Actomyosin motors and malaria parasite invasion of the host cell

Noor Azian Binti Md Yusuf

Division of Parasitology

MRC National Institute for Medical Research

The Ridgeway

Mill Hill, London

NW7 1AA

Department of Structural and Molecular Biology

University College London

This thesis is submitted in part fulfilment of the requirements of University College London for the degree of Doctor of Philosophy

June 2013

Declaration

I, Noor Azian Binti Md Yusuf, confirm that the work presented in this thesis is my own. Where information has been derived from other sources, I confirm that this has been indicated in the thesis

Noor Azian Binti Md Yusuf

June 2013

Abstract

In the blood stream the merozoite is the invasive form of the malaria parasite that must enter a new erythrocyte. Merozoites lack structure for locomotion such as cilia and flagella, but use an actomyosin motor complex that provides the force to drive them into the cell. This molecular motor is located at the pellicle membrane of the parasite. The motor protein complex or glideosome includes a class XIV myosin heavy chain (MyoA), Myosin Tail Interacting Protein (MTIP) and two anchoring proteins known as Glideosome Associated Protein 45 (GAP45) and GAP50. A ternary complex of MyoA-MTIP-GAP45 is first formed and this later associates with GAP50. Using a GFP-tagged MyoA transgenic parasite line the expression of MyoA was examined in both *Plasmodium falciparum* and *P. knowlesi*. The protein was expressed at the periphery of the parasite and associates with MTIP, GAP45 and GAP50. In time course studies it was shown that recruitment of GAP50 to the complex occurs late relative to the onset of GAP50 synthesis, likely reflecting a role for GAP50 in cellular processes prior to host cell invasion. A second class XIV myosin, Myosin B (MyoB) was also tagged with GFP in a transgenic parasite line. Whilst the timing of MyoB expression followed that of MyoA, with clearly detectable protein in segmenting schizonts at 40 hours post invasion, MyoB did not associates with MyoA or any of the other invasion complex proteins. The localisation of MyoB-GFP in *P. falciparum* was at the apical end of the merozoite, in front of other apical organelle markers such as Rhoptry neck protein 4 (RON4). During erythrocyte invasion, MyoB -GFP remained in the same location, whilst RON4 moved out onto the parasite surface as part of the moving junction and migrated to the rear of the parasite. Although the exact role of MyoB is unknown, it is suggested that it may be involved in the invasion process but within its own protein complex that is distinct from the glideosome.

Dedication

To my late father Allahyarham Md Yusuf B. Awang and my late mother Allahyarhamah Rubiah Binti Ismail who always encouraged me to follow my dreams and to my loving and caring stepmother Rokiah Binti Md Noor who took all the responsibilities to let me lift my dreams…….

Acknowledgement

Firstly, I would like to thank my supervisor Dr. Anthony A. Holder for providing me with the opportunity to work in his lab and for the continuous guidance and support throughout my project. I would also like to thank Dr. Robert W. Moon, Dr. Ellen Knuepfer, Dr. Justin Molloy, Dr. Judith L. Green, Dr Claire H. Hastings and Dr. David K. Moss for their generous help and guidance as well as their continuous support and interest in this field of malaria invasion. I also would like to thank my thesis committee panel, Dr. Michael J. Blackman and Dr Roger Buxton for their time and helpful advice.

I also would like to express my gratitude to my home institution, The Institute for Medical Research (IMR), and the Ministry of Health, Malaysia for granting me a full time study leave and The Islamic Development Bank (IDB), Saudi Arabia for awarding me the PhD Merit–scholarship to pursue my study concerning the most intriguing ancient disease in the world in this wonderful country. A special thank you to Dr. Malik Shah B. Mohd Yusoff, Head of Scholarship Programme and Mr. Shaharuqul Huq who spent a lot of their precious time to answer all my emails and who flew from Saudi Arabia to London just to make sure that all concerns of the scholars were taken care of appropriately in order for us to finish this programme, which will benefit our respective home countries.

My appreciation is extended to Ms. Sola Ogun, Dr. Rachel E. Farrow, Dr. Steven Howell, Dr. Madhusudan Kadekopala, Mrs. Munira Grainger, Ms. Oniz Suleyman, Dr. Liz McMinn, Mrs. Rachel Chung, Ms. Suraya Diaz, Ms. Lesley Calder, Ms. Kate Sullivan, Dr. Donna Brown, Ms Jirina Markova and all members of Tony Holder's, Blackman's and Delmiro's Labs who helped me in one way or another. A special thanks to Mrs. Alana Sargent for always helping me with administrative works and dropping by at my house to pick up things early in the morning, Dr. Claire H. Hastings for the 'Haggis Night', Rob Moon for the unforgettable 'ice skating experience', David Moss for the introduction to British delicacies, Mr. Antonio Casal for the coffee indulgence, Mrs. Kush Meghji for the food during Ramadhan, Ms Hayley Wood for photographic advice, Ms. Harsha Seth and Mr. Omar Ayad for their caring

thoughts and last but not least, Dr. Mohd Ridzuan Mohd Abdul Razak for being my unpaid IT manager who always tried to resolved my IT problems.

My most sincere thanks and appreciations goes to Mrs. Salini Halim and her family who were always at my side during both happy and difficult times throughout my stay in London. To my colleagues and friends at the IMR: Dr. Lokman Hakim Sulaiman, Dr. Noor Rain Abdullah, Dr. Shamilah Hisam, Hj.Mohd Yusri Yusof, Mrs Aishah Mahmod, Mrs. Maslawaty Md Noor, Mrs. Parina Ismail, Mrs. Rosilawaty Harun, Mrs Rozie Sarip, Mrs. Paridah Yusuf, Mrs. Rozana Rozali and to the never-ending lists of great and wonderful people in London, Saudi Arabia and Malaysia who in known or unknown ways contributed to the successes of my study, not only in the academic field but also in life experiences.

Last but not least, my endless thanks and never-ending love go to my big family of 12. To my step mother Rokiah, to my elder sisters, Ummi Kalsom, Umi Sofian, Noriza, Noor Zila and Noor Zurawati, to my elder brother Md Amran, to my younger sisters Noor Ziana and Nurul Asyikin, to my younger brothers, Mohd Amirul Azdi, Azrul Hisyam and Mohd Fikry Affendy whom I always refer to by numbers and to all my in- laws, Suhaimi, Razif, Rohaida, Hashimah, Dunian, Amir, Rosli, Azmir, Nazif, and Mira, thank you for your boundless caring, love and support throughout my studies although we are thousands miles apart. To my nephews and nieces: Fahim, Azril, Amzal, Azra, Afza, Azhan, Alia, Aina, Akmal, Shafiq, Firdaus, Balqis, Kamil, Dayana, Hisyamudin, Fahada, Fariha, Firzan, Farisha, Danial, Adam, Hani, Luqman, Elena, Tolia, Fatina, Husna, Damia, Rania and Azfar…Facebook is amazing!!!..I love you all….

…..Thank You….

Table of contents

		Pages
Title Page		1
Declaration		2
Abstract		3
Dedication		4
Acknowledgement		5
Table of contents		7
List of figures		12
List of tables		14
Abbreviations		15
References		170
Appendixes		187
Chapter 1 – Introduction		
1.1	Introduction to malaria	17
1.1.1	The burden	17
1.1.2	The disease	18
1.1.3	The parasite	18
1.2	The *Plasmodium* life cycle	19
1.2.1	The zoites	19
1.2.2	The life cycle	22
1.2.3	The mosquito stage	24
1.2.4	The liver stage	26
1.2.5	The asexual blood stage	27
1.3	The erythrocyte invasion by merozoites	30
1.3.1	Initial attachment	31
1.3.2	Apical orientation	31
1.3.3	Moving junction (MJ) formation	32
1.3.4	Sealing and completion of the parasitophorus vacuole (PV)	34
1.4	The myosin superfamily	35

1.5 The inner membrane complex (IMC) 42
1.6 Acto-myosin motor complex in Apicomplexa 42
1.6.1 *Plasmodium falciparum* myosin A (PfMyoA) 43
1.6.2 Interaction of MyoA with its myosin light chain, MTIP 47
1.6.3 The glideosome associated protein (GAPs) 48
1.6.4 MyoA-actin interrelationship 49
1.7 Apicomplexan Myosin B 54
1.8 Aims of this thesis 55

Chapter 2 – Material and Methods

2.1 DNA manipulation and transformation 57
2.1.1 Oligonucleotides 57
2.1.2 Polymerase Chain Reaction(PCR) 57
2.1.3 Agarose gel electrophoresis 57
2.1.4 Restriction endonuclease digestion 58
2.1.5 Ligation of DNA fragments 58
2.1.6 The propagation and transformation of E.coli by plasmid DNA 58
2.1.7 Isolation of plasmid DNA 59
2.1.8 Sequencing of DNA 59
2.2 *In vitro* Expression and purification of recombinant MyoA, MTIP and GAP45 protein 59
2.2.1 Construction of recombinant DNA 59
2.2.2 Transcription of DNA to mRNA 60
2.2.3 Translation of mRNA to protein 60
2.2.4 Co-translation of proteins 60
2.2.5 SDS-PAGE 61
2.2.6 Immunoblot 61
2.3 Pull down assay and Co-immunoprecipitation assay 62
2.3.1 GST pull down for cell free protein 62
2.3.2 His pull down for cell free protein 62
2.3.3 Co-immunoprecipitation with GFP-TRAP system for parasite lysate 62

2.4 The functional analysis of MyoA 63
2.4.1 *In vitro* motility assay 63
2.4.2 Single molecules studies 64
2.5 *In vitro* parasite culture and maintenance 66
2.5.1 Maintenance of *Plasmodium falciparum* and purification of the schizonts 66
2.5.2 Maintenance of *Plasmodium knowlesi* and purification of the schizonts 67
2.5.3 Freezing and thawing of parasites 67
2.6 The parasite DNA manipulation and transfection 68
2.6.1 Transfection: The construction of single crossover integration constructs for integration of *P. falciparum* and *P. knowlesi* MyoA and MyoB GFP-tags 68
2.6.2 Preparation of DNA construct for transfection 69
2.6.3 Transfection of *P. falciparum* with circular plasmids 69
2.6.4 Transfection of *P. knowlesi* with linear and circular DNA 70
2.6.5 Cloning of transgenic parasite by limiting dilution 70
2.7 Southern Blot 71
2.7.1 DNA digestion 71
2.7.2 Probe generation and labelling 71
2.7.3 Hybridisation 72
2.8 Live imaging and indirect-immunofluorescence microscopy assay (IFA) 72
2.8.1 Live imaging of GFP-tagged parasite 72
2.8.2 Indirect immunofluorescence antibody test (IFA) 72
2.8.3 Fixing live parasite for IFA 73
2.9 Protein complex identification by liquid chromatography- mass spectrometry (LC-MS/MS) 73
2.10 Antibody production 74

Chapter 3 – *In vitro* protein expression and interaction studies

3.1 Introduction 80
3.2 Production of recombinant proteins using the wheat germ cell free 81

system
3.2.1 Co-expression: MyoA co-expression with GST-tag enhances solubility 83
3.2.2 Comparison of His vs GST tagged MyoA solubility 86
3.2.3 MyoA forms a complex with MTIP but not with GAP45 88
3.3 Characterisation of single molecules and the sliding/gliding movement of MyoA 90
3.3.1 Movement of single MyoA molecules and the step size on an actin filament, measured in an optical trapping assay 90
3.3.2 Characterisation of the MyoA-actin interaction 93
3.4 Discussion 97

Chapter 4 - Characterization of Myosin A and Myosin B in asexual blood stages of *Plasmodium*

4.1 Introduction 100
4.2 Production and genotyping of GFP-tagged MyoA (PfMyoA) and MyoB (PfMyoB) *P. falciparum* parasite lines 103
4.2.1 PfMyoA-GFP parasite: cloning and genotyping 104
4.2.2 PfMyoB-GFP parasite: cloning and genotyping 106
4.3 PfMyoA-GFP is part of the established glideosome motor complex whereas PfMyoB is not 109
4.3.1 MyoA-GFP is precipitated with the protein of glideosome motor complex 110
4.3.2 PfMyoB-GFP localises to the extreme apical tip of merozoites 113
4.4 PfMyoA-GFP is localised at the periphery and PfMyoB-GFP is confined to the apical apex as seen by live parasite development 117
4.5 The assembly of PfMyoA-GFP into the glideosome motor complex 122
4.6 Mass spectrometry analysis of proteins associated with PfMyoA-GFP and PfMyoB-GFP 125
4.6.1 Confirmation of MyoA association with the glideosome motor complex 127
4.6.2 MyoB is part of a novel protein complex in the parasite 130
4.7 PF3D7_1118700 protein is a myosin B light chain related to MTIP 134

(MTIP-B)
4.8 Microscopic visualisation of PfMyoA-GFP and PfMyoB-GFP during erythrocyte invasion 137
4.9 Characterisation of anti-MyoA and anti-MyoB antibodies 143
4.10 Generation of anti -MyoA and anti-MyoB antibodies 148
4.11 Discussion 152
4.11.1 The use of transgenic parasites to investigate the timing and localisation of MyoA and MyoB expression 153
4.11.2 MyoA and MyoB share common ancestry but are retained in different complexes. 156
4.11.3 Investigation of PfMyoA-GFP and PfMyoB-GFP localization during erythrocyte invasion 159

Chapter 5 – Research summary
5.1 The reconstitution of the glideosome motor complex *in vitro* using protein produced in the wheat germ cell free translation system 163
5.2 MyoA has a peripheral localization, forms part of the glideosome motor complex and is involved in erythrocyte invasion 163
5.3 MyoB is localised to the apical tip of merozoites, is not part of the glideosome motor complex and may have a role in erythrocyte invasion 165
5.4 Future studies 166
5.5 Concluding remarks 168

List of figures

Figure	Title	Pages
Figure 1.1	The invasive stages of *Plasmodium falciparum* and *Toxoplasma gondii*	21
Figure 1.2	The malaria parasite life cycle	23
Figure 1.3	Gametocytogenesis and gametogenesis	25
Figure 1.4	Asexual stages of *Plasmodium*	29
Figure 1.5	Malaria invasion of the host cell	30
Figure 1.6	Moving junction formation and the role of the AMA-RONs complex	34
Figure 1.7	Myosin superfamily	36
Figure 1.8	Myosin structures	38
Figure 1.9	Clustal alignment of amino acid sequences of PfMyoA and TgMyoA compared to Chiken muscle myosin II (Ckn myoII).	45
Figure 1.10	Putative protein structure of *Plasmodium falciparum* Myosin A (ribbon diagram)	46
Figure 1.11	The power stroke during gliding motility	52
Figure 1.12	Scematic diagram of acto-myosin motor complex	53
Figure 2.1	A schemantic model showing the set up for single molecule myosin studies	76
Figure 3.1	Generation of recombinant DNA, and protein expression in the wheat germ cell free system	82
Figure 3.2	Protein translation in the wheat germ cell free system	85
Figure 3.3	Protein co-expression in the cell free system and determination of MyoA solubility	87
Figure 3.4	GST pull down assays	89
Figure 3.5	Study of MyoA single molecules as measured by optical trapping	92
Figure 3.6	Actin-Myosin interactions	96
Figure 4.1	Generation of parasites expressing PfMyoA-GFP	105

Figure 4.2	Generation of parasites expressing PfMyoB-GFP	108
Figure 4.3	Western blot of uncloned transgene parasites	109
Figure 4.4	PfMyoA-GFP form a tetrameric complex in the glideosome motor complex	1112/3
Figure 4.5	PfMyoB-GFP localised at the apical pole of the parasite	116/7
Figure 4.6	Live microscopy analysis of GFP-tagged MyoA (PfMyoA-GFP) parasite development time course	119/120
Figure 4.7	Live microscopy analysis of GFP-tagged MyoB (PfMyoB-GFP) parasites	121/2
Figure 4.8	PfMyoA-GFP is incorporated into the glideosome motor complex	124
Figure 4.9	Immunoprecipitation of PfMyoA-GFP and PfMyoB-GFP and associated proteins for LC-MS/MS analysis	126
Figure 4.10	Identification of PfMTIP-B	137
Figure 4.11	Stepwise visualisation of PfMyoA-GFP parasites during merozoite invasion of the host cell	140/1
Figure 4.12	Stepwise visualisation of PfMyoB-GFP during merozoite invasion of the host cell	146/3
Figure 4.13	Generation of PkLinA-GFP parasites	146
Figure 4.14	Generation of PkCirB-GFP parasites	147
Figure 4.15	Sequence selection for generation of synthetics peptides to elicit MyoA and MyoB antibodies	150
Figure 4.16	Production of MyoA and MyoB antibodies tested by western blot and IFAs	151
Figure 5.1	A current view of the acto-myosin motor complex and the location of MyoA and MyoB, based on the results of this study	169

List of Tables

Tables	Title	Pages
Table 2.1	The primers used for expression of recombinant protein used in the *in vitro* cell free system	75
Table 2.2	Primers used for construction of a single cross over transfection plasmids and for the diagnostic PCR to analyse transgenic parasites	77
Table 2.3	List of antibodies used in Western blot and IFA.	78
Table 4.1	Members of the glideosome motor complex determined by mass spectrometry analysis of immunoprecipitated PfMyoA-GFP protein	129
Table 4.2	Members of the PfMyoB complex as determined by MS analysis of immunoprecipitated PfMyoB-GFP proteins	132/133

List of Abbreviation

ACT	Artemisinin-combination treatment
ADF	Actin depolymerisation factor
ADP	Adenosine diphosphate
AMA-1	Apical membrane antigen-1
AMP	Adenosine monophosphate
ATP	Adenosine triphosphate
BC	Before Christ
BDM	2,3 –Butanedione monoxine
BSA	Bovine serum albumin
cAMP	3’-5’-Cyclic adenosine monophosphate
CCV	Clathrin-coated vesicle
CDD	Calcium domain database
CDPK 1/2/3/4/5/6	Calcium dependent protein kinase-1/2/3/4/5/6
CME	Clathrin-mediated endocytosis
CR	Complement receptor
CTRP	Circumsporozoite TRAP-related protein
CSP	Circumsporozoite protein
CytB/D	Cytochalasin B/ D
DAPI	4',6-Diamidino-2-phenylindole
DBL	Duffy binding-like protein
DHFR/ DHFR-TS	Dihydrofolate reductase/ DHFR-thymidylate synthase
DDT	Dichlorodiphenyltrichloroethane
DNA/ RNA	Deoxyribonucleic acid/ Ribonucleic acid
DNY/ DrpA/B	Dynamin / Dynamin-related protein A/B
dNTP	Deoxyribonucleotide triphosphate
DTT	Dithiothreitol
EBA/ EBL	Erythrocyte binding antigen/ ligand
EEF	Exoerythrocytic form
EGF	Epidermal growth factor
EDTA	Ethylenediaminetetraacetic acid
EGTA	Ethylene glycol bis(2-aminoethyl ether)-*N*,*N*,*N*'*N*'-tetraacetic acid
EM	Electron microscopy
ER	Endoplasmic reticulum
ES-MS	Electrospray-mass spectrometry
f-MAST	*P. falciparum* merozoites assemblage of subpellicular microtubules
GAP 40/45/50/70	Gliding/glideosome associated protein 40/45/50/70
GAPM 1/2	Glideosome associated protein with multiple membrane spans 1/2
GDP	Global distribution of per-capita gross domestic product
GFP	Green fluorescence protein
GPI	Glycosylphosphatidylinositol
HCl	Hydrochloric acid
HRP	Horse radish peroxidise
Hsp	Heat-shock protein
IFA	Indirect immunofluorescence assay
IgG	Immunoglobulin G
IMC	Inner membrane complex
I PTG	Isopropyl-β-D-thiogalactopyranoside
JAS	Jasplakinolide
KAHRP	Knob associated histidine-rich protein
LAPs	LCCL/lectin adhesive-like protein
LB	Luria-Bertani
LC-MS/MS	Liquid chromatography-tandem mass spectrometry

MCS	Multiple cloning site
MHC/ MLC	Myosin heavy chain/ light chain
MJ/ TJ	Moving junction/ Tight junction
MOPS	Nu-PAGE® 3-(N-morpholino)-propanesulphonic acid
MSP	Merozoite surface protein
MTIP	Myosin tail domain interacting protein
MTOCs	Microtubule organizing centres
MTRAP	Merozoite thrombospondin-related anonymous protein
MyoA/B/C/D/E/F/J/K	Myosin A/B/C/D/E/F/J/K
Ni-NTA	Nickel-nitrilotriacetic acid
NP40	Nonidet P-40
OD/ OT	Optical density/ Optical trapping
PBS/T	Phosphate buffered saline/ tween 20
PCR	Polymerase chain reaction
PFA	Paraformaldehyde
PfCRT	*P. falciparum* chloroquine resistance transporter
PfEMP1/3	*P. falciparum* erythrocyte membrane protein 1/3
PfRh1/2a/2b/4/5	*P. falciparum* reticulocyte binding protein homologue 1/2a/2b/4/5
PfMDR	*P. falciparum* multi drug resistant
PKA/G	Protein kinase A / G
PMSF	Phenylmethanesulfonylfluoride
PM	Plasma membrane
PTRAMP	*Plasmodium* thrombospondin-related apical membrane protein
PV/ PVM	Parasitophorous vacuole/ PV membrane
RAP//2/3	Rhoptry-associated protein 1/2/3
RBC	Red blood cell
RhopH1/2/3	High molecular weight rhoptry protein 1/2/3
RON2/3/4/5	Rhoptry neck protein-2/3/4/5
RPMI	Roswell Park Memorial Institute 1640
SDS	Sodium dodecyl sulphate
SDS-PAGE	Sodium dodecyl sulphate-polyacrylamide gel electrophoresis
SERA	Serine repeat antigen
SOAP	Secreted ookinete adhesive protein
SPECT-1/2	Sprorozoite microneme essential traversal-1/2
SSC	Sodium chloride sodium citrate
TAE	Tris-acetate-EDTA
TRAP	Thrombospondin-related anonymous protein
TSR	Thrombospondin repeat domain
UTR	Untranslated region
UV	Ultra violet
WT	Wild type
WHO	World Health Organisation

Chapter 1

Introduction

1.1 Introduction to malaria

1.1.1 The burden

Malaria is a preventable and treatable disease. Latest WHO estimates can be summarised as 219 million cases reported in 2010 with 660, 000 estimated deaths especially in African children (~90%). These estimated malaria cases were received from 104 malaria endemic countries and territories in 2011 with 99 of these countries having on-going malaria transmission. An estimated 80% of the total malaria cases occur within the 17 most affected countries and the African Region alone gave 47% of cases. However, malaria mortality rates fell by 26% around the world between 2000 and 2010, and remarkable decreases of 33% were reported from the WHO Africa region. During this period, an estimated 1.1 million malaria deaths were averted globally (WHO, 2012).

Recently, a large cluster of human infections caused by *P. knowlesi* has been identified in South East Asian countries including Malaysia (Cox-Singh et al., 2008; Singh et al., 2004), Singapore (Ng et al., 2008), The Philippines (Luchavez et al., 2008), Thailand (Sermwittayawong et al., 2012), the Thai-Myanmar border (Jongwutiwes et al., 2004) and Cambodia (Khim et al., 2011). Other than in South-East Asia *P. knowlesi* cases have only been reported as imported cases where the patient acquired the infection during a vacation in the region. The infections were usually acquired during jungle trekking as a part of eco-tourism activity. The cases reported are from Dutch (Link et al., 2012), New Zealander (Hoosen and Shaw, 2011), French (Berry et al., 2011), Spanish (Ta et al., 2010), Australian (Figtree et al., 2010), and Swedish (Brossier et al., 2003) travelers. Perhaps malaria is a more difficult disease to curtail compared to HIV or tuberculosis owing to the fact of multiple distinct life cycle stages as well as its genetic complexity, which allows *Plasmodium* to adapt rapidly to

drug pressure and challenges by the immune system. In hyperendemic areas, the most affected groups are children under five, pregnant women and other non-immune individuals (Sachs and Malaney, 2002).

1.1.2 The disease

The clinical features are caused by the asexual blood stage of the parasite. These symptoms appear during the parasite's maturation in the blood with the release of antigens during rupture of the host cell (Trampuz et al., 2003). Cases of malaria can be divided into uncomplicated or mild and severe forms. Symptoms of uncomplicated malaria include headache, myalgia and coughing that precedes a typical sequence of shaking chills, fever and sweating for which accurate diagnosis is often difficult. However, uncomplicated malaria can lead to a more severe condition (Weatherall et al., 2002). Severe malaria is a life threatening disease because of the dysfunction of vital organs, i.e. the lungs, kidneys, liver and brain. Further complication such as enlargement of the spleen can occur in untreated cases associated with the increased capacity of the spleen to clear red cells from the circulation (Carter and Mendis, 2002). Cerebral malaria is characterised by deep coma and severe neurological symptoms, seizures, and hypoglycaemia especially in children and has been linked to the sequestration of parasitized erythrocytes in post capillary venules of the cerebral circulation (Weatherall et al., 2002). Severe malarial anemia, including 'black water fever' due to the appearance of haemoglobin in the urine indicating severe intravascular hemolysis leading to hemoglobinuria and hemoglobinemia (White, 2004), and placental malaria causing abortion, premature death of the foetus and maternal death (Weatherall et al., 2002) are two further complications of malaria parasite infection.

1.1.3 The parasite

Malaria is caused by *Plasmodium* species of the phylum *Apicomplexa,* protozoa that are capable of infecting a variety or organisms including certain reptiles, birds and mammals. Malaria species are host specific, however several simian malaria species can be transmitted to man (Coatney, 1971; Escalante et al., 1998; Waters et al., 1993).

There are six species of *Plasmodium* responsible for human malaria: *Plasmodium falciparum, Plasmodium vivax, Plasmodium malariae, Plasmodium ovale curtisi* and *Plasmodium ovale walikeri,* as well as *Plasmodium knowlesi* (Coatney, 1971; Sutherland et al., 2010).

Other than the *Plasmodium spp*., the *Apicomplexa* include *Toxoplasma gondii*, a causative agent of complications in pregnancy and the immunocompromised; *Cryptosporidium spp.*, a causative agent of gastroenteritis; *Theileria spp*. a tick-borne parasite of cattle in Africa and *Eimeria spp.* the causative agent of coccidiosis in livestock (Morrissette and Sibley, 2002). *Apicomplexan* parasites shares common and unique structures known as the apical complex in the motile and invasive stages, which are usually call 'zoites' (Menard, 2001). Zoites are polarized and elongated cells and the integrity of the cell shape is maintained by a set of microtubules anchored to the anterior polar ring and extending longitudinally under the parasite pellicle, which is composed of the plasma membrane (PM) and the inner membrane complex (IMC) (Morrissette and Sibley, 2002).

1.2 The *Plasmodium* life cycle

1.2.1 The zoites

Zoites are motile forms that can be found in the lumen of the mosquito mid-gut (ookinete), in mosquito salivary gland and hepatocyte invasion (sporozoites) and in the red blood cell cycle (merozoites). Although they invade different cells during the different life cycle stages, they share a similar overall morphology. The zoites; the ookinete (~10-13µm long), the sporozoite (~12-15µm long) and the merozoite (~1.5µm long) possess apical secretory organelles namely micronemes, dense granules and rhoptries (only in the sporozoite and merozoite forms) (Figure 1.1). These organelles are only seen in the zoites, secrete their contents at the anterior tip of the zoite during attachment, and invasion of the host cell. Following invasion the parasite resides within a parasitophorous vacuole (PV). The PV is a parasite-derived vacuole formed during infection, primarily by secretion of the lipid-rich rhoptries and partly from later secretion of the dense granules (Baum et al., 2008a; Opitz and Soldati, 2002).

The ookinete's lack of rhoptries is thought to correlate with its special role in traversing the mosquito mid-gut epithelium and the absence of PV formation (Vlachou et al., 2006). Having large rhoptries (club-shaped or elongated) and numerous micronemes, the sporozoites are able to glide, and traverse and infect hepatocytes. On the other hand, the merozoite has large rhoptries and fewer micronemes, shows no gliding motility or cell traversal, but is able to rapidly invade the host cell powered by the conserved gliding machinery (the glideosome) (Cowman and Crabb, 2006). These apical secretory organelles are also present in *T. gondii* tachyzoites (the invasive stage) which suggested that they are conserved across *Apicomplexa* although the composition of their content differs which is a direct consequence of host cell type specificity (Baum et al., 2008a). Except for *Cryptosporidium*, these parasites also contain a non-photosynthetic plastid (of algal origin) known as the apicopalst to play important roles in metabolic activity and possibly in the establishment of the PV (Kim and Weiss, 2004).

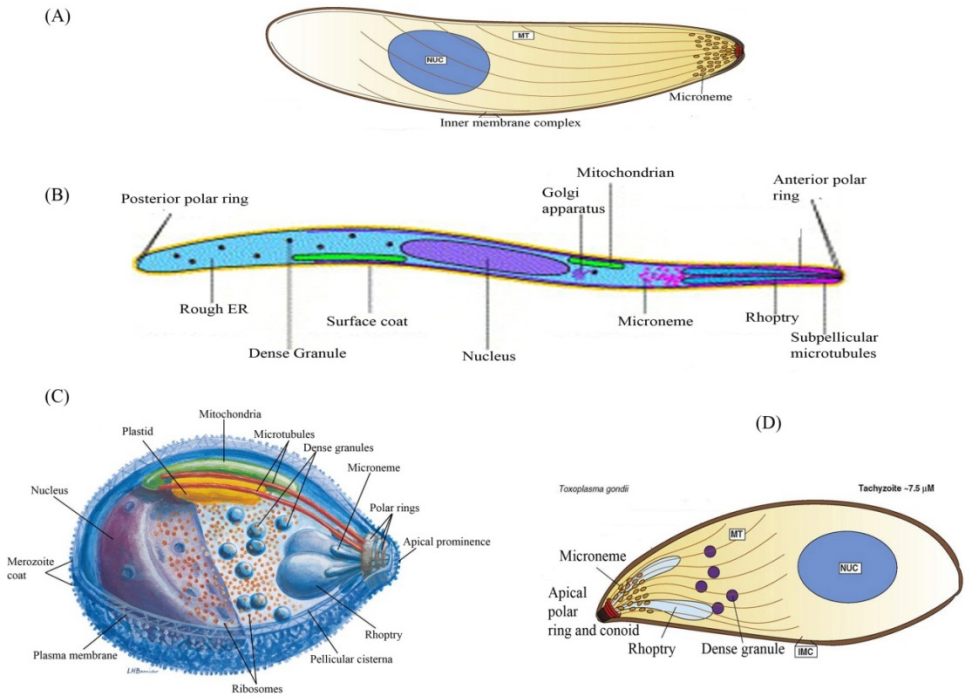

Figure 1.1: The invasive stages of *Plasmodium falciparum* and *Toxoplasma gondii*. Conserved organelles at the apical prominence mainly involved in motility and host cell invasion are the rhoptries, micronemes and dense granules. Ookinetes lack rhoptries. Both *Plasmodium falciparum* and *Toxoplasma gondii* belong to the genus Apicomplexa. Despite the conservation of apical organelles, differences such as the presence of the conoid (only in *T. gondii*) are also depicted here. (A) Ookinete (~10-13µM); (B) Sporozoite (~12-15µM); (C) merozoite (~1.5µM); (D) *T. gondii* tachyzoite (~7.5µM). Panels (A) and (D) taken from (Baum et al., 2008a); Panel (B) from (Frevert, 2004) and Panel (C) from (Bannister et al., 2000b)

1.2.2 The life cycle

The life cycle involves two hosts one being the insect (mosquito stage) and the other the human (vertebrate) host. The life cycle involves two hosts one being the insect (mosquito stage) and the other the human (vertebrate) host. During a blood meal, a malaria-infected female *Anopheles* mosquito inoculates sporozoites into the human host. Sporozoites infect liver cells and mature into merosomes, which rupture and release merozoites into the blood circulation. After this initial replication in the liver (exo-erythrocytic schizogony), the parasites undergo asexual multiplication in the erythrocytes (erythrocytic schizogony). In continuous cycles merozoites infect red blood cells: the initial ring stage develops into a trophozoite and nuclear and cell division leads to a mature schizont, which then ruptures releasing more merozoites. The cycle continues, but some parasites differentiate into sexual erythrocytic stages (gametocytes). The gametocytes, male (microgametocytes) and female (macrogametocytes) are ingested by an *Anopheles* mosquito during a blood meal. In the mosquito's midgut, gametogenesis produces male and female gametes and the microgamete fuses with the macrogamete generating a zygote. The zygote in turn becomes motile and elongated in a form now called an ookinete, which invades the mid-gut wall of the mosquito where it develops into an oocyst. The parasite's multiplication in the mosquito is known as the sporogonic cycle. The oocyst grows and sporogony results in oocyst rupture and release of sporozoites into the hemocoel. The oocyst-derived sporozoites migrate to and infect the mosquito's salivary glands. Inoculation of the sporozoites into a new human host during a blood meal perpetuates the malaria life cycle (Bannister and Mitchell, 2003; Cowman and Crabb, 2006) (Figure 1.2).

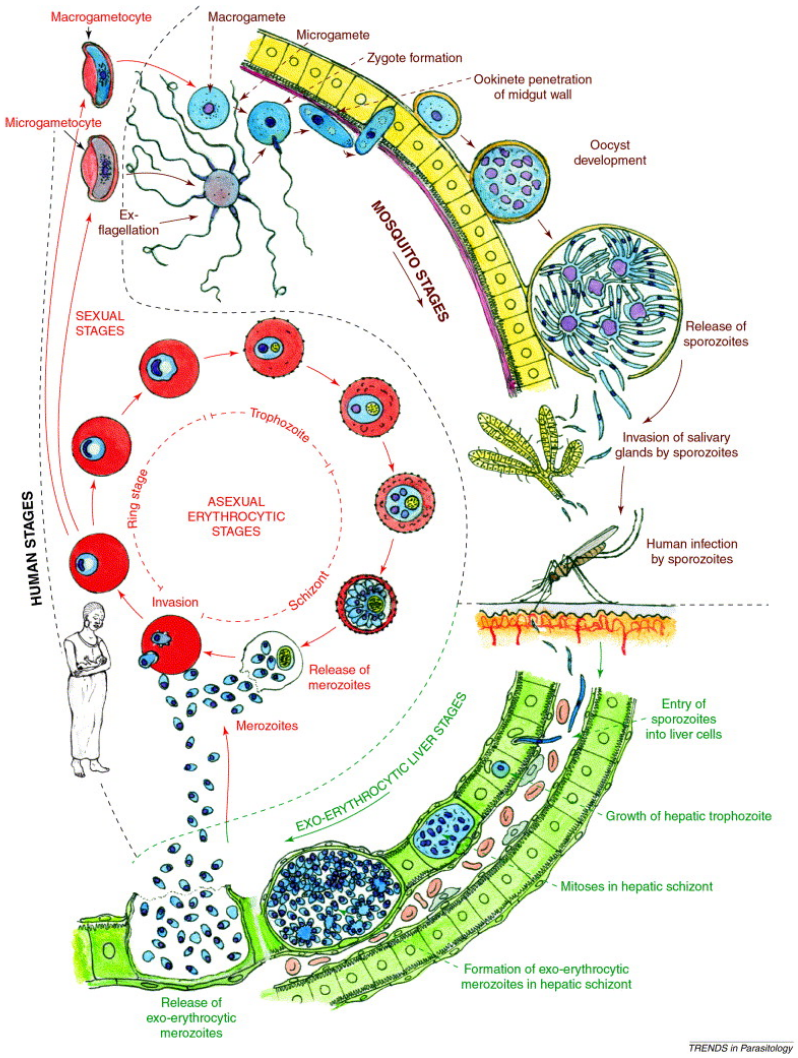

Figure 1.2: The malaria parasite life cycle. Infection of humans occurs by inoculation of sporozoites by the bite of a female infected mosquito. In humans, the sporozoites get carried with the blood stream to the liver where they invade hepatocytes starting the exo-erythrocytic liver stage cycle. In the hepatocyte, the parasite grows through schizogony into a merosome which contains merozoites which then release into the blood circulation starting the asexual erythrocyte cycle. The newly invaded merozoite forms the ring stage, progressing to a trophozoite and following schizogony to a schizont which releases merozoites into the blood circulation. This starts a new asexual erythrocytic cycle. Some of the merozoites after invasion develop into gametocytes which are taken up by feeding mosquitoes and start the sporogonic cycle resulting in the development of infective sporozoites. Diagram adapted from (Bannister and Mitchell, 2003).

1.2.3 The mosquito stage

The gametocytes are the only stages within the life cycle of the malaria parasite that are able to mediate the transition from the human host to the insect host. Gametocytogenesis starts in the erythrocyte cycle 9-12 days after the appearance of the parasite in the human blood and can be influenced by different kinds of stress, including parasite density, anemia, host immune response or drug treatment. When the parasite becomes committed to change from the asexual pathway to the sexual pathway it will involve all merozoites from this schizont and it will result in the production of only one sex (male or female) per schizont (Bruce et al., 1990). This was proven by using female and male-specific markers (pfg377 and α-tubulin II respectively) which showed that the siblings from one schizont were committed to female or male gametocytes exclusively. The switch is believed to have occurred the previous cycle before gametocyte manifestation (Silvestrini et al., 2000). The cellular events of gametogenesis have been described in detailed (Carter and Miller, 1979; Sinden, 1983a, b). During the blood meal from an infected human, the female mosquito takes up gametocytes. By entering the mosquito mid-gut, the gametocytes become activated and round up before egress from their enveloping host cell erythrocyte. Here in the mid-gut the parasite receives environmental signals to switch from a warm blooded host to an insect vector. This extreme change includes sudden drop in temperature (10-15^{o}C) , a pH decrease and the presence of mosquito-derived factors (xanthurenic acid), which trigger the initiation and development of gametes (Billker et al., 1998; Kooij and Matuschewski, 2007). The female macrogametocyte transforms into a macrogamete and the male microgametocyte develops into eight microgametes forming a rosette called an exflagellation center. The microgametes finally detach from the residual body as activated microgametes. Within approximately 20 minutes post-activation, motile microgametes can fertilize macrogametes resulting in a zygote which then transforms into an ookinete within 24 hours (Figure 1.3) (Kuehn and Pradel, 2010).

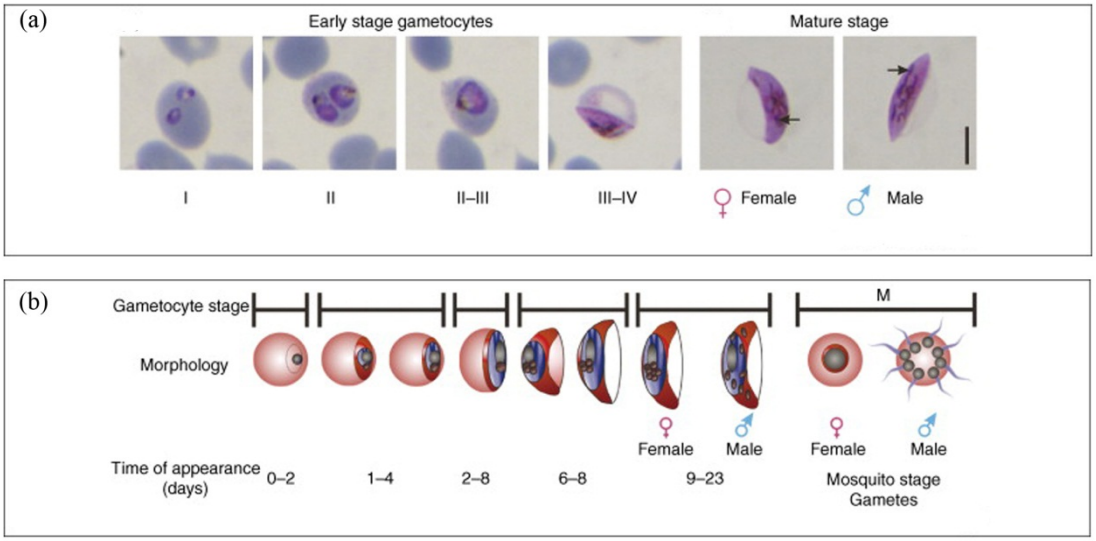

Figure 1.3: Gametocytogenesis and gametogenesis. (a) Giemsa-stained parasites depicting stages of gametocyte development in human blood. (b) schematic of gametogenesis both in human host and in mosquito. Stage-I: oat grain shape of ring stages with simple plasma membrane and small nucleus; Stage-II: D-shaped stage with 8-15 microtubules and an inner pellicle membrane vacuole on the 'straight' side of the cell and a small nucleus with some spindles; Stage II-III: D-shaped parasites and the erythrocyte is distorted; contains 15-40 microtubules,and the inner pellicle membrane vacuole extends around the entire circumference; the nucleus becomes lobed; Stage III-IV: spindle shaped and distorted erythrocyte with microtubules and membrane pellicle surrounding the cell; Stage V or mature stage shows a crescent shape parasite with blunt/ rounded ends within a distorted erythrocyte. The microtubules depolymerise and the inner membrane remains. Females will stained blue, whereas, the male gametocyte is stained pink when using the Giemsa staining technique. Pigmentation of hemozoin differs with a more compact form in the female and a dispersed form in male gametocytes. In the midgut of the mosquito, female gametocytes transform into one macrogamete, meanwhile the male gametocyte forms eight microgametes by exflagellation (Dixon et al., 2008).

1.2.4 The liver stage

The invasive stages of *Plasmodium*, *Toxoplasma* and *Eimeria* have two characteristics to ensure continuity of their life cycle: the capability of cell traversal and invasion by gliding motility (at 1-10µm per second (Sibley et al., 1998). Malarial transmission to the human host is established by sporozoite infection, travelling through the skin in order to reach a blood vessel where they breach the endothelial barrier to enter the circulation and travel to the liver (Garnham, 1966). The circumsporozoite protein (CSP) and thrombospondin-related anonymous protein (TRAP) are essential membrane proteins required for sporozoite motility as well as attachment and invasion of the salivary gland (Baum et al., 2006b). The cytoplasmic domain of TRAP has a penultimate tryptophan residue which is essential to sporozoite motility. TRAP has been shown to be crucial for the sporozoite's ability to infect salivary glands as well as hepatocytes. Other thrombospondin domain-containing proteins in other life cycle stages appear to support a similar function such as circumsporozoite-TRAP-related protein (CTRP: in ookinete stages) (Dessens et al., 1999) and merozoite-TRAP (MTRAP: in merozoite stages) (Baum et al., 2006b). Essential for Kupffer cell transversal motility are two sporozoite micronemal proteins named SPECT-1 and 2 (Ishino et al., 2005; Ishino et al., 2004; Yuda and Ishino, 2004).

Cell traversal by *Apicomplexan* parasites involves the rupturing of the cell PM resulting in the death of several hepatocytes. It is currently unknown how sporozites choose between traversal versus invasion of hepatocytes. It appears that cell traversal is essential for the induction of a cAMP derived signaling mechanism in the sporozoites which together with cytosolic Ca^{2+} levels lead to the secretion of micronemes and rhoptries (Ono et al., 2008). Sporozoites do not develop within the hepatocytes close to space of Disse in the liver, but they migrate through a several hepatocytes before invading the final hepatocyte. The final invasion results in the formation of a PV in the selected hepatocyte. Inside the PV, the sporozoite grows and differentiates into a young exoerythrocytic form (EEF). During the onset of the EEF development cascade, the parasite typically lies close to the nucleus of the infected hepatocyte. Within two days (in rodent) or six to seven days (in primate), the developing EEF grows dramatically resulting in a parasite larger in size than the original host cell. The final step is the release of merozoites into the blood circulation, which occurs not by rupture of the hepatocyte but by the formation of merozoite-filled vesicles, so called

merosomes, which bud off from the infected hepatocytes and release merozoites into the blood circulation (Sturm et al., 2006).

1.2.5 The asexual blood stage

In the blood circulation, the merozoite initially adheres to the erythrocyte surface before invasion proceeds. The initial attachment is reversible, then the merozoite re-orientates to ensure that the apical end which contains the invasion apparatus is juxtaposed to the erythrocyte membrane. The erythrocyte membrane appears thickened at the contact site and at this point the merozoite activates the invasion machinery based on an acto-myosin motor complex. In the erythrocyte, the newly invaded merozoite undergoes several stages of its asexual development and multiplication within a membranous sac called the parasitophorous vacuole (PV). The intracellular stages are named ring, trophozoite, and schizont. Some parasites switch from the asexual pathway to the sexual pathway and develop into gametocytes (Bannister and Mitchell, 2003; Bannister, 2001; Garnham, 1966). During this early developmental stage the parasite feeds on small amounts of haemoglobin ingested through the cytostome or cell mouth, specialised to phagocytose food. *P. falciparum* digests more than 80% of the erythrocyte's haemoglobin to support parasite growth (Francis et al., 1997). The bulk of haemoglobin degradation occurs via a semi ordered process of digestion by proteases which are contained within the food vacuole (Lazarus et al., 2008). The haem products of the haemoglobin digestion are crystallized into a dark pigment called haemozoin which is contained within the food (pigment) vacuole. Any disruption of the haemoglobin degradation process such as that mediated by artemisinin (by damaging the food vacuole or haem polymerization) and chloroquine (by inhibiting the polymerization of haem released during haemoglobin proteolysis) will result in parasite death (Bannister and Mitchell, 2003; Francis et al., 1997). The ring grows more rounded, increasing the size of the PV membrane (PVM) and extends finger-like projections and membranous blebs into the surrounding erythrocyte (Bannister et al., 2003; Bannister et al., 2000a).

Trophozoites are the most metabolically active uni-nucleate stages in asexual parasite development. The numbers of free ribosomes multiply greatly and the ER enlarges, marking the increases of protein synthesis. The parasite feeds on the haemoglobin of the erythrocyte and alters significantly the host cell by exporting

numerous parasite proteins into its cytoplasm and to its surface, resulting in the formation of knobs on the host cell surface. Knobs are relevant to allow sequestration of parasitized erythrocytes in blood vessels preventing splenic clearance (Bannister et al., 2003). The function of the largely extended cleft network within the host erythrocyte is still under debate. Recently using EM, tethers connecting the Maurer's cleft bodies with the erythrocyte membrane have been identified suggesting a role in transport between the clefts and the erythrocyte surface, which may aid the vesicle mediated delivery of PfEMP1 to the surface (Gruring et al., 2011; Hanssen et al., 2010; Tilley et al., 2007). During the development of schizont stages, DNA replication occurs and apical organelles (rhoptries, micronemes and dense granules) are formed. Cytoskeletal components such as microtubules and the apical polar ring are formed beneath the merozoite surfaces which are vital for nuclear segregation and therefore formation of daughter merozoites. Cytokinesis takes place during schizont development and starts from a cleavage furrow on each merozoite. Once cytokinesis is completed, marked by the end of schizogony, and the merozoites are ready to be released into the blood circulation, the host cell membrane and PVM are lysed in a protease-dependent process (Bannister et al., 2000a). Figure 1.4 shows the complete erythrocyte asexual life cycle. Gametogenesis occurs when the parasite switches, changing their pathway from producing merozoites to producing gametocytes.

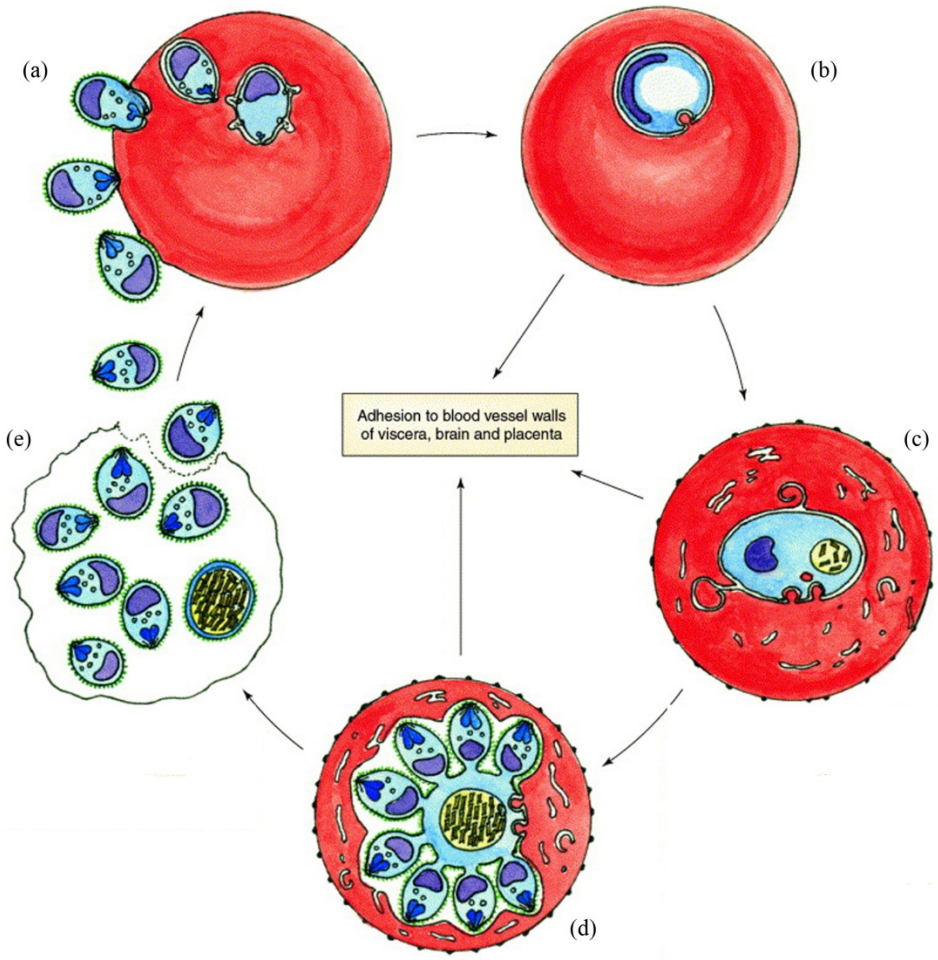

Figure 1.4: Asexual stages of *Plasmodium*. (a) the invasion event starting from attachment to post invasion, (b) ring stages. (c) trophozoite stages, (d) dividing schizont, and (e) schizont rupture releasing merozoites (Bannister et al., 2003)

1.3 The erythrocyte invasion by merozoites

The invasion of erythrocytes by *Plasmodium* merozoites starts with the attachment to the erythrocyte surface followed by a reorientation process in which the apical end of the merozoite is brought to be juxtaposed to the erythrocyte surface. When the tight or moving junction (TJ or MJ) is formed the invasion process becomes irreversible; the molecular motor engages and drives the invasion. At the same time proteases cause the shedding of the surface coat while the parasite is moving into the erythrocyte. Lastly the moving junction seals behind the invading merozoite which is now found within the PV within the host cell (see review by [(Cowman et al., 2012; Cowman and Crabb, 2006)]) (Figure 1.5).

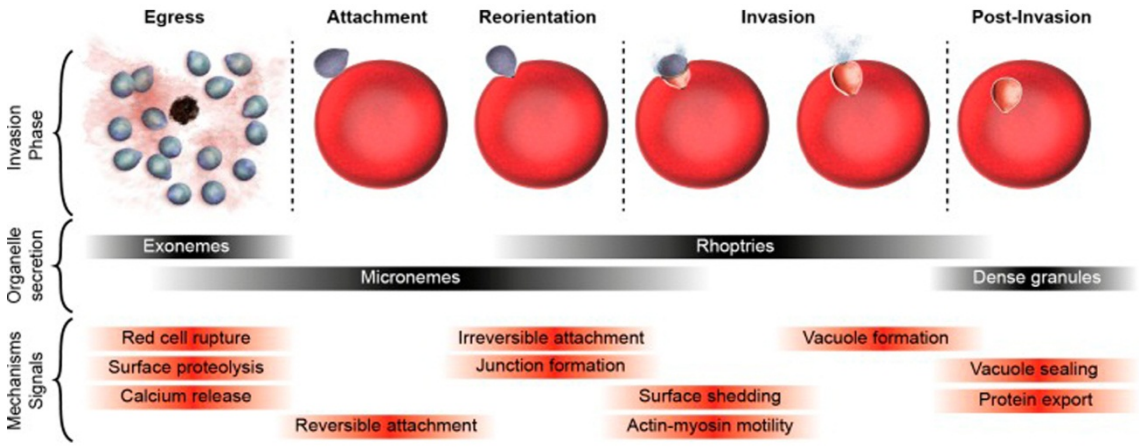

Figure 1.5: Malaria invasion of the host cell. Attachment of merozoites to the erythrocyte surface occurs following egress from schizonts, andis a reversible process. Merozoites then reorientate to bring the apical end in proximity to the erythrocyte membrane. The secretion of apical organelles allows the formation of a MJ and makes the invasion irreversible. The MJ is somehow connected with the acto-myosin motor resulting in the movement of the junction across the merozoite surface. In the same process surface proteins are shed. The PV is formed from the erythrocyte plasmalemma and rhoptry secretions and once the MJ reaches the posterior end of the parasite, the membrane seals (Cowman et al., 2012).

1.3.1 Initial attachment

A few moments prior to merozoites release, the schizont transforms morphologically into a more rounded form. Each merozoite appears defined, tightly packed and symmetrically arranged in a flower-like shape around a centrally located digestive vacuole with condensed haemozoin. A few seconds before actual merozoite egress, the merozoites are released from the PVM into the host cell and then from the erythrocyte, in an explosive event causing the curling of the erythrocyte membrane, into the blood stream (Abkarian et al., 2011; Glushakova et al., 2005). Initial attachment (depending on the receptor-ligand interaction) of the merozoite is believed to be mediated through the adhesive surface coat. This is the first and crucial step of invasion where the merozoite needs to distinguish an erythrocyte from other cells. At this stage the merozoite can detach and re-attach to another erythrocyte (Bannister and Dluzewski, 1990; Dvorak et al., 1975).

The attachment to the erythrocyte can occur anywhere on the surface of the merozoite. A merozoite surface protein (MSP) binds to the erythrocyte plasma membrane and caused adhesion. More than one MSPs, are essential for the erythrocyte adhesion, these included members of EBA and Rh families, which are secreted onto the surface from the internal apical organelles. These protein bind to specific receptors (Tham et al., 2012). Due to the abundance and distribution of MSP1 all over the surface, MSP1 may mediate this initial interaction during the invasion process (Holder et al., 1985). MSP1 processing fragments have been described to bind to erythrocyte receptors, such as the C-terminal $MSP1_{19}$ fragment and erythrocyte receptor band 3 (Goel et al., 2003; Li et al., 2004) or $MSP1_{42}$ and heparin (Boyle et al 2010). EBA175 binds to Glycophorin A and PfRh4 binds complement receptor (CR)-1 (Tham et al., 2012). Gene knockout experiments indicated that the Rh and EBA families function cooperatively, such that EBA genes loss of function resulted in increased transcription of the PfRhs family (Lopaticki et al., 2011).

1.3.2 Apical orientation

After initial attachment the merozoite re-orientates such that the apical complex is juxtaposed to the erythrocyte membrane so that secretion from the apical organelles

(rhoptries and micronemes) can be triggered. The merozoite wraps itself with the erythrocyte to facilitate the reorientation, and AMA1 has been implicated in this reorientation process (Mitchell et al 2004). After reorientation of the merozoite, a tight interaction between parasite and erythrocyte membrane is formed. This junction zone is marked in EM images by an electron-dense undercoating of the erythrocyte membrane and a closer inter-membrane distance of between about 4 nm (Bannister et al., 1986) and ~10nm (Aikawa et al., 1978). This junction formation involves more than one merozoite protein secreted from the apical organelles (micronemes and rhoptry tip) including the rhoptry neck proteins RON2 and RON4 and others such as the erythrocyte binding antigen family (Gaur et al., 2004) and the reticulocyte binding protein homologue family (Rayner et al., 2000; Triglia et al., 2009). The exact sequence of protein secretion from different organelles and the exact external signal that triggers this release are still unknown.

1.3.3 Moving junction (MJ) formation

Much of the invasion process itself is organized around a key interface that forms between the two cells called the MJ. The MJ creates a tight molecular seal between the host and parasite membrane (Aikawa et al., 1978) believed to be comprised of RON2 and RON4 (Besteiro et al., 2011) and other proteins including AMA1 and MTRAP which span the host and parasite membrane and associate with aldolase (on the cytoplasmic face of the parasite PM) The MJ moves from the apical end towards the posterior end of the merozoite, powered by the acto-myosin motor (Baum et al., 2006a; Morrissette and Sibley, 2002), driven by Myosin A (MyoA) via filamentous actin (F-actin). F-actin is present at the apical pole of invading merozoites and then concentrated at the MJ during invasion (Baum et al., 2008b). As the MJ progresses towards the posterior end of the parasite, ligands mediating the adhesion to the host cell must be removed/shed (Cowman and Crabb, 2006). The erythrocyte membrane at the point of attachment is slightly raised and thickened. As the invasion progresses, the indentation deepens and conforms to the curvature of merozoite. Once, the merozoite-erythrocyte junction is initiated, and MJ progresses the thickened, electron-dense zone on the erythrocyte membrane is no longer observed at the site of

initial attachment (Tyler et al., 2011). The junction transforms from a localized patch to an orifice through which the merozoites penetrates into the deepening, forming PV.

The PVM is partially derived from the erythrocyte membrane as well as new membrane material presumed to be derived from the contents of rhoptries. Not all host PM proteins enter the PVM, the MJ sieves some selected proteins (for examples flotilin-1 and -2 are exclusively internalized into the newly form PVM, although some proteins, such as stomatin and nonraft cytoskeletal proteins, are excluded) (Murphy et al., 2007). The secretion of the AMA-1/ RON complex is essential not only for establishment of the MJ but also for the secretion of the rhoptry bulb contents which then allows the establishment of the PV. RON2 is a transmembrane protein which after secretion from the rhoptry neck sits in the erythrocyte plasma membrane. It associates with RON4 and RON5 secreted into the erythrocyte cytoplasm and connects to the host cell cytoskeleton (Tonkin et al., 2011). In *Toxoplasma*, MJ is constituted by the AMA-1 and RON2/4/5 complex, and recent showed the involvement of association with RON8 (Figure 1.6). The complex of RON2/4/8 is injected into the MJ tethered by RON2 (Tonkin et al., 2011). Knockout of the RON8 gene seem to cripple the parasite making it unable to establish firm attachment of the MJ (Straub et al., 2011). AMA-1 is the only member on the parasite surface which so far has been identified in the MJ complex and the best candidate for anchoring the complex on the parasite site. Knockout of AMA-1 impaired parasite attachment to the host cell, invasion and affected rhoptry secretion (Andenmatten et al., 2013; Mital et al., 2005).

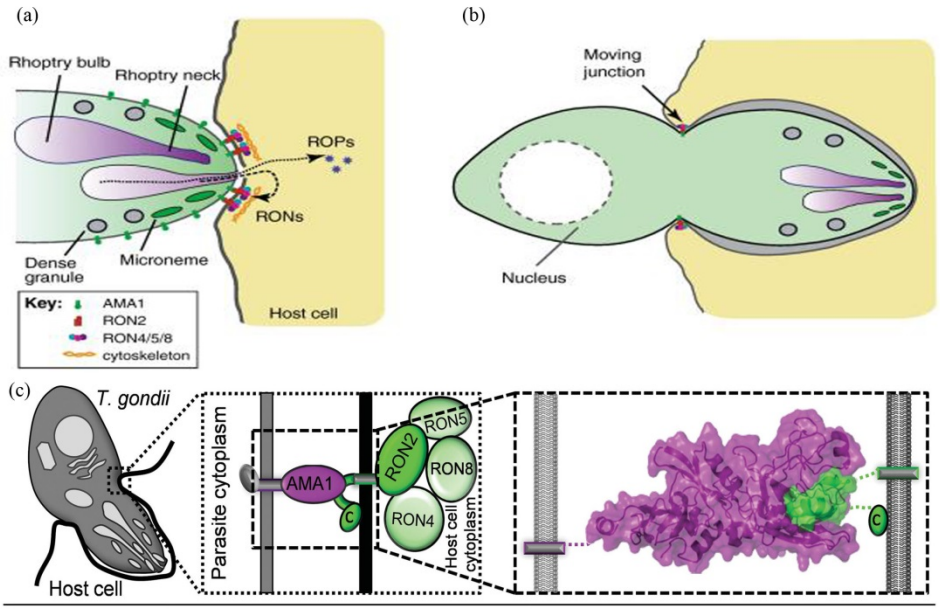

Figure 1.6: Moving junction formation and the role of the AMA-RON complex. (a) Close up of the apical tip displaying secretory organelles; rhoptries (bulb and neck compartment), dense granules and micronemes. Rhoptries are being secreted with the RONs embedding themselves in the erythrocyte membrane and connecting to the host cell cytoskeleton. (b) Zoite partially invaded. The MJ coincides with the parasite contractile apparatus (Tyler et al., 2011). (c) Overview of TgAMA1 and the RON complex. This figure depicts the essential TgAMA1-TgRON2 complex that links the parasite and host cell. The proposed extracellular location of the C-terminus of TgRON2 is indicated (denoted by **[(c)]**) (Tonkin et al., 2011).

1.3.4 Sealing and completion of the parasitophorus vacuole

As the parasite pushes its way into its host cell, it lies within a PV which it forms to seal itself from the host cytoplasm and form an environment hospitable for its development. The membrane of the invagination eventually closes at the posterior end of the merozoites to form the PV (Cowman and Crabb, 2006) . The sealing process is followed by a brief period of echinocytosis of the erythrocyte defined by a morphological spiking of the host cell stimulated by the efflux of potassium and chloride ions. Within 10 min however the erythrocyte returns to its normal shape (Gilson and Crabb, 2009). Progression of the MJ complex over the merozoite, formation of the PV and the sealing events can be followed experimentally by using labeled

PfRON4 and PfRON2 as markers (Zuccala et al., 2012). The internalized parasite known as a ring stage then undergoes rapid, dramatic changes in cell shape (Gruring et al., 2011).

1.4 The Myosin superfamily

Myosins can be defined as a diverse superfamily of molecular motor proteins capable of translocating actin filaments or vesicle cargo on fixed actin filaments. Myosin has the ability to convert energy released by ATP hydrolysis into mechanical work (Sellers, 1999). Even though all myosins have this ability, different myosins perform very different types of functions in the cell. Some myosins are important in cell polarisation, cytokinesis, organelle transport and trafficking as well as signal transduction (Thompson and Langford, 2002). Myosins can be classified into several classes. Previously 18 different classes were distinguished (Hodge and Cope, 2000; Sellers, 2000) whereas more recently 24 have been described (Foth et al., 2006). The characterisation is based on the molecular structure comprising a heavy chain with a conserved head domain, generally near the N-terminus, followed by an alpha-helical light chain-binding domain consisting of one or more IQ motifs and a C-terminal domain. N-terminal extensions are also characteristic of a few classes of myosins (Coluccio, 2008; Lodish et al., 2008; Sellers, 1999; Thompson and Langford, 2002). The more recent classification takes into account similarities of the amino acid sequence in the head domains and phylogeny (Foth et al., 2006) (Figure 1.7).

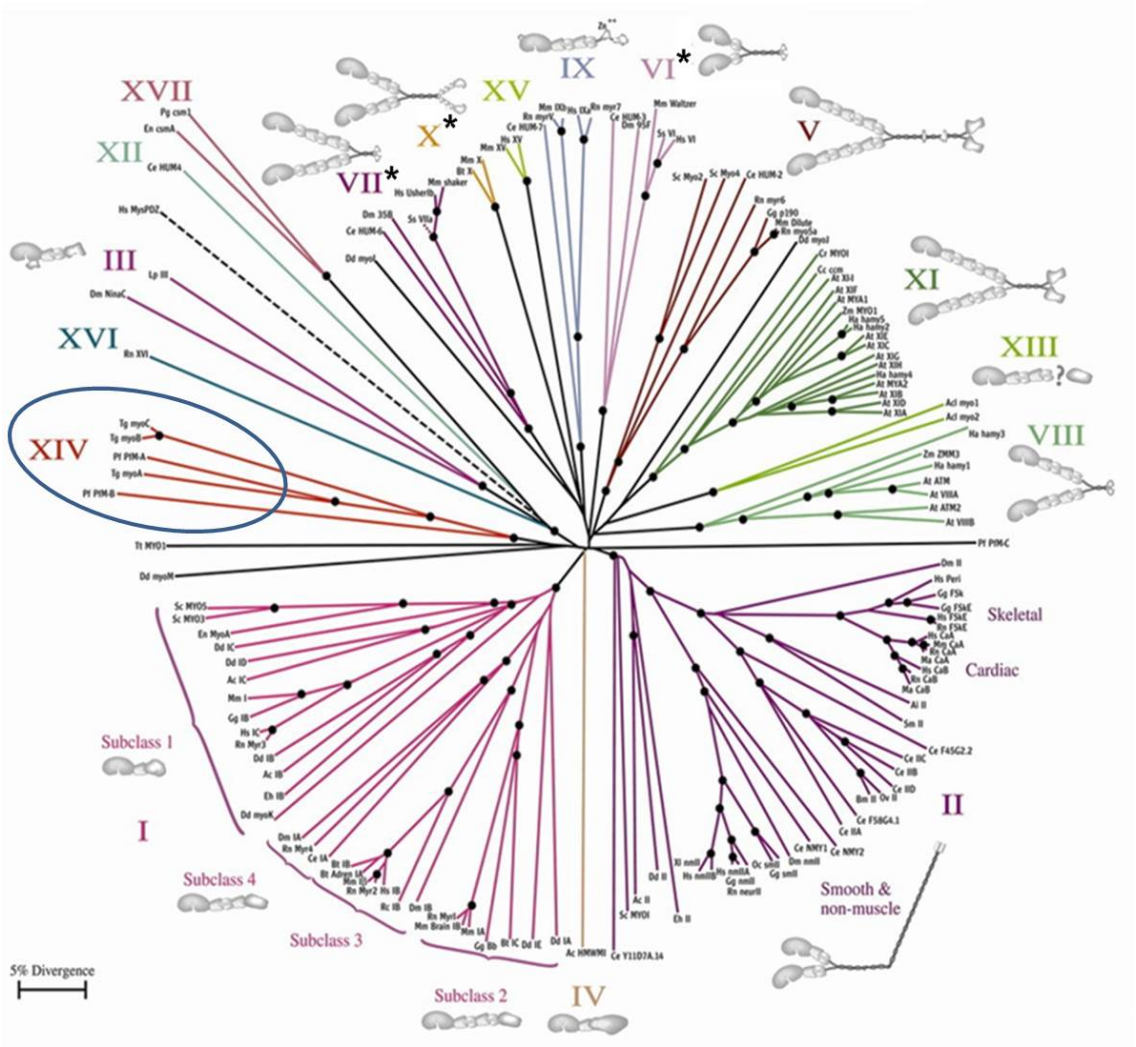

Figure 1.7: Myosin superfamily. Phylogenetic tree of the myosin superfamily. Class XIV contains only Apicomplexan myosins, which are suggested to be similar to classes III, XII, XVII and more distantly related to class I (Hodge and Cope, 2000). Apicomplexa class XIV is highlighted in the blue circle and includes TgMyoC, TgMyoB, TgMyoE, PfMyoA, TgMyoA, TgMyoD and PfMyoB.

All type of myosins consists of at least 3 functional domains (Figure 1.9):

i) the highly conserved head domain or motor domain also known as cross-bridge, which also contains the ATPase activity. Crystal structures for type I, II, V, and VI have been determined and show conservation in the head domain. The head domain consists of a 7-stranded β-sheet surrounded by numerous α-helices. The ATP binding site consists of a P-loop. The head domain also contains the actin binding site which is split by a deep cleft allowing the domain to open and close in response to ATP binding. ATP hydrolysis causes structural conformational changes which are transmitted from the head domain to the lever arm by a small protein region called the converter. This converter region is able to change a linear displacement into a rotation.

ii) the lever arm or neck region which consists of an α-helix of variable length carrying a number of characteristic IQ motifs (between 1 and 6) which have the consensus calmodulin-binding sequences (IQxxxRGxxxR). Each IQ motif serves as a binding site for either a myosin-specific light chain or calmodulin

iii) a tail region of variable length, domain composition and organisation. The cellular localisation and function of the myosins is determined by the tail region. Functions range from filament assembly to cargo binding (Figure 1.8) (Coluccio, 2008; Lodish et al., 2008; Sellers, 1999; Thompson and Langford, 2002).

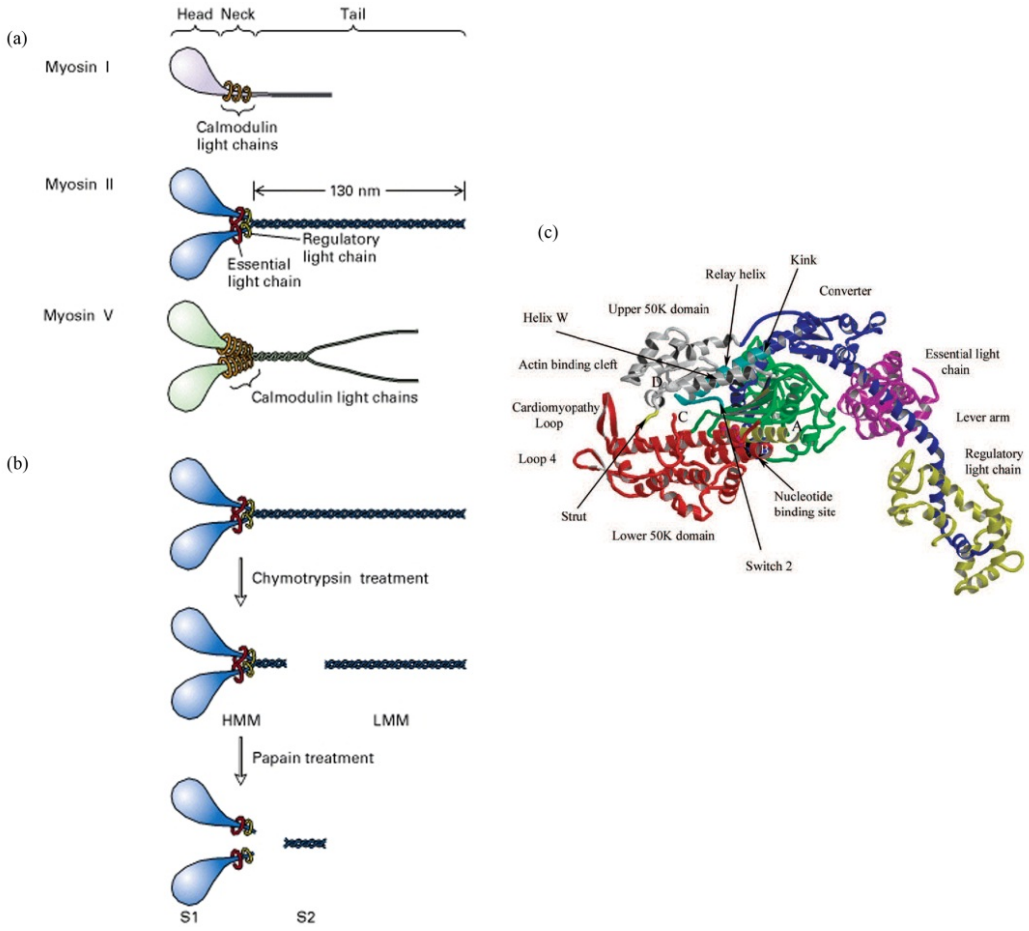

Figure 1.8: Myosin structures. (a) Schematic diagram of myosins. In myosins three different domains can be distinguished: the head domain, neck domain and tail domain. The head domain or motor domain usually serves as an ATP binding site, contains ATPase activity and has the actin binding site. The neck domain serves as the lever arm usually for regulation purposes. This site binds either myosin-specific light chains or calmodulin. The tail domain, defines the specific role of each myosin, serves as a receptor for cargo binding and can form dimers. (b) Schematic diagram of skeletal muscle myosin II which can be broken into fragments by proteolysis. LMM (light meromyosin), HMM (heavy meromyosin), S1 (subfragment1) and S2 (subfragment 2). (c) Crystal structure of myosin II motor domain. The conformation shown is the post rigor state. N-terminus (green), nucleotide binding P-loop and adjoining helix (yellow), upper 50K (red), lower 50K domain (grey), C-terminal long helix (dark blue) with two calmodulin-like chains. Diagram (a) and (b) are adapted from Lodish H, Berk A, Zipursky SL, et al. Molecular Cell Biology. 4th edition. New York: W.H.Freeman; 2000. Available from: http://www.ncbi.nlm.nih.gov/books/NBK21475/) and (c) from (Coluccio, 2008)

Best described myosin belong to classes I, II, V, VI and also XIV, especially important in apicomplexan parasites.

Myosin I is an unconventional myosin with a single head molecular motor due to lack of heptapeptide motifs responsible for coiled-coil association in other myosins. The neck domain of myosin I of *Dictyostelium* and *Acanthamoeba* associates with one or two light chain subunits, whereas in vertebrate cell it contains one to six IQ motifs. The tail domain is relatively short containing TH1 (tail homology 1) domains responsible for membrane binding. Others also contain TH2 domains with are enriched with glycine, proline and alanine or glutamine residues, and may contribute to an ATP-insentive actin-binding site that is believed to serve in anchoring the motor to one actin filament so that it can be moved past another actin filament. Others again contain a *src* homology (SH3 or TH3) domain that is found in several membrane cytoskeletal proteins. These myosin exhibit an ATP-independent actin binding site (Coluccio, 2008; Sellers, 1999).

Myosin II is a conventional myosin. Members of the myosin II class are numerous and well-studied. Myosin II is a hexameric polypeptide that is formed of two heavy chains which contain the actin and nucleotide binding sites, two light chains and two regulatory light chains. Myosin II binds to actin filaments for a short period only. The two heads appear to act independently at the N-terminus which contains the actin and nucleotide binding site. At the C-terminus of two heavy chains, between the two globular head regions and highly elongated coiled-coil α-helical rod lies the binding site for two light chains. Each head is associated with an essential and a regulatory type light chain. The tail region is long and contains α-helical coiled-coil regions that self-assemble and form a variety of filament structures such as in skeletal myosin (Coluccio, 2008; Sellers, 1999).

Myosin V consists of two heavy chains which dimerise via their coiled-coil regions in their tails. The neck domain is extended comparable to that of myosin II and contains six IQ motifs. This allows the association with multiple calmodulins and specific light chains. Myosin V is a cargo-transporting molecule which walks processively along actin filaments in a hand-over-hand mechanism. The dimer is functionally essential and the two heads interact strongly through actin binding. The long range movement occurs outwards towards the plasma membrane and is tightly associated with the short-range

movement of endocytic vesicles achieved via myosin VI (Coluccio, 2008; Sellers, 1999).

Myosin VI is an unusual myosin because it moves backwards toward the minus end of the actin filament. It can be found in distinct locations and is implicated in a wide range of processes such as endocytosis, exocytosis, and maintenance of Golgi morphology and cell migration. The head domain contains a unique insertion of 25 residues which can be found within a surface loop within the 50kDa domain (Kellerman and Miller, 1992). In addition, myosin VI has 50 amino acid inserted N-terminal to the single IQ domain, which is a characterising feature for this class of myosins. The tail domain consists of a short 200 amino acid sequence and is predicted to form coiled-coil structures. (Coluccio, 2008; Sellers, 1999).

Myosin XIV is found only in *Apicomplexa* and ciliates. Myosin XIV appears to have evolved from myosin I in the alveolate protist lineage. The appearance of myosin XIV was coincident with the disappearances of myosin I from alveolates, in accordance with the myosin family tree by Hodge and Cope (2000). Myosin XIV was grouped into a separate class although there is a similarity in the head domain between myosin I and myosin XIV (Thompson and Langford, 2002). The class XIV myosins have been described in ciliates and in *Theileiria, Toxoplasma*, *Plasmodium*, *Cryptosporidium* and *Eimeria*. In *P. falciparum* six class XIV myosins can be distinguished named PfmyoA to F (Chaparro-Olaya et al., 2003; Vale, 2003). PfmyoA was first identified (Pinder et al., 1998) before identification of PfmyoB, PfmyoC and PfmyoD orthologues in *T. gondii* (Heintzelman and Schwartzman, 2001; Hettmann et al., 2000). Recently PfmyoE and F have been described following on from the *P. falciparum* genome project (Chaparro-Olaya et al., 2005; Gardner et al., 2002). Relative transcript abundance of these six myosins was analysed in blood stage parasites and showed that MyoA, MyoB, MyoE and MyoF (currently known as MyoK) are maximally expressed in schizont stages to approximately equal levels (Chaparro-Olaya et al., 2005). *Apicomplexan* myosins were further divided into two subclasses called XIVa and XIVb (Chaparro-Olaya et al., 2005), and even more recently ino four subclasses (Foth et al., 2006). Reclassification of the subclasses resulted from a 'Naming Convention of *Apicomplexan* Myosins' to aid consistency between species. A systematic naming was proposed so that the same letter denotes homologous myosins across taxa. The naming system was based on homology to *T. gondii* myosins since *T. gondii* has the largest

identified myosin repertoire (11 myosins) of any *Apicomplexan.* (Heintzelman and Schwartzman, 1997, 2001; Hettmann et al., 2000). Thus the previously named PfMyoC, PfMyoD and PfMyoE of *Plasmodium* were changed to PfMyoF (~240kDa), PfMyoJ and PfMyoK respectively. MyoB of *Babesia* and *Theileria* was changed to MyoH. During this reclassification, MyoH was regrouped into a new subclass XIVc. The existing 12 ciliate myosins were grouped into subclass XIVd.

Phylogenic comparisons that include *P. falciparum* myosins are difficult due to the A/T rich genome and the insertion of low sequence complexity regions. As a result some *P. falciparum* myosins appear on long branches of the phylogenic tree and are therefore difficult to classify. Consequently, three *P. falciparum* myosins (PfMyoC, PfMyoD and PfMyoF) were excluded from class XIV leaving three sequences in class XIV, of which PfMyoA is segregated in subclass XIVa (~93kDa), together with MyoA from *T. gondii* (TgMyoA), *P. berghei* (PbMyoA), *B. bovis* (BbMyoA) and *C. parvum* (CpMyoA), whereas PfMyoB (~93kDa) and PfMyoE do not unambiguously cluster with other sequences (Foth et al., 2006). MyoA had been described in other Apicomplexan species showing 84% amino acid identity between *P. falciparum* and mouse malaria species *P. berghei* and *P. yoelii* and 62% identity with *T. gondii* (Matuschewski et al., 2001).

The MyoA function in both *Toxoplasma* and *Plasmodium* is important for gliding motility and host cell invasion by interacting with actin and forming a fast, plus-end-directed motor (Herm-Gotz et al., 2002). Only one *Plasmodium* myosin class XIV (PfMyoA) has so far been studied in detail. In *Toxoplasm*a, TgMyoA was implicated in cell invasion (Herm-Gotz et al., 2002; Meissner et al., 2002). MyoD with the apparent molecular weight of ~91kDa localises to the pellicle of tachyzoites and merozoites (Hettmann et al., 2000). Although MyoD is not essential for tachyzoite motility or propagation it might still be involved in motility in the bradyzoite stages of the parasite (Herm-Gotz et al., 2006; Hettmann et al., 2000). TgMyoB/C have been implicated in parasite cell division (Delbac et al., 2001) and there is speculation that myosins belonging to class XIVc are involved in mitosis, cytokinesis or other cell cycle events (Coluccio, 2008; Foth et al., 2006).

1.5 The inner membrane complex (IMC)

Apicomplexan parasites such as *Plasmodium*, *Toxoplasma*, *Cryptosporidium* and *Theileria* share unusual cytoskeletal elements that provide a structural framework for the cell. The motile stages are surrounded by the pellicle, a three-layered structure composed of the plasma membrane and the inner and outer membrane of the inner membrane complex (IMC). The IMC is formed by one or several flattened vesicles underlying the plasma membrane (Morrissette et al., 1997). A group of 2 or 3 microtubules arranged in parallel run from the third polar ring or MTOC, to the merozoite's posterior, underlying the IMC. This structure is known as the *P. falciparum* merozoite assemblage of subpellicular microtubules (f-MAST) and is thought to act as a directional guide, indicating the apical polarity and facilitating a cortical flow of F-actin over myosin (Fowler et al., 2001). The IMC provides stability and shape to the zoite (Aikawa et al., 1981; Tremp and Dessens, 2011; Tremp et al., 2008), as well as functioning as a scaffold for organellogenesis and cytokinesis (Nishi et al., 2008). The IMC also supports the glideosome apparatus that is required for gliding motility and host cell invasion (Gaskins et al., 2004). Deletion of genes for protein components of the IMC such as IMC1 in *Toxoplasma* (TgIMC1), or IMC1a and IMC1b in ookinetes and sporozoites of *P. berghei*, caused altered stability and rigidity of the daughter cell subpellicular network, an abnormal cell shape, reduced speed of motility, decreased mechanical resistance and reduced infectivity (Khater et al., 2004; Mann et al., 2002).

1.6 Acto-myosin motor complex in *Apicomplexa*

In *Apicomplexa* generally, the invasive stages use substrate-dependant motility to invade the host with an invasion machinery powered by an acto-myosin motor known as the glideosome complex (Opitz and Soldati, 2002). This was established clearly by the use of drugs that interfere with actin dynamics such as cytochalasin D, jasplakinolide and latrunculin B as well as myosin ATPase function modulators such as BDM (2,3–butanedione monoxine) which block invasion (Dobrowolski and Sibley, 1996; Matuschewski et al., 2001; Siden-Kiamos et al., 2006a; Wetzel et al., 2003). The gliding motility of *Toxoplasma* and *Plasmodium* and movement during cell invasion is critically dependent on actin polymerization and is powered by a myosin motor (MyoA), which is ubiquitously conserved across the phylum (Baum et al., 2006a; Baum

et al., 2006b). TgMyoA together with the myosin light chain (TgMLC1) and the integral membrane glycoprotein GAP50 (glideosome associated protein 50), which anchors the motor firmly in the IMC, and the lipid modified GAP45 (glideosome associate protein 45) forms the motor in *T. gondii*. Orthologous proteins have been identified in *Plasmodium* with PfMyoA, PfMTIP (Pf myosin tail domain interacting protein), PfGAP45 and PfGAP50, which are conserved across the genus (Gaskins et al., 2004).

It is believed that for gliding motility to occur, the MyoA motor complex somehow needs to be firmly anchored to the IMC/subpellicular microtubule cytoskeleton of the parasite, while actin is firmly attached to a solid substrate outside of the cell via an adhesive protein such as TRAP or MTRAP. It has been established that aldolase, a tetrameric glycolytic enzyme, offers a bridge between the acto-myosin motor and the host receptor-ligand complex (Buscaglia et al., 2003; Jewett and Sibley, 2003). This glycolytic enzyme is unexpectedly able to bind to both the C-terminal domain of a transmembranous adhesin and to parasite actin filaments (Baum et al., 2008a; Bosch et al., 2007a; Buscaglia et al., 2003; Uchime et al., 2012). Adhesin molecules which are able to bind using their cytoplasmic tails to connect via aldolase to actin are TgMIC2, a member of the TRAP family; TRAP and TRAP-like protein (TLP) in *Plasmodium* sporozoites; CSP and TRAP related protein (CTRP) in *Plasmodium* ookinetes, and MTRAP in merozoites. This model of motility requires the posterior translocation of the F-actin-aldolase complex which is bound to the adhesion protein, moving along the myosin track which is firmly anchored in the IMC. This process is able to generate the force required for the parasite to move forward. This chain of interacting components of TRAP/MTRAP-aldolase-actin-MyoA-MLC/MTIP-GAP45-GAP50 together forms the motor complex.

1.6.1 Plasmodium falciparum myosin A (PfMyoA)

PfMyoA like TgMyoA (~90-93kDa, 818 amino acids) is a single headed myosin with no definitive neck region and a very short tail. TgMyoA has 63% identity to chicken skeletal muscle myosin II (Ckn myosin II) with 64% identity in the head alone and 32% identity in the tail region. MyoA is peripherally located and shows a concentration towards the parasite apex. MyoA is expressed in schizonts but not detected in ring stages (Chaparro-Olaya et al., 2005; Foth et al., 2006; Pinder et al.,

1998). MyoA was also identified in sporozoites and merozoites of *P. berghei* (PbMyoA) and *P. yoelii* (PyMyoA) (Matuschewski et al., 2001). MyoA is also present in ookinetes where is essential for motility (Siden-Kiamos et al., 2011). PfMyoA consist of a conserved motor and light chain binding region. The head region displays conserved ATP and actin binding sites with which MyoA generates force upon attachment to an actin filament. MyoA binds to actin and is released from actin in an ATP-dependent manner. In comparison to the head region of Ckn myosin II, PfMyoA shows the least conservation in the loop-2 (less charge) and loop-3 (similar charge) regions with the other elements well conserved (Figure 1.9). In the relay-helix (SH-1) and the converter there is less identity with Ckn myosin II. In Ckn myosin II, the "fulcrum point" (a region that undergoes conformational changes upon actin-myosin-ATP interaction, which lead to lever arm movements for the power stroke (Liang and Spudich, 1998) is where the conserved glycine is replaced by a serine residue (S^{690} in PfMyoA). However, the glycine at the end of the SH-1 helix is conserved in both TgMyoA and PfMyoA (G^{710} and G^{701} in Ckn myosin II and PfMyoA respectively). This residue is believed to allow rotational movement of the converter of PfMyoA (Figure 1.10) (Farrow et al., 2011). Normally, in other myosins, the neck region contains a variable number of IQ motifs, which bind to the EF-hands of calmodulin-like light chains which serve to strengthen and extend the myosin lever arm. In Ckn myosin II this region binds to two light chains known as "essential" and "regulatory" light chain.

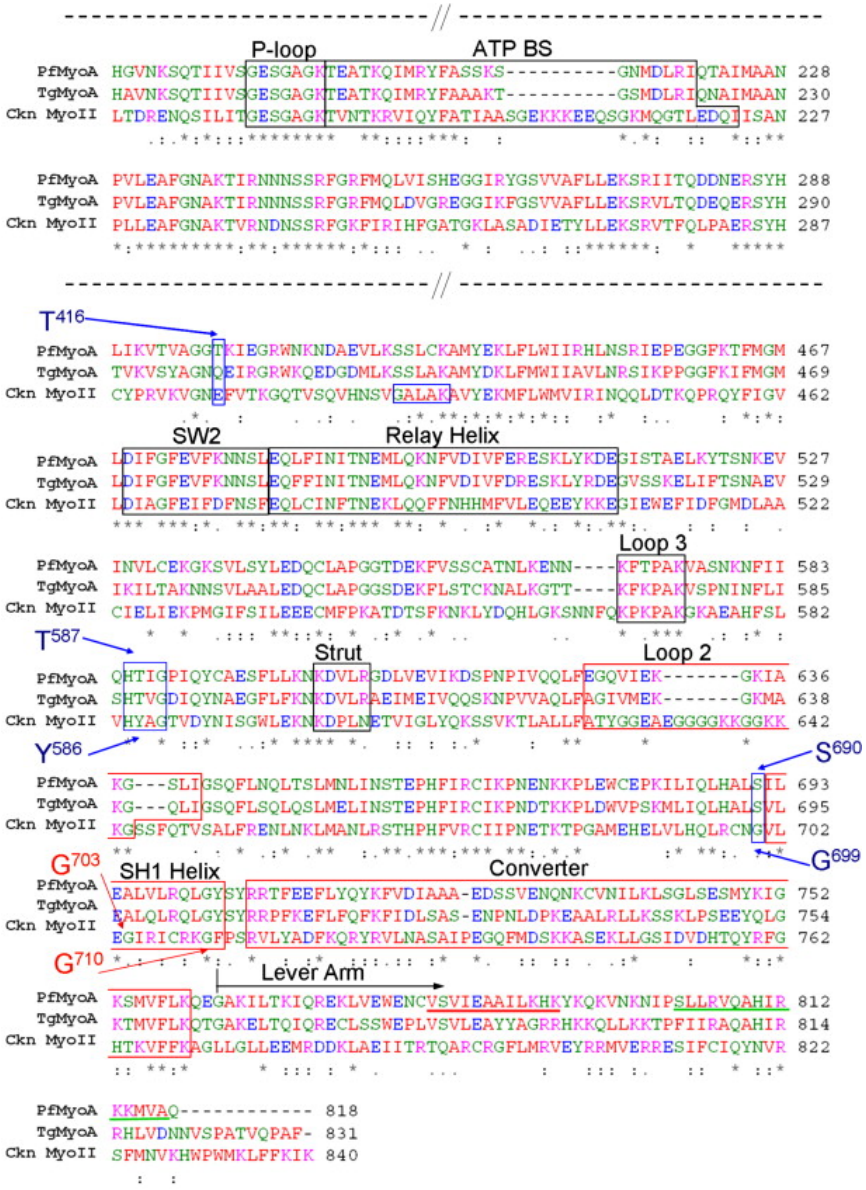

Figure 1.9: Clustal alignment of amino acid sequences of PfMyoA, TgMyoA compared to Chicken muscle myosin II (Ckn myoII). This alignment shows the similarities between PfMyoA, TgMyoA and the less similar Ckn MyoII. The black boxes highlight relatively well conserved regions, while poorly conserved regions are boxed in red. The individual substitution of amino acid was highlighted in blue letters. Residues which are involved in binding to the light chain (MTIP) are underlined in green. A possible degenerate putative IQ motif upstream of the MTIP binding motif is underlined in red. TEDS site, the fulcrum point boxed in blue. The conserved glycine (G699) at the fulcrum point is replaced by serine (S690) in *P. falciparum* (Farrow et al., 2011).

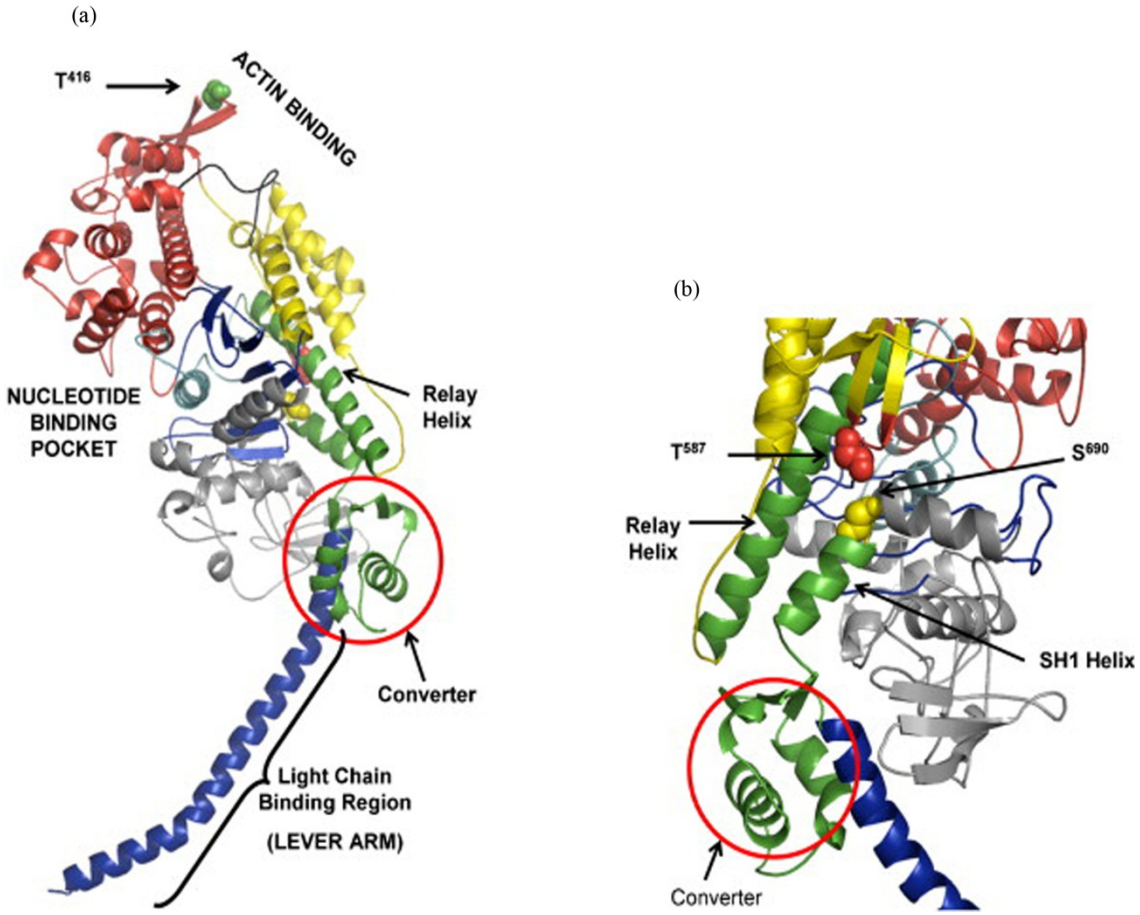

Figure 1.10: Putative protein structure of *Plasmodium falciparum* Myosin A (ribbon diagram). (a) shows the U50K domain (red); L50K domain (yellow); N-terminal domain (grey); central β-sheet (blue); the SH1 helix and rely helix and converter (in green); lever arm (blue); actin binding loop (black). TEDS site (T416-green); T587 of the HTIG sequence (red) and pivotal S690 (yellow spheres). **(b)** the highly conserved glycine (at the end of SH1 helix) is replaced with a serine (S690) in PfMyoA (Farrow et al., 2011).

1.6.2 Interaction of MyoA with its myosin light chain, MTIP

All class XIV myosins are short motor molecules that contain a neck region divergent from other myosins and lack a true, elongated tail domain. The function of the myosin motor can either be modulated by phosphorylation of the myosin heavy chain (MHC), such as at the TEDS rule site, or via the interaction with the myosin light chain (MLC). Normally the TEDS rule site is found in a region of the myosin head which contains a consensus site for Ser/Thr phosphorylation and makes significant contact with actin, so that this interaction can be altered by increasing/decreasing the negative charge. MyoA has been shown to be phosphorylated by CDPK1 and PKA (Lasonder et al., 2012). The TEDS site rule has been deduced from the tendency of many myosins to carry a phosphorylatable residue or an acidic residue (T, E, D, S) at position 16 upstream of the conserved sequence element DALAK. This sequence element however is only partially conserved in MyoA molecules. Some myosins do not adhere to the TEDS rule and it has been proposed that their interaction with actin is regulated differently. MyoA shows unusual features, and therefore it has been a challenge to predict the potential mode of regulation for these molecules. MyoA does not follow the TEDS rule and rather is regulated by MLC1/MTIP which bind to an unusual binding site in the short neck domain, which is devoid of IQ motifs (consensus IQXXXRGXXXR) (Bement and Mooseker, 1995; Foth et al., 2006).

TgMyoA is not directly bound to the IMC but connects to it through MLC. The extreme C-terminus of TgMyoA is important for its peripheral localization. More precisely it is a dibasic motif of two arginines which might be part of a divergent IQ motif (known as 'degenerate' IQ (IQXXXRGXXXR/K) due to the fact that it does not fully conform to the usual IQ motif (Herm-Gotz et al., 2002; Hettmann et al., 2000)), that contributes to the association with TgMLC1/MTIP and via this with the IMC (Bergman et al., 2003; Herm-Gotz et al., 2002; Hettmann et al., 2000; Jones et al., 2006). MLC1 and MTIP contain four degenerate EF-hands missing the canonical calcium-binding motif (Herm-Gotz et al., 2002), and the interaction with MyoA appears to be calcium- independent (Bosch et al., 2006; Green et al., 2006b). Therefore both TgMLC1 and MTIP resemble an atypical EF-hand in which the Ca^{2+} binding site residues are not conserved. The MyoA binds to MTIP via a short, 15 aa sequence and removal of these residues eliminates the MyoA-MTIP interaction. In *Plasmodium*, double or single substitutions of R and K residues in the divergent IQ motif completely

abolish the PfMyoA interaction with PfMTIP (Jones et al., 2006). In addition Bosch et al., (2006, 2007), showed that overall correct conformation of MTIP is important for the interaction between the MTIP C-terminus and the 15 amino acid region in the MyoA-tail.

Phosphorylation occurs at S107 and/or S108 of PfMTIP *in vivo* and mutations at those sites weakens the affinity of MTIP for the C-terminal tail of MyoA. This disruption is likely to have a significant impact on MyoA since the localization to the IMC is dependent of the interaction with MTIP (Douse et al., 2012). The N-terminus of the MTIP homologue, TgMLC1 has been shown to be involved in the interaction with GAP45 (Frenal et al., 2010). A conditional knockout of TgMyoA using a tetracyclin-inducible gene expression system showed that MyoA is important for parasite gliding motility, host cell invasion and egress (Meissner et al., 2002). Since the MyoA-MTIP/MLC1 interaction is important for parasite invasion, any disruption is expected to prevent a continuous parasite life cycle. Thus this interaction could be a good target for anti-malarial compound development. However more recently, using the DiCre system to produce a conditional knockout it was shown that MyoA is not essential for parasite survival, and moreover, the localization of other glideosome proteins (such as MLC and GAP45) is not affected by deletion of MyoA, suggesting the present of a MyoA-independent invasion mechanism (Andenmatten et al., 2013).

1.6.3 The glideosome associated proteins (GAPs)

TgMyoA has been shown to be associated with the IMC as part of a hetero-oligomeric complex termed the glideosome. TgMyoA binds via MLC1 to TgGAP45 and TgGAP50. The pre-complex of MyoA-MLC-GAP45 is anchored to the IMC through association with GAP50, the IMC integral glycoprotein and through acylation of GAP45 (Gaskins et al., 2004; Rees-Channer et al., 2006). At the N-terminus of GAP45 is a predicted myristoylation and palmitoylation site (Rees-Channer et al., 2006), and another two palmitoylation sites were identified at the C-terminus (Frenal et al., 2010). The N-terminus of GAP45 is anchored to the PM (by acylation) and the C-terminus is anchored to the IMC via acylation and protein interactions (Frenal et al., 2010; Ridzuan et al., 2012). The glideosome complex assembles in two steps: MyoA, MLC1 and GAP45 assemble co-translationally prior to transport to the parasite

periphery and then bind to GAP50 which is anchored in the IMC. The complex is also conserved in *Plasmodium* where the assembly occurs in the same manner (Baum et al., 2006b). GAP50 initially is targeted to the secretory pathway by its signal peptide and following insertion into the ER GAP50 is transported to the IMC. MyoA lacks a signal peptide and is translated on ribosomes in the cell cytoplasm before associating with MTIP and GAP45 (Fauquenoy et al., 2011). GAP50 firmly immobilises MyoA in the IMC. GAP50 itself is immobilised within cholesterol rich detergent resistant domains of the IMC not allowing free diffusion and therefore anchoring the whole glideosome within the IMC (Johnson et al., 2007). The current model is that the bulk of GAP50 is located in the lumen of the IMC and binding to other motor complex components occurs via its C-terminal helix extension (Bosch et al., 2012) (Daher and Soldati-Favre, 2009). During early stages of parasite development, GAP50 is localized in the ER but gets redistributed to the apical cap during the formation of daughter cells. Following this GAP50 is incorporated into the IMC and found throughout the parasite development (Yeoman et al., 2011).

Other glideosome associated proteins belong to the GAPM family. These are proteins which contain six-pass transmembrane domains, which are highly conserved in *Plasmodium* and *Toxoplasma*, localize to the IMC and co-purify with cytoskeletal alveolin proteins. GAPMs can also associate with the actomyosin motor in pull down experiments and are suggested to have a role in IMC-anchoring to the cytoskeleton (Bullen et al., 2009). GAP40 is the most recent GAP identified as part of the glideosome motor complex. This protein is a polytopic IMC protein, conserved across the *Apicomplexa* phylum, and believed to play a role as an anchorage protein together with GAP50, although the actual function remains to be investigated (Frenal et al., 2010).

1.6.4 MyoA-actin interrelationship

MyoA involvement in binding to parasite actin and generating motility was suggested as early as the 1970s and 1980s (King, 1988; Vanderberg, 1974). Myosin A haa been described in ookinetes (Siden-Kiamos et al., 2011; Siden-Kiamos et al., 2012; Siden-Kiamos et al., 2006b), sporozoites (Bergman et al., 2003; Matuschewski et al., 2001; Matuschewski et al., 2002) and merozoites (Pinder et al., 1998) and was localized

to an area between the IMC and parasite PM towards the apex (Pinder et al., 2000). Despite a clear contribution of the actomyosin system to gliding and invasion, parasite actin filaments have never been seen formally in the vicinity of the glideosome. In *Toxoplasma* and *Cryptosporidium*, actin is represented by a single gene, whereas in *Plasmodium* two genes are present. Pf-actinI is transcribed in both asexual and sexual stages, whereas Pf-actinII is only transcribed in sexual stages (Dobrowolski et al., 1997b; Wesseling et al., 1988; Wesseling et al., 1989). Actin has a predicted molecular weight of 42-44 kDa. Actin can exist in two forms, globular or monomeric actin (G actin) and filamentous actin (F-actin). The monomeric form can polymerise in a 'head-to-tail' fashion into a right-handed helical spiral. The assembly of monomeric actin usually involves polymerisation into F-actin with addition of monomeric actin onto the 'barbed' (or plus) end and depolymerizes from the 'pointed' (minus) end (Dobrowolski et al., 1997a; Dobrowolski et al., 1997b). *P. falciparum* actin either directly extracted from parasites or produced in heterologous systems displays atypical biochemical properties by forming remarkably short filaments (~100nm in length) that are less stable than those formed by conventional actin (Schmitz et al., 2005). This suggests that filamentous actin is found only for short periods and in the precise locations where it is needed for motility such as areas close to the MJ (Holder and Veigel, 2009). The indication that this is actually the case has been provided by using a *Plasmodium* specific actin antibody, although this antibody does not differentiate between G- and F-actin (Angrisano et al., 2012).

Both actin dynamics and microfilament turnover are suggested to arise from an interaction with actin binding partners. Actin polymerization/ depolymerization may be controlled by intrinsic structural features but also by stabilizing and destabilizing actin associated regulatory proteins. Short actin filaments seem to be nucleated by a yet unknown nucleator from a pool of G-actin sequestered in the cytosol. In other eukaryotes, the ARP2/3 complex nucleates the polymerization of F-actin but *Apicomplexa* lack ARP2/3 and instead use formin to regulate actin polymerization (Angrisano et al., 2012; Baum et al., 2006a). *P. falciparum* formin 1 (PfFormin-1) (Baum et al., 2008b; Holder and Veigel, 2009) and PfFormin-2 (Farrow et al., 2011) localise beneath the parasite plasma membrane and are concentrated towards the parasite apex.

The gliding motility or invasion can be disrupt by certain drugs which interfere with either actin dynamics such as cytochalasin D (CytD), jasplakinolide (JAS), and latrunculin B or interfere with myosin ATPase function such as 2,3-butanedione monoxime (BDM) (Dobrowolski et al., 1997a; Poupel and Tardieux, 1999; Russell and Sinden, 1981; Shaw and Tilney, 1999; Siden-Kiamos et al., 2006b; Wetzel et al., 2003). This was demonstrated by using *T. gondii* mutant lines which are resistant to CytD, which showed that host cell invasion by *T. gondii* tachyzoites was dependent on the polymerization of the parasite actin but not that of the host cell (Dobrowolski and Sibley, 1996). The gliding motility can be blocked by CytD, however the attachment of the parasite to the host cell was unaltered (Dobrowolski and Sibley, 1996; Wetzel et al., 2005). Recently the involvement of host cell actin in invasion was demonstrated. In *T. gondii* tachyzoites and *P. berghei* sporozoites host cell actin participated during parasite invasion by inducing the formation of a ring shaped F-actin structure in the host cell underneath the MJ which remained stable during the invasion process (Gonzalez et al., 2009).

MyoA binds to actin in an ATP-dependent manner. According to the current model of Apicomplexan invasion, myosin grabs onto F-actin filaments and exerts ATP-dependent power strokes which are transmitted via aldolase to parasite ligand-host cell receptor complexes resulting in movement of those to the posterior end of the parasite (Hettmann et al., 2000). PfMyoA moves actin filaments at a speed of 33.3 µm/s and produces short lived working strokes of 5 nm as determined by *in vitro* motility assays and single molecule optical trapping methods. The mechanism of how force is generated (the power stroke) in the myosin actin model by association and disassociation of the myosin head from the filamentous actin has been widely described. In the absence of ATP, the myosin head is firmly attached to the actin filament. Although this state is very short-lived in living muscle, it is this state which is responsible for muscle stiffness after death (rigor mortis). On binding ATP, the myosin head releases from the actin filament. The head hydrolyses ATP to ADP and Pi which induces a rotation in the head with respect to the neck. This ‘cocked state’ stores the energy released by the ATP hydrolysis as elastic energy, similar to a stretched spring. Myosin in the ‘cocked state' binds actin. When bound to actin the myosin head couples the release of Pi with the release of the elastic energy to move the actin filament. This is known as the ‘power stroke’ as it involves moving the actin filament with respect to

the end of the myosin neck domain. The head remains tightly bound to the filament as ADP is released (Cooke, 2004; Vale, 2003) (Figure 1.11).

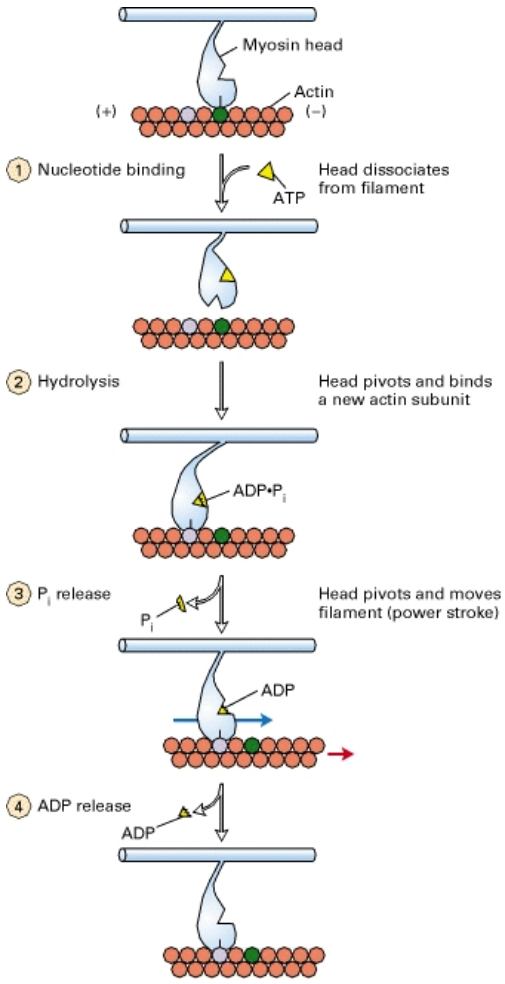

Figure 1.11: The power stroke during gliding motility. During the "rigor state", myosin binds tightly to actin (with no bound nucleotide). (1) Upon ATP binding, the cleft of the ATP binding site "opens" which causes the disruption of the actin-binding site; the interaction becomes weakened releasing the myosin head from the actin filament. (2) Freed of actin the myosin head hydrolyses ATP to ADP+Pi (phosphate). Hydrolysing ATP causes a conformational change in the head. The neck "cocks" and moves to a new position, closer to the (+) end of the actin filament and rebounds the actin filament. (3) Pi dissociates from the ATP binding pocket, the myosin head undergoes the second conformational change, coming into "rigor state" and producing the "power stroke" causing myosin to move the actin filament forward. (4) Myosin head

remains tightly bound to actin as ADP is released. When fresh ATP binds to the binding pocket within the head domain the process continues (Lodish H, Berk A, Zipursky SL, et al. Molecular Cell Biology. 4th edition. New York: W. H. Freeman; 2000. Available from: http://www.ncbi.nlm.nih.gov/books/NBK21475/).

The current model of the acto-myosin motor complex (Figure 1.12) was used as a starting point in this present studies to further investigated the acto-myosin motor complex in *Plasmodium*.

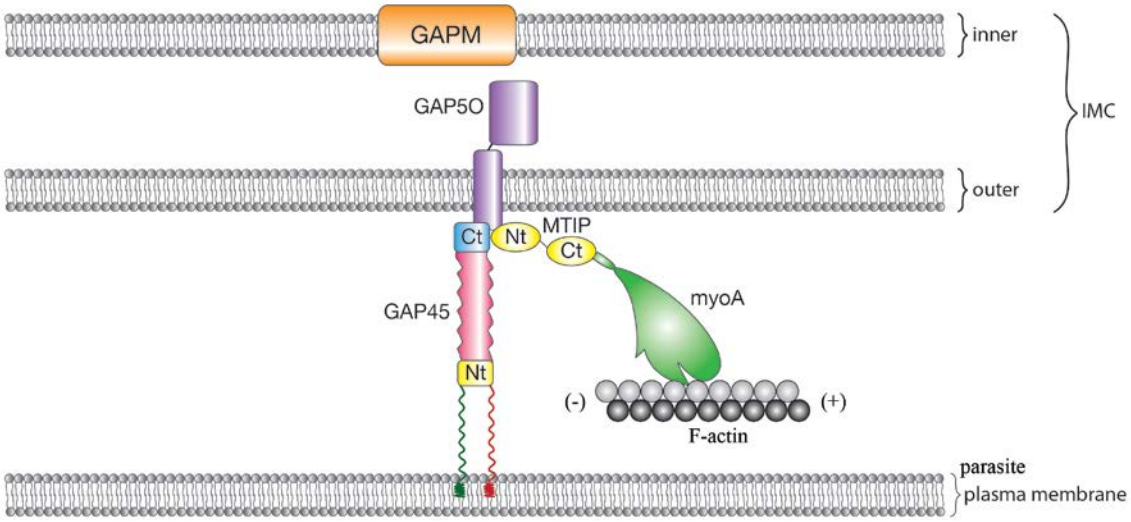

Figure 1.12: Schematic diagram of acto-myosin motor complex. MyoA is linked to the IMC via glideosome associated protein GAP45 (acylated), GAP50 (transmembrane protein) as well as myosin tail domain interacting protein (MTIP). GAPM is a transmembrane protein which is highly conserved and specific to Apicomplexa. The myosin head moves the actin filament from the (+) end towards the (-) end. G-actin is polymerized by formin/profilin. The force generated by the hydrolysis of ATP in the myosin head associates and dissociates the myosin from the actin filament resulting in the forward movement of the parasite into the erythrocyte. Nt; N-terminal; Ct: C-terminal. F-actin (black shape)

1.7 Apicomplexan Myosin B

MyoB like MyoA is classified as a class XIV myosin. As mentioned briefly in section 1.6, MyoB belongs to subclass b of the myosin XIV class (Foth et al., 2006). In *Toxoplasma*, TgMyoB/C arre encoded by one gene and different transcripts are generated by alternative splicing resulting in different C-termini in the proteins. Although both *T. gondii* MyoB and MyoC showed distinct cellular localisation with MyoB spreading throughout the cytoplasm with concentrated punctuate structures and MyoC mostly concentrated at the posterior and weakly at the anterior pole, both myosins have been implicated in parasite cell division (Delbac et al., 2001). In *Plasmodium*, PfMyoB is the smallest myosin in class XIV (88kDa: 801 residues). PfMyoB has been shown to be expressed in mature schizonts and merozoites by RT-PCR, immunobloting and IFA from different stages of the *P. falciparum* parasite (Chaparro-Olaya et al., 2003; Chaparro-Olaya et al., 2005) The hypothesis that PfMyoB might be involved in invasion-related mechanisms was based on the imaging data of MyoB which detected this protein only in late stages of the asexual development and at the merozoite apex (Chaparro-Olaya et al., 2003; Chaparro-Olaya et al., 2005). MyoA and MyoB are also detected in *P. berghei*. PbMyoA was detected in mature ookinetes, whilst PbMyoB was detected in mixed blood stages (containing mostly gametocytes and schizonts), zygotes and mature ookinetes by Western blotting probed with an anti-PfMyoB antiserum, and it shows a punctuated pattern of expression around the entire cell periphery by IFA (Siden-Kiamos et al., 2006b).

1.9 Aims of this thesis

MyoA in Apicomplexan parasites is a well studied molecule and it has been previously shown to be involved in powering the gliding motility of parasites which is important for host cell invasion. Constructing the motor complex is dependent on the association of MyoA with an actin filament, the myosin light chain and the glideosome associated proteins. Even though MyoA has been biochemically characterized and plays a key role in powering invasion (Pinder et al., 2000; Pinder et al., 1998), detailed studies on MyoB which is considered to be structurally similar to MyoA are lacking. In this study we aim to address the following:

i) ***In vitro assembly of the* P. falciparum *motor complex.*** Using the wheat germ cell free system attempts will be made to express and assemble MyoA, MTIP and GAP45 into a complex *in vitro* in order to examine in detail the protein-protein interactions between these molecules. Reconstituition of the invasion motor *in vitro* will also allow functional, biophysical studies of the complex, some of which previously were only attempted with parasite lysate. Compared to that from parasite lysate, MyoA produced with this system can be considered free from other protein components that exist together in the parasite and therefore will give us the oppportuity to work with MyoA molecules alone in order to clarify their function.

ii) ***Study of MyoA* in vivo.** This study will attempt to produce a transgenic MyoA-GFP parasite line by insertion of *gfp* at the C-terminus of the endogenous *MyoA* locus. Although the localisation and timing of protein expression of MyoA can be predicted as it has been examined in many previous studies, GFP-tagging will allow us to follow MyoA throughout the life cycle in real time. Using the transgenic parasite detailed characterisation of protein partners in the motor complex such as the newly characterised GAP40 (in *T. gondii*) and GAPMs, and potential novel candidates will be attempted. Overall, a transgenic parasite would allow a better understanding of the motor complex in space and time and especially during the process of invasion.

iii) ***Characterisation of MyoB and its cellular function***. An identical approach as that described for MyoA to GFP-tag MyoB by targetting the endogenous PfMyoB locus will be attempted. This part of the thesis will be directed to studying MyoB timing of protein expression, localisation and interactions with other proteins in order to predict a role and function for MyoB. As for MyoA, efforts will be made to visualise MyoB-GFP during the process of invasion.

iv) ***Characterisation of MyoA and MyoB in other Plasmodium species***. The generation of transgenic MyoA-GFP and MyoB-GFP *P. knowlesi* parasites was attempted. *P. knowlesi* has merozoites which are significantly larger than *P. falciparum* and also viable for longer once released. The aim was to generate transgenic parasites to study real time invasion in this fifth human malaria parasite.

Chapter 2

Material and Methods

2.1 DNA manipulation and transformation

2.1.1 Oligonucleotides

Oligonucleotides were purchased from Sigma-Aldrich Company Ltd and used in the *in vitro* expression system (Table 2.1) and to prepare DNA constructs for transfection (Table 2.2).

2.1.2 Polymerase Chain Reaction (PCR)

DNA was amplified from plasmid DNA using high fidelity AccuPrime™ *Pfx* DNA polymerase. The reactions consisted of 50 - 200 ng DNA templates, 2 - 4 mM dNTPs, 0.1 - 0.3 µM each oligonucleotide, 10 mM $MgSO_4$, 1.0 - 2.5 units of polymerase and polymerase buffer (supplied by manufacturer) diluted in dH_20 to a final volume of 50 µl. The PCR reactions were performed in a DNA engine® thermocycler (Eppendorf). Amplified DNA was purified using a QIAquick PCR purification kit (Qiagen) according to the manufacturer's instructions.

2.1.3 Agarose gel electrophoresis

DNA fragments were analysed using 0.8 - 1.0% agarose gel electrophoresis. Agarose gel was prepared by dissolving agarose powder (BioRad) in 1X TAE buffer (45 mM Tris-acetate [pH 8.0], 1 mM EDTA). For UV detection, 0.5 µg/ml ethidum bromide or the same concentration of GelRed (Life Technologies) was added before pouring the agarose into the gel cast. Once cooled, gels were immersed in 1X TAE and DNA samples were mixed with 1X DNA loading dye (QIAGEN) before loading into wells. Separation was conducted at 80-100V using an EPS 500/400 DC Power Supply (Pharmacia). Hyperladder™ I (Bioline) DNA size markers were included for reference. If required, DNA was purified from gel pieces using a gel extraction kit (Qiagen) according to manufacturer's instructions.

2.1.4 Restriction endonuclease digestion

In a basic reaction, 1 µg DNA was digested for 2 h at 37°C, in reaction buffer supplied with the specific enzyme being used. All enzymes were purchased from New England Biolabs, 1 Unit being defined as the amount of enzyme required to digest 1 µg DNA in 1 h at 37°C, in a 50 µl reaction. Where more than one enzyme was used in any given reaction, buffers were chosen in order to retain optimal activity of both enzymes.

2.1.5 Ligation of DNA fragments

Where restriction digestion was used in cloning, the resulting cohesive ends were ligated using T4 DNA ligase (Promega). Reactions contained 200U enzyme, 50 ng vector DNA and a 3:1 molar excess of insert to vector DNA. Samples were incubated at 16°C overnight, in the supplied buffer. The vector which was subjected to ligation with the DNA fragment of interest was treated with alkaline phosphatase (AP) before electrophoresis and gel excision. Briefly, 5 µl each of 10X AP buffer and AP were added to digestion mixtures, incubated in the 37^{o}C incubator for 1 h, followed by 50^{o}C for 30 min and finally 75^{o}C for 10 min or treatment with 5 µl of 0.05 M EDTA. This mixture was then electrophoresed and bands were excised and purified. These vectors were then used for ligation with the selected purified DNA fragment.

2.1.6 The propagation and transformation of **E. coli** *by plasmid DNA*

Ligated DNA (1-2 µl or 50 ng) was added and mixed slowly into 25 - 50 µl chemically competent *E. coli* cells (GigaSingle: Novagen). The reaction was then incubated on ice for 5 min, heat shocked for exactly 30 sec in a 42^{o}C water-bath, followed by incubation on ice for another 2 min, then 250 µl SOC medium at room temperature was added and incubated for 1 h at 37°C with agitation at 250 rpm. About 30 - 50 µl of the transformed cells were then plated onto agar plates containing antibiotic for selection (100 µg/ml ampicillin) and incubated at 37°C overnight prior to positive colony picking. Colonies were picked and grown in LB culture containing 100 µg/ml ampicillin at 37°C with agitation at 225 - 250 rpm.

2.1.7 Isolation of plasmid DNA

Plasmid DNA was isolated from *E. coli* overnight cultures using either the QIAprep Spin Miniprep or QIAGEN Plasmid Midi/Maxi kits (Qiagen) following the protocols provided in the QIAGEN plasmid purification handbook. If the resulting DNA was to be used for transformation or sequencing, 2 - 5ml culture was sufficient and DNA was extracted using the Miniprep kit. For electroporation of *P. falciparum*, larger quantities of DNA were required and thus 250 ml cultures were grown and DNA extracted using the QIAGEN-tip 500 from the Maxiprep kit. All DNA was eluted and stored in elution buffer EB (10 mM Tris-HCL, pH 8.5).

2.1.8 Sequencing of DNA

Sequencing reactions were carried out by Cogenic (Beckman Coulter). Sequencing results were aligned and analysed using Sequencher 4.9 (Demo Version).

2.2 *In vitro* expression and purification of recombinant MyoA, MTIP and GAP45 protein

2.2.1 Construction of recombinant DNA

Recombinant plasmid DNA was generated for MyoA, MTIP and GAP45 using specific primers (Table 2.1) designed for the ENDEXT® Technology (CellFree Sciences), for use in their wheat germ cell free protein synthesis system. The recodonised template DNA for MyoA was provided by Rachel Farrow (Physical Biochemistry, NIMR), MTIP and GAP45 were from Rob Moon (Parasitology, NIMR). All vectors used were provided by CellFree Sciences Co., Ltd. (Japan). The DNA was amplified by PCR with a combination of primers 1A and 2A, 3M and 4M and 5G and 6G of MyoA, MTIP and GAP45 respectively. The amplified products were cloned into the multiple cloning site region of the vectors,which for example, had been cleaved between the XmaI and SpeI sites of the pEU-E01H-TEV-N2 (H-pEU) which introduced an N-terminal His-tag. Primer combinations of 7A and 8A, 9M and 10M, and 11G and 12G for MyoA, MTIP and GAP45 respectively, were used for amplification and the products were inserted between the EcoRV and NotI sites of pEU-E01G-TEV-N1 (G-N1) to produceN-terminal GST-tag constructs (Appendix A).

2.2.2. Transcription of DNA to mRNA

For one reaction of mRNA transcription, 2 µl of 1.0 µg/µl highly pure DNA **(**with A260/A280 ratio ranging between 1.7-1.85) were used in a reaction with Transcription Premix (11.5 µl Nuclease free water, 1 X transcription buffer, 2.5 mM NTP mix, 1 U/µl RNase inhibitor, 1 U/µl SP6 RNA Polymerase) in a total volume of 20 µl, mixed and incubated at 37^{o}C for 6 h. The quality of mRNA produced was monitored by gel electrophoresis; if RNase degradation was apparent, the plasmid DNA was further purified.

2.2.3 Translation of mRNA to protein

A Bilayer Reaction System method (CellFree Sciences) was used to translate mRNA into protein. mRNA (10 µl) was added to 10 µl of wheat germ extract (WEPRO® 1240) with 40 ng/µl Creatine Kinase (CK), then the mixture was mixed gently and carefully transferred directly to the bottom of 1 X SUB-AMIX solution (0.3 mM each of amino acids [L-Arg/ L-Asn/ L-Asp/ L-Cys/ L-Gln/ L-Glu/ L-Gly/ L-His/ L-Ile / L-Leu/ L-Lys/ L-Met/ L-Phe/ L-Pro/ L-Ser/ L-Thr/ L-Trp/ L-Tyr/ L-Val], 100 mM potassium acetate, 2.7 mM magnesium acetate, 16 mM disodium creatine phosphate tetrahydrate, 0.4 mM spermidine, 1.2 mM ATP, 0.25 mM GTP, 4 mM dithiothreitol, and 30 mM HEPES-KOH [pH 7.8]). This will form a bilayer phase with the translation mixture in the lower layer and 1 X SUB-AMIX in the upper layer. The translation process was incubated for 20 h at 15-16^{o}C. The expressed proteins were resolved by SDS-PAGE and detected by western blot.

2.2.4 Co-translation of proteins

Two or more proteins can be co-expressed using individually transcribed mRNA. The volume of mRNA used and translation mixtures were optimized so that the efficiency of protein translation was maximized. This co-expression was performed to get the best yield of protein in the soluble fraction for use in interaction studies. The resulting protein concentration was determined using a spectrophotometer (Nanodrop, ThermoScientific) with pre-programmed settings for protein absorbance at λ_{595}.

2.2.5 SDS-PAGE

Protein samples were separated using Sodium Dodecyl Sulphate- Polyacrylamide Gel Electrophoresis (SDS-PAGE) with Nu-PAGE® 10% or 12% pre-cast Bis-Tris gels and an Xcell II™ Mini Cell gel cassette (Invitrogen) in MOPS (Nu-PAGE® 3-[N-morpholino]-propanesulphonic acid) running buffer at 200 Volts (V) using an EPS 500/400 DC Power Supply (Pharmacia). Forty µl of 2X Laemmli sample buffer (100 mM Tris HCl [pH 6.8], 200 mM dithiothreitol [DTT], 4% sodium dodecyl sulphate [SDS], 20% glycerol, 0.2% bromophenol blue) were added to the samples and mixed, then the samples were boiled for 5 min. Precision Plus™ Protein standards (Biorad) were used as size markers. The separated proteins were visualised by staining with Coomassie blue (0.1% [w/v] Coomassie Brilliant Blue R-250, 45% [v/v] methanol, 10% [v/v] acetic acid), or by immunoblot.

2.2.6 Immunoblot

A resolved SDS-PAGE gel was transferred onto nitrocellulose membrane for 1-2 hours at 30V or overnight at 10V at room temperature. The nitrocellulose membranes (Whatman Protran) were immersed in blocking buffer (1% bovine serum albumin [BSA] in PBST) for 30 to 60 min at room temperature or overnight at 4^{o}C with constant slow agitation. The membrane was incubated in the appropriate primary antibody (Table 2.3) for 1 h and washed with PBST 3 times at 10 min intervals. The membrane was incubated with an appropriate secondary antibody for 1 h and washed as before. To visualise protein bands, the membranes were immersed in enhanced chemiluminescene substrate solution (ECL, GE Healthcare) for 1 - 2 min and the protein band signal was detected by exposing the blot to Biomax MR film (Kodak) for an appropriate amount of time before being developed using a Fuji FPM-3800 AD Film developer.

2.3 Pull down assay and co-immunoprecipitation assay

2.3.1 GST Pull Down for cell free protein

Soluble glutathione-S-transferase (GST) fusion protein was purified on glutathione-Sepharose 4B, prepared by washing in 10 volumes of PBS. The tubes were inverted several times to mix the resin before centrifugation at 5000 *g* for 5 min. Supernatants were discarded and washing steps were repeated twice. Soluble protein from the co-expression was added to 10 volumes of PBS and mixed with 1 volume of glutathione-sepharose 4B, under gentle agitation for 2 h at 4^{o}C. The samples were centrifuged for 5 min at 5000 *g*, the supernatant discarded and the gel washed 3 times with PBS. Protease inhibitors were added to the washed beads at an appropriate concentration, then the beads were suspended in SDS-PAGE sample buffer, boiled for 5 min and centrifuged before examination by SDS-PAGE and immunoblot.

2.3.2 His Pull Down for cell free protein

Ni-NTA His•Bind® Resin was washed twice with dilution buffer before binding in batch to the produced protein, rotating at 4°C for 2 h in the presence of 1X protease inhibitor cocktail (Roche). The mixture was then pelleted for 2 min at 2000 *g* and the supernatant was collected. The resin was washed with 500 µl dilution buffer twice and supernatants were collected for every wash. The purified protein was then eluted with 500 µl elution buffer, incubating for 5 min on ice, before centrifugation at 2000 *g* for 5 min. The samples were boiled in 2X SDS-PAGE sample buffer at 94^{o}C for 5 min, centrifuged, and then examined using SDS-PAGE and immunoblot.

2.3.3 Co-immunoprecipitation with GFP-TRAP system for parasite lysate

Purified schizonts were suspended in lysis buffer ([1:10 v/v]: 10 mM Tri-HCl [pH 7.5], 150 mM NaCl, 0.5 mM EDTA, 1% NP40, 1 mM PMSF [Sigma] and 1X protease inhibitor cocktail [Roche]). The mixture was placed on ice for 30 min with extensive mixing by pipetting every 10 min. The cell lysates were spun at 20,000 *g* for 10 min at 4^{o}C, then the supernatant was transferred to a precooled tube and the volume was adjusted to an appropriate volume with dilution buffer (lysis buffer without 1% NP40) GFP-Trap® beads (Chromotek) were washed with dilution buffer at 2700 *g* for 2 min at 4^{o}C. The supernatant was discarded and the washing step was repeated twice. The cell

lysate was incubated with non-coated agarose beads (bab-20, Chromotek) for 30 - 120 min at 4^{o}C with gentle mixing using a rotator to remove nonspecific binding proteins. The mixture was spun down at 2000 *g* for 2 min at 4^{o}C. The supernatant was added to the GFP-Trap® beads and incubated with gentle mixing for 1 to 2 h at 4^{o}C. The mixture was spun down at 2000 *g* for 2 min at 4^{o}C. The supernatant (non-bound materials) was kept for western blotting analysis. The remaining supernatant was discarded and the pellet was washed twice with dilution buffer and washing buffer respectively. The GFP-Trap® beads (30 µl) were re-suspended in 100 µl of 2X Laemmli sample buffer. The re-suspended beads were heated for 10 min at 95^{o}C to dissociate the immuno-complexes from the beads. The beads were collected by centrifugation at 2700 *g* for 2 min at 4^{o}C and SDS-PAGE was performed with the supernatant (referred to as bound material). The presence of GFP and motor proteins was detected by western blot using specific antibodies (Table 2.3).

2.4 The functional analysis of MyoA

2.4.1 In vitro motility assay

A flow cell was constructed from a microscope slide and 22 X 22 mm cover slip (Thermo Scientific). The principle of the flow cell was to allow the motility buffer to be changed by introducing fresh buffer at one end, and drawing it through with a filter paper. 10% nitrocellulose (Earnest F.Fullam) was diluted tenfold with amyl acetate (Sigma Aldrich) and 1 µl spread evenly onto the cover slip. Two pieces of double sided tape (permanent double sided tape, Scotch 3 M) were placed 5-10 mm apart upon a pre-cleaned slide (Super Frost plus, Menzel Glaser, Thermo Scientific) to create a flow cell of approximately 15 µl volumes.

The flow cell was coated with MyoA (15-30 µl) and incubated for 3 - 5 min to allow the MyoA to bind to the pre-coated nitrocellulose and washed three times with AB- (25 mM Imidazole, 25 mM KCl, 4 mM $MgCl_2$, 1 mM EGTA [pH 7.4]), A total of 100 µl AB-/BSA (AB-/ 1.0 mg/ml BSA) was added and allowed to bind for 2-5 min. This binds to the nitrocellulose non-specifically, blocking the surface where no protein has bound. A rabbit actin labeled with Rhodamine-Phaloidin (Molecular Probes Invitrogen,

Life Technologies) (RhPh-actin) was diluted in AB- to a final concentration of 0.6 µg/ml and 20 µl infused into the flow cell and left for 2-5 min to allow actin filaments to bind to the MyoA in the rigor state (MyoA head bound to actin filament). 100 µl AB-/Scavenger (0.02 mg/ml catalase, 0.1 mg/ml glucose oxidase, 3.0 mg/ml glucose, 20 mM DTT) was passed through the chamber of the flow cell to remove unbound actin. To check that actin was bound to the MyoA on the cover slip surface the slide was viewed under the Zeiss epi-fluorescent microscope (Axioskop 40, Zeiss). Motility was initiated by addition of a total of 100 µl AB+/Scavenger (AB+: [AB- / 2mM ATP].

Actin motility was recorded with a modified video camera (ICCD [Photon-P46036A, EEV] linked to a frame grabber [Picolo Tetra, Eurosys], developed by Gregory Mashanov, Physical Biochemistry, NIMR). The user interface GMimPicolo© Software (Gregory Mashanov) was used to collect data.

2.4.2 Single molecule studies

Optical trapping using Optical tweezers (OT) was developed to measure single forces and the displacement that can be recorded using a feedback-enhanced laser trap assay (Finer et al., 1995). The mechanical properties of individual myosin molecules were studied using the three bead assay developed by Spudich and co-workers. (Finer et al., 1994). Reactions occur in a flow cell.

The flow cell preparation: To prepare the flow cell, 1 mg of 2.1 µm diameter silica beads (Bangs Laboratories) was suspended in 1% nitrocellulose in amylacetate (Ernest F. Fullam). Two microlitres of this solution was spread evenly onto a 22 mm by 40 mm coverslip (Menzel Glaser, Thermo Scientific). This concentration of silica beads gave a density of approximately 1 bead per 30 μm^2. Two pieces of double sided tape (permanent double sided tape, Scotch 3 M) were placed 20 mm apart upon a pre-cleaned slide (Super Frost Plus, Menzel Glaser, Thermo Scientific) to create a flow cell of approximately 75 µl volumes. NeutrAvidin coated beads were prepared a day before the experiment. Ten µl of carboxylate modified, biotin labelled, 1 µm polystyrene beads (Sigma Aldrich) were incubated with 10 µl of 0.1 mg/ml RhPh labelled BSA (Sigma Aldrich) and 5 mg/ml NeutrAvidin (Pierce, Thermo-Fisher Scientific) for 1.5 h, rotating at 4^oC. A 100 µl of AB-/BSA was added to the mixture and incubated for 40 min at room temperature. The beads were washed 10 times in 150 µl AB-/BSA by

centrifugation for 2 min at 7,000 rpm (Sepatech Biofuge 13). The washing step reduces non-specific binding and removes free NeutrAvidin from the supernatant. Beads were stored in 100 µl AB- on ice for up to four days.

N-Ethylmaleimide MyoA coated bead preparation: One hundred µl of full length MyoA (25 mg/ml in MyoA preparation solution and 50% glycerol) was diluted into 1 ml of deionised water. MyoA was pelleted by centrifugation at 15,000 rpm for 6 min (Sepatech Biofuge 13). The pellet was resuspended in an equal volume of 2X high salt buffer (1 M KCl, 40 mM potassium phosphate buffer [pH 6.5], 2 mM DTT, 4 mM $MgCl_2$) and 8 µl of freshly prepared N-Ethylmaleimide (NEM) solution (12.5 mg/ml /100 mM NEM [Sigma Aldrich] and 2% v/v ethanol in deionised water) so that the final NEM concentration was 4 mM. The mixture was incubated at room temperature. After 40 min the reaction was quenched and MyoA precipitated by the addition of 1 ml 10 mM DTT (in deionised water). The myosin was pelleted by centrifugation at 15000 rpm (Sepatech Biofuge 13) for 6 min, and resuspended in an equal volume of 2X high salt buffer. The solution was clarified by centrifugation at 15000 rpm for 6 min (Sepatech Biofuge 13). A volume of 30 µl of a 1 in ten dilution of the NEM modified myosin (in 1X high salt buffer) was added to 5 µl of 1 µm pre washed plain latex beads (LB-11, Sigma Aldrich), with 10 µl RhPh labelled BSA, and made up to 100 µl using 1X high salt buffer. The beads and myosin were incubated for 1 h at room temperature before being washed 3 times in AB- (8000 rpm, 3 min, Biofuge 13, Sepatech). Beads were stored in 50 µl AB- on ice for up to two days. Both NeutrAvidin coated beads and NEM myosin coated beads were vortexed and sonicated to disrupt aggregation immediately before use.

Data Acquisition and analysis: The optical trap transducer was constructed by Christopher Batters (Physical Biochemistry, NIMR) and is based around an inverted microscope (Zeiss, Axiovert 135TV). The setup of the laser and illumination and calibrating and testing of the apparatus set up and data acquisition was achieved with the help of Rachel Farrow (Physical Biochemistry, NIMR). A combination of bright-field and fluorescent microscopy was used to view the experiment. A single RhPh-labelled actin filament was captured between two NeutrAvidin beads within the vicinity of the optical trap and the third bead that was a sparsely coated NEM myosin bead was positioned within close proximity of the actin filament (Figure 2.1). Interactions between the surface myosin and the actin filament were then recorded. The procedure to

initiate the interaction was followed as in the motility assay. The reagents and buffers used were the same as in the motility assays. The data acquisition was performed using the custom software, Opittrap (Gregor Mashanov) and data were collected with a sampling rate of 10Hz and analysed using in-house custom software in Igor Pro (Rachel Farrow and Justin Molloy, Physical Biochemistry, NIMR). The data analysis of the single molecule MyoA event (the attachment of MyoA to actin filament), the power stroke and life time analysis was performed with help from Rachel Farrow.

2.5 *In vitro* parasite culture and maintenance

2.5.1 Maintenance of Plasmodium falciparum *and purification of the schizonts*

The *P. falciparum* 3D7 strain was grown in Roswell Park Memorial Institute 1640 (RPMI) medium with supplements (25 mM HEPES, 27 mM $NaHCO_3$, 2 mM L-glutamine, 25 μg/ml gentamycin, 50 μg/ml hypoxanthine and 2 mg/ml glucose and with or without 0.5% [w/v] AlbuMAX II [pH 7.5]) at 2-3% haematocrit. Cultures were gassed with a mixture of 5% O_2, 7% CO_2, and 88% N_2 and incubated at 37°C. To examine parasitaemia and cycle stage, thin blood smears were made on glass slides and stained with Giemsa (10% Giemsa's stain in phosphate buffer [pH 7.2-7.4]) in tap water for 2-3 min. Slides were then viewed using a light microscope. At 10% parasitaemia, the parasite-infected red blood cells were pelleted by centrifugation and washed with the RPMI medium without AlbuMAXII. The pellet was layered on top of 70% Percoll (90% percoll, in phosphate buffered saline and diluted with RPMI) and centrifuged at 1,000*g* for 11 min at room temperature. The concentrated schizont layer was harvested and washed with RPMI medium prior to reinvasion. For reinvasion, purified schizonts were added to the new culture containing fresh non infected red blood cells and incubated with agitation at 37^{o}C for 2-4 h. The newly ring-infected red blood cells were collected by sorbitol treatment to eliminate the schizonts (Lambros and Vanderberg, 1979). The synchronised parasites were grown until they reached 10% parasitemia and harvested at schizont stage. The schizont pellet was washed with RPMI without AlbuMAXII and kept at -80^{o}C prior to use.

2.5.2 Maintenance of **Plasmodium knowlesi** *and purification of the schizonts*

A similar technique to *P. falciparum* culture has been applied to *P. knowlesi* with slightly different use of medium and synchronisation reagents. Normally, parasites were grown in 2% haematocrit in 75 cm^2 flasks with 50 ml RPMI 1640 with AlbuMAXII and 10% human serum (Moon et al., 2013). Medium was change or parasites were diluted every 2 days. Human erythrocytes were tested for expression of the Duffy antigen before use and human serum was tested for parasite growth. Parasites were synchronised using 55% Nycodenz (Axis-Shield, UK; 27.6 g [w/v], 10 ml 100 mM Tris-HCl, [pH 7.0-7.5]) as a cushion instead of percoll. Once layered on top of the cushion, parasites were centrifuged at 1,000 *g* for 11 min at room temperature. The concentrated schizont layer was harvested and washed with RPMI + 10% HS medium prior to reinvasion. For reinvasion, purified schizonts were added to the new culture containing fresh non-infected red blood cells and incubated with agitation at 37^oC for 2-4 h. The newly ring-infected red blood cells were collected by Nycodenz gradient to eliminate the schizonts. The synchronized parasites were grown till they reached 10% parasitaemia and harvested at schizont stage by using Nycodenz as mentioned. Harvested schizont pellets were washed with RPMI without AlbuMAXII and kept at -80^oC prior to use.

2.5.3 Freezing and thawing of parasites

The parasites were frozen in liquid nitrogen for storage. Freezing solution (0.324 g NaCl, 1.512 g D-sorbitol, 14 ml glycerol in 50 ml volume) was added to the pelleted (1000 *g* for 5 min) ring-infected red blood cells with a minimum 5% parasitaemia. Warm freezing solution was added drop wise to the pellets (7:3 v/v). The mixture was transferred to cryopreservation vials and stored in liquid nitrogen. The cryopreserved samples were thawed in a 37^oC water bath and transferred to a 15 ml centrifuge tube. The original volume of thawing solution (3.5% NaCl) was added drop wise and centrifuged at 250 *g* for 5 min and the step repeated twice. The pellet was mixed with warm RPMI plus AlbuMAXII medium (*P. falciparum*) and addition of 10% HS for *P. knowlesi*. The culture was incubated at 37^oC for maintenance.

2.6 Parasite DNA manipulation and transfection

2.6.1 Transfection: The construction of single crossover integration constructs for integration of P. falciparum *and* P. knowlesi *MyoA and MyoB GFP-tags*

Parasite vectors for single homologous genomic integration and GFP expression in *P. falciparum* were based on the pHH4-GFP transfection plasmid (Dr E. Knuepfer, unpublished). This plasmid contain the human dihydrofolate reductase (hDHFR) and GFP cassettes, allowing WR99210 drug selection and introducing a GFP tag at the C-terminus of the chosen protein. In order to introduce the GFP tag at the C-terminus of each protein, a region of homology corresponding to MyoA (PlasmoDB ID PF3D7_1342600) and MyoB (PlasmoDB ID PF3D7_0503600) from the 3' end of each ORF lacking the stop-codon was selected. The region of homology was amplified by PCR using the primer combination of 3F1/3R2 for MyoA and 4F1/4R2 for MyoB (Table 2.2). The DNA from the 3' end of each ORF lacking the stop-codon was cloned into the vector pHH4-GFP at the restriction site of XmaI/AvrII generating the constructs, pHH4-PfMyoA-GFP and pHH4-PfMyoB-GFP for *Plasmodium falciparum* MyoA and MyoB respectively.

DNA constructs used in the *P. knowlesi* transfection experiment were similar to the *P. falciparum* constructs with the addition of a unique site in the middle of the homology region for MyoA (PlasmoDB ID PKH_121190) and MyoB (PlasmoDB ID PKH_102930) for linearization purposes. NruI and AfIII were introduced as unique sites to generate the pHH4-PkMyoA-GFP and pHH4-PkMyoB-GFP for MyoA and MyoB respectively from 3' end of each ORF lacking the stop-codon. PCR was carried out for different fragments for each DNA using specific primers which were designed to create a unique site. For the MyoA construct, to introduce the NruI site, the first fragment was amplified with the primer combination of 1F1/1R1 and cloned into the construct using the XmaI/AvrII sites. Finally, the second fragment was amplified with the primer combination of 1F2/1R2 and cloned into the construct containing the first fragment using XmaI/AvrII sites. For the MyoB construct, the AfIII site was introduced by cloning an amplified PCR product of fragment 1 and fragment 2 into the vector at XmaI/AvrII sites. For diagnostic purposes the construct was digested with XmaI/AvrII to obtain the full length of the region of homology, AvrII/ SacI for the GFP fragment, XmaI/NruI and NruI/AvrII for the MyoA fragment 1 and fragment 2

respectively, and XmaI/ Af1II and AfIII/ AvrII for fragment 1 and fragment 2 of MyoB respectively.

2.6.2 Preparation of DNA constructs for transfection

For circular and linear transfection, the plasmid DNA (100 µg for *P. falciparum* and 10-20 µg for *P. knowlesi*) was purified by ethanol precipitation and mixed with TE buffer (10 mM Tris HCL, 1 mM EDTA, [pH 8.0]) and kept at –20^{o}C. Briefly, 1/10 volume of 3M sodium acetate was added to the DNA sample, followed by 2 volumes of 100% ethanol. DNA was left to precipitate overnight at -20°C and pelleted by centrifugation (20,000 *g*, 20 min). The pellet was washed in 70% (v/v) ethanol and spun again prior to air-drying and resuspended in 30 µl of TE buffer. In addition, for *P. knowlesi* linear transfection, the construct was linearized using appropriate enzymes prior to transfection.

2.6.3 Transfection of **P. falciparum** *with circular plasmids*

Electroporation of parasites was carried out using the BioRad Gene Pulser Electroporator. *P. falciparum* 3D7 parasites were synchronised to a 10% early ring parasitaemia (section 2.5.1). Purified plasmid DNA (100 µg) in 30 µl TE buffer was mixed with 385 µl cytomix solution (120 mM KCl, 0.15 mM $CaCl_2$, 2 mM EGTA, 5 mM MgCl, 10 mM K_2HPO_4/KH_2PO_4, 25 mM HEPES [pH 7.6]) by gently pipetting to dissolve the DNA (Fidock and Wellems, 1997; Wu et al., 1995). The mixture was then added to 150 µl of the ring-infected blood culture, and using a sterile Pasteur pipette the cell suspension was immediately transferred into the Gene Pulser cuvette. Electroporations were done one at a time at 0.310 kV/950 µF with the resistance (ohms) set to infinity. The electroporated samples were transferred into petri dishes containing 10 ml culture medium with a 3% haematocrit of non-infected red blood cells. The petri dish was placed into a culture chamber, gassed with a mixture of 5% O_2, 7% CO_2, and 88% N_2 and transferred to an incubator at 37^{o}C. The culture of transfected parasites was fed every day for 6 to 7 days then every other day for 2 weeks. At the end of the second week, the parasite culture was fed and maintained with RPMI 1640 medium containing

2.5 nM WR99210 (Merck). Once the transfected cultures had recovered, they were scaled up for several purposes such as cryopreservation, preparation of genomic DNA (gDNA), and microscopy to detect GFP expression. This first growth and treatment was termed Cycle-0. The transfected cultures were then subjected to cycling in the absence of drug and with WR99210 selection until GFP was expressed. Transfected parasites expressing GFP were subjected to genotype and phenotype analysis and cloned.

2.6.4 Transfection of **P. knowlesi** *with linear and circular DNA*

Nycodenz-purified schizonts were used for transfection of *P. knowlesi* with both circular and linear DNA. Electroporation of parasites was carried out using the Amaxa 4D Electroporator (Lonza) and the P3 Primary cell 4D Nucleofector X kit L (Lonza). For each transfection, 20 µg of DNA (section 2.5.2) was dissolved in 10 µl TE buffer and added to 100 µl of supplemented P3 primary cell solution. Approximately 5 - 10 µl of schizonts (~5 x 10^7-10^8) were resuspended in the DNA plus P3 Primary cell solution and immediately electroporated in the 4D Nucleofactor X Kit L cuvette (Lonza) using programme FP158. Electroporated parasites were transferred to a 1.5 ml Eppendorf tube containing 500 µl pre-warmed complete RPMI 1640 medium and a 3% haematocrit of fresh RBC. The transfected parasites were incubated at 37^{o}C in a thermomixer with agitation for about 30-60 min and then the transfected parasites were transferred to a 6 well plate, each well containing 5 ml warm complete medium. The plate was then placed at 37^{o}C in a gassed chamber. The medium was replaced with fresh medium containing 2.5 nM WR99210 after 24 hours and the cultivation was continued. The transfected parasites were subjected to genotype and phenotype analysis.

2.6.5 Cloning of transgenic parasites by limiting dilution

Limiting dilution was carried out to obtained a suspension containing three parasitised cells per ml by diluting 100 µl of diluted parasite culture in complete medium containing RBC (2% haematocrit) into each well of a U-bottom microtiter plate. Plates were incubated at 37^{o}C in a gas chamber, and then fed at 3 - 4 days intervals with medium containing RBCs (1% haematocrit) once a week. Wells containing growing parasite clones were identified by light microscopy of Giemsa stained thin films after approximately ~2 weeks. Clones were confirmed by genotype and phenotype analysis.

2.7 Southern Blot

2.7.1 DNA digestion

Approximately 5 to10 µg of DNA was digested with 30 units of the selected restriction enzyme and incubated at 37^{o}C overnight. The digested DNA was separated by gel electrophoresis, using a 0.7% agarose gel in TBE buffer containing 0.5 µg/ml ethidium bromide at 40V overnight and then photographed under UV with a fluorescent ruler for measurements. The gel was then incubated in depurinating solution (0.25 M HCl) for ~10 min on a shaker, washed with MilliQ water followed by denaturing buffer (0.5 M NaOH, 1.5 M NaCl) for a minimum of 30 min and followed by two ~30 min washes in neutralising buffer (1.5 M NaCl, 0.5 M Tris-HCl, 1 mM EDTA, [pH 7.4]). The DNA was then transferred from the agarose gel to Gene Screen Plus membrane (Whatman) by assembly of a semi-dry blot. To do this the membrane was first soaked in 10X SSC buffer (saline-sodium citrate: 0.3 M NaCl, 30 mM sodium citrate, [pH, 7.0]) for ~15 min. The agarose gel was placed upside down on saran wrap and the wet membrane placed on top followed by 3 layers of Whatman 3M filter paper. A layer of paper towels was then placed on top and the blot was weighted and left to blot overnight by capillary transfer (Sambrook, 1989). The blot was then disassembled, the DNA on the membrane was denatured by quickly rinsing in 100 ml 0.4 M NaOH for ~1 min, then neutralised with neutralising buffer (1.5 M NaCl, 0.5 M Tris-HCl, 1 mM EDTA, [pH 7.4]) and the membrane was air-dried before cross-linking under a CL-1000 Ultraviolet Cross linker (UVITEC Cambridge). The membrane was then left to air dry on Whatman filter paper and stored at -20°C until required.

2.7.2 Probe generation and labelling

Hybridisation probes were generated by PCR (section 2.1.2) or excision from a transfection vector and were specific for each gene of interest. Probes were radioactively labelled with α-^{32}P dATP (Perkin Elmer®) by random priming using the Decaprime II kit (Ambion) according to manufacturer's instructions. Unincorporated labelled nucleotides were removed using a ProbeQuant™ G-50 Micro-column (Amersham Biosciences). The labelled probe was then denatured at 98°C for 5 min and used straight away for hybridisation.

2.7.3 Hybridisation

The cross-linked membrane was pre-hybridised with 20ml hybridization solution (6X SSC, 5X Denhardt's solution [1% (w/v) BSA, 1% (w/v) polyvinylpyrrolidone, 1% (w/v) Ficoll 400], 0.2 mg/ml salmon sperm DNA), rotating at 62°C for 1 h. The labelled probe was then added to the hybridisation solution and allowed to hybridise under rotation at 62°C overnight. The labelled probe was poured off, and the membrane washed twice for 30 min with 6X SSC + 0.1% SDS at 62°C. The background radiation was checked and, if necessary, additional washes with 2X SSC were applied. When only a low background was detected the membrane was wrapped in Saran wrap, placed in contact with film (Kodax® BioMax™ MR) and incubated overnight at -80^{o}C for autoradiography. If necessary, the probe was stripped off the membrane by boiling in 0.05X SSC, 0.01 M EDTA, 0.1% SDS to allow re-probing.

2.8 Live imaging and indirect-immunofluorescence microscopy assays (IFA)

2.8.1 Live imaging of GFP-tagged parasites

GFP-tagged parasites were synchronized and purified as described previously and then diluted 1:10 with RPMI 1640 containing AlbumaxII. DNA (the nuclei) was stained with 0.1 µg/ml Hoechst 33342 DNA reagent (Invitrogen) with incubation for 10 min at room temperature. Approximately 2-5 µl of the stained schizonts were dropped onto a glass slide and overlaid with a Vaseline-rimmed coverslip for live microscopy.

2.8.2 Indirect immunofluorescence assay (IFA)

For IFA, the thin films of stage-specific parasite material were made. The slides were fixed with 4% paraformaldehyde (PFA) for 10 min at room temperature. The fixed slides were washed 3 times with PBS and permeablised with PBS containing 0.5% Triton X-100 for 5 min at room temperature. Then the slides were washed twice with PBS and blocked overnight with 4% BSA in PBS at 4^{o}C. After blocking, the slides were incubated with GFP-Booster (a specific GFP-binding protein coupled to the fluorescent dye ATTO 488) (Chromotek) or α-GFP antibody (mouse monoclonal or affinity purified rabbit) for 1 hour at room temperature. The slides were washed 3 times with PBS prior to an incubation step with protein marker antibodies (Table 2.3). The slides

were then incubated with IgG-specific second antibody coupled with Alexafluor 594/488 (Sigma) (Table 2.3) for 60 min at room temperature and washed 3 times with PBS. The slides were mounted with Prolong® Gold anti-fade reagent with DAPI (Invitrogen) overnight. Then the slides were sealed with a coverslip and nail polish prior to imaging by epifluorescence microscopy on an Axio Imager M1 microscope (Zeiss). Images were overlaid using Axio Imager software and edited using Adobe™ Photoshop.

2.8.3 Fixing live parasites for IFA

Parasite populations were synchronised tightly (within 1 h) prior to the experiment. Mature schizonts (~ 44-45 h post invasion) of ~7-8% parasitemia were purified and maintained in complete culture medium without red blood cells. The parasite cultures were monitored closely by Giemsa staining until schizont rupture was detected. The cultures were then pelleted and ~5 µl of parasites were placed into 6 microcentrifuge tubes containing 500 µl complete medium with 5% haematocrit, for harvesting at 6 time points starting from egress to 30 min post egress. For each time point, the tube was taken out from a 37^{o}C shaking incubator and smeared for Giemsa staining to provide a stage-specific reference. Immediately 500 µl of fixing solution (8% PFA+ 0.02% glytaraldehyde in PBS) was added to the tube, and incubated for 60 min. Cells were permeablised with 0.1% Triton-X100, resuspended in 3% BSA, and then kept at 4^{o}C until used. The set time points were T1 (2 min), T2 (5 min), T3 (10 min), T4 (15 min), T5 (20 min) and T6 (30 min). Each selected time point was further analysed with IFA, using the procedure as in section 2.8.2.

2.9 Protein complex identification by liquid chromatography- mass spectrometry (LC-MS/MS)

Proteins or immunoprecipitation products (Section 2.3.3) from *P. falciparum* transgenic parasites expressing GFP-tagged MyoA and MyoB were resolved by short run SDS-PAGE (4mm). The protein was stained with colloidal blue stain (Invitrogen) following the manufacturer's instructions. The stained gel was destained (200 mM ammonium bicarbonate, 50% acetonitrile) for 30 min with shaking. Then the destaining solution was removed and the step repeated prior to washing with ultrapure water twice at 5 min

intervals. All the protein bands were excised and processed. The gel pieces were placed into a non-coloured 0.5 ml Eppendorf tube. The SDS and stain were further extracted by incubating in 500 µl of destaining solution for 30 min at room temperature and this step was repeated twice. The protein was then reduced by incubating in 200 µl reducing solution (20 mM DTT, 200 mM ammonium bicarbonate, 50% acetonitrile) for 1 h at room temperature. The DTT was removed by washing with 500 µl destaining solution. The cysteines of the protein were then alkylated by incubating in 100 µl of freshly prepared alkylation solution (5 mM iodoacetamide, 200 mM ammonium bicarbonate, 50% acetonitrile) for 20 min in the dark at room temperature. The alkylation solution was removed and the gel washed twice with 500 µl washing solution (20 mM ammonium bicarbonate, 50% acetonitrile). The washed gel piece was incubated in 500 µl of neat acetonitrile for 15 min till it turned white, then the acetonitrile was removed and the gel piece was left to dry in a laminar hood for about an hour. The dried gel containing protein was stored at room temperature prior to the trypsinization step. The dried gel was incubated in 12 µl of trypsin solution (1 µg/ml of trypsin in 5 mM ammonium bicarbonate) at 37^{o}C overnight; the trypsin solution was added so that it covered the gel piece. The released peptides were used for protein identification by LC-MS/MS using an LTQ Orbitrap Velos mass spectrometer (Thermo Scientific), which was run and the data analysed by Dr. Steven Howell, (NIMR).

2.10 Antibody production

Antibodies to recombinant MyoA (α-MyoA Rc) protein were raised in a rat by Harlan Ltd, UK following a standard protocol. Anti-peptide antibodies were generated by Pepceuticals Ltd, UK, in either rat or rabbit following the standard protocol. The resulting antibodies and their working dilutions are listed in Table 2.3**.**

Table 2.1: The primers used for expression of recombinant protein used in the *in vitro* cell free system. The coloured letters indicate restriction sites.

Primers	ID	Restriction site	Sequence (5'-3')
N-terminal His-tagged			
Forward			
MyoA/pEU-F	1A	SmaI	**TACCTTAACCCGGGATGGCTGTGACCAACG**
MTIP/pEU-F	3M	SmaI	**TGGCAGTCCCGGGATGAAACAAGAATGC**
GAP45/pEU-F	5G	SmaI	**GCAGTGTCCCGGGATGGGAAATAAATGTTC**
Reverse			
MyoA/pEU-R	2A	SpeI	**GCCAAGCACTAGTCTACTGAGCCACCATCTT**
MTIP/pEU-R	4M	SpeI	**GCGGGCCCTCACTAGTTTATTGTAATATATC**
GAP45/pEU-R	6G	SpeI	**GCCGAGGCCACTAGTTTAGCTCAATAAAGG**
N-terminal GST-tagged			
Forward			
G-N1/MyoAF	7A	EcoRV	**CGTTTATCTGATATCATGGCTGTGACCAACGAGGAGATC**
G-N1/MTIPF	9M	EcoRV	**CGGCCGACGGATATCATGAAACAAGAATGCAATGTATGT**
G-N1/GAP45F	11G	EcoRV	**CCGGGTCGAGATATCATGGGAAATAAATGTTCAAGAAGC**
Reverse			
G-N1/MyOAR	8A	NotI	**AAATAGCGGCCGCTCACGGACACGCAGTTCTCCCAC**
G-N1/MTIPR	10M	NotI	**GCCCGGGCGGCCGCTTGTAATATATCTTCACAGAATAATTTG**
G-N1/GAP45R	12G	NotI	**GGGAATTGCGGCCGCTTAGCTCAATAAAGGTGTATCGG**

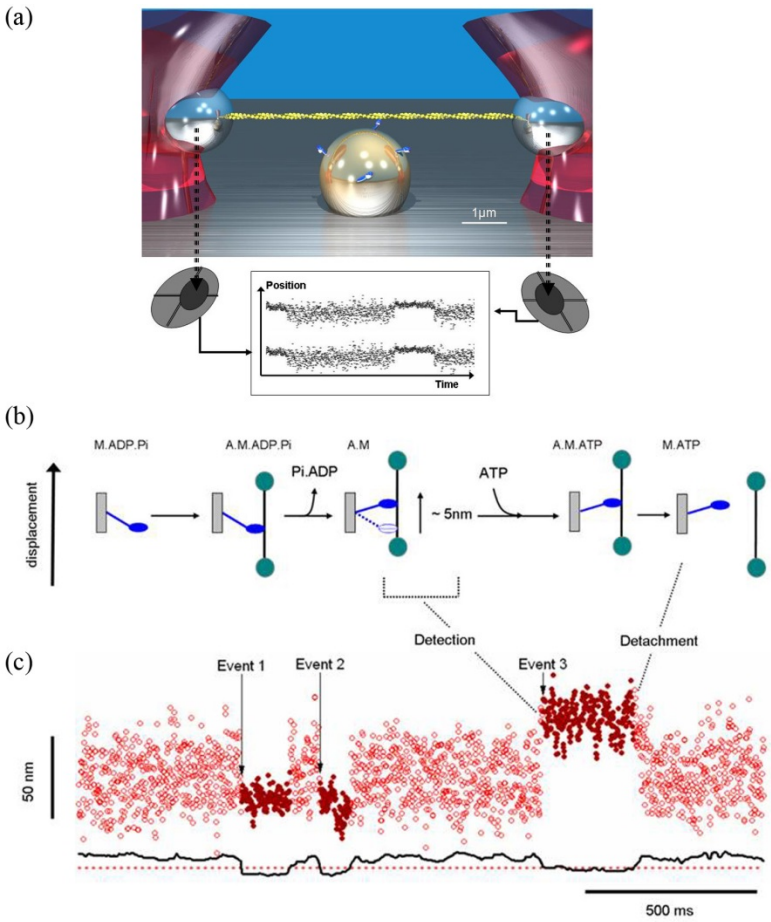

Figure 2.1 A Schematic model showing the set up for single molecule myosin studies. (a) The positioning of the beads in the laser trap. An actin filament (yellow line) was held between two beads trapped by a laser beam (red beam). The third bead is coated with myosin (blue shape). Image is adapted from the Block laboratory website at Stanford University; http://www.stanford.edu/group/blocklab/kinesin/kinesin.htm. (b) A diagram of the Acto-myosin "events" as determine by optical trapping. Under the conditions used throughout this thesis (low temporal resolution) only the rigor state can be detected as the second phase of the power stroke (ADP isomerization or release) occurs within the limit of temporal resolution. The "lifetime" of these events is, therefore, dependent upon ATP concentration. The components are: myosin (blue shape), actin filament (black line), two beads in a laser trap (green shape), and myosin coated bead (rectangle shape). (c) Example of the raw displacement data (red dots) and the corresponding standard deviation (red line). (b) and (c) are a schematic diagram produced by Rachel Farrow.

Table 2.2: Primers used for construction of single cross over transfection plasmids and for the diagnostic PCR to analyse transgenic parasites. Coloured letters show the restriction site, whilst the background coloured letters indicate the unique sites introduce into the DNA sequences.

Primers	ID	RE	Sequence (5'-3')
Primers used for flanking regions			
Forward			
PfMyoA-F	3F1	XmaI	CCCGGGCAAGAATTGAACCAGAAGGAGGATTTAAAAC
PfMyoB-F	4F1	XmaI	CCCGGGGGACATCCTTTCGCCTAACATTTTGAAA
PkMyoA-F1	1F1	XmaI	CCCGGGGGTATGTTGGACATTTTCGGTTTTGAG
PkMyoA-F2	1F2	NruI	TCGCGAAGGGATCACTCATAGGATCTCAGTTC
PkMyoB-F1	2F1	XmaI	CCCGGGTCGATCGTGGGAGTTTACACGAAC
PkMyoB-F2	2F2	AflII	CTTAAGAAAATCAGCTCCTATTTGAAAAACACAAATATAT
Reverse			
PfMyoA-R	3R2	AvrII	CCTAGGTTGAGCTACCATTTTTTTTCTTATATGAGCTTGTA
PfMyoB-R	4R2	AvrII	CCTAGGTTCGTGTTCCTTAATATATTTATATTTCCTAAAATATGC
PkMyoA-R1	1R1	Avr/ NruI	CCTAGGGATCCCTTCGCGATTTTTCCCTTTTCTATAACTTGACCT TCAAAC
PkMyoA-R2	1R2	AvrII	CCTAGGCACGGTGAGTCTCTTCCTTATGTG
PkMyoB-R1	2R1	Avr/ AflII	CCTAGGAGCTGATTTTCTTAAGATTCTCCAAATATTTAAATGTGA TTAAGTTTTTCCTTC
PkMyoB-R2	2R2	AvrII	CCTAGGCTTCAGCTGTGCAATGTACTTATGTTTC
Primers used in diagnostic PCR			
Forward			
PfMyoAs+F1	1	-	GGGAAATATTAATTAAGGTAACTGTTGCTGGAGGAAC
PfMyoBs+F1	3	-	CATAACGGAAAGTTTTGTAATTAAGCATACTGTAAGTGATG
PfMyoB	3a	-	CTAAGAATGAACATTATTCAGTATGTAAG
PfMyoB	3b	-	CATAACGGAAAGTTTTGTAATTAAGCATACTG
PfMyoB	3c	-	ATTAAGTCGATCGTAAGTGTTTATACA
PkMyoAs+F1	5	-	CGCTGGAGGAAATAAGATCGAAGGTAGATG
PkMyoA	5a	-	CAAGGTTACCAACGCTGGAGGAAATAAGATCG
PkMyoA	5b	-	GAGCGATGCAGAAGTGTTGCAGTTATCCCTTTG
PkMyoBs+F1	7	-	CTGGCCCCAGGAAAGAAGGACGAGGTGAGCATCGCGCAAGTG
PkMyoB	7a	-	GTGCATGTGTGAAGGGGAGGCACATTTGCA
PkMyoB	7b	-	CTGGCCCCAGGAAAGAAGGACGAGGTG
Reverse			
PfMyoAs+R1	2	-	CACTCATAGATGCAACATGTAAGTATACAAATAAATATGGTATGT AG
PfMyoBs+R1	4	-	GGATGACCAGAAAGTTGTAACTTTGGCAAATTTATTC
PkMyoAs+R1	6	-	GGTCATTAAGGGGGTAAAAAGGGGGGG
PkMyoBs+R1	8	-	CTTTGATGAGGTCCAACTGGTTGGTGTTC

Table 2.3: List of antibodies used in Western blot and IFA

ID	Antibody	Raised in	Dilution WB/IFA	Source
Polyclonal antibodies to recombinant proteins				
α-MyoA	Polyclonal MyoA	Rabbit	1:5000/1:1000	Dr JC Fordham
α-MTIP	Polyclonal MTIP	Rabbit	1:5000/1:1000	Dr JL Green
α-GAP45	Polyclonal GAP45	Rabbit	1:20000/1:1000	R Rees-Channer et al., 2006
α-GAP45	Polyclonal GAP45	Mouse	-/1:1000	R Rees-Channer et al., 2006
α-GAP50	Polyclonal GAP50	Rabbit	1:1000/1:200	Raised in house
α-GFP	Affinity purified GFP	Rabbit	1:5000/1:500	Dr E Knuepfer
Commercial antibodies				
GFP Booster	Camelid GFP antibody	Camel	-/1:200	Cromotek
α-GFP	Monoclonal mouse GFP	Mouse	1:1000/1:200	Roche
Tub	Tubulin	Mouse	-/1:200	Roche
Act	Actin (AC-40)	Mouse	-/1:100	Roche
Polyclonal antibodies to peptides				
α-MyoA-Rc	MyoA Full length (generated from protein produced with wheat germ cell free system)	Rat	1:500/1:200	This study
Pf/k MyoA	MAVTNEEIKTASKIVRRVSNVEAFDKSGSVC (Antibodies to this sequence should bind to both Pf and Pk MyoA)- Peptide produce by Pepceuticals Ltd.	Rat	1:200/1:200	This study
Pf/k MyoA-rabbit	MAVTNEEIKTASKIVRRVSNVEAFDKSGSVC	Rabbit	1:200/1:200	This study
Pk/f MyoB	IPLSVEESLSIARSISKDIYNKIFEC (Antibodies to this sequence should bind to both Pf and Pk MyoA)- Peptide produce by Pepceuticals Ltd.	Rabbit	1:200/1:200	This study
Pk/f MyoB-rat	IPLSVEESLSIARSISKDIYNKIFEC	Rat	1:200/1:200	This study
PkMyoB	MNKASELSNYFRINSEFVNKIENE Peptide produce by Pepceutical Ltd	Rat	1:200/1:200	This study
PfMyoB	MVNKINELNNYFRINSTFINKSENE Peptide produce by Pepceutical Ltd	Rat	1:200/1:200	This study

Table 2.3 continued: List of antibodies used in western blot and IFA

ID	Antibody	Raised in	Dilution WB/IFA	Source
Organelles marker antibodies				
AMA1	Apical membrane antigen-1	Rabbit	-/1:3000	Arnot et al., 2008
PTRAMP	Thrombospondin-related apical membrane protein	Rabbit	-/1:5000	Dr JL Green (NIMR)
EBA175	Erythrocyte binding antigen-1	Rabbit	-/1:800	MR4
RhopH2	Rhoptry-H2	Rabbit	-/1:4000	Ling et al., 2003
RON3	Rhoptry neck-3	Mouse	-/1:1000	Dr E Knuepfer (NIMR)
RON4	Rhoptry neck-4	Mouse	-/1:1000	Dr E Knuepfer (NIMR)
RAP1	Rhoptry body-1	Mouse	-/1:800	Dr E Knuepfer (NIMR)
MSP7	Merozoite surface protein-7	Rabbit	-/1:3000	Dr E Knuepfer (NIMR)
Secondary antibodies				
α-Rat/Rabbit/Mouse IgG HRP	Alexafluor® 594	Rat/ Rabbit/ Mouse	-/1:5000	Invitrogen
α-Rat/Rabbit/Mouse IgG HRP	Alexafluor® 488	Rat/ Rabbit/ Mouse	-/1:5000	Invitrogen
-	HRP-conjugated goat anti mouse	Mouse	-/1:2000	Biorad
-	HRP-conjugated goat anti rabbit	Rabbit	-/1:2000	Biorad
-	HRP-conjugated goat anti rat	Rat	-/1:2500	Sigma

Chapter 3

In vitro Protein Expression and Interaction Studies

3.1 Introduction

One of the challenges faced by scientists attempting to express *P. falciparum* proteins in heterologous systems, is a lack of an efficient recombinant protein synthesis system. This limits not only the initial synthesis and characterisation of a protein, but also functional studies and downstream assessment for drug discovery, for example. What is required is optimised protein expression systems that can decoded A/T-rich malaria parasite genes, often coding for low complexity amino acid sequence, into high quality folded protein. These features have been proposed as major factors limiting *P. falciparum* protein expression in heterologous cell based systems (Tsuboi et al., 2010). The improvements were achieved by the development of so-called bilayer translation methods in which a diffusion system enables the continuous supply of substrates, while continually removing small, low molecular mass by-products. This is achieved via a phase partition between the translation mixture and the substrate mixture, mimicking the normal cell physiology (Sawasaki et al., 2002a).

Endo et al. (2003) suggested that although classical recombinant protein technology is well developed it still has limitations, such as the fact that the proteins produced may not be correctly modified by the host cell, and generally it is time consuming to prepare the recombinant proteins. On the other hand, using a cell-free synthesis system had several advantages over conventional recombinant expression. These advantages are: the proteins produced are stable at higher concentration due to the fact that wheatgerm contains all necessary requirements for the translation that can be added in a controlled way, the procedure is less time consuming (typically completed within 2 days), and the proteins are correctly folded (Endo and Sawasaki, 2003; Sawasaki et al., 2002a; Sawasaki et al., 2002b). Thus cell-free expression can prove

very useful in systematic studies to examine protein structure-function relationships, in delineating the scope of modern proteomics, in crystallisation studies, and in exploring protein-protein interactions (Sawasaki et al., 2002b; Sawasaki et al., 2002c).

The *Plasmodium* molecular motor complex or glideosome, which includes myosin, is located between the IMC and PM of the parasite and is considered to be the most important driving force responsible for parasite gliding motility and cell invasion, such as merozoite invasion of red blood cells. This motor is powered by ATP hydrolysis allowing the myosin to move f-actin. In many systems it has proved extremely difficult to produce myosins in recombinant form to facilitate their study (Dr Justin Molloy, personal communication). Therefore, in the context of this study it was decided to examine expression of the proteins of the motor complex using the wheat germ *in vitro* expression system, with a view to studying protein-protein interactions and rebuilding the glideosome motor complex *in vitro*.

In this chapter, attempts to express the glideosome motor proteins by wheat germ cell free system are described. The N-terminal and C-terminal tagging with His- and GST- tags of MyoA, MTIP and GAP45 were undertaken in order to produce different tagged proteins to be used in protein-protein interaction studies. Therefore His- or GST- pull down assays can be used to isolate the protein and other associated proteins.

3.2 Production of recombinant proteins using the wheat germ cell free system

Re-codonized full-length genes encoding *P. falciparum* Myosin A (MyoA, 2454 bp) (donated by Rachel Farrow, NIMR), Myosin Tail domain Interacting Protein (MTIP, 615 bp) (Judith Green, NIMR) and Glideosome Associated Protein 45 (GAP45, 615 bp) (Ridzuan Razak, NIMR) were available in the laboratory and therefore chosen for these studies. The sequences were PCR amplified using pairs of primers (Chapter 2, Table 2.1) specifically designed for each gene to allow them to be cloned and expressed in either the His- or GST-tag wheat germ *in vitro* expression vectors (Appendix A). All DNA sequences were confirmed by Sanger sequencing (Beckman Genomics) before

being used in the expression protocols. The recombinant plasmid DNA produced was used as a template for mRNA transcription. Transcript analysis showed that all mRNAs encoding N-terminal His- and GST-tagged proteins were transcribed successfully. Following *in vitro* translation the soluble (S) and insoluble (P) fractions of the reaction were analysed using Western blotting with specific antibodies for the His- or GST-tags to examine the level of protein expression and each protein's solubility. In initial studies looking at expression of His-MTIP (M1), His-GAP45 (G1), GST-MTIP (M5) and GST-GAP45 (G5), it was found that the majority of each protein was soluble (Figure 3.1). Unfortunately, His-MyoA (A1) was largely in the insoluble fraction. Although GST-MyoA (A5) was also in the insoluble fraction, some product was in the soluble fraction (Figure 3.1). Therefore the GST-MyoA was purified from this soluble fraction using glutathione-Sepharose beads (GE Healthcare), and the eluate (E3) was used further as described in Section 3.3.

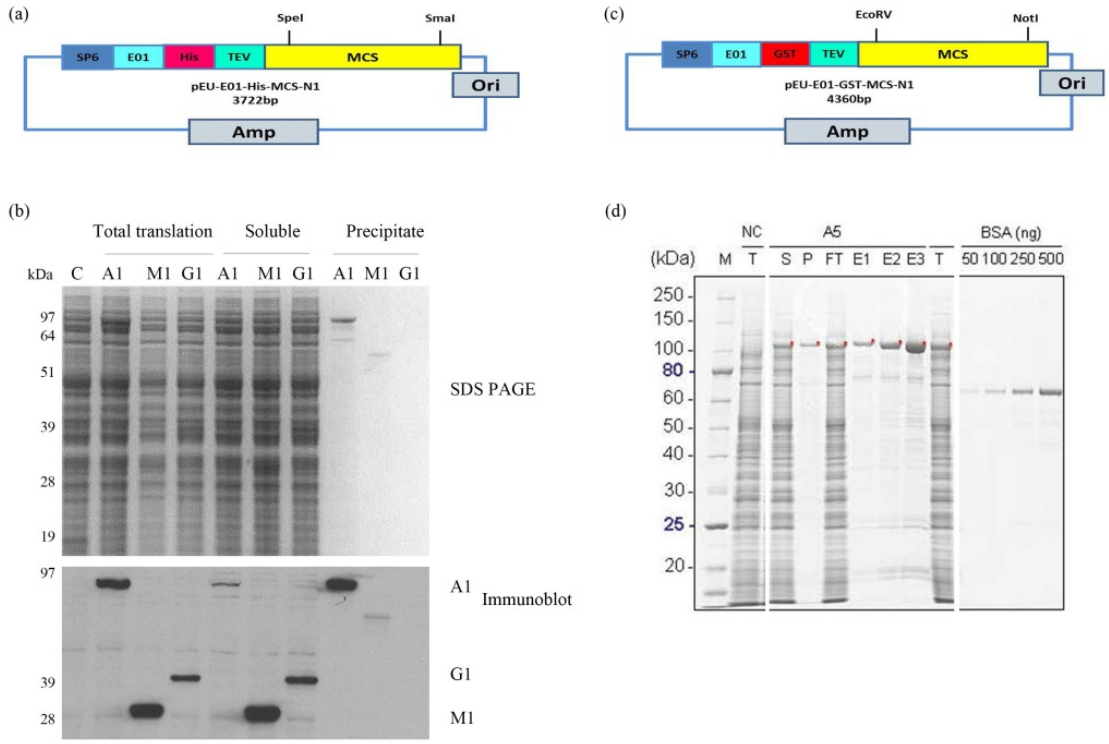

Figure 3.1: Generation of recombinant DNA, and protein expression in the wheat germ cell-free system. (a) Map of the plasmid used for expression of His-tagged proteins in the wheat germ cell-free system; all genes were inserted following

SpeI/SmaI digestion into the multiple cloning site (MCS) region. (b) SDS-PAGE and western blot analysis of *in vitro* translation of His-tagged proteins. The gel was stained with Coomassie blue (SDS-PAGE gel) and the immunoblot probed with anti-hexaHis antibody. Total protein translation reactions were also separated into soluble and insoluble (precipitate) protein fractions following centrifugation. The reactions to express His-MyoA (A1), His-MTIP (M1) and His-GAP45 (G1) respectively were examined. His-MTIP and His-GAP45 were essentially soluble whereas most of the His-MyoA was in the precipitate (insoluble) fraction. Fraction C is a control reaction without added mRNA. The mobility of molecular mass markers (kDa) is indicated on the left of the panel (c) Map of the plasmid used for expression of GST-tagged proteins in the wheat germ cell-free-expression system; all genes were inserted following EcoRI/NotI digestion into the multiple cloning site (MCS) region. (d) SDS-PAGE analysis of GST-MyoA (A5) expression and purification; proteins were detected by staining with Coomassie blue. M-molecular mass markers; NC - negative control, reaction to express DHFR; T - total translation reaction; S - soluble and P - insoluble fractions following centrifugation; FT - flow through of glutathione-Sepharose column; E1 to E3 are column elution fractions 1, 2 and 3, respectively. Bovine serum albumin (BSA) in the amounts specified was included on the gel to facilitate estimation of the yield of specific protein.

3.2.1 Co-expression: MyoA co-expression with GST-tag enhances solubility

The poor solubility of the MyoA protein is consistent with previous studies that showed it is a difficult protein to fold, leading to aggregation and insolubility (Rachel Farrow, Ph.D. thesis, 2010). Therefore the initial question was whether the MyoA protein produced in this study was incorrectly folded leading to its aggregation. Several attempts were made to optimize the level of expression and solubility of the protein including varying the salt (NaCl) concentration, the use of non-ionic detergents (Triton-X100 and Nonidet P40), and addition of reducing agent (DTT) or the divalent cation chelator, EDTA. However, none of these factors significantly altered MyoA solubility (data not shown). In previous studies, MyoA has been shown to interact with MTIP through its short tail (Bergman et al., 2003; Green et al., 2006b; Thomas et al., 2010) . Considering MTIP's good solubility, it was hypothesised that its addition may aid

MyoA folding and solubility, and following MyoA expression an excess of recombinant MTIP protein was added directly to the sample. However, this had a minimal effect on MyoA solubility (data not shown).

In another attempt to increase MyoA solubility in both His- and GST- tagged forms, a series of co-expression studies were carried out. MyoA was co-expressed with combinations of MTIP and GAP45 (see Chapter 2, section 2.2.4). With His-MyoA, initial attempts using a ratio of 1:2 (His-MyoA: MTIP) mRNAs to provide an excess of MTIP showed no appreciable effect. However, by using equal volumes of MyoA and MTIP mRNA in the translation mixture, the solubility of His-MyoA shifted to almost ~50% in the soluble fraction (Figure 3.2). With respect to GST-MyoA, which when expressed alone was approximately 50% soluble, further co-translation with MTIP and GAP45 was carried out. Co-expression of GST-MyoA with either MTIP or GAP45 increased the proportion of soluble MyoA, although co-expression of all three proteins together had no notable effect on MyoA solubility (Figure 3.2.b). Overall from these studies it was determined that there are no major significant differences between His- or GST-MyoA (Figure 3.2.c), but co-expression with MTIP or GAP45 always increased GST-MyoA solubility to greater than 60% (Figure 3.2.d). Unfortunately a consequence of co-expression (with all three proteins) was a reduction in the total amount of MyoA production, the result being that compared to MyoA expression alone the total amount of soluble MyoA protein was lower in the presence of MTIP or GAP45.

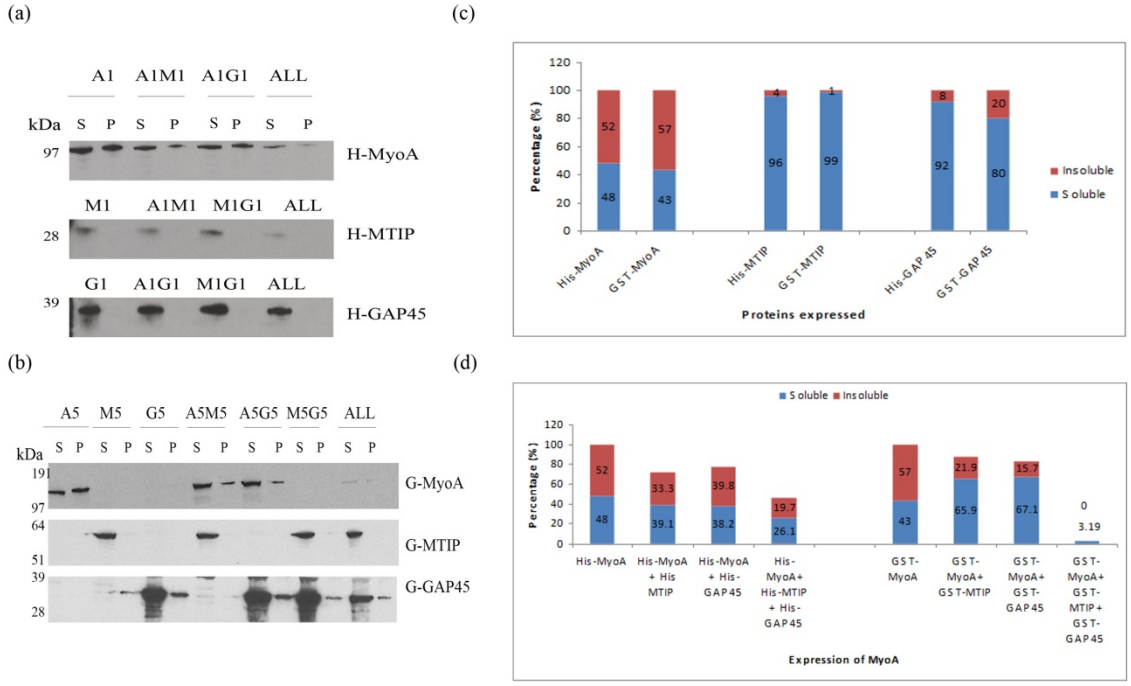

Figure 3.2: Protein translation in the wheat germ cell-free system. Each translation mix was separated into soluble and insoluble fractions and probed for its tagged protein content using SDS-PAGE/Western blotting and α-MyoA, α-MTIP and α-GAP45 antibodies. (a) N-terminal His-tagged MyoA expressed alone (A1), or together with MTIP (A1M1) and GAP45 (A1G1) or together with both MTIP and GAP45 (ALL). The western blots were probed with antibodies specific to MyoA, MTIP and GAP45. (b) N-terminal GST-tagged MyoA expressed alone (A5), or together with MTIP (A5M5) and GAP45 (A5G5), or together with both MTIP and GAP45 (ALL). The western blots were probed with antibodies specific to MyoA, MTIP and GAP45. (c) Estimation of the amount of the expressed single proteins with His- or GST-tags in the soluble and insoluble fractions. The numbers indicate the percentage of the amount of protein in either the soluble (blue) or insoluble (red) fraction, as determined using western blotting and analysed using densitometry (Image J software). (d) Measurement of MyoA solubility when co-expressed with either MTIP or GAP45 individually or both together. The amount of MyoA protein was analysed by western blot (using anti-MyoA antibody) and densitometry and is expressed as the percentage of the control, with indication of the amount in the soluble and insoluble fractions.

3.2.2 Comparison of His vs GST tagged MyoA solubility

In the previously described experiments the same tag was used on each of the expressed proteins, in order to give some idea of the ability of the cell-free system to produce soluble protein. To facilitate studies of protein-protein interactions, a series of protein co-expressions was carried out with GST- or His-tagged MyoA and MTIP or GAP45 modified with the alternative tag. Of particular interest is the fact that MyoA solubility was substantially improved when GST-MyoA was co-expressed with a His-tagged second product (Figure 3.3.b), although the overall amount of MyoA protein produced was reduced (as previously mentioned). The same bias was also evident in reactions where all three products were co-expressed (Figure 3.3.c).

These levels of protein represent general trends in their expression/solubility over several independent experiments, although it should be noted that the total amount of MyoA produced varied quite widely from experiment to experiment, as determined by western blotting. This variation is likely due to inconsistencies in the quality of the transcription and translation preparations, given the multiple stages and the sensitivity of the process. Despite this, some soluble protein was always produced, enabling us to further investigate protein-protein interactions within the motor complex.

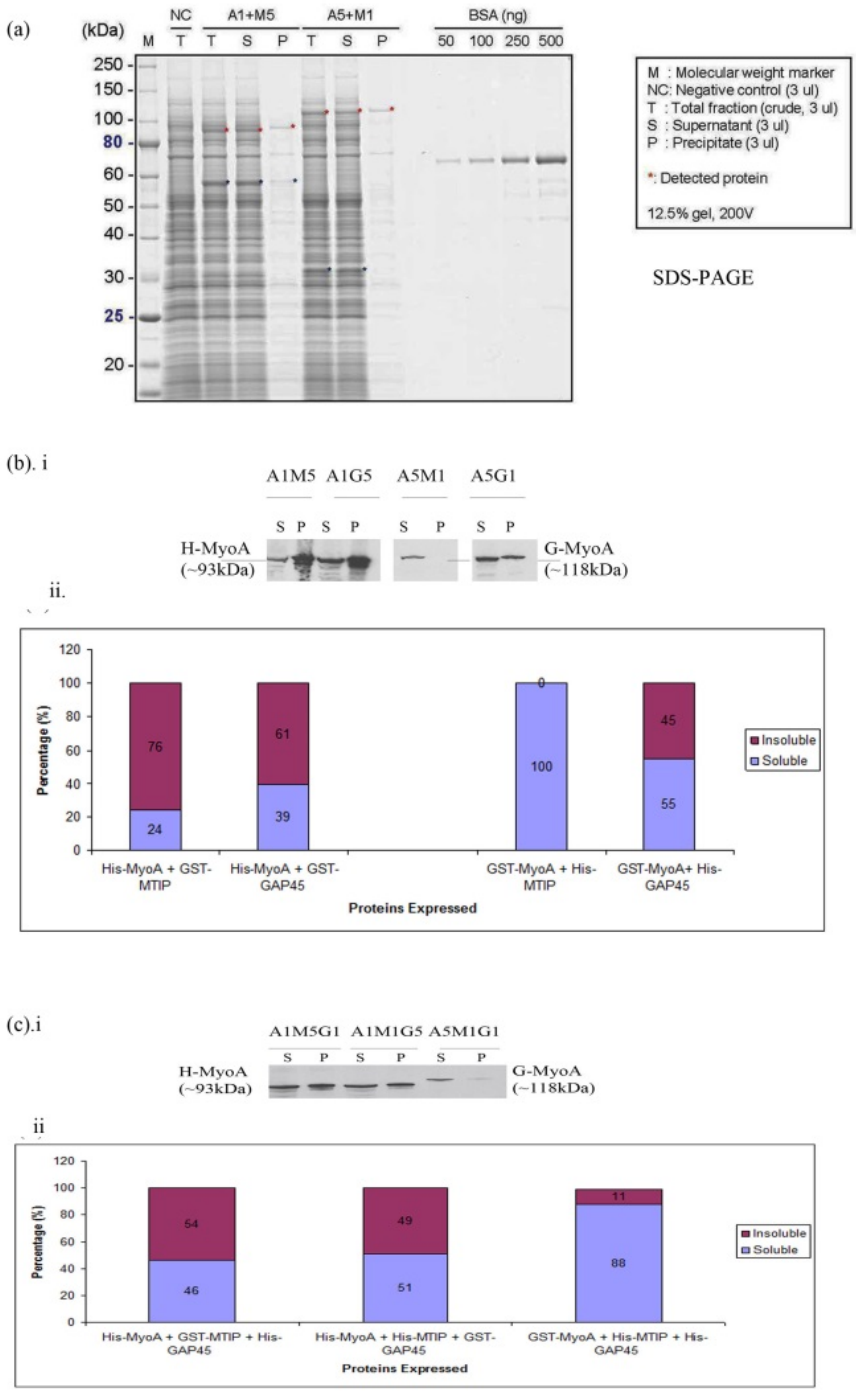

Figure 3.3: Protein co-expression in the cell-free system and determination of MyoA solubility. (a) Total protein from the wheat germ expression system resolved by SDS-PAGE and detected by Coomassie Blue staining following co-expression. His-MyoA coexpressed with GST-MTIP (A1+M5) and GST-MyoA co-expressed with His-MTIP (A5+M1); total reaction mix (T) and soluble supernatant (S) or insoluble precipitate (P) fractions following centrifugation were analysed together with a negative

control (NC) reaction. Molecular weight markers (M) are shown, together with their sizes (kDa) on the left side of the gel. Known amounts (ng) of BSA standard were used to gauge the amount of protein produced. Proteins of the expected size were present in the experimental samples and are highlighted (*). (b) Co-expression of MyoA with MTIP or GAP45 using different tags as detected by western blotting using α-MyoA antibodies (i). The bar chart indicates the percentage of MyoA in the soluble and insoluble fractions as determined by densitometry (Image J) (ii). (c) Expression of MyoA, MTIP and GAP45 all together. The percentages represent the relative expression of MyoA in pellet and soluble fractions in total translation. Western blots using α-MyoA antibodies (i) and bar chart (i) to indicate the amounts of MyoA in the soluble and insoluble fractions (as determined by densitometry). The amount of MyoA production was lower when all three protein were expressed together although the total solubility was increased.

3.2.3 MyoA forms a complex with MTIP but not with GAP45

To determine whether or not MyoA produced in the cell-free system is able to form a complex with other glideosome motor components, we performed pull-down assays using each of the components in the co-expression reactions to precipitate the other proteins from the complex. Although an interaction between MyoA and MTIP was observed using GST-MTIP in GST-pull down assays, this result could not be replicated with other tagging combinations (Figure 3.4). In addition no interaction between either MyoA or MTIP with GAP45 was detected (Figure 3.4).

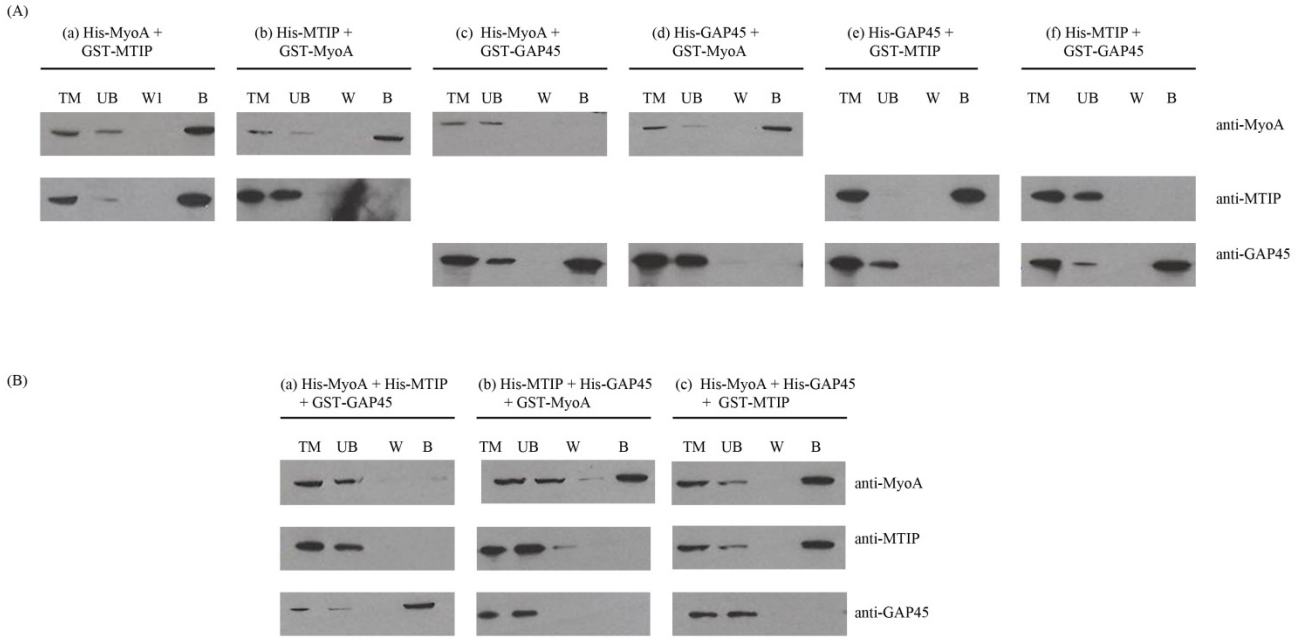

Figure 3.4 GST pull-down assays. Combinations of His- and GST-tagged proteins were co-expressed and used for GST pull-down assays, in which GST-tagged proteins were used to pull-down associated proteins. Precipitated proteins were resolved by SDS-PAGE, transferred to membrane and then probed for the presence of MyoA, MTIP and GAP45 using specific antibodies. (A) Reactions with two components co-expressed. (B) Reactions with all three components co-expressed. Specific interactions with MyoA were observed when GST-MTIP was used, indicating an interaction between these two proteins (in reactions where both MyoA and MTIP and all three proteins were expressed). No interaction was observed between GAP45 and either of the other two proteins. Western blots were probed with α-PfMyoA, α-MTIP and α-GAP45 antibodies. TM= total protein expressed, UB (unbound) = protein not bound to beads, W (wash)= protein after washing step and B (Bound) = protein bound to beads.

3.3 Characterization of single molecules and the sliding/gliding movement of MyoA

MyoA interacts with actin filaments to move the parasite forward during gliding motility or invasion into the host cell, and previous studies have focused on the crucial role of this type XIV myosin in parasite gliding motility. There have been several attempts to express in recombinant form and study the functional properties of MyoA (personal communication, Justin Molloy and Rachel Farrow, NIMR) However expression proved to be very difficult, the produced protein was truncated and improperly folded, and no activity was detected. We attempted to overcome these limitations using the wheat germ cell-free system. Having produced soluble MyoA in this study, we next investigated the functional properties of the protein, specifically its interaction with actin using a combination of motility- and actin binding assays, and also a single molecule study via optical trapping.

3.3.1 Movement of single MyoA molecules and the step size on an actin filament, measured in an optical trapping assay.

Optical traps (OT), also known as optical tweezers, are a system for manipulating refractive dielectric particles such as silica or latex beads, or biological materials such as cells (Ashkin et al., 1987). The technique uses a combination of proton pressure and electric field gradients generated when light of the same magnitude as the particle size, is directed at the particle. This effectively traps the particle and any displacement can be measured. In these studies we used a three-bead assay (Finer et al., 1994). Here an actin filament is suspended between two optically trapped beads and positioned in close proximity to a surface bead that has been coated with myosin (Ruff et al., 2001). This assay is best suited to studying the non-processive motors such as myosin II and XIV, which detach from actin during each ATPase cycle and remain in the detached state for the majority of the mechanical cycle.

An actin filament was suspended between two optically trapped beads and placed over a third, surface bound myosin coated bead. Any binding event can be

detected by the displacement of the beads. Upon myosin binding to the actin filament, the binding event can be detected by a decrease in the running standard deviation of the bead displacements (see Figure 3.5.a for details). MyoA binds to actin when ADP and Pi are bound in a reversible weak-binding state. On binding the ADP-Pi is released forming a strong actin binding complex. This effectively 'holds' the actin filament, restricting its Brownian motion, and is referred to as in a 'myosin bound' or in a 'rigor' state. Pi release occurs simultaneously with the power stroke (known as the 'event'). OT does not detect the power stroke directly but allows measurement of the displacement of the trapped beads attached to the actin filament. Following the power stroke, ADP is released. As mentioned earlier (Chapter 2, section 2.4.2, Figure 2.1), this release is associated with a further smaller power stroke, which can be also be detected by optical trapping nanometry. Following ADP release the myosin head is in a rigor state and tightly bound to the actin filament. Upon ATP binding the myosin cleft opens and myosin dissociates from the actin filament resulting in normal Brownian motion being restored. This is referred to as the 'myosin unbound' state (Figure 3.5.a-b).

In these studies we used GST-tagged MyoA principally because of its greater solubility. A total of 244 acto-myosin events were recorded in 2 µM ATP (a concentration based on the affinity of TgMyoA for 2'-/3'-O-(N'methylanthraniloyl)-ADP (mant ADP) (Herm-Gotz et al., 2002)). For ease of visualization the beads were moved backwards and forwards using a 10 Hz triangle wave applied to both beads and enabling us to observe approximately 20 interactions (Figure 3.5 c). This is considered to be an extremely low event occurrence compared to that of some other myosin studies, which typically reach into thousands of events (Ishijima et al., 1998). At this low frequency of interaction it needed to be established whether there was any specific myosin-actin interaction or were the changes noted due to a random association. To eliminate this possibility, we repeated the experiments using different ATP concentrations of 300 nM and 8 µM to induce variation in the period of actin-myosin interaction. At 300 nM ATP we expected to see interactions lasting on average 10 s^{-1} ($N_{filament}$ =1: $N_{obs=}$79) and at 8 µM ATP lasting 76 s^{-1} ($N_{filament}$=1: N_{obs}=165). This expectation was based on the principle that at higher ATP concentrations myosin would undergo increased ATP hydrolysis causing disassociation from actin and reducing the time of interaction. Conversely, in a low ATP environment ADP will remain bound to

the myosin head longer and in turn the myosin will remain bound to the actin filament longer (Figure 3.5.d, also see Chapter 1, Figure 1.1.7). The results showed that the interactions detected in these experiments are true interactions between MyoA and actin filament. Even though the results were not ideal due to the low frequency of events, the data were sufficient to show that MyoA was binding to actin filaments. Furthermore, by measurement of the lever-arm displacement induced on ATP hydrolysis (referred to as 'displacement') we observed a shift of ~3 nm (range of ~2-5 nm) (Figure 3.5.e). This displacement is similar to the *T. gondii* MyoA shift (~5 nm) and that of skeletal muscle myosin II (~4.8 nm) (Herm-Gotz et al., 2002; Molloy et al., 1995). Overall these data indicate that some of the MyoA produced in the cell-free system is active.

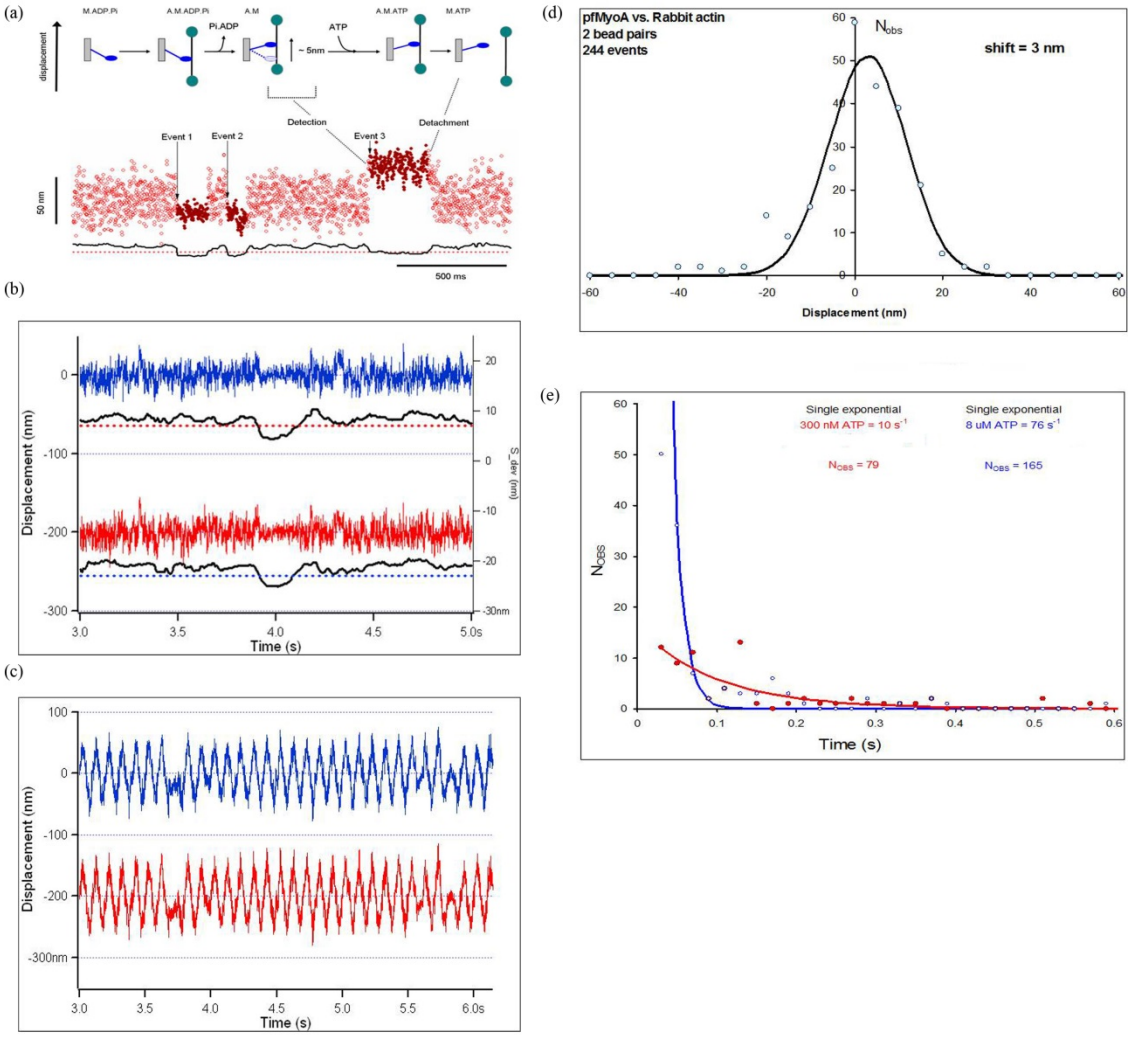

Figure 3.5 Study of MyoA single molecules as measured by optical trapping. (a): illustrated diagram of the acto-myosin 'event' as determine by OT. The actin filament

was held between 2 beads (circles coloured green); a left hand bead and a right hand bead. The third bead (square grey shape) held the MyoA molecule (coloured blue). The background displacement movement (noise) seen is due to Brownian motion. Event1, Event 2 etc. were marked decreases in the standard deviation of the displacement due to the myosin head binding to the actin filament. (b) Acto-myosin 'event' as determine by OT with MyoA. The movement of bead one (the right hand bead) is shown in blue. The movement of the left hand bead is shown in red (and offset by -200 nm for display purposes). The standard deviation for both beads is shown in black (black line). The standard deviation of the left hand bead is offset by -30 nm. The sudden decrease in standard deviation (dash lines) indicates that MyoA bound to the actin filament. Movement below the dotted red/ blue line indicates an 'event' (bound MyoA) whereas above the dotted red/blue line no 'events' were recorded and the MyoA remained 'unbound'. (c) To make the effects easier to visualise, the beads were moved backwards and forwards using a 10Hz triangle wave. (d) MyoA displacement histogram collected for acto-myosin events and fitted Gaussian distribution. On the x-axis is the average of the beads held in the optical trap during binding. The y-axis is the number of observations at that value (N_{obs}). The displacement of MyoA was detected as 3 nm. If MyoA only bound actin and did not do anything, the expected histogram would have a maximum at zero. (e) MyoA lifetime displacement distribution histogram**.** The x-axis is the duration in seconds of the binding events; the y-axis, is the number of observations at that value when the event occurred. The data at 300 nM are in red and the 8 μM data are in blue. This duration of event was fit to a single exponential as the myosin-actin binding is a 'stochastic' process.

3.3.2 Characterisation of the MyoA-actin interaction

Knowing that single MyoA molecules were capable of actin binding and movement, next we carried out motility assays to observe actin filament gliding and to determine translocation velocity. The motility assay displays the sliding/gliding of actin filament caused by myosin bound to a solid substrate (the coverslip). Actin labelled with Rhodamine-Phaloidin (RhPh) forms filaments that are observed via fluorescence microscopy and their movement can be tracked, enabling calculation of myosin speed/velocity.

GST-MyoA was used for the *in vitro* motility assay and rabbit skeletal heavy mero myosin (HMM) was used as a control. In a control experiment, rabbit F-actin bound strongly to HMM (~40 µg/ml) and upon addition of ATP, moved at a velocity of 2.9 µm/s. However, with GST-MyoA (~48 µg/ml) although there was an indication that the MyoA was binding to actin, on addition of 2 µM ATP the actin filaments were washed off of the surface. Although no gliding was seen, the loss of the actin from the surface provides some indication that MyoA was functional, as in the presence of ATP the myosin head will release actin. Unfortunately, it is unclear why they do not rebind following ATP hydrolysis as this is the normal behaviour enabling actin translocation. In an attempt to increase binding the MyoA concentration was increased, however, even at ~92 µg/ml, there was no indication of gliding movement (Figure 3.6).

A series of optimisations was performed in an attempted to improve the conditions for gliding movement. For example, we reasoned that using a combination of MyoA/MTIP might help MyoA translocate actin, allowing gliding movement to be observed and recorded. MyoA lacks the long tail that normally binds to cargo but possesses a neck, which binds to MTIP (Green et al., 2006b) and MLC1 in *Toxoplasma*, bringing MyoA to its site of action. Other changes included immobilisation with MTIP antibody and adding methylcellulose to the scavenger buffer, AB+, to restrict the diffusion of actin filaments away from the surface of the cover slip when the effective MyoA concentration used was too low for smooth motility. Although MyoA showed properties characteristic of actin-binding as mention above (MyoA bound to actin filaments in the absent of ATP), unfortunately we failed to observed any gliding movement under the new conditions. We further investigated the actin-myosin interaction by performing the most straight forward assay, which takes advantage of the ability of actin to co-sediment MyoA on ultracentrifugation (Dobrowolski et al., 1997b). This method is based on a simple observation which is that if MyoA binds to actin in the absence of ATP, then by ultracentrifugation MyoA-actin will co-sediment in the pellet fraction. Conversely in the presence of ATP, MyoA will be in the soluble fraction, while actin will be pelleted. Following analysis of these fractions by Western blots probed with specific antibody to actin and MyoA, none of these expectations were fulfilled (data not shown), and therefore this experiment also failed to show MyoA-actin binding.

Since MyoA was soluble and functional as showed by OT, but failed to promote actin filament gliding in the motility assay, and the inconclusive result of MyoA-actin binding in the actin sedimentation assay, we decided to look at the interaction of actin with MyoA by transmission Electron Microscopy (EM). This experiment was carried out with help from Ms Lesley Calder (Physical Biochemistry, NIMR). EM should enable us to see the MyoA bound to or decorating the actin filament. The result obtained indicated that MyoA was abundant in the sample preparation but unfortunately most of it seemed to be aggregated or precipitated. Therefore, the expected decoration of the actin filament was rarely seen (Figure 3.6). Finally, the unfolded structure of MyoA was confirmed by Far UV circular dichroism (CD) analysis (data not shown). Taking into consideration all of the results obtained, we decided not to investigate further this MyoA produced in the cell free system.

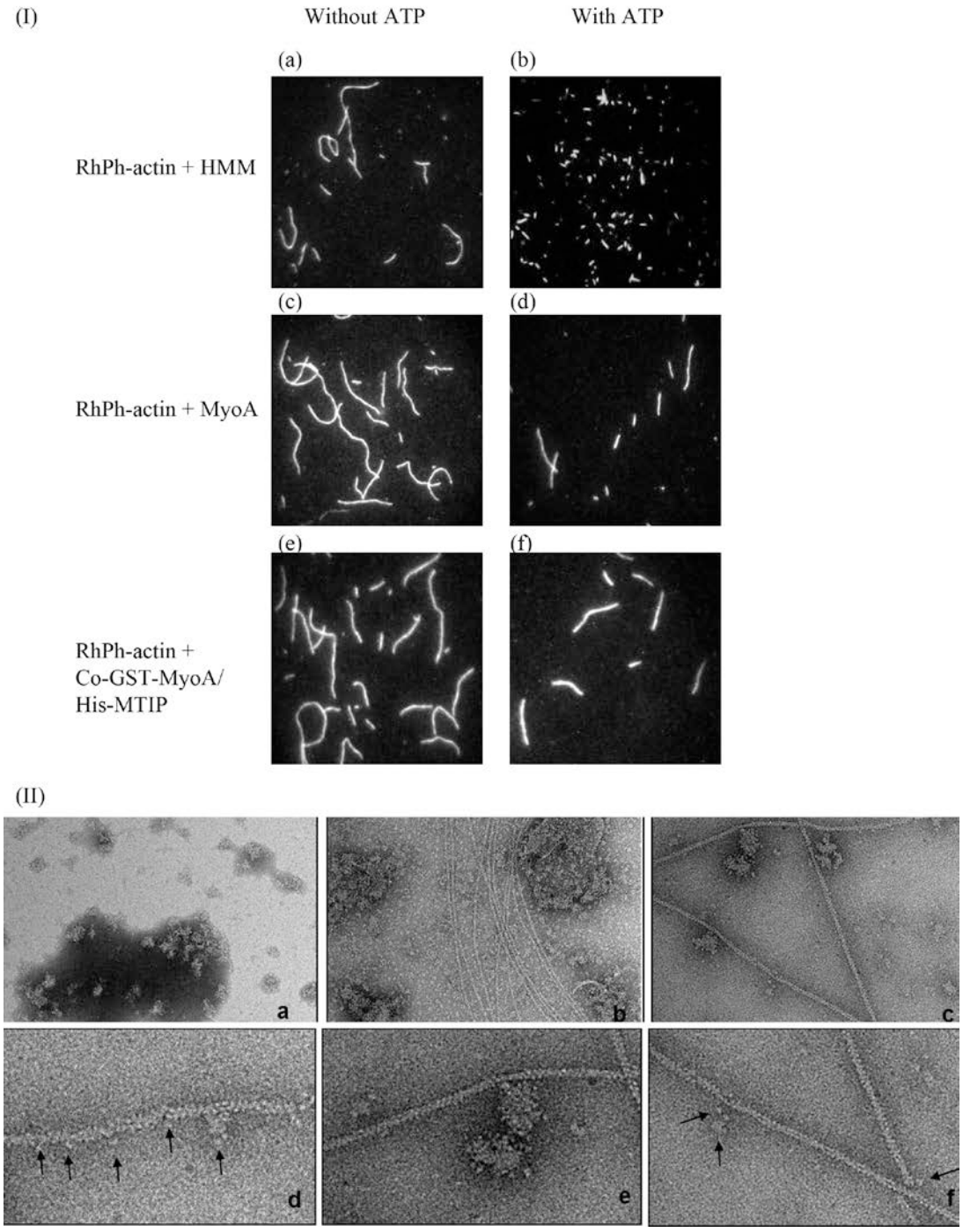

Figure 3.6 Actin-Myosin interactions. (I) (a and b) Control experiments using RhPh labelled rabbit actin (RhPh-actin) and rabbit heavy-meromyosin (HMM) in the presence or absence of ATP. Upon addition of 2 µM ATP, HMM translocated actin filaments with an observed gliding velocity of 2.8 µm s^{-1}. (c and d) RhPh-actin and MyoA in the presence or absence of ATP. Upon addition of ATP, actin filaments were washed away as the MyoA head released the actin filament, with no evidence of re-binding or gliding

motility. (e and f) A combination of GST-MyoA and His- MTIP with and without ATP. As with the MyoA alone, the addition of ATP allowed the actin filaments to be washed away indicating that the presence of MTIP caused no additional improvement to activity. (II) Transmission EM of expressed MyoA and actin filaments. (a) MyoA alone; protein was abundant but highly aggregated. (b) Actin alone; a control showing long filaments of rabbit skeletal actin. (c) MyoA mixed with rabbit-actin filaments; only a small proportion of the MyoA was observed bound to actin filaments with the majority of the protein aggregated. (d-f) Expanded images from that shown in (c) showing some MyoA molecules (arrows) decorating actin filaments.

3.3 Discussion

The aim of this study was to produce soluble MyoA protein that could be used to reconstitute the invasion motor complex in a test tube. An additional aim was to study protein-protein interactions and the functional properties of MyoA in association with glideosome complex proteins, and the interaction with actin.

In order to rebuild the glideosome complex *in vitro*, we required a soluble and functional MyoA protein together with the associated glideosome complex proteins, MTIP and GAP45. These two proteins had been established to be in association with MyoA as a part of the invasion machinery during parasite invasion (Baum et al., 2006b; Bergman et al., 2003; Gaskins et al., 2004; Herm-Gotz et al., 2002). MyoA has proved to be difficult to express in a folded form using heterologous recombinant systems (personal communication with Rachel Farrow and Justin Molloy, NIMR). However, no attempted had been made to express MyoA in the wheat germ cell free extract, and therefore this system was our choice to produce soluble MyoA protein. Using this system we produced MyoA, MTIP and GAP45 individually. We also produced MyoA co-expressed with MTIP or GAP45, or all three proteins expressed together. Previously MTIP and GAP45 had been expressed successfully in another heterologous system, however it was important to produce all the protein in the same system as they needed to be synthesized together for the purpose of establishing an *in vitro* protein-protein interaction study using pull down assays.

The results showed that MyoA and MTIP would associate when expressed together *in vitro*, but no interaction was detected between MyoA and GAP45 and between MTIP and GAP45. The interaction of between MyoA and MTIP has been well studied previously (Bergman et al., 2003; Green et al., 2006b; Thomas et al., 2010) , but not in this format. Tagging at the N-terminus of MyoA was used so as not to affect the binding to MTIP, since the MyoA-MTIP interaction occurs at the extreme C-terminal end of MyoA. Direct interaction, either between MyoA and GAP45 or MTIP and GAP45, has never been reported (Bosch et al., 2006; Bosch et al., 2007b; Green et al., 2006b; Thomas et al., 2010). Frenal et al (2010) showed that the N-terminal region of *T. gondii* MLC1 (the orthologue of MTIP) was important for interaction with GAP45 and the GAP45 C-terminal domain was essential to recruite MLC1 and indirectly MyoA to the IMC.

The study was extended to investigate the functional properties of the MyoA produced and its interaction with actin using OT and gliding motility assays. A single molecule study using OT showed that the MyoA was functional due to the detection of interactions occurring with actin during this assay. Although the binding to actin or the detection of a working stroke (displacement) was not extensive due to the very few binding events (244 events examined during this study), a working stroke of ~3 nm was measured. The number of events was ten times lower compared to what was found in studies on other myosins such as myosin II (Ishijima et al., 1998). However, the results are comparable to what was reported with TgMyoA (598 events, with a measured working stroke of ~5.3 nm), for PfMyoA from a parasite lysate (measured working stroke, 4.7 nm; Rachel Farrow, NIMR, unpublished data) and with myosin II (working stroke ~5-6 nm; (Veigel et al., 1999)). It is possible that the presence of MTIP on the MyoA from the parasite lysate increases the binding with the actin filament, helped by the unusual extended conformation of MTIP which can completely wrap around the IQ motif. In addition the lever arm may be extended into the myosin head adding a further 2 nm to the lever arm length (if PfMyoA goes through a $60/70^{o}$ lever arm swing as in myosin II, then the lever arm will be greater than 5 nm which could easily explain the 4.7 nm power stroke, Rachel Farrow personal communication and (Farrow, 2007)).

Generally *Apicomplexan* MyoA has a very short or almost no tail domain (Chaparro-Olaya et al., 2005; Hodge and Cope, 2000), but still they can propel the

parasite at speeds of 0.05 to 0.1 μm s^{-1} and move actin filaments at an average velocity of 3.5 μm s^{-1} (Herm-Gotz et al., 2002), 3.51 μm s^{-1} (Green et al., 2006b) and 3.0 μm s^{-1} (Schmitz et al., 2005) in an *in vitro* motility assay using parasite lysate. Here, we expected to see the gliding movement of F-actin at this velocity by MyoA produced from the *in vitro* expression system. There was no question about the concentration of MyoA added to the flow cell, or the density of attachment to the motility surface because MyoA was produced in sufficient abundance. However we failed to detect movement, most likely because most of the MyoA was aggregated and unstructured as shown in the EM micrograph, and later confirmed by CD.

We had also intended to explore the regulation of MyoA by phosphorylation with kinases such as CDPK1, PKA and PKG and the possibility to extend the study into investigating the effect of MyoA phosphorylation during motility assay or optical trapping as well as analysis of the sites of modification by mass spectrometry. CDPK1 and PKA is believed to phosphorylate MyoA (Lasonder et al., 2012) and CDPK1 had been shown to phosphorylate MTIP and GAP45 (Gilk et al., 2009; Green et al., 2006b; Rees-Channer et al., 2006; Ridzuan et al., 2012). Unfortunately, due to the failure to demonstrate that the MyoA produced in the *in vitro* system was able to support actin motility, planned future experiments including studies of MyoA regulation *in vitro* were abandoned.

As a conclusion, we felt that this aspect of the project could not go any further at this time. It proved impossible to reconstitute the motor complex *in vitro* because the experiments could not be performed with unstructured protein. In the future it is possible that fresh approaches might allow this, but for now new directions were required and the focus this project shifted to using transgenic parasites to address all the questions which we lay out in our aims.

Chapter 4

Characterisation of Myosin A and Myosin B in asexual blood stages of *Plasmodium*

4.1 Introduction

It has been previously established that MyoA is involved in the glideosome motor complex in both *Toxoplasma* and *Plasmodium*. In previous studies both TgMyoA and PfMyoA have been shown to be localised to a space between the plasma membrane and the IMC, where the glideosome motor complex is thought to lie. MyoA is expressed during late schizogony, almost at the same time as the other glideosome proteins, GAP45, MTIP/ MLC1 and GAP50, thus MyoA is found at the right time and place, which is during parasite segmentation and the assembly of the glideosome complex, consistent with the parasites gearing themselves up for invasion of the host cell (Baum et al., 2008a; Gilk et al., 2009; Herm-Gotz et al., 2002; Hettmann et al., 2000; Johnson et al., 2007; Pinder et al., 2000). Furthermore, genetic knock down of MyoA in *Toxoplasma* tachyzoites (Meissner et al., 2002) and *Plasmodium* ookinetes (Siden-Kiamos et al., 2011) was shown to abrogate gliding motility, impairing both egress and host cell invasion, whereas no effect on intracellular replication or secretion of micronemal proteins was observed, consistent with a role in the glideosome complex (Meissner et al., 2002; Siden-Kiamos et al., 2011; Soldati and Meissner, 2004). The failure to express functional MyoA *in vitro*, using the cell free system (Chapter 3), prevented further *in vitro* characterisation of the MyoA motor complex. However, the role of MyoA in merozoite red blood cell invasion is still unclear and the motor complex may also play a role beyond invasion, for example in cytokinesis in the segmenting schizont, so further examination of its function *in vivo* was warranted. Little is known about the function of the other type XIV myosins. MyoB, for instance, is the smallest myosin in this particular myosin class. PfMyoB has been described as expressed in late schizonts and merozoites and therefore may also be involved in

invasion (Chaparro-Olaya et al., 2005). However, the precise location of MyoB and its function are still unknown.

A key technology for exploring protein trafficking and localisation is the use of reporter molecules such as GFP. This method has given valuable information on protein localisation in *Plasmodium*. The technique relies on genetic manipulation to create a transgenic parasite encoding the GFP sequence introduced within or at the N- or C-terminus of the ORF. Transgenic parasites are generated by transfection – the introduction of foreign DNA into the parasite in order, for example, to alter normal gene expression. Transfection of *Plasmodium* blood stage parasites has been developed relatively recently and requires the translocation of DNA through four membranes before finally reaching the nucleus, making transfection of *Plasmodium* a difficult and complicated technique (Carvalho and Menard, 2005). For integration of the DNA into the genome, a single or double cross-over recombination event can occur; this relies on a vector carrying a homologous sequence to facilitate targeting to locus by homologous recombination as well as a positive selection cassette conferring drug resistance (Waterkeyn et al., 1999). Fortunately, the methodology has been improved significantly since the first reported transfection of zygotes and gametocytes, which was done in the absence of a drug selection cassette in the avian malaria parasite, *Plasmodium gallinaceum* (Goonewardene et al., 1993). Wu and colleagues managed to transfect ring stage parasites which lead to the transformation of *P. falciparum* by homologous integration into the genome (Wu et al., 1996; Wu et al., 1995). Using this approach, DNA is able to be maintained transiently as an episome or integrated into the parasite's haploid genome (Crabb et al., 1997; Wu et al., 1996).

Transfection has also been highly successful in other malaria parasite species, for example rodent malaria parasites, particularly in *P. berghei* (van Dijk et al., 1995), but also in other rodent malaria such as *P. yoelii* (Ono et al., 2007) and *P. chabaudi* (Reece and Thompson, 2008; Spence et al., 2011). *P. knowlesi* transfection can be performed successfully in *in vitro* culture either with monkey blood (Kocken et al., 2002) or using *P. knowlesi* A1-H.1, a parasite clone recently adapted to culture in human blood (Moon et al., 2013). Genetic manipulation of *P. knowlesi* is an important new tool to study malaria parasites as this species is phylogenetically close to *P. vivax*, which lacks an *in vitro* culture system, and is itself a human malaria pathogen, causing a large number of cases of infection in South-East Asia (Cox-Singh et al., 2008). *P.*

knowlesi also has the experimental advantage of being a bigger parasite, which is more amenable to genetic manipulation than *P. falciparum*, and therefore the parasite's asexual blood stages are more tractable to study (Moon et al., 2013). The recent development of improved transfection methods such as the use of the Amaxa electroporation system (Janse et al., 2006) and new selectable markers (de Koning-Ward et al., 2000; Wel et al., 2004), has increased transfection efficiency and facilitated the possibility of double and triple transfectants. Together with whole genome transcript profiling and proteomic analysis, the production of transgenic parasites (for example gene knockouts, allelic replacements and transgene expression) will be a very valuable functional analysis tool.

In this chapter, attempts to GFP-tag both MyoA and MyoB and the characterisation of the resultant transgenic lines are described. This was carried out in order to localise the fusion-protein within the parasite as well as to identify potential interacting proteins and improve our understanding of the roles of MyoA and MyoB in host cell invasion by *Plasmodium*. The GFP-tag allows direct visualisation of the endogenous protein in live parasites using epifluorescence microscopy and avoids the need for protein-specific antibody generation. Using these transgenic parasites, the expression of MyoA and MyoB throughout the asexual blood stage cycle of *P. falciparum* was analysed. First, the fusion proteins were localised within the parasite by live imaging and IFAs relative to known organelle marker proteins; second, immunoprecipitation and mass spectrometry studies were undertaken to explore potential associations with other proteins or protein complexes; and third to establish the role and localisation of MyoA and MyoB during parasite invasion into the host cell, in comparison with the established marker of the moving junction, RON4. Further characterisation of MyoA and MyoB was performed by GFP-tagging of both proteins in *P. knowlesi* in order to enhance their microscopic visualisation as the merozoites are bigger in size than those of *P. falciparum*, and to confirm the similarity across the genus. For the same purposes, we also generated MyoA- and MyoB-specific antibodies to be used in co-localisation studies and to be used in other techniques such as Western blotting and immunoprecipitation.

4.2 Production and Genotyping of GFP-tagged MyoA (PfMyoA) and MyoB (PfMyoB) *P. falciparum* parasite lines

The GFP-tagging of the endogenous MyoA and MyoB genes of *P. falciparum* was achieved by integration of DNA constructs, via single crossover homologous recombination, into the parasite's genome. In order to introduce the GFP tag at the C-terminus of each protein, a region of homology corresponding to 1057bp (MyoA) and 1069bp (MyoB) from the 3' end of each ORF and lacking the stop-codon was selected. The region of homology was amplified from genomic DNA by PCR using primer combination 3F1/3R2 for MyoA and 4F1/4R2 for MyoB (Chapter 2, Table 2.2). These regions of homology were cloned between the XmaI/AvrII sites of the pHH4-GFP plasmid (Knuepfer et al., unpublished) and the correct sequence confirmed by Sanger sequencing (Beckman Genomics), generating the constructs pHH4-PfMyoA-GFP and pHH4-PfMyoB-GFP, respectively. In each case the cloning resulted in the targeting fragment being placed upstream of the GFP ORF followed by the Pbdhfr 3'UTR. The strategy for integration is summarised in Figure 4.1 for MyoA and Figure 4.2 for MyoB. The pHH4-GFP transfection vector map which includes the human DHFR resistance cassette as a selectable marker is depicted in Appendix B- pHH4-GFP vector.

Genomic integration of DNA constructs is generally achieved in *P. falciparum* through transfection of episomal constructs, followed by cycles of drug selection to select for the rare integration events. In each cycle drug pressure is withdrawn for a period of time to allow plasmid loss, and then resistant parasites are reselected by reapplication of drug pressure. Removal of drug pressure results in loss of episome over time due to uneven segregation of plasmid in daughter cells (Waterkeyn et al., 1999), whereas integrant parasites grow steadily during this time. Normally several cycles of drug pressure are required taking at least ~ 3 months. This compares to *P. knowlesi* and *P. berghei* to which the integrant can be obtained in ~3 weeks. The lengthy period of time is due to the procedure used to select for integration (de Koning-Ward et al., 2000; Tonkin et al., 2004), which in turn is required due to the extremely low efficiency of both transfection and genomic integration in *P. falciparum*.

After transfection with 100 µg plasmid DNA for each construct into ring stage parasites, 2.5 nM WR99210 was added and the parasites cultured continuously under drug selection for approximately 3 weeks. The parasites that grew after this time were

designated cycle 0, and whilst resistant to WR99210, as expected, this was predominantly due episomal maintenance of the targeting construct. The transfected cultures were then grown for 3 weeks without drug selection, to allow loss of the episomal construct (due to uneven segregation of the episome) followed by a further week of growth under WR99210 selection again. The resultant parasite populations were designated cycle 1 and this was repeated a further time; parasites were obtained from cycle 2 for both MyoA and MyoB. Cultures were checked after each cycle for integration of the construct by both diagnostic PCRs and monitoring for GFP expression. The MyoA and MyoB fragments cloned into the transfection vectors lack a promoter, thus the GFP tagged version can only be expressed once the plasmid has integrated and expression can be driven by the endogenous promoter. This means that expression of GFP can be taken as a strong indication of correct integration of the plasmids.

4.2.1 PfMyoA-GFP parasites: cloning and genotyping

GFP-expression was detectable in the PfMyoA-GFP transfected parasites as early as in cycle 1, and in the PfMyoB-GFP transfected parasites in cycle 2. Correct integration in the un-cloned lines was confirmed by PCRs (data not shown). Preliminary live fluorescent imaging of PfMyoA-GFP showed strong GFP fluorescence associated with the periphery of developing merozoites, providing further evidence for the correct integration of the tagging construct. Western blots of PfMyoA-GFP parasite lysates, probed with an anti-GFP antibody also confirmed the MyoA fusion protein was at the expected ~120kDa size (Figure 4.3). The PfMyoA-GFP parasites were then cloned by limiting dilution and 6 clones (C1-C6) screened for integration by PCR. One single band was detected for each cloned parasite when using the 1/GFP primers for detection of parasite integrants, whereas, when using primers 1/2 to detect wild type sequence, none of the cloned parasites produced a band. These data indicate that all the clones produced contain the construct integrated into the parasite genome. The integrant clones were further validated by Southern blotting, where the expected band for integration was detected in four cloned lines tested. The same band was also visible in cycle 0 (A0), suggesting that integrated parasites formed a high proportion of the parasites even at this early stage. A band diagnostic of wild type was present only in

the 3D7 parasites; therefore the PfMyoA-GFP sequence was integrated correctly by homologous recombination into the genomic locus (Figure 4.1).

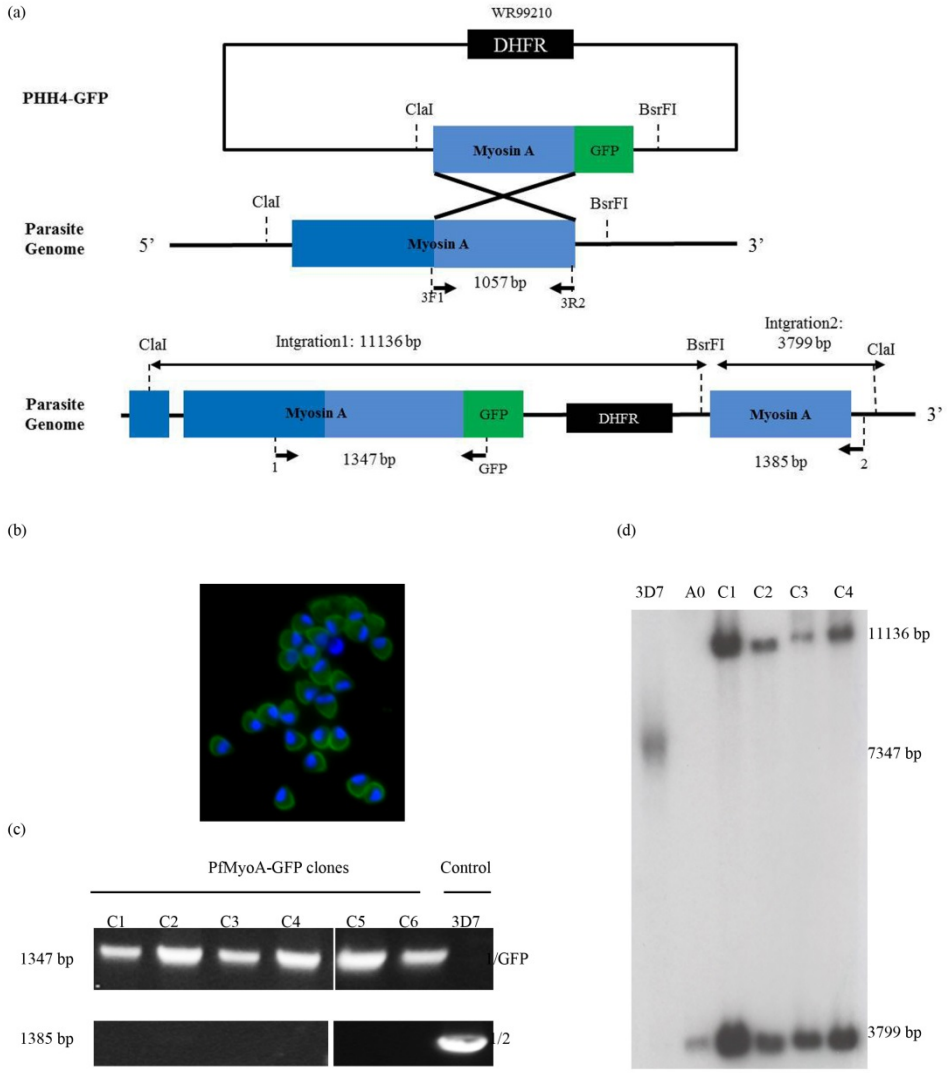

Figure 4.1: Generation of parasites expressing PfMyoA-GFP. (a) Schematic representation of the GFP tagging of MyoA by single cross-over homologous recombination into the MyoA locus, with primers for PCR (arrows with primer 3F1/3R2) and Southern blot probe and restriction sites labelled. (b) The uncloned PfMyoA-GFP parasites as viewed by live fluorescence microscopy. Merge of GFP and DAPI channels shows that GFP signal is distributed to the parasite periphery in schizonts. (c) Diagnostic PCR on genomic DNA showing integration of PfMyoA-GFP (Primers 1/GFP) and wild type (Primers 1/2).Six PfMyoA-GFP clones (C1to C6) were

examined. (d) Southern blot analysis of cloned PfMyoA-GFP parasites. Probes to the 5' homologous flanking region gave the expected two integration bands at 11136 bp and 3799 bp. A0: PfMyoA-GFP parasites at cycle 0 and 3D7 is the wild type control (7347 bp).

4.2.2 PfMyoB-GFP parasites: cloning and genotyping

Genotyping of PfMyoB-GFP parasite was carried out in the same way as for PfMyoA-GFP. Diagnostic PCR was performed initially on the un-cloned PfMyoB-GFP parasites, and then later with cloned parasite lines using primers for integration (3/GFP). The PfMyoB-GFP parasites were cloned by limiting dilution and 3 clones (C1-C3) screened for integration. Integration was detected by diagnostic PCR, indicating correct integration of the PfMyoB-GFP construct into the MyoB locus on chromosome 5. The integration PCR consistently produced a doublet band, despite the use of several alternative forward primers in the PCR (Table 2.2). We also used primer 1/GFP, a primer set designed for PfMyoA, in order to eliminate the possibility that the PfMyoB-GFP construct had additionally integrated into the MyoA locus, and the result was confirmed by Southern blot Southern blot analysis revealed that two bands for integration were detected in all clones as predicted (7994 and 5439 bp). Interestingly, an additional band at the same size as the episomal transgene band was also present in two clones of PfMyoB-GFP (clone C1 and C3). As our strategy targets the locus using single crossover homologous recombination, it is possible for multiple copies of the plasmid to integrate into the target locus. In the current result, the additional band of episomal size might indicated either the maintenance of an episomal construct in addition to the integrated copy or it might be due to multiple copies integrated into the targeted locus. Fortunately, an episomal transgene will not interfere with the one integrated into the genome and can be removed by reapplication of drug pressure cycling until loss. In wild type 3D7, only a band corresponding to the endogenous gene sequence was detected and in cycle 0 (B0), two bands were detected which correspond to this wild type and an episomal copy, therefore PfMyoB-GFP was detected as an integrant in the correct locus (Figure 4.2). Expression of GFP was detectable in the PfMyoB-GFP transfected parasites during cycle 2, (although Southern blot indicated that integration was detectable as early as in cycle 1).

Preliminary live fluorescence imaging of PfMyoB-GFP showed GFP fluorescence in the developing merozoite. However, this technique revealed a very different localisation compared to that of PfMyoA-GFP (Figure 4.2). Even though the GFP fluorescence signal was seen, it was less strong than that of PfMyoA-GFP and faded very quickly. In this preliminary observation, the PfMyoB-GFP signal seemed to locate to a single discrete dot possibly at the apical end of merozoites in mature schizonts. Although the localisation of PfMyoA-GFP was very easily observed and monitored, work with PfMyoB-GFP was a challenging task: the fluorescence signal bleached rapidly in only a few seconds. Finally after several attempts, we managed to capture live images of PfMyoB-GFP parasitesby using only transmitted light to focus the microscope and setup the cell to minimize exposure to UV light before the images were collected. Western blots of PfMyoB-GFP parasite lysate, probed with an anti-GFP antibody confirmed that the MyoB fusion protein was at the expected ~120 kDa size (Figure 4.3).

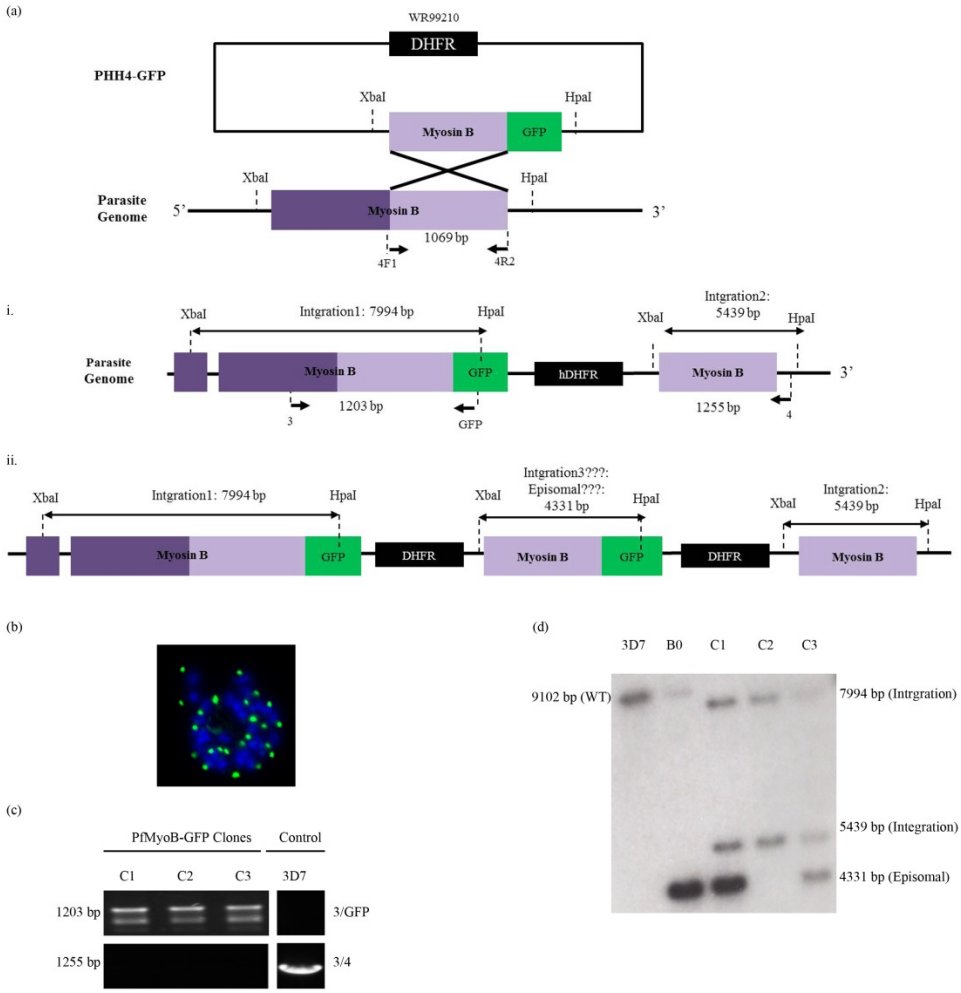

Figure 4.2: Generation of parasites expressing PfMyoB-GFP. (a) Schematic representation of the GFP tagging of MyoB by single cross over homologous recombination into the MyoB locus with primers for PCR (arrows: 4F1/4R2) and Southern blot probe and restriction sites labelled. An additional schematic (a. ii) shows the result of possible integration of multiple plasmid copies into the same locus. (b) The uncloned PfMyoB-GFP parasites as viewed by live fluorescence microscopy. The merge of GFP and DAPI channels shows that GFP signal is localised to the parasite apex in schizonts. (c) Diagnostic PCR on genomic DNA showing integration of PfMyoB-GFP (Primers: 3/GFP) and wild type (Primers: 3/4). Three PfMyoB-GFP clones (C1 to C3) were examined. (d) Southern blot analysis of cloned PfMyoB-GFP parasites. Probes to the 5' homologous flanking region gave the expected two integration bands at 7994 bp and 5439 bp. PfMyoB-GFP Cycle 0 (B0) shows the presence of wild type (9102 bp) and episomal (4331 bp) bands; 3D7 parasites only show the wild type band.

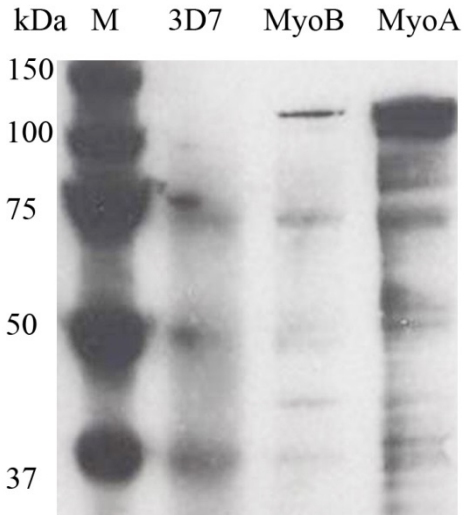

Figure 4.3: Western blot of uncloned transgenic parasites. Bands corresponding to PfMyoA-GFP (MyoA) and PfMyoB-GFP (MyoB) were clearly detected in the corresponding parasite lysate, whereas no band detected in the wild type (3D7). Schizont lysates were probed with α-GFP.

4.3 PfMyoA-GFP is part of the established glideosome motor complex whereas PfMyoB is not

To determine whether PfMyoA-GFP and PfMyoB-GFP participate in the glideosome motor complex, we can use anti-GFP antibodies to immunoprecipitate the motor complex components from the transgenic parasite lines. Mature schizont-stage parasites were enriched and solubilised using an NP-40 containing buffer. Soluble lysates were immunoprecipitated with α-GFP antibodies coupled to agarose beads. The GFP antibodies should only bind the GFP-tagged protein, and wild type 3D7 parasites, prepared in the same way, can be used as negative control. The GFP-TRAP (Chromotek) system utilises camelid monoclonal anti-GFP "nanobodies". Camelid antibodies do not contain a light chain and the heavy chain variable region is sufficient for highly specific antigen recognition. Nanobodies are composed of only these short

variable regions and so are highly stable and only 13 kDa in size. Since cross reactivity is a common problem with many antibodies, this GFP-TRAP is very suitable for the purposes of this experiment.

4.3.1 MyoA-GFP is precipitated with the protein of glideosome motor complex

When a Western blot of the precipitated samples was probed with a GFP-specific mouse mAb, bands corresponded to PfMyoA-GFP and PfMyoB-GFP (both ~120 kDa) were detected. There was band detected in lysates from wild type 3D7 parasites. The relative intensity of the bands in the two parasite samples indicated that PfMyoA-GFP is much more abundant than PfMyoB-GFP, as an equal amount of total parasite protein was loaded in each case. This is unsurprising when considering the live imaging data described above. The PfMyoA-GFP immunoprecipitate also contained both PfGAP45 and PfGAP50. Rabbit α-GAP45 detected a doublet band at ~37 and 39 kDa, while rabbit α-GAP50 detected a ~42 kDa band corresponding to GAP50.

The precipitated lysate also contained MTIP, as a rabbit α-MTIP antibody detected a band at ~27 kDa. These data demonstrated that PfMyoA-GFP is in the glideosome motor complex together with endogenous MTIP, GAP45 and GAP50 (Figure 4.4a). On the other hand, when the same antibodies were used to probe the PfMyoB-GFP precipitated lysate no MTIP, GAP45 or GAP50 was detected. None of the glideosome complex proteins was precipitated together with PfMyoB-GFP (Figure 4.4a) demonstrating that MyoB does not form a complex with the same proteins as MyoA. This co-immunoprecipitation was carried out in the absence of Ca^{2+}, and therefore any Ca^{2+}-dependent proteins potentially associated with the glideosome motor complex, such as calmodulin, would not be co-precipitated with the GFP-tagged protein. There are also other proteins that are known to bind with the glideosome complex in either *Plasmodium* or *Toxoplasma* such as GAP40, GAP70 and GAPMs, however we currently lack antibodies to these proteins.

To confirm the co-localisation of PfMyoA-GFP with the glideosome motor complex, we performed IFA on the transgenic PfMyoA-GFP parasite. It is critical for the proposed function for PfMyoA-GFP to be located at the parasite's periphery,

between the PM and IMC. To determine whether this is indeed the case, we used our specific antisera to each glideosome sub unit (MTIP, GAP45 and GAP50) and mouse monoclonal α-GFP (for MyoA) for an IFA analysis of late schizonts and merozoites of the clonal PfMyoA-GFP line. The PfMyoA-GFP signal was concentrated around the periphery of each merozoite, both within schizonts as well as free merozoites. As expected, all subunits of the putative glideosome complex were also confined to the periphery of the parasite pellicle, overlapping with PfMyoA-GFP. Co-staining with antiserum against RON3, which labels the rhoptries at the very anterior end of the parasite, suggested that the glideosome protein complex is co-localised with the IMC, as the components are present around a major proportion of the parasite periphery, consistent with their proposed role as members of an active motor complex that drives parasite invasion (Figure 4.4b).

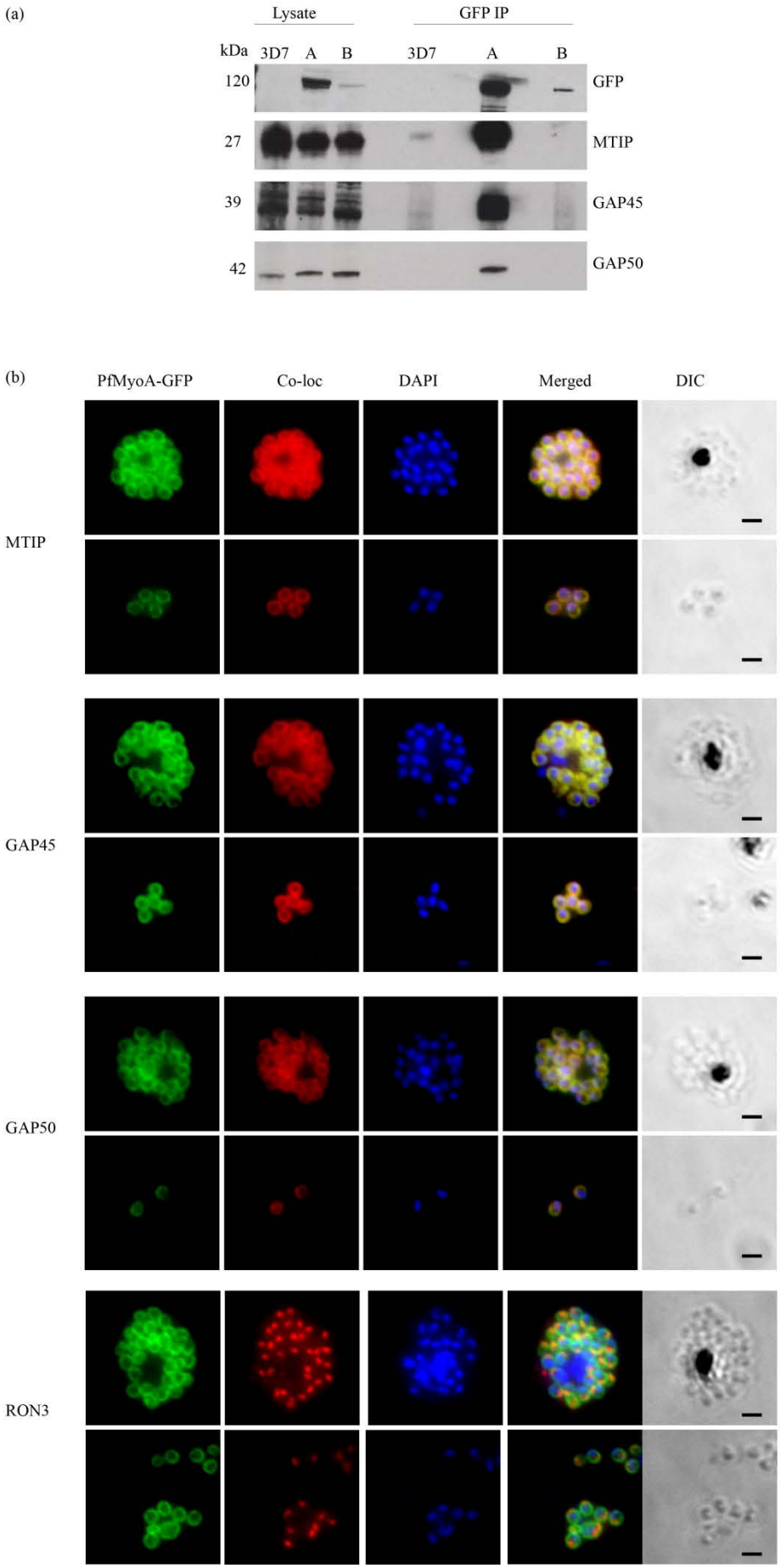
(a)
Lysate
GFP IP
kDa
3D7
A
B
3D7
A
B
120
GFP
27
MTIP
39
GAP45
42
GAP50
(b)
PfMyoA-GFP
Co-loc
DAPI
Merged
DIC
MTIP
GAP45
GAP50
RON3

Figure 4.4: PfMyoA-GFP forms a tetrameric complex in the glideosome motor complex. (a) The left hand side shows the whole parasite lysate (Lysate) for PMyoA-GFP (A), PfMyoB-GFP (B) and 3D7 parasites before imuunoprecipitation with GFP-TRAP (Chromotek). GFP-IP, on the right hand side, shows the precipitated proteins probed with rabbit α-GFP, α-MTIP, α-GAP45 and α-GAP50. Wild type 3D7 parasite lysates were used as a control. Single bands corresponding to MyoA-GFP, MyoB-GFP, MTIP and GAP50 were detected, whereas a doubled band was detected for GAP45. PfMyoA-GFP interacts with MTIP, GAP45 and GAP50, whereas PfMyoB-GFP is not in association with the glideosome complex proteins. Proteins were detergent solubilised from enriched mature schizont stages of clonal PfMyoA-GFP and PfMyoB-GFP parasites. (b) Co-localisation of PfMyoA-GFP with MTIP, GAP45 and GAP50 confirming the association of PfMyoA-GFP with the glideosome motor complex by location at the parasite periphery. Co-localisation with RON3 that is located in the rhoptry neck is used as a marker for the apical end of the parasite. DAPI stained nucleus. Scale bar is 2μM.

4.3.2 PfMyoB-GFP localises to the extreme apical tip of merozoites.

Based on the preliminary data, PfMyoB-GFP appeared to be localised to the apical end of the merozoite (Figure 4.2.b) and, from the IP experiments, it had no association with the glideosome motor complex (Figure 4.4a). In order to determine a more exact location of PfMyoB-GFP, co-localisation IFA was performed using a range of antibodies against known apical organelle markers such as the micronemal markers AMA1 and EBA175, the rhoptry neck marker RON3 and RON4 and the rhoptry bulb markers RAP1 and RhopH2. Co-localisation was also carried out for the merozoite surface marker PfMSP7. We also further co-localised PfMyoB-GFP with a cytoplasmic component of the invasion machinery, α-actin (AC-40: Sigma), and with α-tubulin (Sigma) antibodies to identify the location of this cytoskeletal component. The α-AMA1, α-EBA175 and α-MSP7 were raised in rabbit, whereas α-RON4, α-RON3 and α-RAP1 were raised in mouse. The best fluorescent anti-GFP signal was obtained from an affinity purified rabbit polyclonal α-GFP (rabbit-GFP: Dr Ellen Knuepfer, NIMR) which gave a very stable and strong fluorescent signal (at 1:500 up to 1:5000 dilution)

compared to both mouse monoclonal α-GFP (mouse-GFP: Roche), and camel monoclonal α-GFP-booster-atto4880 (Chromotek). Despite the lower sensitivity of the mouse mAb compared to the rabbit antibody, this mAb was used in co-localisations with antibodies raised in rabbits.

In mature schizonts and merozoites, PfMyoB-GFP produced a compact 'dotty' pattern of GFP fluorescence located at the very apical end of the parasite, near to the localisation of the apical markers AMA1, EBA175, RON4, RON3 and RAP1. However, whilst in some cases the fluorescent signal partially overlapped with these markers, MyoB appears to be in a distinct location within the cell. Examination of the localisation in detail revealed that the protein appeared to be anterior to the micronemes, organelles visible as a speckled pattern at the anterior one third of the parasite. The protein was also anterior of RAP1, in the rhoptry bulb and even to the RON4 and RON3 signal at the very anterior end of the rhoptry neck. The signal for that latter appeared as a single or double dot close together (Figure 4.5). We also co-localised PfMyoB-GFP with the other apical markers RhopH2 and PTRAMP, as well as the surface membrane marker MSP7, and the glideosome proteins MTIP, GAP45 and GAP50 but due to poor imaging and little additional information gathered, the data are not shown. For more precise localisation of MyoB, immuno-electron microscopy (IEM) would be required. Gold labelling of α-GFP antibodies to detect PfMyoB-GFP was carried out, but likely due to the poor performance of the antibody in IEM, this experiment was unsuccessful (data not shown). The other good apical markers to use would be antisera to the Rh proteins which locate at the rhoptry head (Cowman et al., 2012) and the late marker of the apical polar ring, RNG1 (Tran et al., 2010). However, unfortunately the appropriate antibodies are unavailable in our lab and therefore this additional experiment could not be performed.

We also complemented this co-localisation by performing IFA against proteins such as actin and tubulin which might provide some information regarding the association of PfMyoB-GFP. Normally, actin and tubulin are located in the anterior two-thirds of the parasite, beneath the parasite membrane complex, with tubulin forming the subpellicular microtubules known in merozoites as f-MAST (Fowler et al., 2001). Actin has also previously been shown to be concentrated at the apical tip of merozoites (Angrisano et al., 2012; Baum et al., 2008b; Field et al., 1993). Given its pattern of expression and anterior localisation we co-localised PfMyoB-GFP with α-

actin and α-tubulin antibodies. The anti- actin mAb AC-40 (A3853; Sigma) we used recognises an epitope located at the C-terminal end of actin, which is also conserved in all actin isoforms. This IFA showed that PfMyoB-GFP resides at the apical pole of merozoites in front of the rhoptries and co-localised with actin detected with α-actin antibodies, which revealed that both proteins might be located in the same region (Figure 4.5). This localisation also appeared to be coincident with the apical polar ring and microtubule organising centre from which microtubules originate, which might indicate an association of PfMyoB-GFP with the polar ring. Anti-α-tubulin mAb clone DM 1A (T9026: Sigma) was used to detect the parasite α-tubulin. Tubulin is expected to be a major component of the two or three microtubules and was localised at the apex and running in parallel along the merozoite periphery spreading towards the posterior of the merozoite. The localisation of microtubules was confirmed in previous studies by immunofluorescence (Fowler et al., 2001; Read et al., 1993) and EM (Bannister and Mitchell, 1995). As can be seen, the localisation of PfMyoB-GFP partially overlaps with tubulin at the apical part of the merozoite, further supporting the putative association with the apical polar ring.

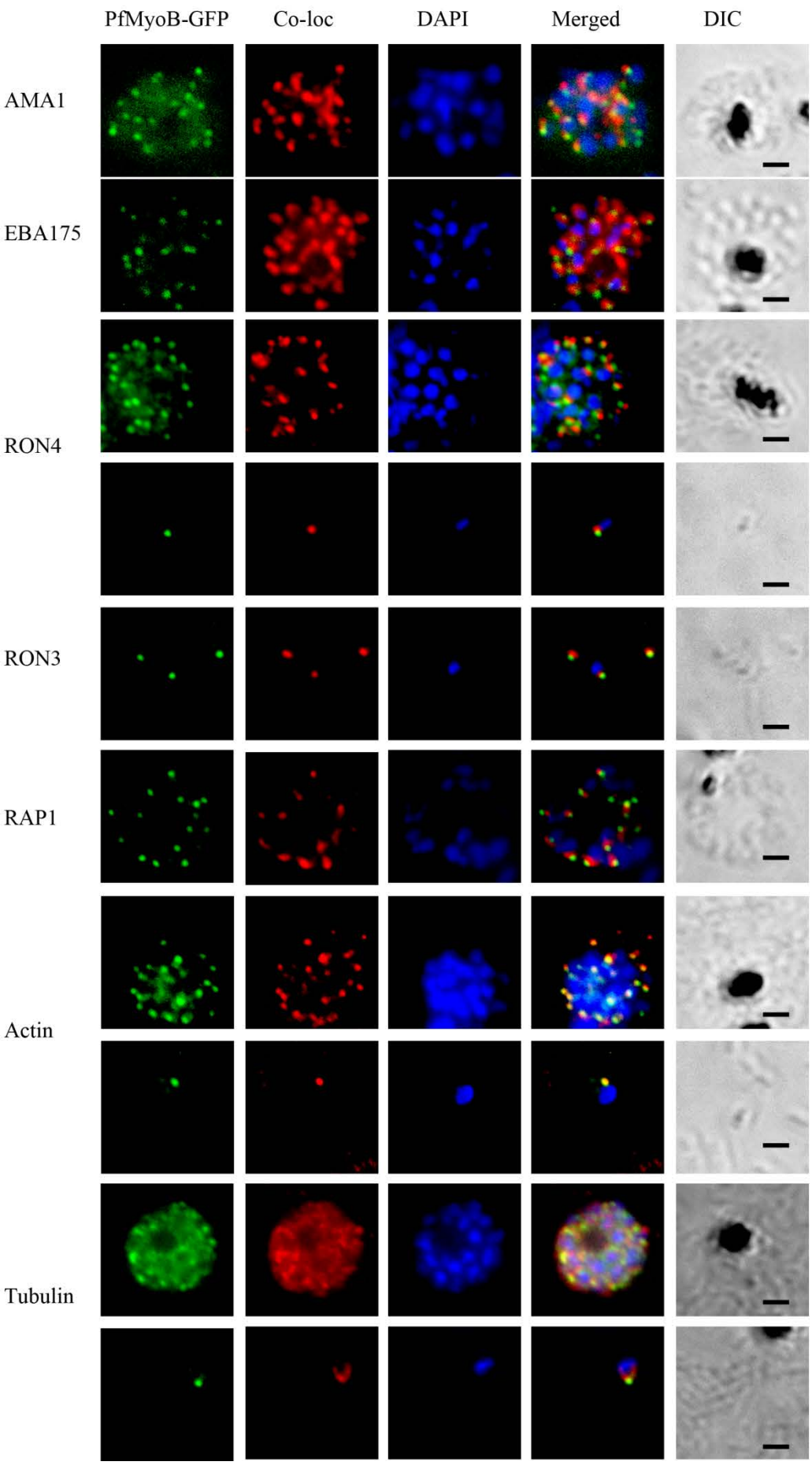
PfMyoB-GFP
Co-loc
DAPI
Merged
DIC
AMA1
EBA175
RON4
RON3
RAP1
Actin
Tubulin

Figure 4.5: PfMyoB-GFP localised at the apical pole of the parasite. Co-localisation of PfMyoB-GFP in schizonts and merozoites as determined by IFA with various merozoite organelle components, using rabbit antisera to AMA1 and EBA175 (the micronemes); mouse antisera to RON4, RON3,and RAP1 (the rhoptries); and commercial mouse antisera to actin and α-tubulin (a component of sub-pellicular microtubules). The distribution of PfMyoB-GFP was clearly at the apical end of the merozoite. Samples were counterstained with DAPI. Scale bar is 2μM.

4.4 PfMyoA-GFP is localised at the periphery and PfMyoB-GFP is confined to the apical apex as seen by live parasite development.

We have demonstrated that the GFP-tagged MyoA and MyoB are successfully expressed in *P. falciparum*. In order to examine expression of the tagged proteins over the parasite's development in the red blood cell we carried out a live time course microscopy study over the latter half of the parasite's development in these cells. Although the peripheral localisation of MyoA was reported by Pinder et al., (1998, 2000) and others, presumably the GFP-tagged MyoA must locate to the correct site, which is at the IMC, in order to function correctly. Tightly synchronised GFP-tagged parasite lines were harvested at two to three hour intervals from 24 h to 46 h post invasion, corresponding to a period from late trophozoites up to merozoite release and early ring formation (~30 min after egress). This also corresponds to the period when most of the MyoA associated proteins were expressed, for example onset of MTIP and GAP45 synthesis starts at ~24-30 h (Baum et al., 2006b; Ridzuan et al., 2012) which is consistent with the initial formation of IMC and assembly of the glideosome complex. In the earlier stages, from ~24 to 38 h post invasion, MyoA-GFP produced a diffuse green fluorescence pattern throughout the cytosol, and at this time the typical peripheral localisation was not yet visible. At later stages, from 40-46 h, the GFP fluorescence signal was highly visible especially when the parasites started to segment at approximately ~40 h post invasion and displayed a distinctive peripheral localisation in later schizont and merozoites (~42-46 h post invasion) (Figure 4.6). The association and the assembly of MyoA into the motor complex were further investigated by co-localisation of PfMyoA-GFP with MTIP, GAP45 and GAP50 using IFA in the time

course experiment and the same results were obtained, confirming these data (data not shown because no additional information was gathered). The peripheral localisation was also observed in *P. berghei* ookinetes expressing GFP-tagged MyoA (Rita Tewari, unpublished data) supporting the earlier findings reported in other publications of MyoA localisation detected by IFA and EM using anti-MyoA antibody (Baum et al., 2006b; Pinder et al., 2000; Pinder et al., 1998),

The experimental protocol designed for the PfMyoB-GFP live microscopy imaging time course experiment followed that used for PfMyoA-GFP. The initial results were a bit unclear and disappointing, especially at the earlier time points because of the faint GFP signal for this line, along with problems of overlap with the Hoechst nuclear staining. The strong DNA staining caused some crossover into the green (GFP) channel giving a false GFP fluorescence signal that overlapped with Hoechst staining. However, although at earlier stages a diffuse green fluorescence was detected, the distinctive discrete dot at the apical end as determine in the preliminary studies was clearly not seen until around ~40-48 h post invasion (data not shown) giving a rough idea of the timing of the MyoB expression. To determine the expression and localisation of MyoB during parasite development, we instead took images of parasites at various stages of development, based on visible morphology and the number of nuclei, in mixed stage cultures. We compared the number of nuclei in individual cells from these images to the number of nuclei from the real live time course images and examined the GFP fluorescence, revealing a pattern of GFP expression as we would have predicted which is at the apical end of the parasite and with maximum expression at 40 h (Figure 4.7). At the earlier time points from 21- 38 h post invasion, there was no clear green fluorescence signal detected, although a very faint ‘dot’ pattern was observed at ~36 and ~38 h. The GFP signal with a clear apical end localisation became visible at around ~40 h and more prominent as the parasite development continued to mature schizonts (42-44 h) and merozoites (46 h). This localisation and timing of the MyoB expression were further confirmed by performing further IFAs (data not shown).

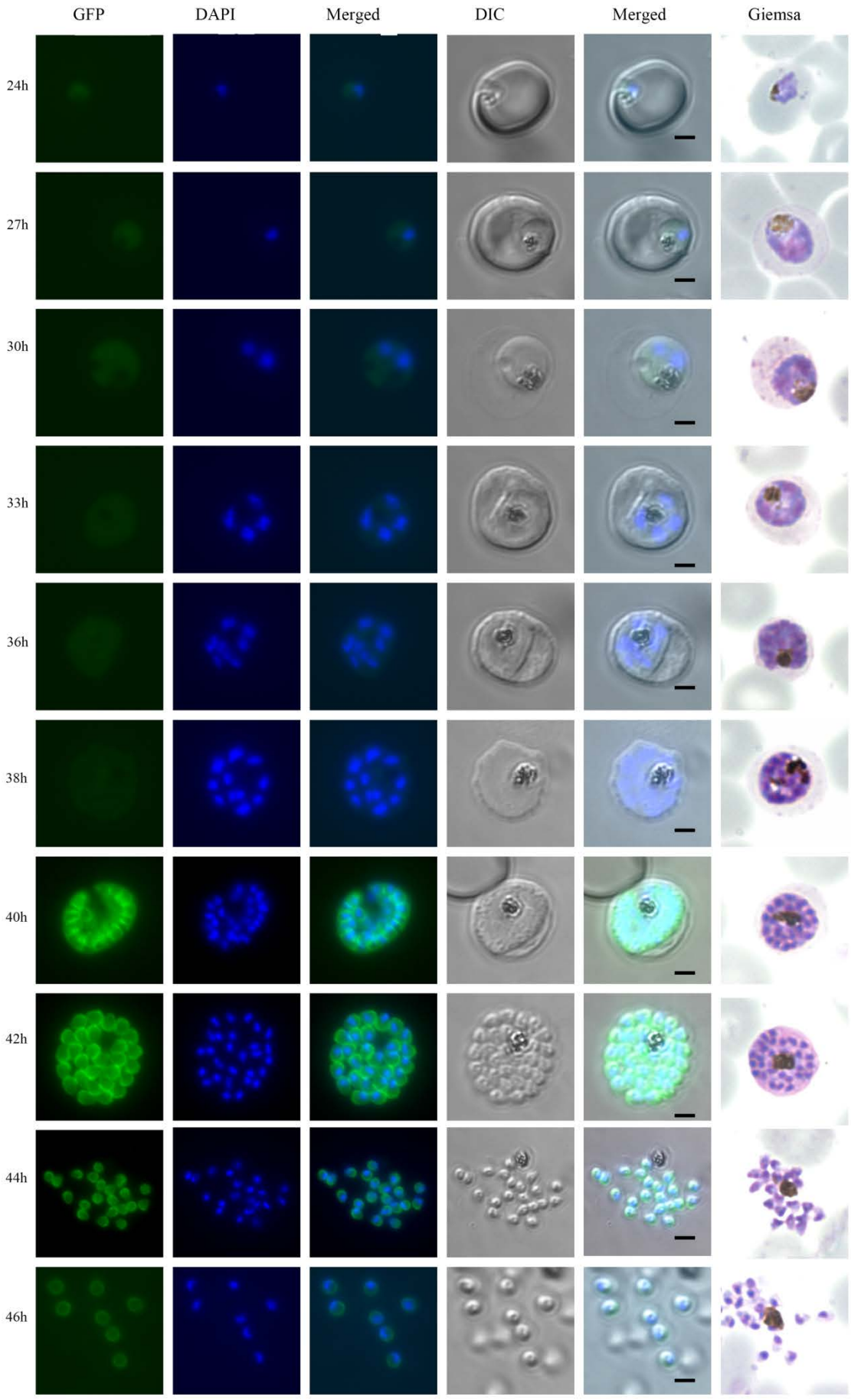
GFP
DAPI
Merged
DIC
Merged
Giemsa
24h
27h
30h
33h
36h
38h
40h
42h
44h
46h

Figure 4.6: Live microscopy analysis of GFP-tagged MyoA (PfMyoA-GFP) parasite development time course. A synchronised PfMyoA-GFP parasite population was separated into several cultures. Cultures were harvested starting at 24 h post invasion, and every two or three hours until 46 h post invasion. The harvested parasites were visualised and analysed by fluorescencet microscopy. The nucleus was labelled with Hoechst stain prior to microscopic analysis at 1000X magnification. In the early schizont stages, the GFP signal was very faint giving a diffuse green fluorescence. In the segmented parasite (40 h post invasion), the GFP signal was observed around the parasite's periphery, typical of a localisation at the IMC. The peripheral pattern continued until the parasite was fully segmented and divided into merozoites. Images of Giemsa-stained parasites were produced to aid comparison of the stages during parasite development. Scale bar is 2µm.

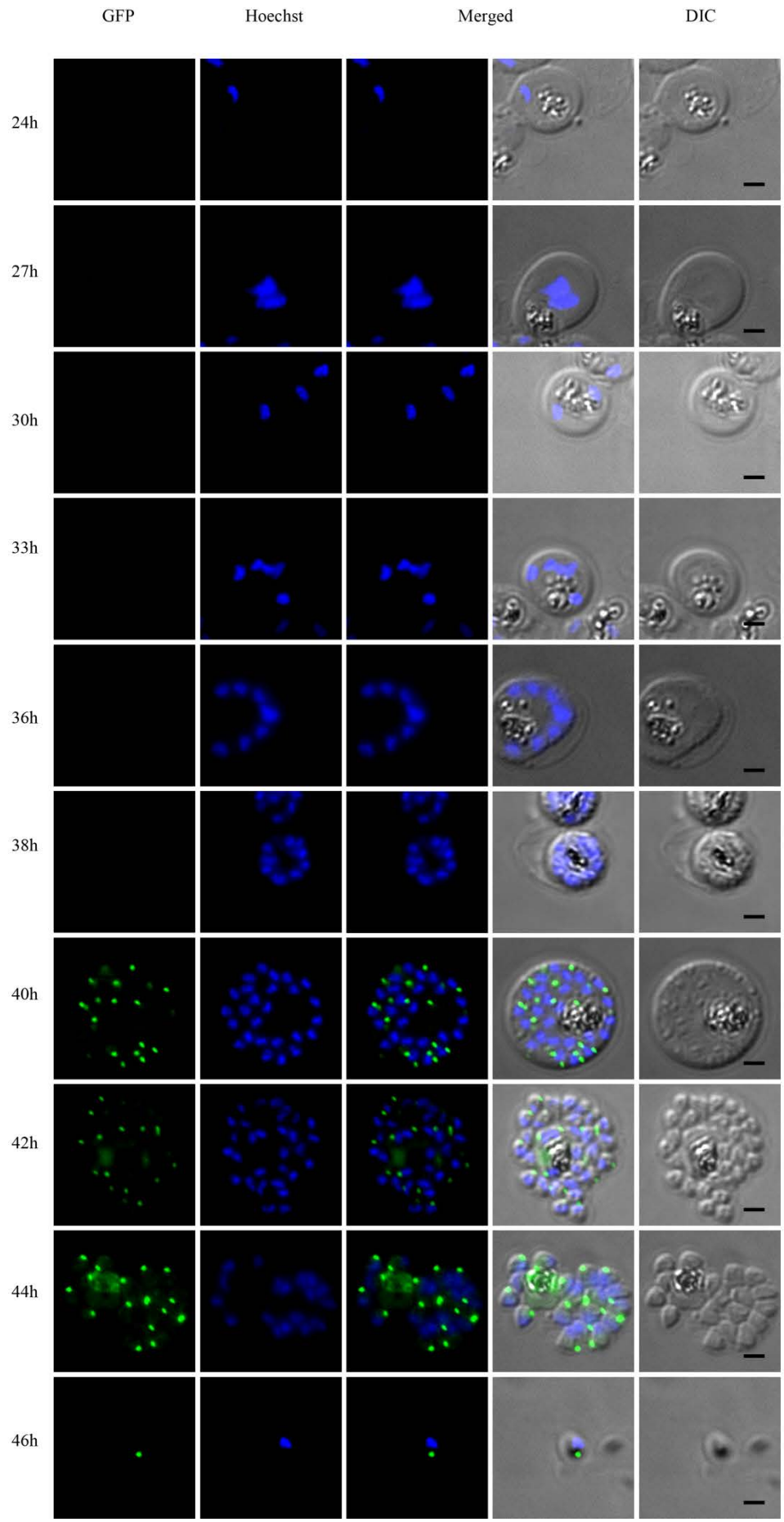
GFP
Hoechst
Merged
DIC
24h
27h
30h
33h
36h
38h
40h
42h
44h
46h

Figure 4.7: Live microscopy analysis of GFP-tagged MyoB (PfMyoB-GFP) parasites. A mixed population of the transfected parasite was harvested, visualised and analysed by fluorescence microscopy. The nucleus was labelled with Hoechst stain prior to microscopic analysis at 1000X magnification. The images were assembled by comparing the number of nuclei to represent the stages of parasite development. In the trophozoite and early schizont stages, GFP signal was undetectable. In the segmented parasite (40 h post invasion and later), the GFP signal was observed at the parasite's apical end. The apical end pattern was retained in the fully segmented schizont and free merozoites. Scale bar is 2µm.

4.5 The assembly of PfMyoA-GFP into the glideosome motor complex

Endogenous MyoA bound to MTIP/MLC1, GAP45 and GAP50 forms part of the glideosome complex that is associated with the IMC (Baum et al., 2006b; Bergman et al., 2003; Frenal et al., 2010; Yeoman et al., 2011). Having shown that the expression of PfMyoA-GFP was at the periphery, we further investigated the association of MyoA with the other glideosome motor complex components. We used parasite lysates collected during the time course analysis and performed co-immunoprecipitation with GFP-TRAP (Chromotek) (see section 4.3). These experiments complement the studies on the time of MyoA expression that were difficult to interpret due to the weak GFP signal detected during the earlier time points of parasite development in the live microscopy analysis. The parasite lysates used were collected during the time course experiment from 21 h to 46 h post invasion (section 4.6). We used our specific antisera to each glideosome component (MTIP, GAP45 and GAP50) and mouse α-GFP mAb (for MyoA) for this immunoblot analysis of the time course, probing parasite lysates (Lysate) and immunoprecipitated proteins from the clonal PfMyoA-GFP line (GFP-IP). We also used the same batch of antibodies as in the immunoblot (section 4.3.1) and IFA (section 4.3.2) analyses to minimise any discrepancies that might occur. An equivalent amount of PfMyoA-GFP protein lysate from each time point was probed with the antibodies. The results showed that MyoA-GFP was expressed at the trophozoite stages starting from ~24 h (Figure 4.7) (confirming the diffuse green fluorescence detected in the live microscopy imaging:

Figure 4.6). Early expression also occurred for GAP50 at ~21 h, whereas MTIP was first detected later at ~33 h (Figure 4.8: Parasite lysate panel). Although GAP45 was first detected here at around ~36 h (Figure 4.8: Parasite lysate) it has previously been detected as early as ~30 h post infection by Ridzuan et.al., (2012) using live imaging and IFA of the transgenic GFP-tagged GAP45 parasite. This discrepancy could be due to several factors such as the amount of protein being expressed at the ~30 h time point in this study was low and the sensitivity of detection was less than that which can be achieved by direct tagging of GAP45 with GFP as performed by Ridzuan et al., (2012), although the exact cause is not clear.

The PfMyoA-GFP immunoprecipitate from the lysate (GFP-IP panel) also contained the glideosome complex proteins as mention above. However the comparison between these results and those from examining the timing of protein expression in parasite lysates indicated that although, the expression of of PfMyoA-GFP and GAP50 started during the earlier stages compared to MTIP and GAP45, they only come together in the formation of the complex at around ~38 h together with MTIP and GAP45 (Figure 4.8: GFP IP). It appears that even though PfMyoA-GFP was expressed earlier, it was only assembled together with MTIP and GAP45 into the motor complex and anchored to the IMC via GAP50 at a later time. Yeoman et al., (2011) showed the earlier transcription and expression of GAP50 in *T. gondii* that may reflect a role in another cellular process outside of host cell invasion and the early synthesis could be required for its proper processing and insertion into the IMC. Therefore, the role of PfGAP50 might be similar to that of TgGAP50.

Even though in these particular studies we do not know exactly which proteins interact first in the complex formation, previous studies have shows that GAP45 will interact with the MyoA-MTIP complex first, which is then followed by binding of GAP50 to the pre-assembled complex of MyoA-MTIP-GAP45 (Bergman et al., 2003; Gaskins et al., 2004; Herm-Gotz et al., 2002; Johnson et al., 2007; Rees-Channer et al., 2006; Yeoman et al., 2011). Although, PfMyoB-GFP does not associate with known motor proteins, similar time course samples were taken. When candidate binding partners for MyoB have been identified, and antibody reagents generated, these samples will be used in the same way as for the analysis of MyoA interactions.

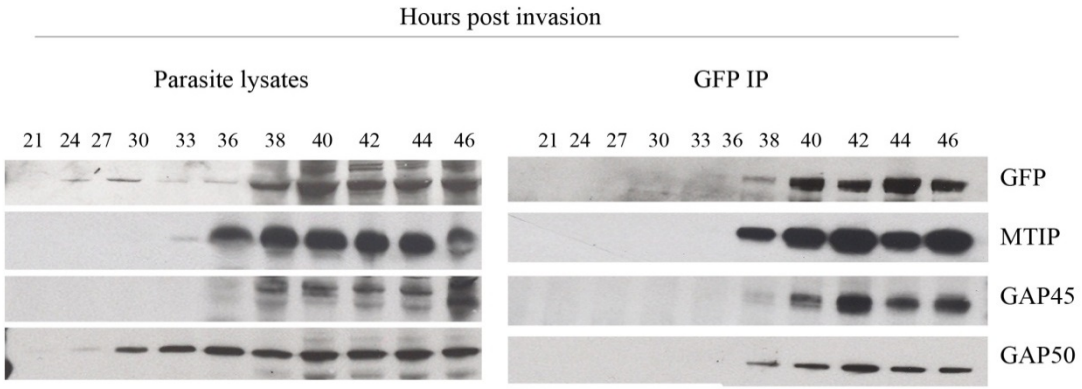

Figure 4.8: PfMyoA-GFP is incorporated into the glideosome motor complex. The immunoblot samples were collected during the time course experiment from 11 time point, from 21 h to 46 h post invasion. Parasite cultures collected at each time point were saponin lysed and kept on dry ice to avoid protein degradation and then proteins were detergent solubilised. On the left hand side are the total parasite lysates (Parasite lysate), whereas on the right hand side are the samples immunoprecipitated with GFP-TRAP (GFP-IP) and probed with mouse α-GFP, rabbit α-MTIP, α-GAP45 and α-GAP50. Single bands corresponded to MyoA, MTIP and GAP50 were detected, whereas a doublet band was detected for GAP45. MyoA and GAP50 were expressed at the earlier stages compared to MTIP and GAP45. The assembly of the motor complex occurred from ~38 h post invasion onwards.

4.6 Mass spectrometry analysis of proteins associated with PfMyoA-GFP and PfMyoB-GFP

We further characterised the possible interaction of PfMyoA-GFP and PfMyoB-GFP with unknown proteins in the parasite, through IP using GFP-TRAP (Chromotek). We intended to confirm PfMyoA-GFP as part of the glideosome motor complex as well as identify any new and interesting proteins associated with either PfMyoA-GFP or PfMyoB-GFP using mass spectrometry (MS) analysis. The identification of known and unknown proteins associated with *P. falciparum* MyoA and MyoB was performed by liquid chromatography mass spectrometry (LC-MS), implementing the electrospray ionisation methodology. Generally, MS is a powerful tool for measuring the mass of proteins using either intact or proteolytically digested molecules. Protonated proteins are fragmented and detected by the mass spectrometer corresponding to their mass/charge ratio (m/z). The mass spectrum is characterised by a series of peaks caused by multiple charges on the protein molecules, which then can be de-convoluted by an algorithm into a single peak of protein mass with an accuracy typically within 1 Da in every 10 kDa (Mann and Wilm, 1995). MS has been used for proteome analysis in *P. falciparum* of a range of selected life cycle stages, which has provided a wealth of information for malaria research (Lasonder et al., 2002).

The IP of GFP-tagged MyoA and MyoB was performed as described in Chapter 2 (section 2.3.3) prior to LC-MS/MS analysis. The immunoprecipitated proteins were separated by SDS-PAGE and stained with Sypro-Ruby (Invitrogen) for determination of precipitation efficiency. Wild type 3D7 parasites were used as a control and were treated in the same way as the samples from the GFP tagged parasite lines. A distinct ~120 kDa protein band corresponding to MyoA-GFP was seen in the immunoprecipitate from the PfMyoA-GFP line (lane A) (Figure 4.9). Other protein bands suggested the presence of MTIP, GAP45, GAP50 and GAP40 although the clarity was poor due to the presence of a background of other proteins. Due to low intensity, a distinct band corresponding to MyoB could not be distinguished from other potentially nonspecific bands as shown in lane B and lane 3D7 (Figure 4.9).

For the purpose of LC-MS/MS analysis, the anti-GFP precipitated proteins were subjected to SDS-PAGE for a short electrophoresis period (run length: 4 mm) and then the whole gel piece was excised and prepared for trypsin digestion prior to protein

identification by LC-MS/MS (Chapter 2, section 2.9). Results from the deconvoluted LC-MS/MS spectra were converted into molecular weights by the ExPASy ProtParam tool, and showed MyoA and MyoB were present as major proteins at the expected molecular weight of ~120 kDa in each case. The other proteins present in these samples were tabulated after comparison with spectra hits in the control. Any protein detected in the GFP tagged samples but also present in the wild type control sample was excluded from this analysis table.

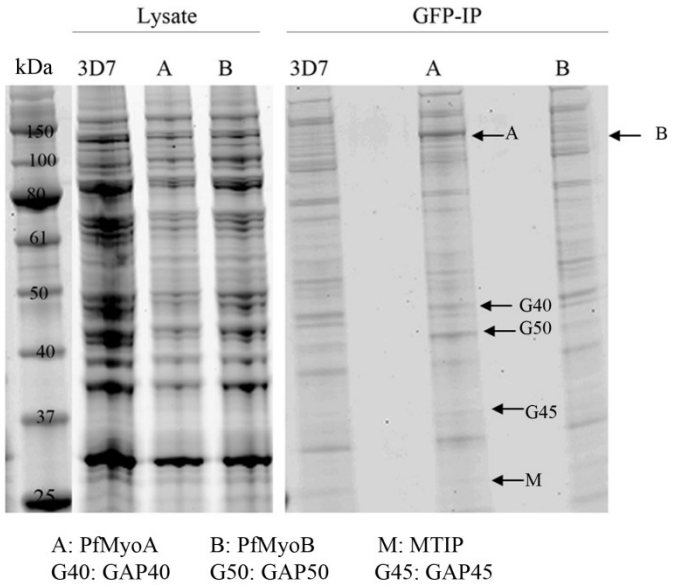

Figure 4.9: Immunoprecipitation of PfMyoA-GFP and PfMyoB-GFP and associated proteins for LC-MS/MS analysis. On the left hand side (Lysate) are lysates before immunoprecipitation with GFP-TRAP from wild type (3D7), PfMyoA-GFP (A) and PfMyoB-GFP (B) parasites. On the right hand side (GFP-IP) are immunoprecipitated proteins from each of the lysates. Each sample were resolved by SDS-PAGE and stained with Sypro-ruby (Invitrogen) staining. Only the band corresponding to PfMyoA (A can be distinguished from the other protein bands. The respective bands of GAP40, GAP50, GAP45 and MTIP should be within the areas indicated.

4.6.1 Confirmation of MyoA association with the glideosome motor complex

From a total of 221 proteins identified by LC-MS/MS in the MyoA-GFP sample, only 21 proteins were selected and tabulated, whereas 200 proteins were excluded. This selection of proteins was based on comparison with the proteins detected in the control sample from the WT parasite line, and each protein had to be represented by two or more peptides. Only proteins which did not appear in the WT sample were selected (Table 4.1). This excluded some important proteins such as actin, tubulin, apical organelle and merozoite surface proteins and others were present in both MyoA and WT datasets. LC-MS/MS of the MyoA-GFP complex identified MyoA along with the known glideosome proteins MTIP, GAP45 and GAP50 (Table 4.1). Moreover, MyoA was identified with the highest coverage (72.49%) and with the number of peptides identified correspondingly high (66 peptides), which confirmed the MyoA protein. As expected, the known glideosome proteins were also detected in this MS dataset. The coverage of each protein was also high, with 31.37% (7 peptides), 29.80% (9 peptides) and 19.61% (4 peptides) for MTIP, GAP50 and GAP45, respectively. These results validated the previous IP (Figure 4.3.a and section 4.5), which confirmed MyoA as belonging to the glideosome complex.

Interestingly, the 51.8 kDa GAP40 was also precipitated with MyoA. The orthologue of this protein in *T. gondii*, TgGAP40, was first described by Frenal et al., (2010) and identified as an additional member of the glideosome motor complex by co-IP and MS analysis of MLC1-Ty-expressing parasites (Frenal et al., 2010) and affinity purification of GAP50 (Fauquenoy et al., 2011). By reference to the *Plasmodium* genome database (PlasmoDB: http://plasmodb.org), PfGAP40 transcriptional profiling (Bozdech et al., 2003) showed that it is highly expressed in schizonts and so also likely forms part of the glideosome motor complex in *P. falciparum* as has been shown for TgGAP40. Therefore, in this study we have provided evidence of the glideosome complex in *P. falciparum* consisting of MyoA-MTIP-GAP45-GAP50-GAP40. GAPM proteins (GAPM2 and GAPM3) were also identified in the complex by LC-MS/MS. These proteins have also been suggested to be involved with the glideosome motor complex (Bullen et al., 2009). GAPMs in both *T. gondii* and *P. falciparum* localise to the IMC where they form highly SDS resistant oligomeric complexes which are conserved throughout *Apicomplexa*. GAPMs co-purify with the cytoskeletal alveolin proteins and are also thought to interact with the actin-myosin motor itself. These

might be strong candidates for providing an IMC-anchoring role, either directly or indirectly tethering the motor to the cytoskeleton (Bullen et al., 2009). It would also be interesting to further characterise the root hair defective 3 GTP-binding protein (RHD3). RHD3 (110 kDa) is a protein involved in the transport of secreted and Golgi marker proteins between the ER and Golgi apparatus (Zheng et al., 2004) . In addition to these proteins, there were a number of other previously unknown proteins, some at low level, which were detected in the PfMyoA-GFP immunoprecipitated product with low coverage and low peptide representation. These proteins include, for example the Cu^{2+} -transporting ATPase, putative (CUP), a tetratricopeptide repeat family protein, and nucleoside transporter 2 (NT2). LC-MS/MS analysis identified four hypothetical proteins which are PF3D7_0822900, PF3D7_1409400, PF3D7_0912400, and PF3D7_1017500. PlasmoDB contains little extra interesting information about these hypothetical proteins at the moment, upon which to carry out further investigation (Table 4.1). To validate further the novel MyoA interacting proteins identified here one possibility would be to undertake a reciprocal IP approach through the use of either antibodies or tagged version of the target proteins. This work is currently on-going within the lab.

Table 4.1 Members of the glideosome motor complex determined by mass spectrometry analysis of immunoprecipitated PfMyoA-GFP protein. Each protein identified by MS is listed with their PlasmoDB accession number (column 1); a description of the protein identified (column 2) and the molecular weight (column 3). Column 4 gives the percentage probability MS score and number of peptides hits (column 5). Column 6 (C5: Area), and 7 (D5: Area) represent the duplicates of the MS datasets obtained. The highlighted proteins are those that have been previously shown to be in the motor complex (blue) and those that are judged potentially associated with the glideosome complex (grey).

Accession	Description	MW [kDa]	ΣCoverage	Σ# Peptides	C5: Area	D5: Area
PF3D7_1342600	myosin A (MyoA)	92.2	72.49	66	7.237E8	7.553E8
PF3D7_0423500	glideosome associated protein with multiple membrane spans 2 (GAPM2)	42.6	12.37	2	3.339E7	3.242E7
PF3D7_0515700	glideosome-associated protein 40, putative (GAP40)	51.8	7.46	4	2.769E7	3.194E7
PF3D7_1246400	myosin light chain 1,myosin A tail domain interacting protein (MTIP)	23.5	31.37	7	9.911E6	2.653E7
PF3D7_0822900	conserved Plasmodium protein, unknown function	138.2	16.24	15	1.765E7	1.581E7
PF3D7_1033200	early transcribed membrane protein 10.2 (ETRAMP10.2)	38.9	22.82	6	4.274E6	7.205E6
PF3D7_0918000	glideosome-associated protein 50,secreted acid phosphatase (GAP50)	44.6	29.80	9	6.927E6	7.140E6
PF3D7_1409400	conserved Plasmodium membrane protein, unknown function	30.5	10.69	5	1.556E7	7.136E6
PF3D7_1416100	root hair defective 3 GTP-binding protein (RHD3) homolog, putative	110.5	12.17	10	3.568E6	5.461E6
PF3D7_0824400	nucleoside transporter 2 (NT2)	67.6	3.76	2	4.518E6	4.523E6
PF3D7_0912400	conserved Plasmodium protein, unknown function	52.7	5.83	2	2.666E6	4.327E6
PF3D7_1032500	DER1-like protein, putative (Der1-2)	31.0	10.27	3	3.856E6	3.963E6
PF3D7_1444300	apicoplast 1-acyl-sn-glycerol-3-phosphate acyltransferase, putative	33.7	12.67	2	3.154E6	3.458E6
PF3D7_1406800	glideosome associated protein with multiple membrane spans 3 (GAPM3)	32.9	6.69	2	0.000E0	3.256E6
PF3D7_1017500	conserved Plasmodium protein, unknown function	15.7	24.63	2	0.000E0	3.157E6
PF3D7_0204700	hexose transporter (HT)	56.4	5.36	2	1.175E6	2.587E6
PF3D7_1457000	signal peptide peptidase (SPP)	47.5	8.01	3	3.204E6	2.444E6
PF3D7_1222700	glideosome-associated protein 45 (GAP45)	23.6	19.61	4	3.547E6	2.406E6
PF3D7_0500800	mature parasite-infected erythrocyte surface antigen,erythrocyte membrane protein 2 (MESA)	168.2	6.90	6	2.843E6	1.694E6
PF3D7_0904900	Cu2 -transporting ATPase, putative (CUP)	298.6	1.13	2	3.369E6	1.166E6
PF3D7_1420200	tetratricopeptide repeat family protein, putative	147.9	1.93	2	8.916E5	6.173E5

4.6.2 MyoB is part of a novel protein complex in the parasite

LC-MS/MS analysis of the immunoprecipitated GFP-tagged MyoB identified 229 proteins. By comparison to the WT dataset, proteins present in both MyoB-GFP and WT samples were excluded. Only 27 proteins were selected. Table 4.2 shows the resulting data and includes only proteins identified by two or more peptides. The numbers of peptides representing MyoB was high (40 peptides) confirming the presence of MyoB-GFP protein. None of the confirmed proteins from the glideosome complex (MyoA, MTIP, GAP45, and GAP50) nor the potential proteins for glideosome complex (GAP40 and GAPMs) was identified in this MyoB dataset. This result of the analysis of PfMyoB-GFP by LC-MS/MS confirmed the earlier result presented in sections 4.3 and Table.4.1 which revealed no association between PfMyoB-GFP and known glideosome motor complex proteins.

The most interesting protein present in the LC-MS/MS analysis is designated as 'a conserved *Plasmodium* protein of unknown function' (PF3D7_1118700; 78.7 kDa; 11.66% coverage and 6 peptides) (Table 4.2) which later we designate PfMTIP-B. Some of the proteins identified in the MoB-GFP complex are involved in protein trafficking and endocytosis, such as protein transport protein (SEC31: 3.74% coverage; 4 peptides); Pf332 (0.36% coverage; 2 peptides); clathrin heavy chain, putative (2.35% coverage; 4 peptides); and Dynamin-like protein (DYN2: 3.24% coverage; 2 peptides). Although this number of peptides hits is within the threshold range, the result is considered less convincing due to low coverage (less than 5%). This might be due to the low abundance of MyoB and associated proteins giving a lower signal to noise ratio. These vesicular trafficking proteins may be worth investigating further: Plasmodium SEC31 protein is a homologue of COPII in mammalian cells which is involved in trafficking clathrin coated vesicles (CCV) from the ER to the Golgi, (Adisa et al., 2001; Taraschi et al., 2001), whereas DYN2 is involved in membrane scission (Charneau et al., 2007). Protein involved in other functions also identified by this LC-MS/MS approach include polyubiquitin (PfpUB) (61.68% coverage; 4 peptides) which is present in all cellular compartments of the parasite and is involved in non-lysosomal, ATP-dependent degradation of misfolded, short-lived proteins (such as transcription factors) and cell cycle regulatory proteins (Horrocks and Newbold, 2000).

There are proteins in the MyoB-GFP dataset that were also detected in the MyoA-GFP dataset (Table 4.1), such as mature parasite-infected erythrocyte surface antigen/erythrocyte membrane protein 2 (MESA/EMP2), which may be binding non-specifically and other proteins which may be present because of their generally high abundance such as Hsp40/90 organising protein (HOPs), acyl-CoA-synthase (AC11) and translocon component (PTEX88) (Table 4.2 non-highlighted proteins).

Table 4.2 Members of the PfMyoB complex as determined by MS analysis of immunoprecipitated PfMyoB-GFP proteins. Each protein identified by MS is listed with their PlasmoDB accession number (column 1); a description of the protein identified (column 2) and the molecular weight (column 3). Column 4 gives the percentage probability MS score and the number of peptides hits is in column 5. Columns 6 (C5: Area), 7 (D5: Area) and 8 (E5: Area) represent the triplicates of the MS datasets obtained. MyoB and its potential light chain are highlighted in blue, and proteins potentially associated with vesicular trafficking and endocytosis are highlighted in grey.

Accession	Description	MW [kDa]	ΣCoverage	Σ# Peptides	C5: Area	D5: Area	E5: Area
PF3D7_0503600	myosin B (MyoB)	93.1	49.56	40	3.948E7	3.545E7	4.150E7
PF3D7_1211700	minchromosome maintenance (MCM) complex subunit, putative (MCM5)	85.8	11.87	7	5.720E5	6.153E5	1.240E6
PF3D7_1118700	conserved Plasmodium protein, unknown function	78.7	11.66	6	7.533E5	7.408E5	6.616E5
PF3D7_0619500	acyl-CoA synthetase (ACS12)	163.8	3.88	5	3.721E5	2.640E5	4.180E5
PF3D7_1211800	polyubiquitin (PfpUB)	42.8	61.68	4	1.054E7	4.692E6	0.000E0
PF3D7_1219100	clathrin heavy chain, putative	232.8	2.35	4	2.752E5	0.000E0	2.242E5
PF3D7_0214100	protein transport protein sec31 (SEC31)	166.6	3.74	4	2.587E5	0.000E0	7.721E5
PF3D7_1238800	acyl-CoA synthetase, PfACS11 (ACS11)	92.0	4.42	3	9.231E5	5.842E5	6.957E5
PF3D7_1208900	conserved Plasmodium protein, unknown function	166.8	2.50	3	1.527E5	2.884E5	0.000E0
PF3D7_1213800	bifunctional aminoacyl-tRNA synthetase, putative	86.6	5.50	3	1.607E5	2.289E5	2.753E5
PF3D7_0305200	conserved Plasmodium protein, unknown function	135.7	9.92	3	3.350E5	3.018E5	2.755E5
PF3D7_1434300	Hsp70/Hsp90 organizing protein (HOP)	66.0	4.08	2	2.894E5	2.634E5	2.689E5
PF3D7_0309500	asparagine synthetase, putative	69.8	3.93	2	1.211E6	0.000E0	7.280E5
PF3D7_0812100	conserved Plasmodium protein, unknown function	314.3	1.17	2	0.000E0	9.594E4	5.986E5
PF3D7_0500800	mature parasite-infected erythrocyte surface antigen,erythrocyte membrane protein 2 (MESA)	168.2	2.58	2	1.829E5	1.620E5	0.000E0
PF3D7_1105600	translocon component PTEX88 (PTEX88)	90.7	3.60	2	0.000E0	3.459E5	3.202E5
PF3D7_1420700	surface protein, Pf113 (Pf113)	112.5	2.37	2	0.000E0	8.654E5	1.037E6
PF3D7_0918900	gamma-glutamylcysteine synthetase (gammaGCS)	124.4	2.54	2	0.000E0	2.409E5	3.233E5
PF3D7_1447900	multidrug resistance protein 2 (heavy metal transport family) (MDR2)	118.9	2.54	2	1.361E5	4.973E5	2.682E5
PF3D7_0204100	conserved Plasmodium protein, unknown function	271.3	1.35	2	0.000E0	1.635E5	1.881E5
PF3D7_0917600	pre-mRNA-splicing factor ATP-dependent RNA helicase PRP43, putative (PRP43)	94.1	2.93	2	1.395E5	0.000E0	2.727E5
PF3D7_1457300	conserved Plasmodium protein, unknown function	75.9	3.91	2	3.939E5	2.580E5	1.959E6
PF3D7_1027300	peroxiredoxin (nPrx)	43.9	7.38	2	4.796E5	4.065E6	5.993E5
PF3D7_1037500	dynamin-like protein (DYN2)	81.5	3.24	2	2.151E5	2.493E5	2.479E5
PF3D7_1149000	antigen 332, DBL-like protein (Pf332)	688.9	0.36	2	0.000E0	8.858E5	1.908E5
PF3D7_1136400	conserved Plasmodium protein, unknown function	107.0	2.71	2	4.650E5	4.140E5	3.921E5

4.7 PF3D7_1118700 protein is a myosin B light chain related to MTIP (MTIP-B)

Immunoprecipitation and LC-MS/MS analysis of PfMyoB-GFP and associated proteins revealed seven proteins of unknown function, i.e. with PlasmoDB ID of PF3D7_1118700, PF3D7_1208900, PF3D7_0305200, PF3D7_0812100, PF3D7_0204100, PF3D7_1457300 and PF3D7_1136400, proteins for which no function could be deduced by homology to known proteins in public databases and suggesting that they might be Plasmodium-specific molecules. Among these unknown proteins, the protein coded by PF3D7_1118700 was further investigated *in silico* due to the fact that it contained an EF-hand domain identified by the InterPro programme. Referring to PlasmoDB (http://plasmodb.org/plasmo/), this protein was predicted to have a myosin light chain domain. Bioinformatics searches showed that this protein contained at least one EF-Hand domain (Accession: SSF47473; Coordinates from residues 513 to 646) which was used to BLAST search the Calcium Domain Database (CDD). The result confirmed that the protein belonged to the EF-Hand Superfamily and that this protein contained Ca^{2+}-binding protein motifs (FRQ1: COG5126). These calcium binding domains are a common feature of Myosin Light Chains. For comparison, MTIP (PF3D7_1246400) was found to contain 2 EF-hands (PlasmoDB: Accession: SSF47473; coordinate 84-202) as identified by the EF-hand Superfamily database and Accession: PS50222; coordinate 139-174 as identified by the Profile database (Bosch et al., 2006).

A clustal alignment of the full length of MTIP (204 residues) and the C-terminal 232 residues (from 652 residues) of PF3D7_1118700 (henceforth called PfMTIP-B) revealed that they have 56% similarity and 31% identity within this region (Figure 4.9a). We discard the first 420 aa of MTIP-B because it has much longer N-terminus than MTIP giving a distinct size of 78.8 kDa for PfMTIP-B relative to the 23.5 kDa of MTIP (Table 4.1 and 4.2). The transcriptional profiling of PfMTIP-B showed that it is highly expressed in late asexual blood stages as is also the case for MTIP (Figure 4.9.b). Furthermore, this protein is also found in *P. berghei* (PBANKA_092940), *P. chabaudi chabaudi* (PCHAS_091490), *P. knowlesi* (PKH_091610) and *P. yoelii yoelii* (PYYM_0930800) (PlasmoDB) which shows it has homologues across *Plasmodium* species (Appendix C). This protein was absent in the MyoA-GFP pull down indicating that MTIP-B does not associate with MyoA. From studies conducted previously, MTIP (MLC1 in *Toxoplasma*) had been identified as the light chain for MyoA and the the

association occurred through the degenerate IQ motif at the extreme C-terminal end of MyoA (Bergman et al., 2003; Green et al., 2006b; Herm-Gotz et al., 2002). (Appendix D). Considering the association of PfMyoA and MTIP through binding of the MyoA-tail by the C-terminal domain of MTIP, a 12 residue peptide (EPQRKPLSIEESFENSE) was identified (Green et al., 2006b); this domain is also present in the PfMyoB sequence (QKIEIPLSIEESLSICR), thus PfMTIP-B might be associated with PfMyoB and a further investigation needs to be carried out in order to confirm this MTIP-B as a MyoB light chain.

The first step that we need to carry out is to establish the residues of MyoB binding to MTIP-B followed by studies on the expression profile of MTIP-B in developing parasite by generating a GFP- or HA-tagged MTIP-B transgenic parasite. The localisation of MTIP-B can be determined using IFA or IEM with specific antibodies against MTIP-B, or live imaging microscopy. The function of the protein may be investigated by mutagenesis studies or the generation of a knockout parasite. The important features of the structure of MTIP-B and MyoB-MTIP-B complexes need to be established. As a start, the interactions of MyoB and MTIP-B can be examined using methods developed to study the MyoA – MTIP complex (Douse et al., 2012; Green et al., 2006b; Thomas et al., 2010).

(a)

```
MTIP            ---------------------------------------------MKQECN-------- 6
MTIP-B          KIEELEMNISYCEQQINYLKDDLDFKMEELRNTTLYTEEVKNEASYFKQELSKNNDLLLE 360
                                                             :*** .

MTIP            -------------------------VCYFN------------LPDPESTLGPYDNELNYF 29
MTIP-B          VMEHFHQMINNVDEFIYKNKDKNELITYMNKKKKKYGDITKKISEKNKELNLKVKNFVPY 420
                                  : *:*           :.: :. *.   :::  :

MTIP            TWGPGFEYEPEPQRKPLSIEESFENSEES------EESVADIQQLEEKVDESDVRIYFNE 83
MTIP-B          NFSMGTELKKHEEYLKIQMDEMKKKEEEEKRKRREEEEEEQKKRKEEEEEEQKKRKEEEE 480
                .:. * * : . :   :.::*  ::.**.      **.  : :: **: :*.. *   :*

MTIP            KSSGGKISIDNASYNARKLGLAP-------SSIDEKKI-------KELYGDNLTYEQYLE 129
MTIP-B          KIEKKKKEEEEEKRKKEEQELLEEKDIKNNETFEEKKIRLVKELMKEVNEETLSLEKCVD 540
                * .  * . :: . : .:  *         .:::****       **:  :.*: *: ::

MTIP            YLS-------------------------------ICVHDKDNVEELIKMFAHFDNNCTGY 158
MTIP-B          IIYKANLPLTQNKLNKLKNMGDIKKDELVTFVKTLMLNEQEAFENMKTFFEIWDIMKTGY 600
                 :                                : ::::: .*:: .:*  :*   ***

MTIP            LTKSQMKNILTTWGDALTDQEAIDALNAFS--SEDNIDYKLFCEDILQ---- 204
MTIP-B          MHKNLIISILKQFGDNLTEEESNYIQKELNQMSESNISYVKLLKKWIYGTEE 652
                : *. : .**. :** **::*:    : :.  **.**.*  : :. :
```

(b)

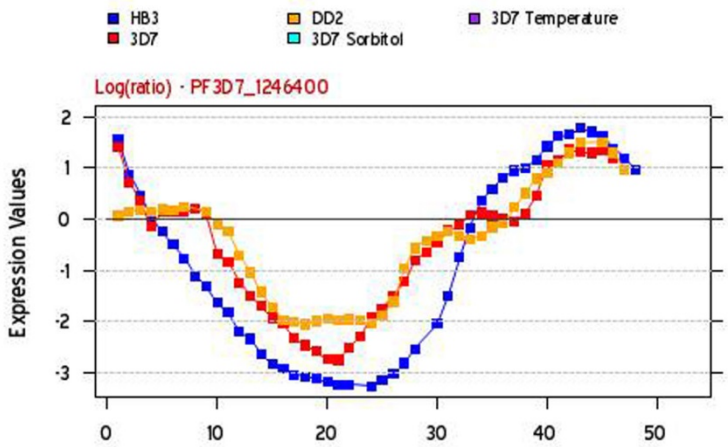

(c)

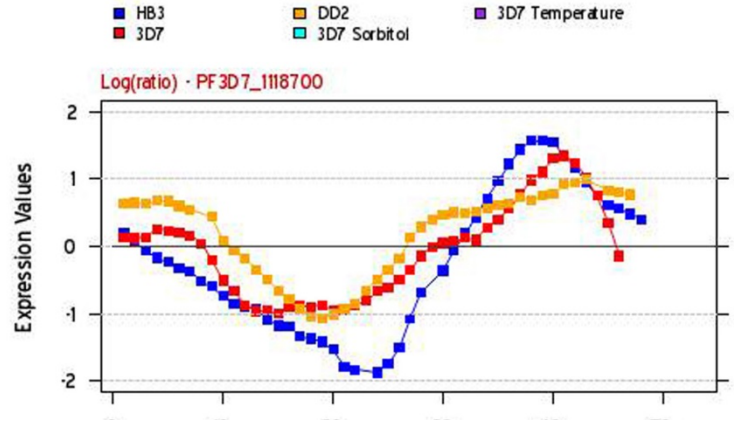

Figure 4.10: Identification of PfMTIP-B. (a) Clustal alignment of the MTIP sequence with the C-terminal 232 amino acids of MTIP-B. This alignment clearly shows the similarity between PfMTIP and PfMTIP-B. The residues in red and blue indicate the EF hand domains. *, identity; :, strong similarity; .(b) The expression profile of PfMTIP and (c) The expression profile of PF3D7_1118700 (PfMTIP-B) as reported in the *Plasmodium* database. The expression level of both PfMTIP and PfMTIP-B (peaks at later stages) during the erythrocyte cycle. The blue, red and orange colours represent expression profiles of the HB3, 3D7 and DD2 strains. The x-axis shows hours post invasion of the parasite and the y-axis represent the signal obtained for the protein expression.

4.8 Microscopic visualisation of PfMyoA-GFP and PfMyoB-GFP during erythrocyte invasion.

Merozoite invasion of the host erythrocyte is a necessary stage in *Plasmodium* infection and essential for malaria parasite survival. The first EM visualisation of invasion was in the 1970s by Aikawa (Aikawa et al., 1978; Aikawa et al., 1981; Bannister et al., 1975) and more recently using high resolution epifluorescence imaging technologies (Riglar et al., 2011; Zuccala et al., 2012). Although the moving junction (MJ) has been recognised morphologically for many decades, the proteins that contribute to this interface were only recently identified. The rhoptry neck proteins (RONs) along with micronemal protein AMA1 form a complex which was found to be localised to the MJ forming a ring at the site of invasion. Several RON proteins are inserted into the host cell plasma membrane and function as the parasite's own receptor transferred into the host cell, which also provides a point of anchorage for the invasion process. According to Boyle and colleagues merozoites invade the host cell within 10 min at 37^{o}C (Boyle et al., 2010). With a reliable and quick method of fixation of *P. falciparum* merozoites during the invasion process the localisation of merozoite proteins relative to the moving junction can be visualised during this whole process. RON4 has been established as a key protein in the moving junction. Therefore we decided to use antibodies to RON4 to facilitate the visualisation and determination of the stage of invasion. PfMyoA-GFP and PfMyoB-GFP were visualised during invasion

relative to RON4, which can be traced by IFA from a single point at the apex of the merozoite during attachment through to junction closure upon completion of the entry and formation of the PV. The localisation of PfMyoA-GFP and PfMyoB-GFP during erythrocyte invasion is shown in Figure 4.11 and Figure 4.12 respectively.

As described in section 2.9 (Chapter 2) tightly synchronised PfMyoA-GFP or PfMyoB-GFP late stage schizonts were mixed with uninfected erythrocytes and shaken at 37^{o}C for 30 min. Samples were taken at 2, 5, 8, 10, 20 and 30 min and fixed and permeabilised in solution. RON4 was detected with mouse α-RON4 mAb (24C6) followed by goat anti mouse secondary antibody coupled with Alexa 594. To investigate the PfMyoA-GFP and PfMyoB-GFP localisation, affinity purified rabbit α-GFP antibodies were applied followed by goat-anti rabbit Alexafluor 488-labeled antibodies. DNA was stained with 0.1µg/ml DAPI. In free merozoites RON4 showed a single dot at the apical tip of the cell. PfMyoA-GFP localised at the periphery of free merozoites (Fig 4.11 top row) and PfMyoB-GFP (Fig 4.12 top row) at the anterior end of the merozoites apical to RON4. In live host cell invasion, the initial attachment is reversible, here this event has been frozen and was identified by RON4's localisation, changing from a single point at the merozoite apex to a slightly elongated band when the actual moving junction has been formed. Also the erythrocyte shows a slight indentation at the point of attachment and protuberances of the erythrocyte's membrane mark the formation of a moving junction. Protuberances are detected associated with echinocytosis, which was triggered by the internalisation and sealing events when a merozoite enters into the erythrocyte. The protuberances may result from the increased erythrocyte membrane deformability that is probably due to changes of rigidity and flexibility in the underlying cytoskeleton and resulting from stimulation of signalling receptors (β-adrenergic) which increase the cyclic AMP level (Gilson and Crabb, 2009). PfMyoA-GFP remained circumferential throughout the invasion process, whereas PfMyoB-GFP at initial attachment showed a partial co-localisation with RON4 (Fig 4.12, second row). As the merozoite moves into the developing PV, RON4 forms a circumferential zone of labelling around the attachment point of the parasite to the cell, which appears as a ring in three dimensions or two points of fluorescence in a two-dimensional cross section and depicts the movement of the tight junction (Riglar et al., 2011).

In this experiment, the stage of RON4 ring formation as mention above was not clearly displayed, however RON4 appeared as an elongated band marking the progression of the junction. As can be clearly seen from Fig 4.11 PfMyoA-GFP still showed peripheral merozoite staining. The staining did not seem to follow the moving junction but rather be circumferential throughout. PfMyoB-GFP also did not follow the moving junction but rather stayed in the apical position of the merozoite with the moving junction, as visualised by RON4, moving over the merozoite. In Figure 4.12 (row 3) RON4 shows a partial co-localisation with PfMyoB-GFP and in row 4 RON4 is located anterior to PfMyoB-GFP suggesting the secretion of RON4 from the rhoptry neck into the host cell. Finally the parasite has finished invading the erythrocyte and RON4 is localised in the remnant junction, which has closed the developing PV and plasma membrane at the posterior of the parasite. After completion of invasion PfMyoA-GFP lies on the inside of the sealing PV (RON4 demarking the host cell side of the PVM), whereas PfMyoB-GFP stayed at the original apical localisation at the opposite end to PfRON4 and before RON4 spreads in patches around the expanding PV membrane (PVM), suggesting loss of structural integrity of the junction at this stage.

During early ring stages PfMyoA-GFP seems to localise inside the PVM however it is gradually lost until it is expressed prominently again during parasite segmentation, which suggests a role for it in the invasion motor complex as discussed in section 4.4 and 4.5. On the other hand, PfMyoB-GFP still appeared as a single dot localised inside the PVM. We knew from the time course studies that PfMyoB-GFP was expressed later in the intracellular life cycle starting around ~40 hours post invasion during parasite segmentation and localised at the apical end anterior to the RONs (section 4.3 and Figure 4.5). We assume that after invasion has been completed that PfMyoB-GFP will gradually be lost. If this is the case we may hypothesize that PfMyoB-GFP is crucial for invasion although the actual role remains unknown. More investigations need to be performed to answer this question, for example by generating gene knockout parasites.

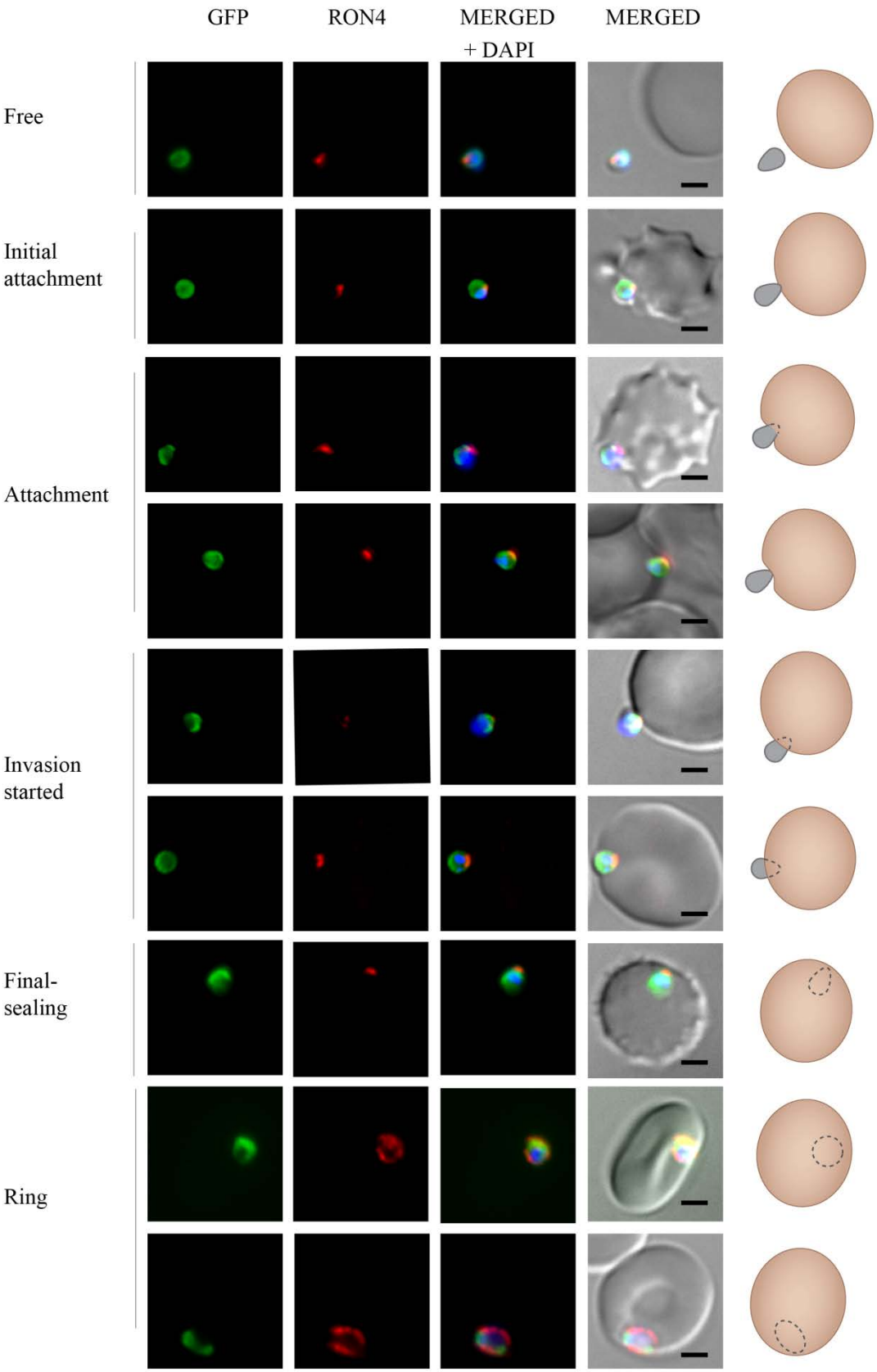
GFP
RON4
MERGED
+ DAPI
MERGED
Free
Initial attachment
Attachment
Invasion started
Final-sealing
Ring

Figure 4.11: Stepwise visualisation of PfMyoA-GFP parasites during merozoite invasion of the host cell. The PfMyoA-GFP parasite was fixed during various stages of invasion. MyoA-GFP was localised using rabbit anti GFP antibodies (1:200), RON4 was detected using mouse monoclonal antibody 24C6 (1:400), and the nucleus stained with DAPI. The invasion steps were divided into free merozoites, initial attachment, followed by attachment and invasion as well as the final steps depicted as final sealing of the parasite within the host cell and establishment in the PV for development (ring). PfMyoA-GFP (green), RON4 (red) and nucleus (blue) are shown as well as a cartoon of the invasion. Scale bar is 2µM.

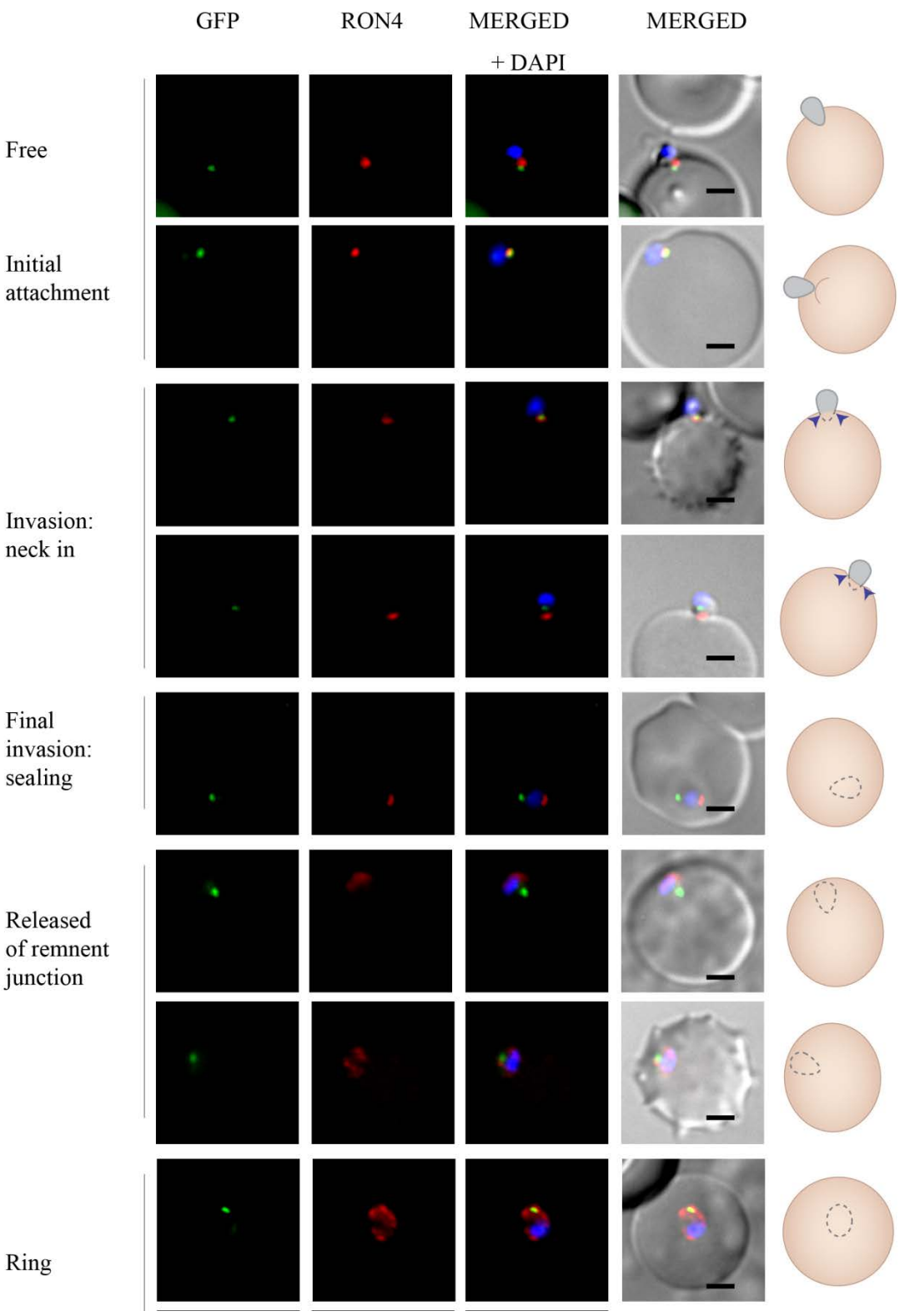
GFP
RON4
MERGED
+ DAPI
MERGED
Free
Initial attachment
Invasion: neck in
Final invasion: sealing
Released of remnent junction
Ring

Figure 4.12: Stepwise visualisation of PfMyoB-GFP during merozoite invasion of the host cell. The PfMyoB-GFP parasite was fixed during various stages of invasion. MyoB-GFP was localised using rabbit anti GFP antibodies (1:200), RON4 was detected using mouse monoclonal antibody 24C6 (1:400) and the nucleus stained with DAPI. The invasion steps were divided into free merozoites, initial attachment, followed by early and late stages of invasion (neck in versus final invasion) as well as the finishing steps of invasion with the release of the remnant junction and the formation of ring stage. PfMyoA-GFP (green), RON4 (red) and nucleus (blue) are shown as well as a cartoon of the invasion. Scale bar is 2µM.

4.9 Characterisation of MyoA and MyoB in *Plasmodium knowlesi*

Despite the successful GFP-tagging of MyoA and MyoB in *P. falciparum*, the localisation, especially for MyoB, proved to be very challenging to establish due to the size of the parasite. By comparison, *P. knowlesi* merozoites are about twice the length of *P. falciparum* (1.5 versus 3.7 µm) and are viable for a longer period after egress (Aikawa et al., 1978; Aikawa et al., 1981). Therefore *P. knowlesi* may enable more detailed observation of protein localisation. In this section we performed transfections with linear and circular DNA to generate *P. knowlesi* MyoA and MyoB transgene parasite lines. Single cross over transfection using circular DNA is widely used in *P. falciparum*, whilst linear DNA is the preferred substrate for homologous recombination in *P. knowlesi*. Whilst linear DNA may integrate more readily, it cannot be replicated in the parasite and so is rapidly degraded. As transfection efficiency is lower in *P. falciparum* there is very small chance that it is integrated straight away. The advantage of using linear DNA is that the time required for selecting integrants is about 2 weeks versus the 3-4 months required for transfection with circular DNA. This is because the transgenic population that initially grows contains a high proportion of parasites with integrated DNA and few carrying the plasmid as an episome. In *P. knowlesi*, MyoA-GFP DNA and MyoB-GFP DNA were transfected using both linear and circular constructs. Both were tried as this work was carried out at an early stage in the development of the *P. knowlesi in vitro* transfection system in 100% human blood (Moon et al., 2013), and we were not sure of the efficiency of transfection.

The GFP-tagging of the endogenous MyoA and MyoB genes of *P. knowlesi* was achieved by integration of a tagging construct via single cross over homologous recombination into the parasite genome. In order to introduce the GFP tag at the C-terminus of each protein, a region of homology corresponding to 1097 bp (MyoA) and 1064 bp (MyoB) from the 3' end of each ORF lacking the stop-codon was selected. The region of homology was amplified by PCR using primer combination 1F1/1R2 for MyoA and 2F1/2R2 for MyoB (Chapter 2, Table 2.2). These regions of homology were cloned between the XmaI/AvrII sites of pHH4-GFP (Knuepfer et al., unpublished) and the correct sequence confirmed by Sanger sequencing (Beckman Genomics), generating the constructs pHH4-PkMyoA-GFP and pHH4-PkMyoB-GFP respectively. In each case the cloning resulted in the targeting fragment being placed upstream of the GFP ORF followed by the Pbdhfr 3'UTR. The strategy for integration followed the work in *P. falciparum* and is summarised in Figure 4.13 for MyoA and Figure 4.14 for MyoB.

Prior to linear transfection, plasmid DNA was linearized with NruI and AflII for MyoA and MyoB respectively. After transfection of 20 µg plasmid DNA (linear and circular plasmid) for each construct into schizont stage parasites, 2.5 nM WR99210 was added and the parasites cultured continuously under drug selection for approximately 2 to 3 weeks. The parasite that grew after these times were depicted as cycle 0, and whilst resistant to WR99210, as expected; this resistance was predominantly due episomal maintenance of the targeting construct. The transfected cultures were then grown for 3 weeks without drug selection, to allow loss of the episomal construct (due to uneven segregation of the episome) followed by a further week of growth under WR99210 selection again. The resultant parasite populations were designated cycle 1 and this was repeated further until transgenic parasites were obtained. Cultures were checked after each cycle for integration of the construct by both diagnostic PCRs and monitoring for GFP expression. The plasmids transfected into the parasites lack a promoter to drive expression of the tagged genes, thus the GFP tagged version can only be expressed once the plasmid has integrated and expression can be driven by the endogenous promoter. This means that expression of GFP can be taken as a strong indication of correct integration of the plasmid.

Expression of MyoA-GFP was detected in parasites following transfection with a linear construct (henceforth called PkLinA-GFP) and for MyoB-GFP following transfection with a circular construct (henceforth called PkCirB-GFP). Preliminary

live fluorescent imaging of PkLinA-GFP and PkCirB-GFP showed a pattern of GFP signal similar to that as detected in *P. falciparum*. A strong GFP fluorescence signal associated with the periphery of developing merozoites was detected in PkLinA-GFP (Figure 4.13), and a PkCirB-GFP signal with an apical end localization was also detected (Figure 4.14). These results were further confirmed by IFA using GFP antibody. Although transfection with these constructs eventually produced *P. knowlesi* transgenic parasite lines for MyoA and MyoB, cloning of these transgenic parasite lines was unsuccessful due to the relatively low proportion of integrated parasites. To improve the efficiency of the transgene's expression, we plan in the future to transfect using newly produced vectors specifically designed for *P. knowlesi* (produced by Robert Moon, NIMR). This work is in progress. These vectors replace *P. falciparum* promoter regions with *P. knowlesi* sequence, resulting in better expression of the selectable marker, and much higher integration efficiency.

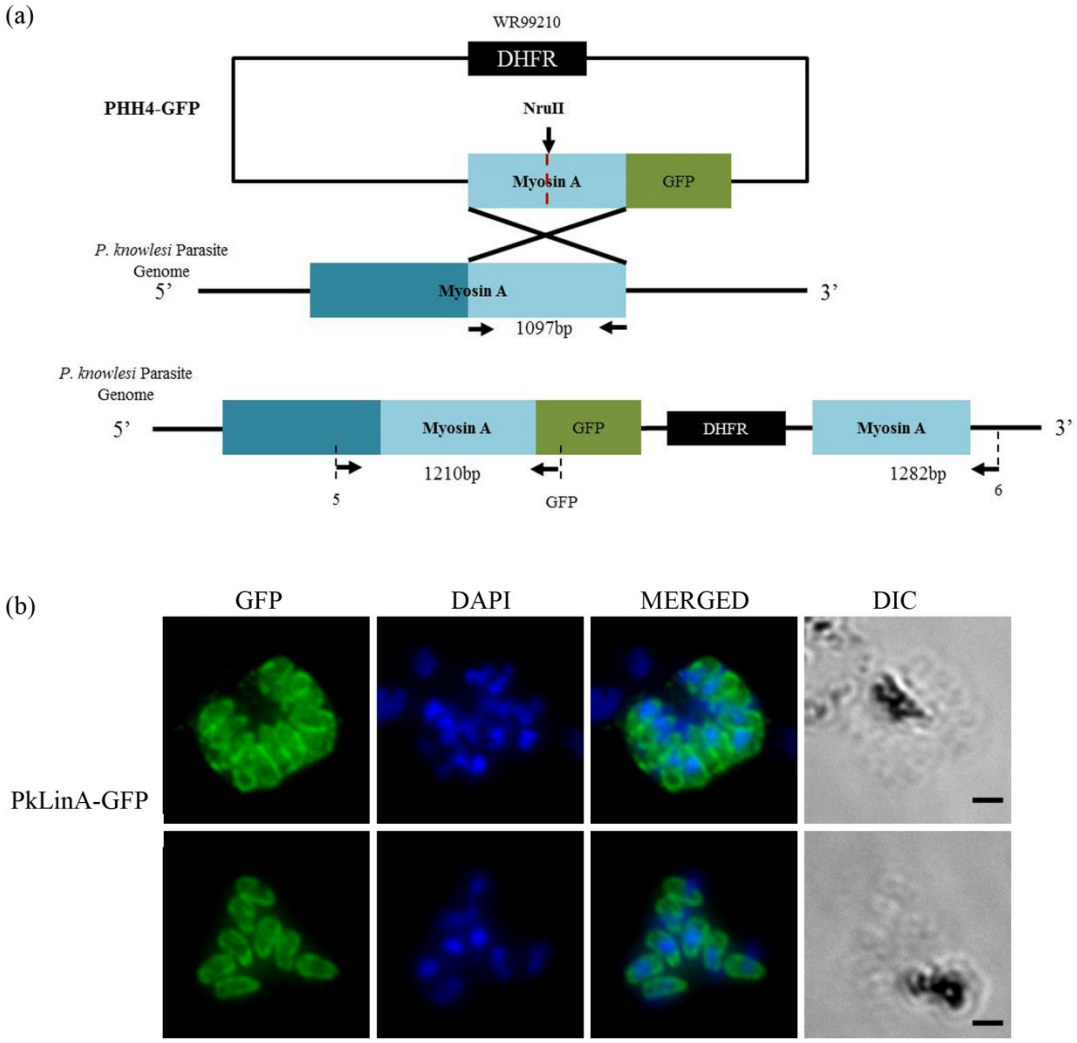

Figure 4.13: Generation of PkLinA-GFP parasites. (a) Plasmid DNA used for circular and linear transfection. This illustrated diagram depicts the unique site (NruI) for linearization purposed. Schematic representation of the gene replacement strategy by single cross over MyoA homologous recombinant and integration into the *P. knowlesi* genome with primers for PCR (arrows), and containing the pyrimethamine-resistant DHFR selectable marker and a complete integration strategy. The 1097bp homology region of PkMyoA gene is also present. (b) The un-cloned PkLinA-GFPIFA probed with GFP antibody (1:300) and analysed at 1000X magnification. PkLinA-GFP is evenly distributed at the parasite periphery as shown in *P. falciparum*. .Nucleus stained with DAPI. Scale bar is 2µM.

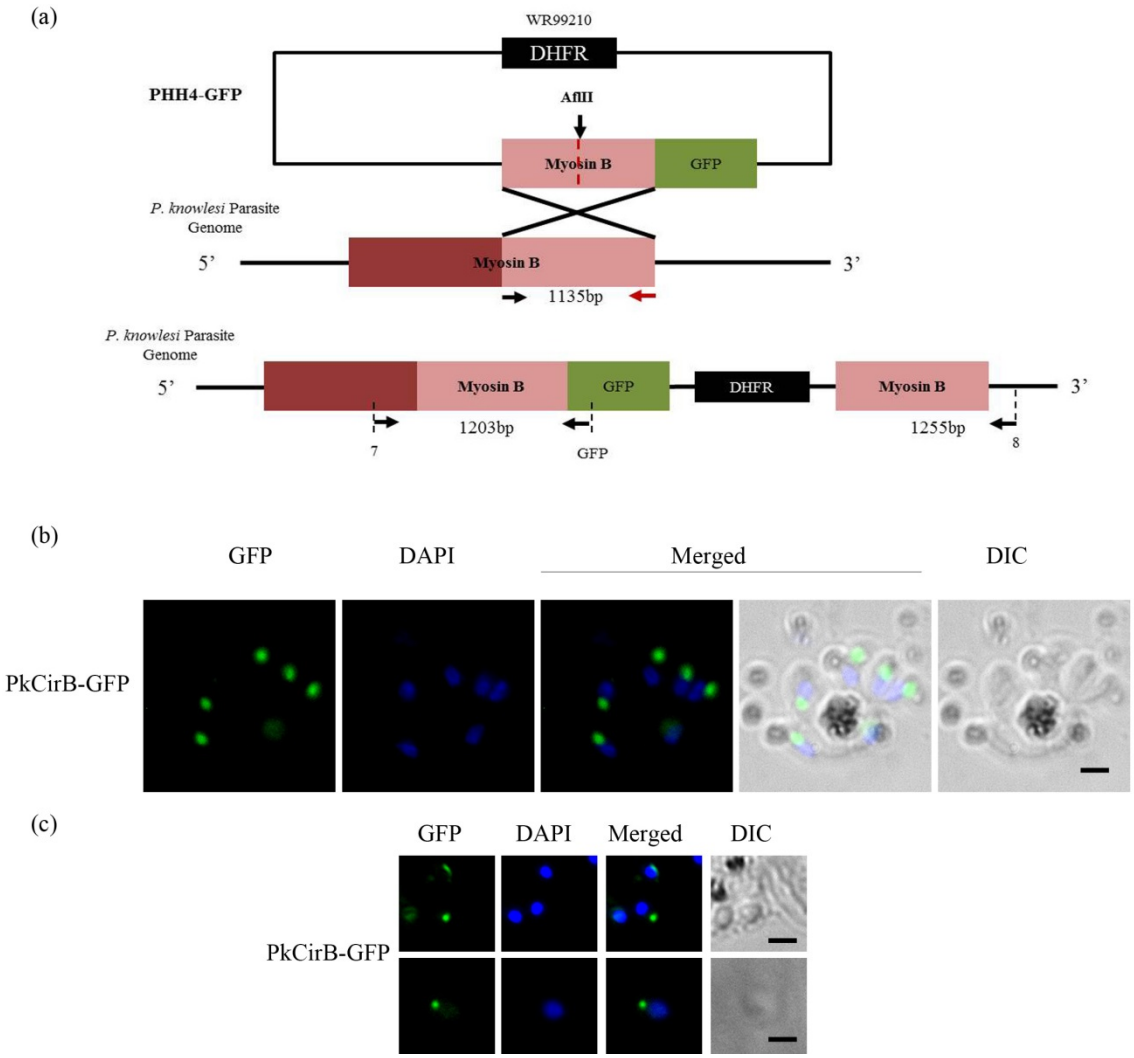

Figure 4.14: Generation of PkCirB-GFP parasites. (a) The vector is linearized at the unique Af1II site generated in the homology region. Schematic representation of the gene replacement strategy by single cross over MyoB homologous recombination and integration strategy into *P. knowlesi* with primers for PCR (arrows) and containing the pyrimethamine-resistant DHFR selectable marker and a complete integration strategy. The 1064bp homology region of PkMyoA gene is also present. (b) and (c) The un-cloned PkCirB-GFP transgene parasite as viewed by live fluorescence microscopy. PkCirB-GFP is eventually located at the parasite anterior at the apical end as demonstrated for PfMyoB-GFP. Nucleus stained with DAPI. Scale bar is 2µM

4.10 Generation of anti -MyoA and anti-MyoB antibodies

In addition to the generation of transgenic parasites expressing proteins of interest, specific antibodies to these proteins will also be important tools, for example for use with western blots, IFAs and immunoprecipitation. Although in this scenario it is not crucial due to the use of commercial α-GFP antibodies for transgene expression detection, it is an advantage to have those specific antibodies to complement this strategy or to serve as controls for these tagged lines.

Four peptide sequences were chosen to generate MyoA and MyoB antibodies. The MyoA peptide was selected based on a region conserved between *P. falciparum* and *P. knowlesi* to increase the chance antibodies would cross-react between the two species (Figure 4.15.i), and this was used to raise antibodies in rats. MyoB antibody was raised in rabbits using MyoB sequences selected to be conserved between both *P. falciparum* and *P. knowlesi* (Figure 4.15.ii). Based on previous experience of producing antibody in rabbit, there was the possibility that the antibody produced would not be very specific, and therefore antibodies for another 2 peptide sequences specifically targeting either MyoB in *P. falciparum* (anti-PfMyoB) or *P. knowlesi* (anti-PkMyoB) were raised in rats (Figure 4.15.iii). Synthesis of all peptides and production of the antibody was carried out by Pepceutical Ltd following a standard protocol. In addition, an antibody to full length MyoA (MyoA-FL) was also generated against the recombinant protein produced in the cell free system. The immunization was carried out in rats by Harlan Biosciences following the 34 day standard protocol. Animals to be used were pre-screened by western blot prior to inoculation to avoid previously existing cross reacting antibodies. Terminal bleeds were used in immunoblot to detect MyoA and MyoB. Immunoblot analysis showed that the MyoA-FL antibody reacted strongly with a *P. falciparum* parasite lysate in western blot (Figure 4.16.a), whereas Pf/k-MyoA and Pk/f-MyoB antibodies strongly detected a single band corresponding to native MyoA (~93 kDa) in both *P. knowlesi* and *P. falciparum* western blot (Figure 4.16.b and c) with a stronger band detected for MyoA compared to MyoB as expected due to the abundance of the proteins.

We used MyoA-FL, Pf/k-MyoA, Pk/f-MyoB, anti-PfMyoB and anti-PkMyoB antibodies to establish whether or not the signal co-localised with the GFP signal in PkLinA-GFP and PfMyoA-GFP parasites by IFA. Although, MyoA-FL and Pk/f-

MyoB antibodies strongly recognized a band corresponding to MyoA and MyoA/MyoB, respectively on a western blot, unfortunately no fluorescence signal was detected in either GFP-tagged parasite lines (data not shown). Co-localization of PkLinA-GFP with Pf/k-MyoA antibody gave a strong peripheral fluorescent signal that indicated a strong recognition of MyoA by Pf/k-MyoA antibody (Figure 4.16.d). Co-localisation of PkLinA-GFP and PfMyoA-GFP with anti-PkMyoB antibody showed that MyoB was recognized by these antibodies (Figure 4.16.e and f). Although the localization of MyoB at the apical end of the parasite had been shown in section 4.2 and 4.3, this is the first time we observed the MyoB pattern as recognized by antibodies. In *P. falciparum*, MyoB antibody gave a single discrete dot at the apical end as predicted (Figure 4.16.f). On the other hand, in *P. knowlesi*, MyoB gave a slightly different pattern: in microscopy imaging of the *P. knowlesi* transgenic parasite, MyoB appeared as a doubled dot. This may be due to possible cross reaction with unspecified antigen (we used crude serum), alternatively it might be a consequence of the bigger size of *P. knowlesi* compared to *P. falciparum*, allowing us to resolve the labeled structure in greater detail. This is a very interesting finding and further investigation is needed. Due to some technical difficulties and time limitations, the IFA for PkCirB-GFP parasites with all the generated antibodies was not performed, thus we can't confirm by reciprocal analysis the antibody activities. We hope to resolve the technical problems and further clarify the protein's location by performing IEM.

Figure 4.15: Sequence selection for generation of synthetics peptides to elicit MyoA and MyoB antibodies. (I*) P. falciparum* sequence (pink residues) used for MyoA antibody production that can be used in both *P. falciparum* and *P. knowlesi*. (II) *P. knowlesi* sequence (pink residues) used for production of MyoB antibody that can be used in both *P. falciparum* and *P. knowlesi*. (III) Species specific sequences used to produce *P. knowlesi* MyoB and *P. falciparum* MyoB (pink residues). In general, the red and blue residues are for sequence comparison between *P. knowlesi* MyoA and MyoB, and *P. falciparum* MyoA and MyoB respectively

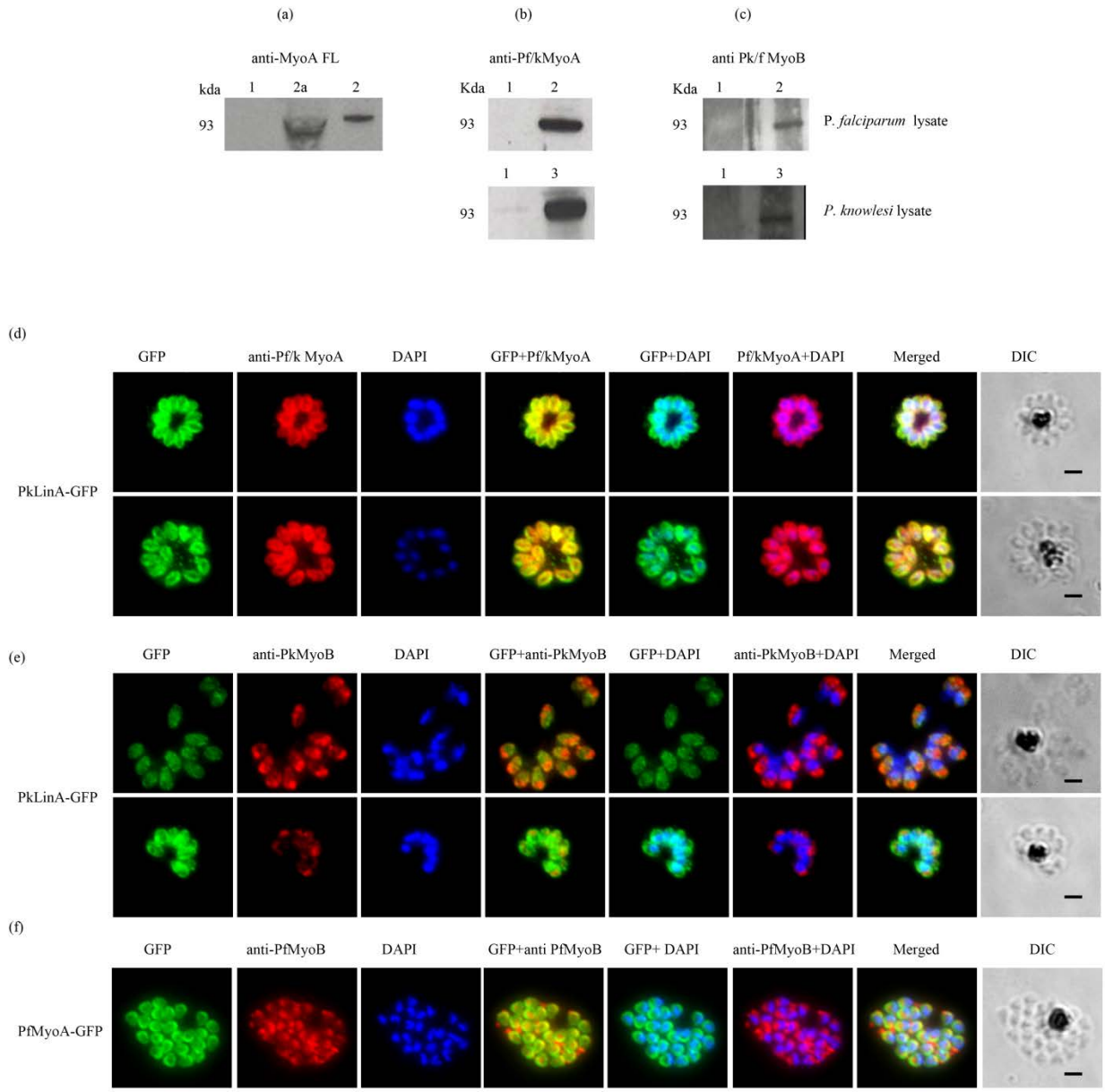

Figure 4.16: Production of MyoA and MyoB antibodies tested by western blot and IFAs. (a) to (c) Western blot of the full length MyoA (MyoA-FL), Pf/k-MyoA and Pk/f-MyoB antibodies (1:200) against *P. falciparum* and *P. knowlesi* wild type parasite lysate. Single band (~93 kDa) indicated the recognition of MyoA or MyoB by these antibodies. RBC (1); 3D7 schizont NP-40 lysate (2a); 3D7 crude schizont lysate (2) and *P. knowlesi* schizont lysate (3). (d) and (e) Co localisation of PkLinA-GFP with GFP antibody and Pf/k-MyoA or with anti-PfMyoB antibodies. Pf/k-MyoA antibody gave a strong fluorescence signal at the periphery of the parasite indicating the recognition of MyoA. (f) Co localisation of PfMyoA-GFP with GFP antibody and anti

PfMyoB antibodies. Anti-PfMyoB antibody also gave a strong fluorescence signal at the apical end of the merozoite in both PkLinA–GFP and PfMyoA-GFP indicating the recognition of MyoB. GFP-antibody shown in green (Alexa 488), the Pf/k-MyoA and anti-PfMyoB antibody in red (Alexa 594), nucleus stained blue. 1000x magnification. Scale bar is 2 µm.

4.11 Discussion

Myosins are molecular motor proteins that are capable of either translocating actin filaments using ATP hydrolysis to provide energy, and driving cellular movement in eukaryotes or of translocating vesicles or cargo on fixed actin filaments. In this chapter, *Plasmodium* Myosin A and B are characterised *in vivo*.

Myosins A and B are the smallest members of the myosin superfamily (Foth et al., 2006), both displaying a similar molecular weight (~93kDa each), and like their homologue in *T. gondii*, they each are characterised by a short or almost nonexistent tail which cannot be defined easily. Compared to the other myosins, MyoA appears to possess a very divergent neck with one degenerate IQ motif. The degenerate IQ motif, present at the extreme C-terminus of MyoA, associates with the calmodulin-like protein, TgMLC1 or PfMTIP (Bergman et al., 2003; Herm-Gotz et al., 2002). In *T. gondii* it has been proposed that the N-terminal extension of MLC1 substitutes for the tail of MyoA. MyoA along with at least four additional proteins makes up the invasion motor complex, which consists of MyoA-MLC1/MTIP-GAP45-GAP50 (Baum et al., 2006b; Frenal et al., 2010; Green et al., 2006b; Heaslip et al., 2010; Herm-Gotz et al., 2002; Jones et al., 2006; Soldati and Meissner, 2004). General conservation of the glideosome components has been demonstrated between at least six *Apicomplexa* genera, indicating that this complex plays an important role in host cell invasion and motility (Bergman et al., 2003; Gaskins et al., 2004). An important role for MyoA and the motor complex in host cell invasion is supported by the successful genetic knock down of MyoA in *T. gondii* and *P. berghei* ookinetes (Siden-Kiamos et al., 2011) which led to a severe impairment of cell entry (Meissner et al., 2002), although this result has been contradicted by recent studies which show by the generation of a MyoA

knockout that this protein is not absolutely necessary for cell invasion (Andenmatten et al., 2013). Although MyoA has been biochemically characterised by various studies in both *Plasmodium* and *Toxoplasma*, little is known about MyoB. This study was intended to characterise PfMyoB further in particular to investigate where it is located and which proteins it forms a complex with.

4.11.1 The use of transgenic parasites to investigate the timing and localisation of *MyoA and MyoB expression*

The localisation of MyoA and MyoB has been clearly demonstrated in this study. PfMyoA-GFP shows a strong and stable peripheral localisation suggestive of the pellicle. Meanwhile, the signal from PfMyoB-GFP indicates a different localisation, at the apex of the merozoite. Using *P. knowlesi,* newly adapted to continuous culture in human blood (Moon et al., 2013), the GFP sequence was inserted into the endogenous locus of PkMyoA and PkMyoB. Interestingly, PkMyoA-GFP showed a peripheral merozoite staining similar to that of PfMyoA-GFP, whereas PkMyoB-GFP gave a signal at the extreme apex of the merozoite. Using GFP has allowed the direct localisation of MyoA and MyoB to be achieved in a living cell in real time by live fluorescence microscopy. A similar pattern of localisation of MyoA and MyoB at the periphery and apical tip respectively has been shown recently in ookinetes of *P. berghei* (personal communication, Rita Tewari, University of Nottingham). The addition of GFP to the protein's C terminus has overcome the need to fix and label proteins with specific antibodies to the protein of interest, eliminating possible fixation problems and artefacts. Nevertheless, antigen-specific antibodies were used to identify MyoA and MyoB in both transgenic parasite species, which has aided the characterisation and localisation of MyoA and MyoB in the parasite. Due to time constraints, the characterisation of MyoA and MyoB from only one species of the parasite - *P. falciparum* – was pursued. Any further characterisation of *P. knowlesi* MyoA and MyoB will be carried out in the future but is beyond the scope of this thesis.

Upon successfully generating PfMyoA-GFP parasites, the expression and localisation pattern previously described was confirmed (Pinder et al., 1998). MyoA colocalises with the glideosome motor complex at the IMC. The peripheral location of

MyoA has previously been shown in *P. falciparum* by immuno-EM imaging (Pinder et al., 2000) and by immunofluorescence using specific antibodies to MyoA in *T. gondii* (Hettmann et al., 2000; Opitz and Soldati, 2002) and *P. yoelii* sporozoites (Matuschewski et al., 2001). Although the peripheral localisation of PfMyoA is established, this study demonstrates for the first time the development of PfMyoA-GFP throughout the intra-erythrocytic cycle by live cell imaging and Western blot as well as immunoprecipitation of PfMyoA-GFP from time course protein samples. Using tightly synchronised parasites and live cell imaging, we found that PfMyoA-GFP was highly expressed at the parasite periphery during segmentation (~40 h post invasion), marked by a high intensity of fluorescence around the parasite pellicle. PfMyoA-GFP also colocalised with PfMTIP, PfGAP45 and PfGAP50 throughout the segmentation process, as determined by IFA over the time course. This co-localisation complements previous work which located the other motor complex components to the periphery of several Apicomplexan zoites by live microscopy and IFA: GAP45 (Frenal et al., 2010; Gaskins et al., 2004; Ridzuan et al., 2012), GAP40 (Frenal et al., 2010), GAP50 (Gaskins et al., 2004; Yeoman et al., 2011), and MTIP (Bergman et al., 2003; Green et al., 2006b). Therefore in this study we support and confirm the earlier findings of MyoA's involvement in the motor complex. In addition, Rizduan et al., (2012) showed that the episomally expressed GFP tagged GAP45 start as dots or rings that elongate and spread rearward as the IMC forms starting at 30 h, but MyoA did not show the same development pattern suggesting that, MyoA only binds to fully formed IMC. As mention earlier in section 4.5, the expression of GAP45 was not detected at 30 h as found in a previous study (Ridzuan et al., 2012); it was only found at around 36-38 h by GFP-IP, suggesting that it only comes into association with MyoA at a later stage (38 h) when the IMC is fully developed.

As well as providing confirmation of the location and expression of MyoA, this study presented a novel insight into PfMyoB-GFP expression and localisation. PfMyoB-GFP displays a distinct expression profile: very late during schizont development and at the extreme apex of the cell. Although MyoA and MyoB are from the same class of myosins (XIV), and have a similar molecular weight (~93 kDa) and amino acid sequence (>50% similarity), they appear very different under the microscope. As described above, PfMyoA-GFP is located at the parasite periphery, whereas PfMyoB-GFP is located at the apex of merozoites. The timing of PfMyoB-

GFP expression indicates that the protein is relatively abundant at the time of parasite segmentation, around ~40 h or later post invasion. It might be expressed earlier than that, probably from around~36 h post invasion, but in low abundance. Live time course experiments showed that at the earlier times, the expression of PfMyoB-GFP is very faint and diffuse. This can not be ignored, because as also shown for PfMyoA-GFP expression, although only faint diffuse fluorescence was detected during earlier time points (from 21 h post invasion) in the time course analysis, the expression was confirmed by western blot, indicating that the protein was clearly expressed. Therefore, PfMyoB-GFP may also be expressed as early as the faint diffuse fluorescence was detected in the time course analysis, which is ~36 h post invasion. This result needs to be confirmed by western blotting of the time course protein samples, but unfortunately, this experiment will be beyond the scope of the thesis. This issue was also discussed briefly by Chaparro and colleagues (Chaparro-Olaya et al., 2005), where the authors used RT-PCR to analyse cDNA from different stages of parasite development, and suggested a role for MyoB in invasion due to the fact that MyoB was transcribed in late schizonts and merozoites. In order to determine the exact location of PfMyoB-GFP within the parasite, colocalisation studies were carried out with apical markers, such as micronemal proteins (AMA1 and EBA175), rhoptry proteins (RON3, RON4 and RAP1) and antibodies to actin and microtubules (α-tubulin). Consistent with the earlier hypothesis that MyoB is involved in invasion; this study showed the localisation of PfMyoB-GFP to be at the very apical tip of the merozoite, in front of other apical organelle markers. There was some overlap with the actin marker (AC-40). However due to the small size of the cell (1 µm) and a resolution limit of 0.2 µm for light microscopy we cannot be certain about this.

Due to PfMyoB's distinct location separate from these known apical markers, further investigation was required. At the extreme apical tip of the merozoite lies a microtubule organising centre (MTOC) unique to Apicomplexa and named the apical polar ring (Morrissette and Sibley, 2002; Russell and Burns, 1984). The polar ring is made up of three tubulin ring-like structures, the third of which (anterior to posterior) is believed to be the site of subpellicular microtubule organisation, which maintains the cell's shape and polarity (Bannister et al., 2000a). Due to the extreme apical location of PfMyoB-GFP, it is possible that this protein interacts with or forms part of the polar ring. IFAs were performed using actin and tubulin antibodies to investigate this

hypothesis. PfMyoB-GFP co-localised partially with actin, meanwhile co-staining with tubulin antibodies showed a localisation in between two connecting microtubules. Since the minus ends of sub-pellicular microtubules reside inside the polar ring and are laterally attached to MTOC through a shallow depression, there is a linkage between both polar ring and microtubules (Morrissette and Sibley, 2002; Russell and Burns, 1984). According to the apparent location of MyoB at the opposite end to the nucleus, in front of the apical markers, partially overlapping with actin and overlapped with the two tubulin ring, perhaps it is a component related to the sub-pellicular microtubules. In *Toxoplasma*, the apical polar ring can be identified using antibodies to a recently discovered component of the apical polar ring - RNG1(Tran et al., 2010). This protein appears to be unique to coccidian Apicomplexa as it is absent from *Plasmodium spp.* and therefore could not be used for co-localisation studies. However *Plasmodium* may share an orthologous proline-rich protein which is yet to be characterised. The location of RNG1 seems to be comparable to PfMyoB-GFP localisation. Potential interactions between MyoB and the apical ring complex remain to be studied.

4.11.2 MyoA and MyoB share common ancestry but are retained in different complexes.

Due to the small size of merozoites, localisation by fluorescence microscopy is not a definitive method of identifying a protein's subcellular location. If MyoA and B were shown to interact with a protein of known location and role within the cell then more reliable conclusions could be drawn regarding these proteins' function. The method of choice to complement the microscopy results in this study was immunoprecipitation (IP), followed by mass spectrometry or western blotting. IP using α-GFP specific antibodies demonstrated that PfMyoA-GFP assembled into the glideosome motor complex as it co-precipitated other motor components - PfMTIP, PfGAP45 and PfGAP50. Previous work on the complex has shown that PfGAP50 is synthesized before other components of the complex, and its role is likely to reflect the formation of the IMC and the host cell invasion by merozoites (Yeoman et al., 2011). The results showing the association of MyoA with the glideosome motor complex complements earlier studies in both *Toxoplasma* and *Plasmodium*. Since the first

characterisation of MyoA in T*oxoplasma* (Heintzelman and Schwartzman, 1997) and *Plasmodium* (Pinder et al., 1998), the role of MyoA in the acto-myosin motor has been widely discussed (Herm-Gotz et al., 2002; Meissner et al., 2002). A dibasic motif in the MyoA tail was shown to be essential to determine membrane localization (Hettmann et al., 2000), due to it's role in binding to myosin light chain (TgMLC1) (Herm-Gotz et al., 2002), and anchoring to the IMC by TgGAP45 via TgGAP50 (Gaskins et al., 2004; Johnson et al., 2007) in the invasion motor complex.

In *Plasmodium*, PfMyoA, PfMTIP, PfGAP45 and PfGAP50 (orthologous proteins of TgMyoA, TgMLC1, TgGAP45 and TgGAP50, respectively) were demonstrated to participate in gliding motility and host cell invasion (Baum et al., 2006a). MyoA interacts with MTIP (Bergman et al., 2003; Bosch et al., 2007a; Bosch et al., 2006; Green et al., 2006a; Thomas et al., 2010) and is anchored to GAP50 (Bosch et al., 2012; Yeoman et al., 2011) in the IMC via GAP45 (Gilk et al., 2009; Rees-Channer et al., 2006; Ridzuan et al., 2012; Thomas et al., 2012). Therefore the expression of PfMyoA-GFP at the periphery occurs at the right location and the right time to be part of the motor complex.

LC-MS/MS analysis of PfMyoA-GFP immunoprecipitated proteins revealed novel motor complex-associated proteins such as several members of the PfGAPM protein family, GAPM2 and GAPM3. These proteins are multi-pass membrane proteins and may provide additional anchoring of the motor complex to the IMC, and have also been identified in *T. gondii*. Using HA-tagged GAPM3 co-localised with GAP45 identified by IFA, GAPM3 localised at the IMC and co-localised with GAP45 but not with $MSP1_{19}$ (Bullen et al., 2009). This study showed for the first time in *Plasmodium* an interaction between GAP40 and the motor complex. GAP40 (Accession ID: PF3D7_0515700) with a molecular weight of 51.8kDa is highly expressed during late schizogony (PlasmoDB: http://plasmodb.org/plasmo/). This association had only previously been described in *T. gondii* (Frenal et al., 2010). According to Frenal et al., GAP40 which contains nine transmembrane spanning domains might play an important role in anchoring the motor complex to the IMC and partnering with GAP50.

Interestingly, this study provides direct evidence that PfMyoB-GFP does not have any relationship with the previously described glideosome motor complex. IP

experiments were performed using GFP specific antibodies on lysates of PfMyoB-GFP-schizonts and no interaction with MTIP, GAP45 or GAP50 was detected (Figure 4.3(i)). LC-MS/MS analysis clarified the western blot finding and identified several potential interaction partners for PfMyoB-GFP that are not identified in a complex with PfMyoA-GFP. Interestingly, PfMyoB-GFP associated with what is believed to be PfMTIP-B. It is not clear whether the interaction of PfMyoB and MTIP-B is the basis for a separate invasion motor which has not previously been identified. This requires further investigation but is beyond the scope of this thesis. PfMyoB-GFP seems to also interact with dynamin 2 (DNY2) and clathrin, as identified by MS analysis. Dynamin and clathrin are known to be involved in vesicular protein trafficking, endocytosis and cytokinesis (Breinich et al., 2009; De Camilli et al., 1995; Rao et al., 2012; Taraschi et al., 2001; van Dooren et al., 2009).

The classical eukaryotic secretory pathway involves budding and fusion of small vesicles between the intracellular organelles. In *Plasmodium*, this classical vesicle mediated secretory pathway is present within the cytoplasm and is involved in protein trafficking to the parasite PM (Foley and Tilley, 1998). DYN2 and clathrin are two proteins precipitated from the GFP-tagged MyoB lysate during the GFP-TRAP analysis and identified by MS analysis (Table 4.2). DYN2 is involved in membrane scission and actin reorganisation (Menon and Schafer, 2013), plays a role in cytokinesis and may contribute to multiple forms of endocytosis. DYN2 is required for scission of endocytotic vesicles by acting as a mechanoenzyme or molecular switch, and the mechanism of action is best understood in the context of its interaction with clathrin in clathrin-mediated endocytosis (CME) (Royle, 2006, 2012). A further literature search of both proteins revealed that together with F-actin they play important roles in clathrin coated vesicle (CCV) formation and vesicle endocytosis (Breinich et al., 2009; Ferguson and De Camilli, 2012; Li et al., 2004; Merrifield, 2004; Praefcke and McMahon, 2004; Royle, 2006, 2012; van Dooren et al., 2009; Zhou et al., 2009). CCV are generated at a single Golgi apparatus and subsequently are delivered to the IMC (Bannister et al., 2000b).

Phylogenetic analysis of the *Apicomplexa* dynamin family shows PfDYN2 belongs to dynamin related proteins, DrpB together with TgDrpB (*Toxoplasm*a) and PvDYN2 (*P. vivax*) (van Dooren et al., 2009). PfDYN2 was implicated in vesicular

trafficking and/or organelle fission. PfDYN2 was found to bind to GTP and hydrolyse it into GDP, and also self-associated in low-salt conditions. The expression of PfDYN2 is restricted to late stages of parasite development in the asexual blood stages as determined by western blot and it's localised by IFA in punctuate structures within the parasite cytoplasm, suggesting its role is to participate in protein trafficking (Charneau et al., 2007). Data obtained from other studies of DrpB showed more evidence of DrpB proteins involved in replication to generate vesicles for the regulated secretory pathway that forms the unique secretory organelles such as micronemes, dense granules and rhoptries, and for protein sorting for targeting to the food vacuole in *Plasmodium* and the apicoplast (a unique chloroplast-like organelle) for other *Apicomplexa* (Breinich et al., 2009). In this study, clathrin and dynamin were in association with MyoB either directly or indirectly to form a complex. Exactly where or when MyoB comes into contact with these proteins or is assembled into the possible complex is not known.

Putting together the results of the PfMyoB-GFP time course experiment (the protein is expressed highly during segmentation), the co-localisation with actin (a partial localisation) and tubulin (at the microtubule connection), and the association with proteins involved in trafficking, it could be hypothesised that MyoB has a role in vesicular transport or an involvement in cytokinesis, where during this final act of cell division, the cytoplasm is pinched off as shown by the role of Myosin II in the assembly of the actin contractile ring for cell division (DeBiasio et al., 1996; Pelham and Chang, 2002). However, further investigation is needed. The results of the IP experiments using MyoA- and MyoB-GFP tagged lines suggest that these two proteins have completely distinct roles.

4.11.3 Investigation of *PfMyoA-GFP and PfMyoB-GFP localization during erythrocyte invasion*

Invasion occurs in distinct stages: initial attachment; apical reorientation; MJ formation and the movement of the MJ from apical to posterior end of the parasite before host cell membrane sealing and PV formation. Although erythrocyte invasion has been the focus of many laboratories for a number of decades, there are several basic questions that remain unanswered such as: what are the molecules involved in initial

attachment and how do they facilitate reorientation; what are the actual molecules involved at the MJ; what causes erythrocyte deformation; what molecules are involved in PV formation; is the vacuolar membrane of parasite or erythrocyte origin; what proteins are involved in gliding motility? Some of the proteins involved in invasion have been successfully identified but there are many more proteins yet to be characterised. Some of the proteins involved directly in the invasion processes have been thoroughly investigated such as the apical rhoptry neck proteins RON2, 4 and 5, micronemal proteins such as AMA1 and EBA-175, several surface proteins, and the glideosome complex. With new technologies emerging, proteins involved in invasion can be labelled and followed over time by microscopy, including 3D imaging and EM.

Our ability to image cellular events during *P. falciparum* invasion provides a unique window into the processes of erythrocyte invasion by these deadly parasites. In this study, fluorescence imaging was used to track GFP-tagged MyoA and MyoB throughout the invasion process. RON4 was used as a cellular invasion marker as the timing of release as well its location at the moving junction has been established (Riglar et al., 2011; Zuccala et al., 2012). Co-localisation IFAs on merozoites arrested within the invasion process were conducted by using α- GFP and α-RON4 antibodies. PfMyoA-GFP and PfMyoB-GFP did not follow the movement of RON4 but remained at the same location within the merozoite during and after invasion as they did prior to release at the end of schizogony. The role of MyoB here remains unclear. One hypothesis is that MyoB is involved in the release of the contents of the apical organelles but remains attached to a structure within the parasite. Alternatively, it might have a role early in ring stage development. The actual role of MyoB is still open for discussion and is under investigation. In order to gather more information the methodology could be improved, for example by the isolation of viable merozoites, as suggested by (Boyle et al., 2010) to ensure that each step of invasion can be visualised easily.

Generation of a knockout parasite line seem to be crucial for defining the role of MyoA in the glideosome motor complex and of MyoB. Although, Meissner et al., (2002) reported that a TgMyoA conditional gene knockout only decreased the host cell invasion it did not prevent the invasion, confirming the important role of MyoA. In more recent work Meissner and co-workers used the DiCre system to generate knockouts of MyoA, a micronemal protein (MIC2) and Actin (Act1) of *T. gondii* in

order to disrupt the function of the glideosome motor complex. MyoA deletion or the absence of MIC2 did not inhibit invasion although some growth defect was observed, whilst the knockout of Act1 showed that actin is essential for parasite survival (Andenmatten et al., 2013). Therefore, the generation of PfMyoA and PfMyoB knockouts using the DiCre system may provide information regarding the functions of both MyoA and MyoB in *P. falciparum*. The application of this conditional knockout approach is a powerful way to generate a rapid and efficient system to examine the phenotype for stage- specific disruption of particular genes. Expanding the investigation to *P. knowlesi* may provide additional advantages such as improvement of image clarity due to a larger cell size. Visualisation by IEM would confirm the location of MyoB during invasion. Although IEM was attempted, imaging was unsuccessful due to an incompatibility of the antibody with the fixation process.

The localisation and interaction between MyoA and the glideosome motor complex has been studied by other groups either in *T. gondii* or *Plasmodium*, producing similar conclusions about both localisation and association of MyoA with the invasion complex. In addition, our studies have also demonstrated the presence of additional proteins in the *Plasmodium* glideosome complex, including GAP40 and the GAPMs family. However, the studies on the actual association should be carried further in the future. Most notably, these studies have provided the first information on PfMyoA-GFP protein expression in live parasites (using live imaging of GFP) and most importantly, the visualisation of MyoA during parasite progression into the host cell during invasion. Although, MyoB was briefly discussed especially during classification of the myosin superfamily, MyoB possesses a different localisation and a different protein complex from MyoA. This is the first study of PfMyoB-GFP protein expression and its localisation in parasite development and during parasite invasion of host cells and the possible MyoB protein complexes.

If MyoB plays a role in gliding motility and invasion as MyoA does, then several questions arise. First, we do not know the mechanism of how a MyoB motor is controlled, although the regulation might involve a mechanism similar to that for MyoA. MyoA is regulated by phosphorylation at the consensus TEDS phosphorylation site, which is serine residue 19 in MyoA, whereas for MyoB, the phosphorylation site(s) are likely to be serine 16 and/or threonine 17. Microtubules have been shown to have signalling roles (Bejon et al., 1997) and a role in translocating AMA1 (within

mcronemes) during merozoites development (Bannister et al., 2003). Although, myosins use actin as their track for translocation, the association of MyoB with microtubules is open for discussion. One possibility is that if MyoB is involved in initiation of invasion by squeezing or stiffening the cisternal membrane to release the secretory organelles, microtubules might support this, and assist with the scission of the opening by PfDNY2. Thirdly, does MyoB play an important role in invasion such as becoming transiently involved withthe same complex as MyoA to determine the direction of movement, as well as anchoring cytoskeletal structures and defining the polar ring structure.

These data indicate that MyoB may have a very interesting role in parasite biology. Future work should therefore include the generation of a MyoB knockout, detailed localization studies using IEM, protein interaction studies with PfMTIP-B, and analysis of functional activities with actin and the association with tubulin. Further analysis of the proteins in *P. knowlesi* may provide significant advantages. All together this will gave a better understanding of the role of the MyoB protein.

Chapter 5

Research Summary

5.1 The reconstitution of the glideosome motor complex *in vitro* using protein produced in the wheat germ cell free translation system

- Attempts to reconstitute the glideosome complex were relatively unsuccessful due to a largely unstructured MyoA protein produced by the cell free system. Although, a proportion of the MyoA was structured to some extent and active, as determined by the optical trapping methods with single molecules, there wasn't sufficient in the protein preparations for their successful use in motility or actin-binding based assays. This study was, therefore, unable to produce the high quality and quantity of soluble MyoA required. Although there was some suggestion of interaction between MyoA and MTIP, these experiments failed to give conclusive evidence of the protein-protein interactions required to reconstruct the motor complex *in vitro,* or to demonstrate the association of MyoA with actin filaments to establish gliding motility (Chapter 3). Initially, it was intended that MyoB should also be produced in the cell free *in vitro* expression system for characterisation and functional studies, but the decision was taken to suspend these plans. Therefore, no future work was planned for this study.

5.2 MyoA has a peripheral localization, forms part of the glideosome motor complex and is involved in erythrocyte invasion

- Characterisation of MyoA by producing a GFP-tagged MyoA in both *P. falciparum* and *P. knowlesi*. With the current technology, the best way to monitor MyoA expression and localisation is by following the GFP-tagged MyoA throughout parasite development, by tagging the endogenous MyoA gene. The successful addition of GFP to the C-terminus of both proteins revealed that MyoA was present around the periphery of invasive merozoites

and expressed in abundance during parasite segmentation, in schizonts and merozoites (Chapter 4; Figure 4.1, 4.6 and 4.13) which is consistent with the findings of Pinder *et al* (1998), where the authors confirm the peripheral localisation with IEM (Pinder et al., 1998).

- The assembly of MyoA to the glideosome motor complex. This study found that MyoA co-localises with MTIP, GAP45 and GAP50 by IFA (Chapter 4; Figure 4.4). This result was further validated by co-immunoprecipitation of GFP-tagged MyoA with the glideosome complex proteins where MyoA was precipitated together with these proteins. The structure of the motor complex was further confirmed by MS analysis of the precipitated GFP-tagged MyoA and associated proteins. The MS results showed that all the proteins previously identified as associated with the glideosome complex including MyoA were present as expected, with the addition of GAP40 (previously identified in *Toxoplasma* by Frenal et al., 2010) and GAPMs (Chapter 4; Table 4.1). GAPMs were previously isolated in *P. falciparum* and *Toxoplasma* where they were proposed as candidates for an IMC anchoring role (Bullen et al., 2009). Prior to this study as shown in Figure 1.12, the *P. falciparum* glideosome motor complex was thought to consist of MyoA (Pinder et al., 1998), MTIP (Bergman et al., 2003; Green et al., 2006b), GAP45, GAP50 (Baum et al., 2006b) and GAPM (Bullen et al., 2009). In this present study, PfGAP40, GAPM2 and GAPM3 were detected by MS analysis of the MyoA IP and have been added to the diagram depicted in Figure 5.1a.

- The redistribution of GFP-tagged MyoA during parasite invasion. It was important to follow the stages of MyoA's progress during invasion until parasite internalisation, in order to clarify its role. This is the first study to investigate the progression of MyoA during the invasion process. Using RON4 as a marker to follow the stages of invasion, MyoA could be seen to progress into the host cell as expected, however the sub-cellular location of MyoA was distinct to that of RON4. MyoA remained associated with the parasite during PV formation, whereas RON4 diffuses into the PVM (Chapter 4; Figure 4.11).

5.3 MyoB is localised to the apical tip of merozoites, is not part of the glideosome motor complex and may have a role in erythrocyte invasion

- Characterisation of GFP-tagged MyoB in *P. falciparum* and *P. knowlesi.* The gene encoding C-terminal GFP-tagged MyoB was successfully integrated into the parasite genome. Whilst MyoA localised to the parasite periphery, MyoB localised at the apical end of the merozoite and the expression was optimum during parasite segmentation through out parasite development to merozoites (Chapter 4; Figure 4.2, 4.7 and 4.14), a result which is also complemented by the studies carried out by Chapparo-olaya et. al., (2003) where the authors used IFA of schizont stages probed with Pfmyo-B antibody. In addition, the present study has also showed MyoB localised at the apical tip of the merozoite ahead of the RON and microneme specific antibodies as determined by IFA co-localisation studies. Futhermore, using the same approach, co-localisation with tubulin and actin showed MyoB was partially overlapped with actin and might be overlapped with tubulin at the MTOC (Chapter 4; Figure 4.5). MyoB seems to be in the wrong place to be directly involved in gliding motility, but it could be involved in the initiation of invasion due to its association with microtubules or by controlling release of the contents of the apical organelles. Microtubules have been shown to have signalling roles (Bejon et al., 1997) and are important in translocating AMA1 (within micronemes) during merozoite development (Bannister et al., 2003).
- This study was also carried out in order to determine wether MyoB was part of the glideosome motor complex and what is the potential MyoB contribution to the invasion process. Attempts to co-localise MyoB with proteins from the glideosome complex (MTIP, GAP45 and GAP50) showed none of these proteins co-precipitated with GFP-tagged MyoB, indicating MyoB does not associated with the known glideosome complex proteins. This result was validated by western blot and MS analysis (Chapter 4; Figure 4.4a). However, MyoB forms part of a novel complex, potentially including the vesicular transport-related proteins such as PfDYN2, clathrin, SEC31 and Pf332. In addition a potential MyoB light chain, PfMTIP-B was also identified (Chapter 4; Table 4.2) (Figure 5.1b).

- Further investigation to determine the role of MyoB during erythrocyte invasion was carried out as in MyoA,. using RON4 as a MJ marker. Results showed MyoB did not followed the characteristic RON4 pattern during invasion; instead MyoB stayed exactly where it was associated with the parasite's apex throughout the progression of the merozoite into the erythrocyte. One interesting characteristic is that during MJ formation, RON4 initially localised behind MyoB moved forward ahead of MyoB to go to the front of the merozoite for the TJ formation (Chapter 4; Figure 4.12).

5.4 Future Studies

The present study has discussed two myosin of type XIV in Apicomplexa The first protein is MyoA which is known to be involved in the gliding motility of the merozoite to invade erythrocytes. The second protein is MyoB which might be potentially involved in the invasion process.

1) The study has shown that the endogenous GFP-tagged MyoA is able to interact with the other glideosome motor complex protein components and the merozoites invaded erythrocytes suggesting it is functional. Therefore, further phenotype identification is needed to fully understand its functionalities.
2) In addition, it is also important to study the function of the newly identified glideosome component, the PfGAP40 protein. The posttranslational modification of GAP40 and its IMC localisation also need to be established in order to confirm its association and the assembly of the glideosome complex.
3) Generation of parasite lines with inducible knockouts of endogenous MyoA and GAP40 needs to be carried out in the future. The conditional knockout can be performed using the DiCre system which was recently developed. Together with IEM analysis of MyoA and GAP40, such experiments will elucidate further the glideosome motor complex components which have been shown to consist of GAP45-MTIP-MyoA-GAP50-GAP40 *T.gondii*.

On the other hand, the endogenous GFP-tagged MyoB is not interacting with any protein from the glideosome complex although the apical localisation suggests that it may be involved in the invasion processes. It is important to study MyoB in more detail

in order to understand its possible role in the parasite. There are several experiments that should be carried out for this purposes which are:

1) Immuno-EM- In this study the localisation of MyoB was only determine by live microscopy imaging and co-localisation IFAs for which the resolution was limited. Therefore, it needs to be confirmed by IEM analysis. A new endogenous HA-tagged MyoB to replace the GFP-tagged version is required in order to characterise the actual localisation, due to failure of IEM using the available GFP antibody.
2) Establishment of the MyoB novel complex. There are several protein identified during this study which have possible interactions with MyoB. The interaction of MyoB with the vesicular transport proteins such as clathrin, DNY2, Sec31 and the MyoB light chain which is MTIP-B, as well as tubulin and actin should be further investigated. As MTIP-B was shown to have interaction with MyoB, a close investigation should be carried out for example of the binding affinity to MyoB. The association of MyoB-MTIP-B can be examined using the experimental approach which was carried out previously for MyoA-MTIP. In addition, generation of GFP-tagged MTIP-B, Clathrin, DNY2 and Sec31 will further clarify the associations of this novel complex.
3) Western blot and IFAs using newly produced MyoA and MyoB antibodies can be used in protein interaction studies.
4) An alternative approach to identify MyoB functionalities can be carried out by generating a knockout parasite line for MyoB and its potential complex components. This experiment will give clear ideas on how MyoB and its binding partners work.
5) The live invasion studies should be repeated by using higher resolution microscopy such as the 3D-SIM, time-lapse microscopy or EM/ IEM imaging. Although the exact function is not yet known, this experiment should give evidence of MyoB function during the invasion process.

5.5 Concluding remarks

Invasion of the erythrocyte involves multiple cellular steps: from merozoite egress and red cell rupture, followed by initial merozoite attachment, reorientation and tight junction formation, invasion powered by the acto-myosin motor in parallel with shedding of the surface coat, PV formation and post invasion events marked by vacuole sealing (Cowman et al., 2012). In this study, the results provide evidence for the association of MyoA with the glideosome complex. On the other hand, MyoB appears to play a different role from MyoA although it may also contribute to the invasion process. The data presented here indicate an independent role for both myosins during the invasion process. This is backed up by the fact that depletion of MyoA impaired host cell invasion (Meissner et al., 2002) and is not essential for invasion (Andenmatten et al., 2013), and MyoB appears at the right location and the right time to be implicated in erythrocyte invasion by a different pathway. This is the first detailed study, to our knowledge, to investigate the location and timing of expression of MyoA and MyoB throughout the parasite's asexual life cycle of development and erythrocyte invasion. Figure 5.1 shows an illustrated diagram of the additional proteins added to the current model of the acto-myosin motor (Figure 1.12) as provided by this study.

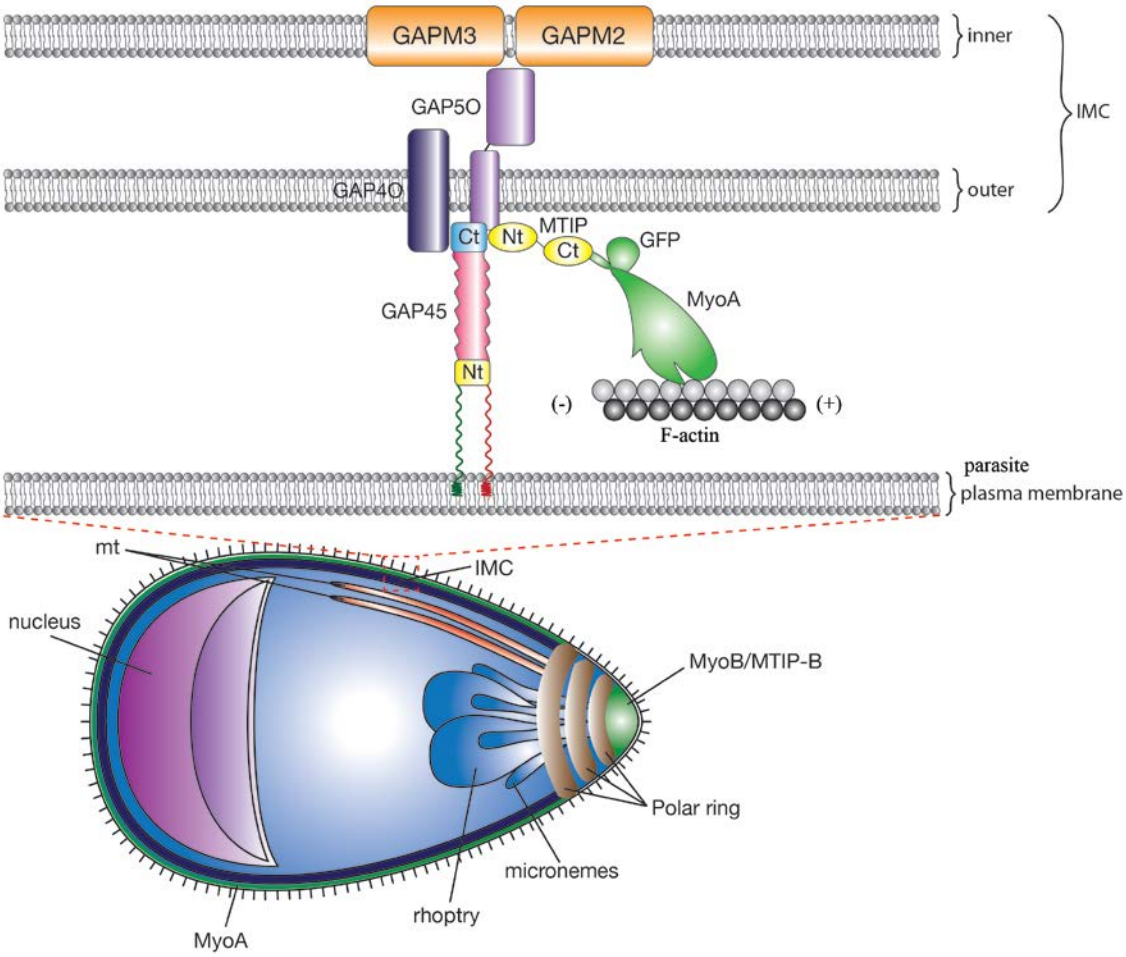

Figure 5.1: A current view of the acto-myosin motor complex and the location of MyoA and MyoB, based on the results of this study. GAP40, GAPM2 and GAPM3 have possible interactions with the MyoA glideosome complex as identified by MS in this study. The merozoite illustration shows MyoA localised at the periphery of the merozoite (green line) and MyoB and its MTIP-B localised at the apical prominence (green) ahead of rhoptries and micronemes. Also shown are MTIP (yellow circles), GAPMs (orange); GAP45 (pink shape with blue and yellow Ct and Nt, respectively), transmembrane GAP50 (purple) and GAP40 (deep purple), and F-actin (black and grey circles). Nt: N-terminal; Ct: C-terminal; mt: microtubule.

REFERENCES

Abkarian, M., Massiera, G., Berry, L., Roques, M., and Braun-Breton, C. (2011). A novel mechanism for egress of malarial parasites from red blood cells. Blood *117*, 4118-4124.

Adisa, A., Albano, F.R., Reeder, J., Foley, M., and Tilley, L. (2001). Evidence for a role for a *Plasmodium falciparum* homologue of Sec31p in the export of proteins to the surface of malaria parasite-infected erythrocytes. Journal of cell science *114*, 3377-3386.

Aikawa, M., Miller, L.H., Johnson, J., and Rabbege, J. (1978). Erythrocyte entry by malarial parasites. A moving junction between erythrocyte and parasite. The Journal of cell biology *77*, 72-82.

Aikawa, M., Miller, L.H., Rabbege, J.R., and Epstein, N. (1981). Freeze-fracture study on the erythrocyte membrane during malarial parasite invasion. The Journal of cell biology *91*, 55-62.

Andenmatten, N., Egarter, S., Jackson, A.J., Jullien, N., Herman, J.P., and Meissner, M. (2013). Conditional genome engineering in *Toxoplasma gondii* uncovers alternative invasion mechanisms. Nature methods *10*, 125-127.

Angrisano, F., Riglar, D.T., Sturm, A., Volz, J.C., Delves, M.J., Zuccala, E.S., Turnbull, L., Dekiwadia, C., Olshina, M.A., Marapana, D.S*., et al.* (2012). Spatial localisation of actin filaments across developmental stages of the malaria parasite. PloS one *7*, e32188.

Ashkin, A., Dziedzic, J.M., and Yamane, T. (1987). Optical trapping and manipulation of single cells using infrared laser beams. Nature *330*, 769-771.

Bannister, L., and Mitchell, G. (2003). The ins, outs and roundabouts of malaria. Trends Parasitol *19*, 209-213.

Bannister, L.H. (2001). Looking for the exit: How do malaria parasites escape from red blood cells? Proceedings of the National Academy of Sciences of the United States of America *98*, 383-384.

Bannister, L.H., Butcher, G.A., Dennis, E.D., and Mitchell, G.H. (1975). Structure and invasive behaviour of *Plasmodium knowlesi* merozoites *in vitro*. Parasitology *71*, 483-491.

Bannister, L.H., and Dluzewski, A.R. (1990). The ultrastructure of red cell invasion in malaria infections: a review. Blood cells *16*, 257-292; discussion 293-257.

Bannister, L.H., Hopkins, J.M., Dluzewski, A.R., Margos, G., Williams, I.T., Blackman, M.J., Kocken, C.H., Thomas, A.W., and Mitchell, G.H. (2003). *Plasmodium falciparum* apical membrane antigen 1 (PfAMA-1) is translocated within micronemes along subpellicular microtubules during merozoite development. Journal of cell science *116*, 3825-3834.

Bannister, L.H., Hopkins, J.M., Fowler, R.E., Krishna, S., and Mitchell, G.H. (2000a). A brief illustrated guide to the ultrastructure of *Plasmodium falciparum* asexual blood stages. Parasitol Today *16*, 427-433.

Bannister, L.H., Hopkins, J.M., Fowler, R.E., Krishna, S., and Mitchell, G.H. (2000b). Ultrastructure of rhoptry development in *Plasmodium falciparum* erythrocytic schizonts. Parasitology *121 (Pt 3)*, 273-287.

Bannister, L.H., and Mitchell, G.H. (1995). The role of the cytoskeleton in *Plasmodium falciparum* merozoite biology: an electron-microscopic view. Annals of tropical medicine and parasitology *89*, 105-111.

Bannister, L.H., Mitchell, G.H., Butcher, G.A., Dennis, E.D., and Cohen, S. (1986). Structure and development of the surface coat of erythrocytic merozoites of *Plasmodium knowlesi*. Cell and tissue research *245*, 281-290.

Baum, J., Gilberger, T.W., Frischknecht, F., and Meissner, M. (2008a). Host-cell invasion by malaria parasites: insights from *Plasmodium* and *Toxoplasma*. Trends Parasitol *24*, 557-563.

Baum, J., Papenfuss, A.T., Baum, B., Speed, T.P., and Cowman, A.F. (2006a). Regulation of apicomplexan actin-based motility. Nat Rev Microbiol *4*, 621-628.

Baum, J., Richard, D., Healer, J., Rug, M., Krnajski, Z., Gilberger, T.W., Green, J.L., Holder, A.A., and Cowman, A.F. (2006b). A conserved molecular motor drives cell invasion and gliding motility across malaria life cycle stages and other apicomplexan parasites. The Journal of biological chemistry *281*, 5197-5208.

Baum, J., Tonkin, C.J., Paul, A.S., Rug, M., Smith, B.J., Gould, S.B., Richard, D., Pollard, T.D., and Cowman, A.F. (2008b). A malaria parasite formin regulates actin polymerization and localizes to the parasite-erythrocyte moving junction during invasion. Cell host & microbe *3*, 188-198.

Bejon, P.A., Bannister, L.H., Fowler, R.E., Fookes, R.E., Webb, S.E., Wright, A., and Mitchell, G.H. (1997). A role for microtubules in *Plasmodium falciparum* merozoite invasion. Parasitology *114 (Pt 1)*, 1-6.

Bement, W.M., and Mooseker, M.S. (1995). TEDS rule: a molecular rationale for differential regulation of myosins by phosphorylation of the heavy chain head. Cell motility and the cytoskeleton *31*, 87-92.

Bergman, L.W., Kaiser, K., Fujioka, H., Coppens, I., Daly, T.M., Fox, S., Matuschewski, K., Nussenzweig, V., and Kappe, S.H. (2003). Myosin A tail domain interacting protein (MTIP) localizes to the inner membrane complex of *Plasmodium* sporozoites. Journal of cell science *116*, 39-49.

Berry, A., Iriart, X., Wilhelm, N., Valentin, A., Cassaing, S., Witkowski, B., Benoit-Vical, F., Menard, S., Olagnier, D., Fillaux, J.*, et al.* (2011). Case Report: Imported *Plasmodium knowlesi* Malaria in a French Tourist Returning from Thailand. Am J Trop Med Hyg *84*, 535-538.

Besteiro, S., Dubremetz, J.F., and Lebrun, M. (2011). The moving junction of apicomplexan parasites: a key structure for invasion. Cellular microbiology *13*, 797-805.

Billker, O., Lindo, V., Panico, M., Etienne, A.E., Paxton, T., Dell, A., Rogers, M., Sinden, R.E., and Morris, H.R. (1998). Identification of xanthurenic acid as the putative inducer of malaria development in the mosquito. Nature *392*, 289-292.

Bosch, J., Buscaglia, C.A., Krumm, B., Ingason, B.P., Lucas, R., Roach, C., Cardozo, T., Nussenzweig, V., and Hol, W.G. (2007a). Aldolase provides an unusual binding site for thrombospondin-related anonymous protein in the invasion machinery of the malaria parasite. Proceedings of the National Academy of Sciences of the United States of America *104*, 7015-7020.

Bosch, J., Paige, M.H., Vaidya, A.B., Bergman, L.W., and Hol, W.G.J. (2012). Crystal structure of GAP50, the anchor of the invasion machinery in the inner membrane complex of *Plasmodium falciparum*. Journal of Structural Biology *178*, 61-73.

Bosch, J., Turley, S., Daly, T.M., Bogh, S.M., Villasmil, M.L., Roach, C., Zhou, N., Morrisey, J.M., Vaidya, A.B., Bergman, L.W.*, et al.* (2006). Structure of the MTIP-MyoA complex, a key component of the malaria parasite invasion motor. Proceedings of the National Academy of Sciences of the United States of America *103*, 4852-4857.

Bosch, J., Turley, S., Roach, C.M., Daly, T.M., Bergman, L.W., and Hol, W.G. (2007b). The closed MTIP-myosin A-tail complex from the malaria parasite invasion machinery. Journal of molecular biology *372*, 77-88.

Boyle, M.J., Wilson, D.W., Richards, J.S., Riglar, D.T., Tetteh, K.K., Conway, D.J., Ralph, S.A., Baum, J., and Beeson, J.G. (2010). Isolation of viable *Plasmodium falciparum* merozoites to define erythrocyte invasion events and advance vaccine and drug development. Proceedings of the National Academy of Sciences of the United States of America *107*, 14378-14383.

Bozdech, Z., Llinas, M., Pulliam, B.L., Wong, E.D., Zhu, J., and DeRisi, J.L. (2003). The transcriptome of the intraerythrocytic developmental cycle of *Plasmodium falciparum*. PLoS biology *1*, E5.

Breinich, M.S., Ferguson, D.J.P., Foth, B.J., van Dooren, G.G., Lebrun, M., Quon, D.V., Striepen, B., Bradley, P.J., Frischknecht, F., Carruthers, V.B.*, et al.* (2009). A Dynamin Is Required for the Biogenesis of Secretory Organelles in *Toxoplasma gondii*. Current Biology *19*, 277-286.

Brossier, F., Jewett, T.J., Lovett, J.L., and Sibley, L.D. (2003). C-terminal processing of the *Toxoplasma* protein MIC2 is essential for invasion into host cells. The Journal of biological chemistry *278*, 6229-6234.

Bruce, M.C., Alano, P., Duthie, S., and Carter, R. (1990). Commitment of the malaria parasite Plasmodium falciparum to sexual and asexual development. Parasitology *100 Pt 2*, 191-200.

Bullen, H.E., Tonkin, C.J., O'Donnell, R.A., Tham, W.H., Papenfuss, A.T., Gould, S., Cowman, A.F., Crabb, B.S., and Gilson, P.R. (2009). A novel family of Apicomplexan glideosome-associated proteins with an inner membrane-anchoring role. The Journal of biological chemistry *284*, 25353-25363.

Buscaglia, C.A., Coppens, I., Hol, W.G., and Nussenzweig, V. (2003). Sites of interaction between aldolase and thrombospondin-related anonymous protein in *Plasmodium*. Molecular biology of the cell *14*, 4947-4957.

Carter, R., and Mendis, K.N. (2002). Evolutionary and historical aspects of the burden of malaria. Clinical microbiology reviews *15*, 564-594.

Carter, R., and Miller, L.H. (1979). Evidence for environmental modulation of gametocytogenesis in *Plasmodium falciparum* in continuous culture. Bulletin of the World Health Organization *57 Suppl 1*, 37-52.

Carvalho, T.G., and Menard, R. (2005). Manipulating the *Plasmodium* genome. Current issues in molecular biology *7*, 39-55.

Chaparro-Olaya, J., Dluzewski, A.R., Margos, G., Wasserman, M.M., Mitchell, G.H., Bannister, L.H., and Pinder, J.C. (2003). The multiple myosins of malaria: The smallest malaria myosin, Plasmodium falciparum myosin-B (Pfmyo-B) is expressed in mature schizonts and merozoites. Eur J Protistol *39*, 423-427.

Chaparro-Olaya, J., Margos, G., Coles, D.J., Dluzewski, A.R., Mitchell, G.H., Wasserman, M.M., and Pinder, J.C. (2005). *Plasmodium falciparum* myosins: transcription and translation during asexual parasite development. Cell motility and the cytoskeleton *60*, 200-213.

Charneau, S., Bastos, I.M., Mouray, E., Ribeiro, B.M., Santana, J.M., Grellier, P., and Florent, I. (2007). Characterization of PfDYN2, a dynamin-like protein of *Plasmodium falciparum* expressed in schizonts. Microbes and infection / Institut Pasteur *9*, 797-805.

Coatney, G.R. (1971). The simian malarias: zoonoses, anthroponoses, or both? Am J Trop Med Hyg *20*, 795-803.

Coluccio, L.M.e. (2008). Myosin: a superfamily of molecular motor. Netherland, Springer, 1-54; 421-440; 289-352 and 421-434.

Cooke, R. (2004). The sliding filament model: 1972-2004. J Gen Physiol *123*, 643-656.

Cowman, A.F., Berry, D., and Baum, J. (2012). The cellular and molecular basis for malaria parasite invasion of the human red blood cell. The Journal of cell biology *198*, 961-971.

Cowman, A.F., and Crabb, B.S. (2006). Invasion of red blood cells by malaria parasites. Cell *124*, 755-766.

Cox-Singh, J., Davis, T.M., Lee, K.S., Shamsul, S.S., Matusop, A., Ratnam, S., Rahman, H.A., Conway, D.J., and Singh, B. (2008). *Plasmodium knowles*i malaria in humans is widely distributed and potentially life threatening. Clinical infectious diseases : an official publication of the Infectious Diseases Society of America *46*, 165-171.

Crabb, B.S., Triglia, T., Waterkeyn, J.G., and Cowman, A.F. (1997). Stable transgene expression in *Plasmodium falciparum*. Mol Biochem Parasitol *90*, 131-144.

Daher, W., and Soldati-Favre, D. (2009). Mechanisms controlling glideosome function in apicomplexans. Curr Opin Microbiol *12*, 408-414.

De Camilli, P., Takei, K., and McPherson, P.S. (1995). The function of dynamin in endocytosis. Current opinion in neurobiology *5*, 559-565.

de Koning-Ward, T.F., Janse, C.J., and Waters, A.P. (2000). The development of genetic tools for dissecting the biology of malaria parasites. Annual review of microbiology *54*, 157-185.

DeBiasio, R.L., LaRocca, G.M., Post, P.L., and Taylor, D.L. (1996). Myosin II transport, organization, and phosphorylation: evidence for cortical flow/solation-contraction coupling during cytokinesis and cell locomotion. Molecular biology of the cell *7*, 1259-1282.

Delbac, F., Sanger, A., Neuhaus, E.M., Stratmann, R., Ajioka, J.W., Toursel, C., Herm-Gotz, A., Tomavo, S., Soldati, T., and Soldati, D. (2001). *Toxoplasma gondii* myosins B/C: one gene, two tails, two localizations, and a role in parasite division. The Journal of cell biology *155*, 613-623.

Dessens, J.T., Beetsma, A.L., Dimopoulos, G., Wengelnik, K., Crisanti, A., Kafatos, F.C., and Sinden, R.E. (1999). CTRP is essential for mosquito infection by malaria ookinetes. The EMBO journal *18*, 6221-6227.

Dixon, M.W., Thompson, J., Gardiner, D.L., and Trenholme, K.R. (2008). Sex in *Plasmodium*: a sign of commitment. Trends Parasitol *24*, 168-175.

Dobrowolski, J.M., Carruthers, V.B., and Sibley, L.D. (1997a). Participation of myosin in gliding motility and host cell invasion by *Toxoplasma gondii*. Molecular microbiology *26*, 163-173.

Dobrowolski, J.M., Niesman, I.R., and Sibley, L.D. (1997b). Actin in the parasite *Toxoplasma gondii* is encoded by a single copy gene, ACT1 and exists primarily in a globular form. Cell motility and the cytoskeleton *37*, 253-262.

Dobrowolski, J.M., and Sibley, L.D. (1996). *Toxoplasma* invasion of mammalian cells is powered by the actin cytoskeleton of the parasite. Cell *84*, 933-939.

Douse, C.H., Green, J.L., Salgado, P.S., Simpson, P.J., Thomas, J.C., Langsley, G., Holder, A.A., Tate, E.W., and Cota, E. (2012). Regulation of the *Plasmodium* motor complex: phosphorylation of myosin A tail-interacting protein (MTIP) loosens its grip on MyoA. The Journal of biological chemistry *287*, 36968-36977.

Dvorak, J.A., Miller, L.H., Whitehouse, W.C., and Shiroishi, T. (1975). Invasion of erythrocytes by malaria merozoites. Science *187*, 748-750.

Endo, Y., and Sawasaki, T. (2003). High-throughput, genome-scale protein production method based on the wheat germ cell-free expression system. Biotechnology advances *21*, 695-713.

Escalante, A.A., Freeland, D.E., Collins, W.E., and Lal, A.A. (1998). The evolution of primate malaria parasites based on the gene encoding cytochrome b from the linear mitochondrial genome. Proceedings of the National Academy of Sciences of the United States of America *95*, 8124-8129.

Farrow, R.E., Green, J., Katsimitsoulia, Z., Taylor, W.R., Holder, A.A., and Molloy, J.E. (2011). The mechanism of erythrocyte invasion by the malarial parasite, *Plasmodium falciparum*. Seminars in cell & developmental biology *22*, 953-960.

Farrow, R.E., Rosenthal, P.B., Mashanov, G.I., Holde,A.A., Molloy,J.E. (2007). Optical trapping studies of acto-myosin motor protein. In: Dholakia K, Spalding GC, editor, Proceeding og Society of Photo-optical instrumentation Engineers (SPIE), 66440B66441-66411.

Fauquenoy, S., Hovasse, A., Sloves, P.J., Morelle, W., Tchilabalo-Dilezitoko, E., Slomianny, C., Werkmeister, E., Schaeffer, C., Van Dorsselaer, A., and Tomavo, S. (2011). Unusual N-glycan

structures are required for trafficking *Toxoplasma gondii* GAP50 to the inner membrane complex and regulate host cell entry through parasite motility. Molecular & cellular proteomics : MCP.

Ferguson, S.M., and De Camilli, P. (2012). Dynamin, a membrane-remodelling GTPase. Nat Rev Mol Cell Bio *13*, 75-88.

Fidock, D.A., and Wellems, T.E. (1997). Transformation with human dihydrofolate reductase renders malaria parasites insensitive to WR99210 but does not affect the intrinsic activity of proguanil. Proceedings of the National Academy of Sciences of the United States of America *94*, 10931-10936.

Field, S.J., Pinder, J.C., Clough, B., Dluzewski, A.R., Wilson, R.J., and Gratzer, W.B. (1993). Actin in the merozoite of the malaria parasite, *Plasmodium falciparum*. Cell motility and the cytoskeleton *25*, 43-48.

Figtree, M., Lee, R., Bain, L., Kennedy, T., Mackertich, S., Urban, M., Cheng, Q., and Hudson, B.J. (2010). *Plasmodium knowlesi* in human, Indonesian Borneo. Emerging infectious diseases *16*, 672-674.

Finer, J.T., Mehta, A.D., and Spudich, J.A. (1995). Characterization of single actin-myosin interactions. Biophys J *68*, 291S-296S; discussion 296S-297S.

Finer, J.T., Simmons, R.M., and Spudich, J.A. (1994). Single myosin molecule mechanics: piconewton forces and nanometre steps. Nature *368*, 113-119.

Foley, M., and Tilley, L. (1998). Protein trafficking in malaria-infected erythrocytes. International Journal for Parasitology *28*, 1671-1680.

Foth, B.J., Goedecke, M.C., and Soldati, D. (2006). New insights into myosin evolution and classification. Proceedings of the National Academy of Sciences of the United States of America *103*, 3681-3686.

Fowler, R.E., Smith, A.M., Whitehorn, J., Williams, I.T., Bannister, L.H., and Mitchell, G.H. (2001). Microtubule associated motor proteins of *Plasmodium falciparum* merozoites. Mol Biochem Parasitol *117*, 187-200.

Francis, S.E., Sullivan, D.J., Jr., and Goldberg, D.E. (1997). Hemoglobin metabolism in the malaria parasite *Plasmodium falciparum*. Annual review of microbiology *51*, 97-123.

Frenal, K., Polonais, V., Marq, J.B., Stratmann, R., Limenitakis, J., and Soldati-Favre, D. (2010). Functional dissection of the apicomplexan glideosome molecular architecture. Cell host & microbe *8*, 343-357.

Frevert, U. (2004). Sneaking in through the back entrance: the biology of malaria liver stages. Trends Parasitol *20*, 417-424.

Gardner, M.J., Hall, N., Fung, E., White, O., Berriman, M., Hyman, R.W., Carlton, J.M., Pain, A., Nelson, K.E., Bowman, S*., et al.* (2002). Genome sequence of the human malaria parasite *Plasmodium falciparum*. Nature *419*, 498-511.

Garnham, P.C.C. (1966). Life cycle and morphology, in Garnham , P.C.C. (ED.), malaria parasites and other Haemosporidia. 1 ed Blackwell Scientific Publication, Oxford, 17-59.

Gaskins, E., Gilk, S., DeVore, N., Mann, T., Ward, G., and Beckers, C. (2004). Identification of the membrane receptor of a class XIV myosin in *Toxoplasma gondi*i. The Journal of cell biology *165*, 383-393.

Gaur, D., Mayer, D.C., and Miller, L.H. (2004). Parasite ligand-host receptor interactions during invasion of erythrocytes by *Plasmodium* merozoites. Int J Parasitol *34*, 1413-1429.

Gilk, S.D., Gaskins, E., Ward, G.E., and Beckers, C.J. (2009). GAP45 phosphorylation controls assembly of the *Toxoplasma* myosin XIV complex. Eukaryotic cell *8*, 190-196.

Gilson, P.R., and Crabb, B.S. (2009). Morphology and kinetics of the three distinct phases of red blood cell invasion by *Plasmodium falciparum* merozoites. Int J Parasitol *39*, 91-96.

Glushakova, S., Yin, D., Li, T., and Zimmerberg, J. (2005). Membrane transformation during malaria parasite release from human red blood cells. Current biology : CB *15*, 1645-1650.

Goel, V.K., Li, X., Chen, H., Liu, S.C., Chishti, A.H., and Oh, S.S. (2003). Band 3 is a host receptor binding merozoite surface protein 1 during the *Plasmodium falciparum* invasion of erythrocytes. Proceedings of the National Academy of Sciences of the United States of America *100*, 5164-5169.

Gonzalez, V., Combe, A., David, V., Malmquist, N.A., Delorme, V., Leroy, C., Blazquez, S., Menard, R., and Tardieux, I. (2009). Host cell entry by apicomplexa parasites requires actin polymerization in the host cell. Cell host & microbe *5*, 259-272.

Goonewardene, R., Daily, J., Kaslow, D., Sullivan, T.J., Duffy, P., Carter, R., Mendis, K., and Wirth, D. (1993). Transfection of the malaria parasite and expression of firefly luciferase. Proceedings of the National Academy of Sciences of the United States of America *90*, 5234-5236.

Green, J.L., Hinds, L., Grainger, M., Knuepfer, E., and Holder, A.A. (2006a). *Plasmodium* thrombospondin related apical merozoite protein (PTRAMP) is shed from the surface of merozoites by PfSUB2 upon invasion of erythrocytes. Mol Biochem Parasitol *150*, 114-117.

Green, J.L., Martin, S.R., Fielden, J., Ksagoni, A., Grainger, M., Yim Lim, B.Y., Molloy, J.E., and Holder, A.A. (2006b). The MTIP-myosin A complex in blood stage malaria parasites. Journal of molecular biology *355*, 933-941.

Gruring, C., Heiber, A., Kruse, F., Ungefehr, J., Gilberger, T.W., and Spielmann, T. (2011). Development and host cell modifications of *Plasmodium falciparum* blood stages in four dimensions. Nature communications *2*, 165.

Hanssen, E., McMillan, P.J., and Tilley, L. (2010). Cellular architecture of *Plasmodium falciparum*-infected erythrocytes. Int J Parasitol *40*, 1127-1135.

Heaslip, A.T., Leung, J.M., Carey, K.L., Catti, F., Warshaw, D.M., Westwood, N.J., Ballif, B.A., and Ward, G.E. (2010). A small-molecule inhibitor of *T. gondii* motility induces the

posttranslational modification of myosin light chain-1 and inhibits myosin motor activity. PLoS pathogens *6*, e1000720.

Heintzelman, M.B., and Schwartzman, J.D. (1997). A novel class of unconventional myosins from *Toxoplasma gondii*. Journal of molecular biology *271*, 139-146.

Heintzelman, M.B., and Schwartzman, J.D. (2001). Myosin diversity in *Apicomplexa*. The Journal of parasitology *87*, 429-432.

Herm-Gotz, A., Delbac, F., Weiss, S., Nyitrai, M., Stratmann, R., Tomavo, S., Sibley, L.D., Geeves, M.A., and Soldati, D. (2006). Functional and biophysical analyses of the class XIV *Toxoplasma gondii* myosin D. Journal of muscle research and cell motility *27*, 139-151.

Herm-Gotz, A., Weiss, S., Stratmann, R., Fujita-Becker, S., Ruff, C., Meyhofer, E., Soldati, T., Manstein, D.J., Geeves, M.A., and Soldati, D. (2002). *Toxoplasma gondi*i myosin A and its light chain: a fast, single-headed, plus-end-directed motor. The EMBO journal *21*, 2149-2158.

Hettmann, C., Herm, A., Geiter, A., Frank, B., Schwarz, E., Soldati, T., and Soldati, D. (2000). A dibasic motif in the tail of a class XIV apicomplexan myosin is an essential determinant of plasma membrane localization. Molecular biology of the cell *11*, 1385-1400.

Hodge, T., and Cope, M.J. (2000). A myosin family tree. Journal of cell science *113 Pt 19*, 3353-3354.

Holder, A.A., Lockyer, M.J., Odink, K.G., Sandhu, J.S., Riveros-Moreno, V., Nicholls, S.C., Hillman, Y., Davey, L.S., Tizard, M.L., Schwarz, R.T*., et al.* (1985). Primary structure of the precursor to the three major surface antigens of *Plasmodium falciparum* merozoites. Nature *317*, 270-273.

Holder, A.A., and Veigel, C. (2009). Formin' an invasion machine: actin polymerization in invading *Apicomplexan*s. Trends Parasitol *25*, 1-3.

Hoosen, A., and Shaw, M.T. (2011). *Plasmodium knowlesi* in a traveller returning to New Zealand. Travel medicine and infectious disease *9*, 144-148.

Horrocks, P., and Newbold, C.I. (2000). Intraerythrocytic polyubiquitin expression in *Plasmodium falciparum* is subjected to developmental and heat-shock control. Mol Biochem Parasitol *105*, 115-125.

Ishijima, A., Kojima, H., Funatsu, T., Tokunaga, M., Higuchi, H., Tanaka, H., and Yanagida, T. (1998). Simultaneous observation of individual ATPase and mechanical events by a single myosin molecule during interaction with actin. Cell *92*, 161-171.

Ishino, T., Chinzei, Y., and Yuda, M. (2005). A *Plasmodium* sporozoite protein with a membrane attack complex domain is required for breaching the liver sinusoidal cell layer prior to hepatocyte infection. Cellular microbiology *7*, 199-208.

Ishino, T., Yano, K., Chinzei, Y., and Yuda, M. (2004). Cell-passage activity is required for the malarial parasite to cross the liver sinusoidal cell layer. PLoS biology *2*, E4.

Janse, C.J., Ramesar, J., and Waters, A.P. (2006). High-efficiency transfection and drug selection of genetically transformed blood stages of the rodent malaria parasite *Plasmodium berghei*. Nature protocols *1*, 346-356.

Jewett, T.J., and Sibley, L.D. (2003). Aldolase forms a bridge between cell surface adhesins and the actin cytoskeleton in apicomplexan parasites. Mol Cell *11*, 885-894.

Johnson, T.M., Rajfur, Z., Jacobson, K., and Beckers, C.J. (2007). Immobilization of the type XIV myosin complex in *Toxoplasma gondii*. Molecular biology of the cell *18*, 3039-3046.

Jones, M.L., Kitson, E.L., and Rayner, J.C. (2006). *Plasmodium falciparum* erythrocyte invasion: a conserved myosin associated complex. Mol Biochem Parasitol *147*, 74-84.

Jongwutiwes, S., Putaporntip, C., Iwasaki, T., Sata, T., and Kanbara, H. (2004). Naturally acquired *Plasmodium knowlesi* malaria in human, Thailand. Emerging infectious diseases *10*, 2211-2213.

Kellerman, K.A., and Miller, K.G. (1992). An unconventional myosin heavy chain gene from *Drosophila melanogaster*. The Journal of cell biology *119*, 823-834.

Khater, E.I., Sinden, R.E., and Dessens, J.T. (2004). A malaria membrane skeletal protein is essential for normal morphogenesis, motility, and infectivity of sporozoites. The Journal of cell biology *167*, 425-432.

Khim, N., Siv, S., Kim, S., Mueller, T., Fleischmann, E., Singh, B., Divis, P.C., Steenkeste, N., Duval, L., Bouchier, C*., et al.* (2011). *Plasmodium knowles*i infection in humans, Cambodia, 2007-2010. Emerging infectious diseases *17*, 1900-1902.

Kim, K., and Weiss, L.M. (2004). *Toxoplasma gondii*: the model apicomplexan. Int J Parasitol *34*, 423-432.

King, C.A. (1988). Cell motility of sporozoan protozoa. Parasitol Today *4*, 315-319.

Kocken, C.H., Ozwara, H., van der Wel, A., Beetsma, A.L., Mwenda, J.M., and Thomas, A.W. (2002). *Plasmodium knowlesi* provides a rapid in vitro and *in vivo* transfection system that enables double-crossover gene knockout studies. Infection and immunity *70*, 655-660.

Kooij, T.W., and Matuschewski, K. (2007). Triggers and tricks of *Plasmodium* sexual development. Curr Opin Microbiol *10*, 547-553.

Kuehn, A., and Pradel, G. (2010). The coming-out of malaria gametocytes. Journal of biomedicine & biotechnology *2010*, 976827.

Lambros, C., and Vanderberg, J.P. (1979). Synchronization of Plasmodium falciparum erythrocytic stages in culture. J Parasitol *65*, 418-420.

Lasonder, E., Ishihama, Y., Andersen, J.S., Vermunt, A.M., Pain, A., Sauerwein, R.W., Eling, W.M., Hall, N., Waters, A.P., Stunnenberg, H.G*., et al.* (2002). Analysis of the *Plasmodium falciparum* proteome by high-accuracy mass spectrometry. Nature *419*, 537-542.

Lasonder, E., Treeck, M., Alam, M., and Tobin, A.B. (2012). Insights into the *Plasmodium falciparum* schizont phospho-proteome. Microbes and infection / Institut Pasteur *14*, 811-819.

Lazarus, M.D., Schneider, T.G., and Taraschi, T.F. (2008). A new model for hemoglobin ingestion and transport by the human malaria parasite *Plasmodium falciparum*. Journal of cell science *121*, 1937-1949.

Li, X., Chen, H., Oo, T.H., Daly, T.M., Bergman, L.W., Liu, S.C., Chishti, A.H., and Oh, S.S. (2004). A co-ligand complex anchors *Plasmodium falciparum* merozoites to the erythrocyte invasion receptor band 3. The Journal of biological chemistry *279*, 5765-5771.

Liang, W., and Spudich, J.A. (1998). Nucleotide-dependent conformational change near the fulcrum region in *Dictyostelium* myosin II. Proceedings of the National Academy of Sciences of the United States of America *95*, 12844-12847.

Link, L., Bart, A., Verhaar, N., van Gool, T., Pronk, M., and Scharnhorst, V. (2012). Molecular detection of *Plasmodium knowlesi* in a Dutch traveler by real-time PCR. Journal of clinical microbiology *50*, 2523-2524.

Lodish, H., Berk, A., Kaise, C.A., Kriger, M., Scott, M.P., Bretscher, A., and Ploegh, H. (2008). Molecular Cell Biology. 6th edition. New York, WH Freman Company *6th Ed.*, 716-780.

Lopaticki, S., Maier, A.G., Thompson, J., Wilson, D.W., Tham, W.H., Triglia, T., Gout, A., Speed, T.P., Beeson, J.G., Healer, J*., et al.* (2011). Reticulocyte and erythrocyte binding-like proteins function cooperatively in invasion of human erythrocytes by malaria parasites. Infection and immunity *79*, 1107-1117.

Luchavez, J., Espino, F., Curameng, P., Espina, R., Bell, D., Chiodini, P., Nolder, D., Sutherland, C., Lee, K.S., and Singh, B. (2008). Human infections with *Plasmodium knowlesi,* the Philippines. Emerging infectious diseases *14*, 811-813.

Mann, M., and Wilm, M. (1995). Electrospray mass spectrometry for protein characterization. Trends in biochemical sciences *20*, 219-224.

Mann, T., Gaskins, E., and Beckers, C. (2002). Proteolytic processing of TgIMC1 during maturation of the membrane skeleton of *Toxoplasma gondii*. The Journal of biological chemistry *277*, 41240-41246.

Matuschewski, K., Mota, M.M., Pinder, J.C., Nussenzweig, V., and Kappe, S.H. (2001). Identification of the class XIV myosins Pb-MyoA and Py-MyoA and expression in *Plasmodium sporozoites*. Mol Biochem Parasitol *112*, 157-161.

Matuschewski, K., Nunes, A.C., Nussenzweig, V., and Menard, R. (2002). *Plasmodium* sporozoite invasion into insect and mammalian cells is directed by the same dual binding system. The EMBO journal *21*, 1597-1606.

Meissner, M., Schluter, D., and Soldati, D. (2002). Role of *Toxoplasma gondii* Myosin A in powering parasite gliding and host cell invasion. Science *298*, 837-840.

Menard, R. (2001). Gliding motility and cell invasion by *Apicomplexa*: insights from the *Plasmodium* sporozoite. Cellular microbiology *3*, 63-73.

Menon, M., and Schafer, D.A. (2013). Chapter Three - Dynamin: Expanding its scope to the cytoskeleton. In International review of cell and molecular biology, W.J. Kwang, ed. (Academic Press), pp. 187-219.

Merrifield, C.J. (2004). Seeing is believing: imaging actin dynamics at single sites of endocytosis. Trends in cell biology *14*, 352-358.

Mital, J., Meissner, M., Soldati, D., and Ward, G.E. (2005). Conditional expression of *Toxoplasma gondii* apical membrane antigen-1 (TgAMA1) demonstrates that TgAMA1 plays a critical role in host cell invasion. Molecular biology of the cell *16*, 4341-4349.

Molloy, J.E., Burns, J.E., Kendrick-Jones, J., Tregear, R.T., and White, D.C. (1995). Movement and force produced by a single myosin head. Nature *378*, 209-212.

Moon, R.W., Hall, J., Rangkuti, F., Ho, Y.S., Almond, N., Mitchell, G.H., Pain, A., Holder, A.A., and Blackman, M.J. (2013). Adaptation of the genetically tractable malaria pathogen *Plasmodium knowlesi* to continuous culture in human erythrocytes. Proceedings of the National Academy of Sciences of the United States of America *110*, 531-536.

Morrissette, N.S., Murray, J.M., and Roos, D.S. (1997). Subpellicular microtubules associate with an intramembranous particle lattice in the protozoan parasite *Toxoplasma gondii*. Journal of cell science *110 (Pt 1)*, 35-42.

Morrissette, N.S., and Sibley, L.D. (2002). Cytoskeleton of apicomplexan parasites. Microbiology and molecular biology reviews : MMBR *66*, 21-38; table of contents.

Murphy, S.C., Fernandez-Pol, S., Chung, P.H., Prasanna Murthy, S.N., Milne, S.B., Salomao, M., Brown, H.A., Lomasney, J.W., Mohandas, N., and Haldar, K. (2007). Cytoplasmic remodeling of erythrocyte raft lipids during infection by the human malaria parasite *Plasmodium falciparum*. Blood *110*, 2132-2139.

Ng, O.T., Ooi, E.E., Lee, C.C., Lee, P.J., Ng, L.C., Pei, S.W., Tu, T.M., Loh, J.P., and Leo, Y.S. (2008). Naturally acquired human *Plasmodium knowles*i infection, Singapore. Emerging infectious diseases *14*, 814-816.

Nishi, M., Hu, K., Murray, J.M., and Roos, D.S. (2008). Organellar dynamics during the cell cycle of *Toxoplasma gondii*. Journal of cell science *121*, 1559-1568.

Ono, T., Cabrita-Santos, L., Leitao, R., Bettiol, E., Purcell, L.A., Diaz-Pulido, O., Andrews, L.B., Tadakuma, T., Bhanot, P., Mota, M.M.*, et al.* (2008). Adenylyl cyclase alpha and cAMP signaling mediate *Plasmodium* sporozoite apical regulated exocytosis and hepatocyte infection. PLoS pathogens *4*, e1000008.

Ono, T., Tadakuma, T., and Rodriguez, A. (2007). *Plasmodium yoelii yoelii* 17XNL constitutively expressing GFP throughout the life cycle. Experimental parasitology *115*, 310-313.

Opitz, C., and Soldati, D. (2002). 'The glideosome': a dynamic complex powering gliding motion and host cell invasion by *Toxoplasma gondii*. Molecular microbiology *45*, 597-604.

Pelham, R.J., and Chang, F. (2002). Actin dynamics in the contractile ring during cytokinesis in fission yeast. Nature *419*, 82-86.

Pinder, J., Fowler, R., Bannister, L., Dluzewski, A., and Mitchell, G.H. (2000). Motile systems in malaria merozoites: how is the red blood cell invaded? Parasitol Today *16*, 240-245.

Pinder, J.C., Fowler, R.E., Dluzewski, A.R., Bannister, L.H., Lavin, F.M., Mitchell, G.H., Wilson, R.J., and Gratzer, W.B. (1998). Actomyosin motor in the merozoite of the malaria parasite, *Plasmodium falciparum*: implications for red cell invasion. Journal of cell science *111 (Pt 13)*, 1831-1839.

Poupel, O., and Tardieux, I. (1999). *Toxoplasma gondii* motility and host cell invasiveness are drastically impaired by jasplakinolide, a cyclic peptide stabilizing F-actin. Microbes and infection / Institut Pasteur *1*, 653-662.

Praefcke, G.J.K., and McMahon, H.T. (2004). The dynamin superfamily: Universal membrane tubulation and fission molecules? Nat Rev Mol Cell Bio *5*, 133-147.

Rao, Y., Rückert, C., Saenger, W., and Haucke, V. (2012). The early steps of endocytosis: From cargo selection to membrane deformation. European Journal of Cell Biology *91*, 226-233.

Rayner, J.C., Galinski, M.R., Ingravallo, P., and Barnwell, J.W. (2000). Two P*lasmodium falciparum* genes express merozoite proteins that are related to *Plasmodium vivax* and *Plasmodium yoelii* adhesive proteins involved in host cell selection and invasion. Proceedings of the National Academy of Sciences of the United States of America *97*, 9648-9653.

Read, M., Sherwin, T., Holloway, S.P., Gull, K., and Hyde, J.E. (1993). Microtubular organization visualized by immunofluorescence microscopy during erythrocytic schizogony in *Plasmodium falciparum* and investigation of post-translational modifications of parasite tubulin. Parasitology *106 (Pt 3)*, 223-232.

Reece, S.E., and Thompson, J. (2008). Transformation of the rodent malaria parasite *Plasmodium chabaudi* and generation of a stable fluorescent line PcGFPCON. Malaria journal *7*, 183.

Rees-Channer, R.R., Martin, S.R., Green, J.L., Bowyer, P.W., Grainger, M., Molloy, J.E., and Holder, A.A. (2006). Dual acylation of the 45 kDa gliding-associated protein (GAP45) in *Plasmodium falciparum* merozoites. Mol Biochem Parasitol *149*, 113-116.

Ridzuan, M.A., Moon, R.W., Knuepfer, E., Black, S., Holder, A.A., and Green, J.L. (2012). Subcellular location, phosphorylation and assembly into the motor complex of GAP45 during *Plasmodium falciparum* schizont development. PloS one *7*, e33845.

Riglar, D.T., Richard, D., Wilson, D.W., Boyle, M.J., Dekiwadia, C., Turnbull, L., Angrisano, F., Marapana, D.S., Rogers, K.L., Whitchurch, C.B*., et al.* (2011). Super-resolution dissection of coordinated events during malaria parasite invasion of the human erythrocyte. Cell host & microbe *9*, 9-20.

Royle, S.J. (2006). The cellular functions of clathrin. Cellular and molecular life sciences : CMLS *63*, 1823-1832.

Royle, S.J. (2012). The role of clathrin in mitotic spindle organisation. Journal of cell science *125*, 19-28.

Ruff, C., Furch, M., Brenner, B., Manstein, D.J., and Meyhofer, E. (2001). Single-molecule tracking of myosins with genetically engineered amplifier domains. Nat Struct Biol *8*, 226-229.

Russell, D.G., and Burns, R.G. (1984). The polar ring of coccidian sporozoites: a unique microtubule-organizing centre. Journal of cell science *65*, 193-207.

Russell, D.G., and Sinden, R.E. (1981). The role of the cytoskeleton in the motility of coccidian sporozoites. Journal of cell science *50*, 345-359.

Sachs, J., and Malaney, P. (2002). The economic and social burden of malaria. Nature *415*, 680-685.

Sambrook, J.G. (1989). Molecular cloning: A laboratory manual. Cold Spring Harbour Laboratory Press.

Sawasaki, T., Hasegawa, Y., Tsuchimochi, M., Kamura, N., Ogasawara, T., Kuroita, T., and Endo, Y. (2002a). A bilayer cell-free protein synthesis system for high-throughput screening of gene products. FEBS letters *514*, 102-105.

Sawasaki, T., Ogasawara, T., Morishita, R., and Endo, Y. (2002b). A cell-free protein synthesis system for high-throughput proteomics. Proceedings of the National Academy of Sciences of the United States of America *99*, 14652-14657.

Sawasaki, T., Seki, M., Sinozaki, K., and Endo, Y. (2002c). High-throughput expression of proteins from cDNAs catalogue from *Arabidopsis* in wheat germ cell-free protein synthesis system. Tanpakushitsu kakusan koso Protein, nucleic acid, enzyme *47*, 1003-1008.

Schmitz, S., Grainger, M., Howell, S., Calder, L.J., Gaeb, M., Pinder, J.C., Holder, A.A., and Veigel, C. (2005). Malaria parasite actin filaments are very short. Journal of molecular biology *349*, 113-125.

Sellers, J.R. (1999). Myosin. 2nd edition. reprint 2002. New York, Oxford University Press, 1-67.

Sellers, J.R. (2000). Myosins: a diverse superfamily. Biochim Biophys Acta *1496*, 3-22.

Sermwittayawong, N., Singh, B., Nishibuchi, M., Sawangjaroen, N., and Vuddhakul, V. (2012). Human *Plasmodium knowles*i infection in Ranong province, southwestern border of Thailand. Malaria journal *11*, 36.

Shaw, M.K., and Tilney, L.G. (1999). Induction of an acrosomal process in *Toxoplasma gondii*: visualization of actin filaments in a protozoan parasite. Proceedings of the National Academy of Sciences of the United States of America *96*, 9095-9099.

Sibley, L.D., Hakansson, S., and Carruthers, V.B. (1998). Gliding motility: an efficient mechanism for cell penetration. Current biology : CB *8*, R12-14.

Siden-Kiamos, I., Ecker, A., Nyback, S., Louis, C., Sinden, R.E., and Billker, O. (2006a). *Plasmodium berghei* calcium-dependent protein kinase 3 is required for ookinete gliding motility and mosquito midgut invasion. Molecular microbiology *60*, 1355-1363.

Siden-Kiamos, I., Ganter, M., Kunze, A., Hliscs, M., Steinbuchel, M., Mendoza, J., Sinden, R.E., Louis, C., and Matuschewski, K. (2011). Stage-specific depletion of myosin A supports an essential role in motility of malarial ookinetes. Cellular microbiology *13*, 1996-2006.

Siden-Kiamos, I., Louis, C., and Matuschewski, K. (2012). Evidence for filamentous actin in ookinetes of a malarial parasite. Mol Biochem Parasitol *181*, 186-189.

Siden-Kiamos, I., Pinder, J.C., and Louis, C. (2006b). Involvement of actin and myosins in *Plasmodium berghei* ookinete motility. Mol Biochem Parasitol *150*, 308-317.

Silvestrini, F., Alano, P., and Williams, J.L. (2000). Commitment to the production of male and female gametocytes in the human malaria parasite *Plasmodium falciparum*. Parasitology *121 Pt 5*, 465-471.

Sinden, R.E. (1983a). The cell biology of sexual development in *Plasmodium*. Parasitology *86 (Pt 4)*, 7-28.

Sinden, R.E. (1983b). Sexual development of malarial parasites. Advances in parasitology *22*, 153-216.

Singh, B., Kim Sung, L., Matusop, A., Radhakrishnan, A., Shamsul, S.S., Cox-Singh, J., Thomas, A., and Conway, D.J. (2004). A large focus of naturally acquired *Plasmodium knowlesi* infections in human beings. Lancet *363*, 1017-1024.

Soldati, D., and Meissner, M. (2004). Toxoplasma as a novel system for motility. Curr Opin Cell Biol *16*, 32-40.

Spence, P.J., Cunningham, D., Jarra, W., Lawton, J., Langhorne, J., and Thompson, J. (2011). Transformation of the rodent malaria parasite *Plasmodium chabaudi*. Nature protocols *6*, 553-561.

Straub, K.W., Peng, E.D., Hajagos, B.E., Tyler, J.S., and Bradley, P.J. (2011). The moving junction protein RON8 facilitates firm attachment and host cell invasion in *Toxoplasma gondii*. PLoS pathogens *7*, e1002007.

Sturm, A., Amino, R., van de Sand, C., Regen, T., Retzlaff, S., Rennenberg, A., Krueger, A., Pollok, J.M., Menard, R., and Heussler, V.T. (2006). Manipulation of host hepatocytes by the malaria parasite for delivery into liver sinusoids. Science *313*, 1287-1290.

Sutherland, C.J., Tanomsing, N., Nolder, D., Oguike, M., Jennison, C., Pukrittayakamee, S., Dolecek, C., Hien, T.T., do Rosario, V.E., Arez, A.P*., et al.* (2010). Two nonrecombining sympatric forms of the human malaria parasite *Plasmodium ovale* occur globally. The Journal of infectious diseases *201*, 1544-1550.

Ta, T.T., Salas, A., Ali-Tammam, M., Martinez Mdel, C., Lanza, M., Arroyo, E., and Rubio, J.M. (2010). First case of detection of *Plasmodium knowlesi* in Spain by Real Time PCR in a traveller from Southeast Asia. Malaria journal *9*, 219.

Taraschi, T.F., Trelka, D., Martinez, S., Schneider, T., and O'Donnell, M.E. (2001). Vesicle-mediated trafficking of parasite proteins to the host cell cytosol and erythrocyte surface membrane in *Plasmodium falciparum* infected erythrocytes. Int J Parasitol *31*, 1381-1391.

Tham, W.H., Healer, J., and Cowman, A.F. (2012). Erythrocyte and reticulocyte binding-like proteins of *Plasmodium falciparum*. Trends Parasitol *28*, 23-30.

Thomas, D.C., Ahmed, A., Gilberger, T.W., and Sharma, P. (2012). Regulation of *Plasmodium falciparum* glideosome associated protein 45 (PfGAP45) phosphorylation. PloS one *7*, e35855.

Thomas, J.C., Green, J.L., Howson, R.I., Simpson, P., Moss, D.K., Martin, S.R., Holder, A.A., Cota, E., and Tate, E.W. (2010). Interaction and dynamics of the *Plasmodium falciparum* MTIP-MyoA complex, a key component of the invasion motor in the malaria parasite. Molecular bioSystems *6*, 494-498.

Thompson, R.F., and Langford, G.M. (2002). Myosin superfamily evolutionary history. The Anatomical record *268*, 276-289.

Tilley, L., McFadden, G., Cowman, A., and Klonis, N. (2007). Illuminating *Plasmodium falciparum*-infected red blood cells. Trends Parasitol *23*, 268-277.

Tonkin, C.J., van Dooren, G.G., Spurck, T.P., Struck, N.S., Good, R.T., Handman, E., Cowman, A.F., and McFadden, G.I. (2004). Localization of organellar proteins in *Plasmodium falciparum* using a novel set of transfection vectors and a new immunofluorescence fixation method. Mol Biochem Parasitol *137*, 13-21.

Tonkin, M.L., Roques, M., Lamarque, M.H., Pugniere, M., Douguet, D., Crawford, J., Lebrun, M., and Boulanger, M.J. (2011). Host cell invasion by apicomplexan parasites: insights from the co-structure of AMA1 with a RON2 peptide. Science *333*, 463-467.

Trampuz, A., Jereb, M., Muzlovic, I., and Prabhu, R.M. (2003). Clinical review: Severe malaria. Crit Care *7*, 315-323.

Tran, J.Q., de Leon, J.C., Li, C., Huynh, M.H., Beatty, W., and Morrissette, N.S. (2010). RNG1 is a late marker of the apical polar ring in *Toxoplasma gondii*. Cytoskeleton (Hoboken) *67*, 586-598.

Tremp, A.Z., and Dessens, J.T. (2011). Malaria IMC1 membrane skeleton proteins operate autonomously and participate in motility independently of cell shape. The Journal of biological chemistry *286*, 5383-5391.

Tremp, A.Z., Khater, E.I., and Dessens, J.T. (2008). IMC1b is a putative membrane skeleton protein involved in cell shape, mechanical strength, motility, and infectivity of malaria ookinetes. The Journal of biological chemistry *283*, 27604-27611.

Triglia, T., Tham, W.H., Hodder, A., and Cowman, A.F. (2009). Reticulocyte binding protein homologues are key adhesins during erythrocyte invasion by *Plasmodium falciparum*. Cellular microbiology *11*, 1671-1687.

Tsuboi, T., Takeo, S., Arumugam, T.U., Otsuki, H., and Torii, M. (2010). The wheat germ cell-free protein synthesis system: a key tool for novel malaria vaccine candidate discovery. Acta tropica *114*, 171-176.

Tyler, J.S., Treeck, M., and Boothroyd, J.C. (2011). Focus on the ringleader: the role of AMA1 in apicomplexan invasion and replication. Trends Parasitol *27*, 410-420.

Uchime, O., Herrera, R., Reiter, K., Kotova, S., Shimp, R.L., Jr., Miura, K., Jones, D., Lebowitz, J., Ambroggio, X., Hurt, D.E.*, et al.* (2012). Analysis of the conformation and function of the *Plasmodium falciparum* merozoite proteins MTRAP and PTRAMP. Eukaryotic cell *11*, 615-625.

Vale, R.D. (2003). The molecular motor toolbox for intracellular transport. Cell *112*, 467-480.

van Dijk, M.R., Waters, A.P., and Janse, C.J. (1995). Stable transfection of malaria parasite blood stages. Science *268*, 1358-1362.

van Dooren, G.G., Reiff, S.B., Tomova, C., Meissner, M., Humbel, B.M., and Striepen, B. (2009). A novel dynamin-related protein has been recruited for apicoplast fission in *Toxoplasma gondii*. Current Biology *19*, 267-276.

Vanderberg, J.P. (1974). Studies on the motility of *Plasmodium* sporozoites. The Journal of protozoology *21*, 527-537.

Veigel, C., Coluccio, L.M., Jontes, J.D., Sparrow, J.C., Milligan, R.A., and Molloy, J.E. (1999). The motor protein myosin-I produces its working stroke in two steps. Nature *398*, 530-533.

Vlachou, D., Schlegelmilch, T., Runn, E., Mendes, A., and Kafatos, F.C. (2006). The developmental migration of Plasmodium in mosquitoes. Current opinion in genetics & development *16*, 384-391.

Waterkeyn, J.G., Crabb, B.S., and Cowman, A.F. (1999). Transfection of the human malaria parasite *Plasmodium falciparum*. Int J Parasitol *29*, 945-955.

Waters, A.P., Higgins, D.G., and McCutchan, T.F. (1993). Evolutionary relatedness of some primate models of *Plasmodium*. Molecular biology and evolution *10*, 914-923.

Weatherall, D.J., Miller, L.H., Baruch, D.I., Marsh, K., Doumbo, O.K., Casals-Pascual, C., and Roberts, D.J. (2002). Malaria and the red cell. Hematology / the Education Program of the American Society of Hematology American Society of Hematology Education Program, 35-57.

Wel, A., Kocken, C.H., Pronk, T.C., Franke-Fayard, B., and Thomas, A.W. (2004). New selectable markers and single crossover integration for the highly versatile *Plasmodium knowlesi* transfection system. Mol Biochem Parasitol *134*, 97-104.

Wesseling, J.G., Smits, M.A., and Schoenmakers, J.G. (1988). Extremely diverged actin proteins in *Plasmodium falciparum*. Mol Biochem Parasitol *30*, 143-153.

Wesseling, J.G., Snijders, P.J., van Someren, P., Jansen, J., Smits, M.A., and Schoenmakers, J.G. (1989). Stage-specific expression and genomic organization of the actin genes of the malaria parasite *Plasmodium falciparum*. Mol Biochem Parasitol *35*, 167-176.

Wetzel, D.M., Hakansson, S., Hu, K., Roos, D., and Sibley, L.D. (2003). Actin filament polymerization regulates gliding motility by apicomplexan parasites. Molecular biology of the cell *14*, 396-406.

Wetzel, D.M., Schmidt, J., Kuhlenschmidt, M.S., Dubey, J.P., and Sibley, L.D. (2005). Gliding motility leads to active cellular invasion by *Cryptosporidium parvum* sporozoites. Infection and immunity *73*, 5379-5387.

White, N.J. (2004). Antimalarial drug resistance. The Journal of clinical investigation *113*, 1084-1092.

WHO (2012). World Malaria Report 2012.

Wu, Y., Kirkman, L.A., and Wellems, T.E. (1996). Transformation of *Plasmodium falciparum* malaria parasites by homologous integration of plasmids that confer resistance to pyrimethamine. Proceedings of the National Academy of Sciences of the United States of America *93*, 1130-1134.

Wu, Y., Sifri, C.D., Lei, H.H., Su, X.Z., and Wellems, T.E. (1995). Transfection of *Plasmodium falciparum* within human red blood cells. Proceedings of the National Academy of Sciences of the United States of America *92*, 973-977.

Yeoman, J.A., Hanssen, E., Maier, A.G., Klonis, N., Maco, B., Baum, J., Turnbull, L., Whitchurch, C.B., Dixon, M.W., and Tilley, L. (2011). Tracking Glideosome-associated protein 50 reveals the development and organization of the inner membrane complex of *Plasmodium falciparum*. Eukaryotic cell *10*, 556-564.

Yuda, M., and Ishino, T. (2004). Liver invasion by malarial parasites--how do malarial parasites break through the host barrier? Cellular microbiology *6*, 1119-1125.

Zheng, H., Kunst, L., Hawes, C., and Moore, I. (2004). A GFP-based assay reveals a role for RHD3 in transport between the endoplasmic reticulum and Golgi apparatus. The Plant journal : for cell and molecular biology *37*, 398-414.

Zhou, H., Gao, Y., Zhong, X., and Wang, H. (2009). Dynamin like protein 1 participated in the hemoglobin uptake pathway of *Plasmodium falciparum*. Chin Med J *122*, 1686-1691.

Zuccala, E.S., Gout, A.M., Dekiwadia, C., Marapana, D.S., Angrisano, F., Turnbull, L., Riglar, D.T., Rogers, K.L., Whitchurch, C.B., Ralph, S.A*., et al.* (2012). Subcompartmentalisation of proteins in the rhoptries correlates with ordered events of erythrocyte invasion by the blood stage malaria parasite. PloS one *7*, e46160.

Appendix A: Wheat germ His- and GST-tagging vectors used in the wheat germ cell free expression system. pEU-E01-His-TEV-MCS-N1 used for His-tagged protein. pEU-E01-GST-TEV-MCS-N1 used for GST-tagged protein

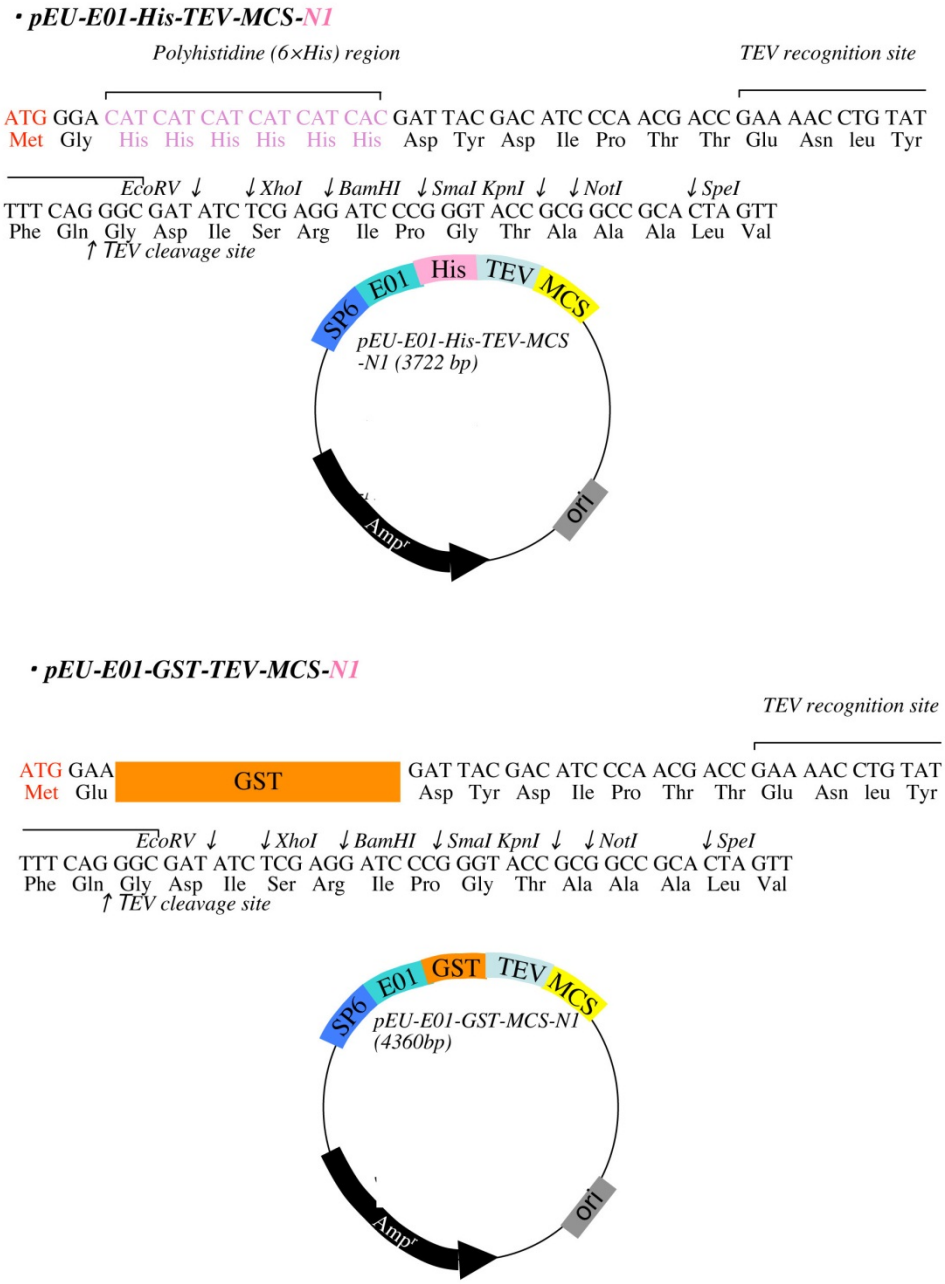

Appendix B: Vector map of (a) **t**he PHH4-PfMyoA-GFP and (b) the PHH4-PfMyoB-GFP plasmids. The diagram shows the vector map of the construct used in single crossover homologous recombination. All unique sites and important features are indicated.

(a)

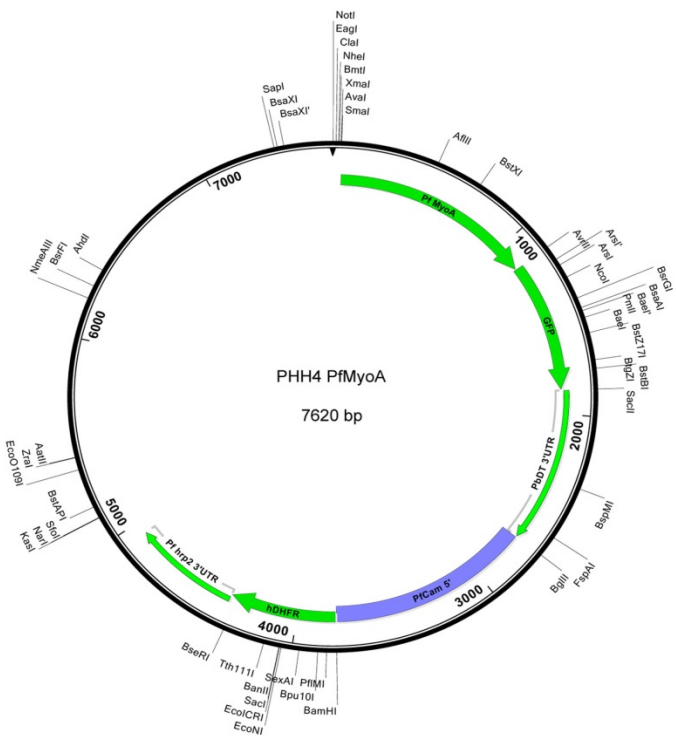

(b)

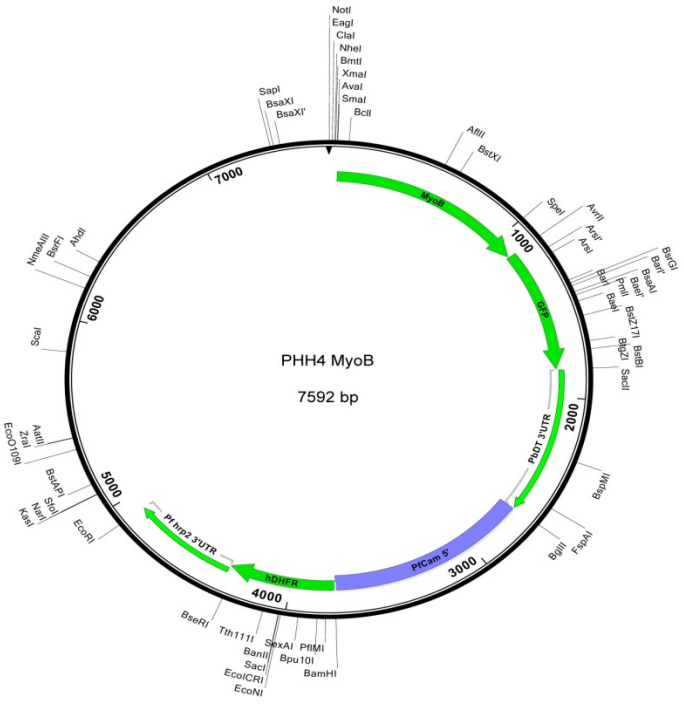

Appendix C: Clustal alignment of *P. falciparum* MTIP-B amino acid sequence with the protein sequence in other *Plasmodium* parasites**.** PCYB - *P. cynomolgi* B strain hypothetical protein; PKH - *P. knowlesi* H strain; PBANKA - *P. berghei* ANKA strain; PCHAS - *P. chabaudi chabaudi* AS strain; PfMTIP-B - *P. falciparum*, 3D7 strain. *, identity; :, strong similarity.

```
PCYB_092480       ----------------------------------------------------MDNFPPPSL 9
PKH_091610        MEILKGSVNKIVNTQRSPLSYDDDGKPFSSLFRKNRVSFYDDLRTEAVLLLWKNSHHPKY 60
PBANKA_092940     -------MIQNLYVPQNNKIKNYNERKTTSLFRNNSVSFYNDVNTEAICLLDRATQP--- 50
PCHAS_091490      -------MIQNLYTPKNNKIKNVNERKNTSLFRNNSVSFYNDVNTEAISLLDRATQQ--- 50
PfMTIB-B          -MKVLKTSKNNFVHPNKSNQYNCNDQPYDSLFRKNCVSFYEDFDTEAIFLLDKGSRP--- 56


PCYB_092480       SSYVTNFRINRECVLFSQGKQIRHTRKK-------------------------QEFEKIN 44
PKH_091610        FAYVTNFRINRECVLFSQGKQIRHIRKKQVLLIMRKGFPQLVLVNMFSLLRLREEFEKIN 120
PBANKA_092940     ---INYKIIKNDCILFKDGNKIQHTKKE-------------------------KEFDKIT 82
PCHAS_091490      ---IDYNMIKNDCILYKDGNKNQHTKKE-------------------------KEFEKIT 82
PfMTIB-B          ---IYHKLKDKEWGSSNNQKDTEKKKKK-------------------------EEFEKID 88
                     :     ..:    .: :. .: :*:                         :**:**


PCYB_092480       DIINNIDYLDTLKEKVHDRNVEKIVEPLGICAPREGIPKGSDGEYGELTYKDKFEALKNK 104
PKH_091610        DILNSIDYLDTLKEKVHDRNVEKIIEPLGICAPREGIPKGSGEEYGELTYKDKFEVMKNK 180
PBANKA_092940     QIVNASNYLNSLKSKIHTTDIEQITKPLGIYFSNE-KSNSLRTKDNDLVYKNKYESLKKE 141
PCHAS_091490      KIVNDADYLNSLKSKIHTTDIEKITQPLGIYSSKE-KSNSHRAKYNDIIYKNKYKSLKKE 141
PfMTIB-B          EIISNAEHLNNLRNKLYSFEYQNILEPLGIYISQQEDKEENIKREMGNFYKDEYEILKKK 148
                  .*:.  ::*:.*:.*::  : ::* :****  ..:   :    .     **:::: :*::


PCYB_092480       YDHLKKNLDTRIHLELIKAGVFYNQDDIKNVLYMVRKYQGDLKTKKSIINVQNGIIQNVM 164
PKH_091610        YNDLKKNMDTRIHLELIKAGVFYNQDDIQNVLHMVRKYQGDLKTKKSIINVQNGIIQNVV 240
PBANKA_092940     YDNLKERMDIKIDLELIKAGAFYNKEDIHDILRLIKKYQSRIKEKKDIIDTQNNVIENIM 201
PCHAS_091490      YDDLKERIDIKIDLELIKSGAFYNKEDIHDILHLIKKYQSKIKEKKDIIDTQNNVIENIM 201
PfMTIB-B          YIHLKENMDTILDVERIKAGLFYTKEDLQKIFEIIRKHQSKINNKNDIIKFQSSMLEKAI 208
                  * .**:.:*  :.:* **:* **.::*::.:: :::*:*. :: *:.**. *..:::: :


PCYB_092480       ERNKLSRNKLLVDKKKNEELMKMCRTYYEQNKSAQTRLRKLKHAFLQYKIALESIVSCCE 224
PKH_091610        ERNKLSRNKLRLDKEKNEGLMKMCRTYYEQNKNTQMRLRKLKHAFLEYKIALESIVSCCE 300
PBANKA_092940     EQTKLNRNKFIVEKKKNEDMAKICHSYYRQSKKTQMKMKMLKYSFLEYKMALENIVSCCE 261
PCHAS_091490      EQTKLNRNKFIVEKKKNEDMAKICNSYYHQSKKTQMKMKMLKYSFLEYKMALENIVSCCE 261
PfMTIB-B          EHNKKNKLTIIKDKRKNEKLLEICKSYYEQNEKAQKKLRHLKYSFLEYKIALENIVSCCE 268
                  *:.* .: .:  :*.*** : ::*.:**.*.:.:* ::: **::**:**:***.******


PCYB_092480       KIGGDKIILMDAVKSARAQTDLSIATDILNTKKIQELEMNICYCEHQINSLKDDLDVMLG 284
PKH_091610        KIGGDKIILMDVVKSARAQTDLSIATDILNTKKIQELEMNICYCEHQINSLKDDLDTMLA 360
PBANKA_092940     QIGGDKIILMDAIKSAKTQTDLSIATEILNIKKIKDLEMSICYCEHHINYLNEELNLKLQ 321
PCHAS_091490      QIGGDKIILMDAIKSAKTQTDLSIATEMLNIKKIKELEMSICYCEHHINYLNEELNLKLQ 321
PfMTIB-B          KIGGDKIILMDGIKSARAQADMSIANDIKNKIKIEELEMNISYCEQQINYLKDDLDFKME 328
                  :********** :***:.*:*:***.:: *  **::***.*.***::** *:::*:  :


PCYB_092480       KLQNEKKEKREVMNQTLRYKEHLEKNNAMLIEALENFRRVMTSVDEHLSREG--NRSDFK 342
PKH_091610        KLQDEKKEKREVMNQALQYKEHLAKNNDMLIEALENFRRVMISVDEHLSRES--DRSDFK 418
PBANKA_092940     ELKNETKEKKEAQNEIYSYKKELTKNNNMIIKILENYHQMMATMEKIIYEND--IANKYK 379
PCHAS_091490      ELKNAAKEKKETQNEIYSYKKELAKNNNMIIKILEDYHQTMATMEKIIYENDNANANKHK 381
PfMTIB-B          ELRNTTLYTEEVKNEASYFKQELSKNNDLLLEVMEHFHQMINNVDEFIYKNK--DKNELI 386
                  :*::    ..*. *:   :*:.* *** :::: :*.::: : .::: : .:     ..


PCYB_092480       ETFDKSKKKYNDFVRKAAEKNKDLQKMGDKLLLTSALSGHELKRHQEYLNRQINEMKKNQ 402
PKH_091610        KTFDNSKKKYNDFVRKAAVKNKELQKMGDKLILMNALSGQELKKHQEYLNRQINQIRKNQ 478
PBANKA_092940     PDFIKDKKKYNDMVKLLLESNKELKNINDKLFLSNNVFKGKLKNHQEFLTKHMNEDN--- 436
PCHAS_091490      TDFIKDKKKYNDLVKKVLESNNELKNNNDKLFLHDNVLKGKLKAHQELLTKHMN------ 435
PfMTIB-B          TYMNKKKKKYGDITKKISEKNKELNLKVKNFVPYNFSMGTELKKHEEYLKIQMDEMKKK- 445
                    : :.****.*:.:    .*::*:   .::.  .     :** *:* *. :::


PCYB_092480       GGVEEEEEQKGHKNGGKVGEAEKSSHEEEQDKKQPLEGESSQGAKEITNDTERKQA-EQK 461
PKH_091610        GGIEEEE-QKGNKNNGKVGEVEKGNQEEEQDQKQTLEGKSCQGVKDIPNDIEGKQG-KEK 536
PBANKA_092940     -------KNKHKDDANKISNLTDQTNETKNIDKS--ETEIIAKENNSTNETVLKN----- 482
PCHAS_091490      -------EHKPKEAVNKAPSLADQKNETENADKP--ETGVMGNENNSTNEVEPKD----- 481
```

```
PfMTIB-B          ---EEEEKRKRREEEEEEQKKRKEEEEEEQKKRKEEEEKIEKKKKEEEEEKRKKEEQELL 502
                         .* ..   :  .  .  .* :: .:   *       ::  ::   *:

PCYB_092480       GEQPTHVDESLEGRKINQVMELLQKKEIDKLTFEDCVDVIYKVNLPLTQSKLNELKAMGE 521
PKH_091610        EEQTKRVDESLEGRIINQVMELLQKKENNKLTFEDCVDVIYKVNLPLTQSKLNELKAMGE 596
PBANKA_092940     -----NIDINVELDKIEKIQEFIKNKNIDKLKFEDCVDIMYKSNIVLTRNKMEELKQMGL 537
PCHAS_091490      -----NQDIPVDLEKIEKIQEFIKNKNVDKLKFEDCLDIMYKSNVVLTRSKMEELKQMDP 536
PfMTIB-B          EEKDIKNNETFEEKKIRLVKELMKEVNEETLSLEKCVDIIYKANLPLTQNKLNKLKNMGD 562
                       . :  .:   *. : *:::: : :.*.:*.*:*::** *: **:.*:::** *.

PCYB_092480       VHKDDLVAFIKTFIVQEEEALQNMITFFEIWDVQKTGYMHKELILLILKQFGDSLTEDEM 581
PKH_091610        VDKEDLIAFIKTFIMDEDEALQNMITFFEIWDVQKTGYMHKELILLILKQFGDKLTEDEM 656
PBANKA_092940     ITANEFVTFIKPFIINEEEALKNMITFFEIWDVKKTGYMHKDLFMPILKYFGDHLSDQEI 597
PCHAS_091490      ITTDEFVTFIKPFIINEEEALKNMITFFEIWDVKKTGYMHKDLFMPILKYFGDHLSDQEM 596
PfMTIB-B          IKKDELVTFVKTLMLNEQEAFENMKTFFEIWDIMKTGYMHKNLIISILKQFGDNLTEEES 622
                  :  :::::*:*.:::::*:**:** ******* ******* .*:: *** *** *:::*

PCYB_092480       EYLR-------ESKK------KR--------- 591
PKH_091610        EYLRGEVNAFKESNISYVDLLKRWIQGTGE-- 686
PBANKA_092940     DYLQKELNLSNEPKISYADILKKWIYGKDQQI 629
PCHAS_091490      DYLQKELSLSNEPNISYVDILKKWIYGKDQQT 628
PfMTIB-B          NYIQKELNQMSESNISYVKLLKKWIYGTEE-- 652
                  :*::       *.:       *:
```

Appendix D: Clustal alignment of amino acid sequences of full length *P. falciparum* MyoA and MyoB**.** *, identity; :, strong similarity